



The  
University  
Of  
Sheffield.

## **Experimental Study of Multiple Outlets in a Siphonic Roof Drainage System**

Kieran J. Williams

A thesis submitted to the Department of Civil and Structural Engineering in partial fulfilment  
of the requirements for the degree of Doctor of Philosophy.

The University of Sheffield

February 2016

## **Abstract**

Recent trends in the development of our urban landscape have seen the introduction of larger buildings with vast roof areas especially in localised business and industry parks. It is anticipated that the onset of climate change will see increased intensities and volumes of rainfall which will place significant pressures on the roof drainage systems for these buildings, potentially leading to failure and major flooding. There is an urgent need to examine alternative forms of roof drainage and a potential future solution is the adoption of siphonic roof drainage systems. However, it has been identified that there is a universal lack of understanding of the hydraulic performance of siphonic systems, particularly with regard to multi-outlet systems.

The work presented in this thesis describes a comprehensive experimental programme of research using novel and sophisticated measurement techniques including flourometry and particle image velocimetry, to increase the understanding of the hydraulic performance of multi-outlet siphonic roof drainage systems. The overall aim was to deliver a step change and better understanding of the performance of such systems and how they may be better designed. A total of 63 steady flow tests were completed using the siphonic roof drainage test facility at the University of Sheffield.

The results from this study support key findings that within a multi-outlet siphonic system the flow rate through each individual outlet is contrary to existing design practice and significantly different flow regimes occurred within the horizontal carrier pipe. Hence, current approaches applied in conventional siphonic roof drainage practice and design software should be reviewed.

The outputs from this study have highlighted the need for further research to better understand the performance of multi-outlet siphonic roof drainage systems. These topics may be addressed with the technology and methodologies developed within the experimental programme of research reported in this thesis.

## Executive Summary

Recent trends in the development of our urban landscape have seen the introduction of larger buildings with vast roof areas especially in localised business and industry parks. It is anticipated that the onset of climate change will see increased intensities and volumes of rainfall which will place significant pressures on the roof drainage systems for these buildings potentially leading to failure and major flooding. There is an urgent need to examine alternative forms of roof drainage and a potential future solution is the adoption of siphonic roof drainage systems. However, it has been identified that there is a universal lack of understanding of the hydraulic performance of siphonic systems, particularly with regard to multi-outlet systems.

The work presented in this thesis describes a comprehensive experimental programme of research to increase the understanding of the hydraulic performance of multi-outlet siphonic roof drainage systems with three outlets, in order to deliver a step change and better understanding of the performance of such systems and how they may be better designed.

The experimental programme of research enhanced and utilised a full-scale siphonic roof drainage test facility owned by the Department of Civil and Structural Engineering at the University of Sheffield, together with a series of novel experimental measurement techniques with computer control. Four methods of measurement were designed and used during the experimental research programme:

1. Water depth measurement within the gutter
2. Pressure measurement at four locations within the horizontal carrier pipe
3. Flow rate measurement within the horizontal carrier pipe downstream of each gutter outlet using flourometry
4. Flow velocity measurement within the horizontal carrier pipe downstream of each gutter outlet using high speed image velocimetry.

A series of feasibility tests were undertaken to independently assess, review and refine the methods of measurement. A full test program of 63 steady flow tests were completed using three outlets within the gutter at overall system flow rates equivalent to 20%, 40%, 60%, 80%, 100%, 117% and 120% of the system design flow rate.

This experimental research presents novelty in several aspects:

- The application of flourometry within the experimental system and methodology refined during this research has for the first time, provided a repeatable, robust and reliable approach to simultaneously measure the relative proportion and components of flow within a multi-outlet siphonic roof drainage system over a range of steady flow tests below, at, and above the design criteria. Significantly, this non-intrusive methodology enabled the continuous measurement of flow through each outlet without affecting the hydraulic performance or generating additional, uncalculated losses. It is concluded therefore, that the provision of such a measurement system

represents a novel and original way in which to measure the flow components in a multi-outlet siphonic roof drainage system;

- Flow rate through the multi-outlet test facility was not equal and flow proportionality through each outlet varied as a function of the magnitude of the total system flow rate. This highlights that current design criteria are fundamentally flawed as the assumption is made that this is the case;
- Commercially available model based software based on steady state hydraulic theory was used to calculate the design and ultimate flow capacity through the system. It was observed that the measured system flow rates and pressure using the experimental test facility differed to the calculated values from the model based design software. The differences can be attributed to five reasons:
  1. Steady state hydraulic theory is based on the pipes within system being full of water and free of air;
  2. Flow observed within the horizontal carrier pipe contained unquantified amounts of air at the crown of the carrier pipe and as a homogenous mixture that varied temporally and spatially;
  3. Steady state hydraulic calculations used within the software are based on certain assumptions, specifically the pipe roughness ( $k_s$ ) and the head loss coefficient ( $K$ );
  4. Head loss due to fittings within the software are assumed to be local to the fitting;
  5. In practice, any slight displacement or imperfection in the pipe joints will affect the head loss at that fitting and be a source of error.
- The change in pressure and flow regime within the horizontal carrier pipe of a siphonic system has been shown to be an extremely complex process with many observed phenomena. The recognised and reported flow regimes within the horizontal carrier pipe of a siphonic roof drainage system varied temporally and spatially from the observations made during the steady flow tests during both sub-primed and primed flow conditions. Current design criteria do not take these observed regimes and changes into account;
- Flow rate, pressure and the quantity of air within the horizontal carrier pipe varied temporally and spatially, even when the system was operating above the design capacity. What is clear is that the quantity of air entrainment is extremely difficult to accurately measure and model as such entrainment varied as a function of the magnitude of flow;
- For the first time, the relationship between localised system pressure, the relative flow through each component outlet of the system and a visual representation of air entrainment along the length of the horizontal carrier pipe, has been clearly demonstrated;
- A sophisticated system of measurement was developed and refined to record the transverse velocity of the flow within the horizontal carrier pipe. This is a unique approach of measuring velocity in siphonic systems and provides a novel, non-intrusive method of measurement without interrupting the flow field. Observations

following analysis of the measured flow velocity using high-speed image velocimetry and PIV analysis showed that the transverse velocity profile within the horizontal carrier pipe was variable and complex. Hence, the use of flow velocity measurement at individual locations within a siphonic drainage system may not be appropriate to estimate flow rate;

- Considerable fluctuations in the velocity profile of the flow within the horizontal carrier pipe were measured during sub-primed conditions and at the system design. Even at full bore flow conditions significantly in excess of the system design, variability in the flow velocity was recorded. This is a new finding that requires further exploration. Previous experimental research using alternative methods of measuring and estimating flow rate and velocity may not be able to accurately determine these conditions at the required resolution and further work is recommended to address this shortfall in knowledge.

In summary, the results from this study support several key findings: within a multi-outlet siphonic system the flow rate through each individual outlet is not the same; that significantly different flow regimes occurred along the length of the horizontal carrier pipe during steady flow tests; that air entrainment is a major influence on system performance and that differences were observed between the experimental pressure and flow rate results with those computed using software based on steady-state hydraulic relationships. Hence, the current approaches applied in conventional siphonic roof drainage design should be reviewed. Design engineers should also be made aware of these findings.

The outputs from this study have highlighted the need for further research to better understand the performance of multi-outlet siphonic roof drainage systems. Specifically, the following topics have been identified:

- Hydraulic design and the applicability of a standard safety factor;
- Design criteria based on the magnitude of flow and changes to system configuration;
- System balancing for a range of outlet and pipework configurations;
- Minimum flow velocities to investigate the applicability of previously reported experimental research;
- Speed of priming to apply the techniques and measurement methodologies developed during this experimental research to a series of time-varying flow tests to inform and update current design standards, software and models;
- Minimum allowable pressures to quantify the effect of flow velocity, temperature, static pressure and atmospheric pressure;
- Quantification of air entrainment within siphonic systems as a function of the magnitude of flow rate, flow velocity, system pressure and pipework configuration.

These topics may be addressed with the technology and methodologies developed within this experimental research.

# Contents

1	Introduction.....	1
1.1	Background.....	1
1.2	Research Aim and Objectives.....	5
1.2.1	Aim.....	5
1.2.2	Objectives.....	6
1.3	Thesis Contents.....	7
2	Literature Review.....	8
2.1	Introduction.....	8
2.2	Siphons.....	8
2.3	Conventional roof drainage.....	10
2.3.1	Limitations of Conventional Roof Drainage Systems.....	12
2.4	Siphonic Roof Drainage.....	13
2.4.1	Siphonic System Priming.....	15
2.4.1.1	Initial gutter inflow.....	17
2.4.1.2	Outlet tail pipe priming.....	17
2.4.1.3	Formation and Movement of Hydraulic Jumps.....	18
2.4.1.4	Formation and Propagation of Full Bore Flow.....	18
2.4.1.5	Depressurisation of Flow.....	18
2.4.1.6	Partial Re-pressurisation of Flow.....	19
2.4.1.7	Fully Primed System.....	19
2.4.2	Current Design Practice.....	19
2.4.2.1	Hydraulic Design.....	20
2.4.2.2	Design Criteria.....	23
2.4.2.3	System Balancing.....	23
2.4.2.4	Minimum Flow Velocities.....	24
2.4.2.5	Speed of Priming.....	25
2.4.2.6	Minimum Allowable Pressure.....	26
2.4.2.7	Air within Siphonic Systems.....	28
2.4.3	Limitations of Siphonic Roof Drainage.....	29
2.4.3.1	Interaction between the Above and Below Ground Systems.....	29
2.4.3.2	System Operating and Design Pressures.....	30
2.4.3.3	Mechanical Failure of Pipework.....	30
2.4.3.4	Inadequate Capacity.....	32
2.4.3.5	Inadequate Maintenance.....	32
2.4.4	Previous Experimental Research.....	33
2.4.4.1	Heriot-Watt University (HWU), Edinburgh, Scotland.....	33
2.4.4.1.1	HWU Experimental Study.....	33

2.4.4.1.1.1	Steady State Design Criteria Rainfall Event (Fully Primed System)	36
2.4.4.1.1.2	Rainfall Events below the Design Criteria.....	36
2.4.4.1.1.3	Design Criteria Rainfall Event Varying Gutter Inflows (Fully Primed System).....	36
2.4.4.1.1.4	Rainfall Events above the Design Criteria .....	36
2.4.4.1.1.5	Total Blockage of one of the Outlets .....	37
2.4.4.1.2	HWU Numerical Model .....	37
2.4.4.2	The University of Sheffield, UK .....	40
2.4.4.2.1	The Interaction of Primary and Secondary Siphonic Rainwater Outlets	40
2.4.4.2.2	The Validity of a Theoretical Methodology for Siphonic Roof Drainage Design .....	40
2.4.4.2.3	The Prediction of Water Depths around Siphonic Rainwater Outlets ...	40
2.4.4.2.4	The Effects of Sub-Atmospheric Pressure .....	41
2.4.4.2.5	Flow Measurement.....	42
2.4.4.3	Geberit International A.G., Switzerland.....	43
2.4.4.4	University of South Australia (UniSA), Melbourne, Australia .....	46
2.4.4.4.1	The Effects of Air Entrainment on System Capacity.....	46
2.4.4.4.2	Controlling Negative Pressures within Siphonic Roof Drainage Systems using Air Entrainment.....	47
2.4.4.4.2.1	Aeration Testing.....	48
2.4.4.4.2.2	Cavitation Testing .....	49
2.4.4.4.2.3	Cavitation Endurance Testing .....	49
2.4.4.4.2.4	Pressure Surge Testing .....	50
2.4.4.4.3	Capacity Loss in Siphonic Systems due to Aeration.....	50
2.4.4.4.4	Measurement of Flows in Partially Filled Pipes in Siphonic Roof Drainage Systems.....	52
2.5	Literature Review Summary .....	58
3	Experimental Study.....	60
3.1	Phase 1 - Enhancement and Configuration of the Experimental Test Facility .....	61
3.1.1	Principles of the Commercially Available Siphonic Roof Drainage Design Software .....	66
3.1.2	Gutter Outlets and Tailpipe Configuration .....	67
3.2	Phase 2 - Calibration of the Experimental Test Facility .....	71
3.2.1	Levelling of the Gutter Sole.....	71
3.2.2	Levelling of the Knife-Edged Weir .....	71

3.2.3	Levelling of the Horizontal Carrier Pipe .....	71
3.2.4	Calibration of the Butterfly Control Valve .....	71
3.3	Water Depth Measurement within the Gutter .....	74
3.3.1	Calibration of the Digital Depth Micrometer.....	74
3.3.2	Methodology .....	74
3.3.3	Summary .....	75
3.4	Pressure Measurement within the Horizontal Carrier Pipe.....	76
3.4.1	Calibration of the Pressure Transducers .....	78
3.4.2	Summary .....	80
3.5	Flow Rate Measurement within the Horizontal Carrier Pipe using Fluorometry ....	81
3.5.1	Calibration of the Fluorometers .....	83
3.5.2	Methodology .....	84
3.5.3	Summary .....	86
3.6	Flow Velocity Measurement within the Horizontal Carrier Pipe using High Speed Image Velocimetry.....	87
3.6.1	Methodology .....	88
3.6.2	Summary .....	92
3.7	Feasibility Test Summary and Introduction to the Full Test Program.....	94
3.7.1	Full Test Program Methodology .....	95
4	Results and Discussion .....	97
4.1	Summary of the Results .....	99
4.1.1	Tests Completed at 20% of the Design Flow Rate .....	108
4.1.1.1	Mass Balance .....	108
4.1.1.2	Flow Proportionality .....	108
4.1.1.3	Time Series Flow Rate and Pressure Measurements.....	110
4.1.1.4	Time Series Flow Rate, Pressure and Image Comparison at P1 .....	113
4.1.1.5	Time Series Flow Rate, Pressure and Image Comparison at P2 .....	114
4.1.1.6	Time Series Flow Rate, Pressure and Image Comparison at P3 .....	115
4.1.2	Tests Completed at 40% of the Design Flow Rate .....	118
4.1.2.1	Mass Balance .....	118
4.1.2.2	Flow Proportionality .....	118
4.1.2.3	Time Series Flow Rate and Pressure Measurements.....	120
4.1.2.4	Time Series Flow Rate, Pressure and Image Comparison at P1 .....	122
4.1.2.5	Time Series Flow Rate, Pressure and Image Comparison at P2 .....	123
4.1.2.6	Time Series Flow Rate, Pressure and Image Comparison at P3 .....	125
4.1.3	Tests Completed at 60% of the Design Flow Rate .....	127
4.1.3.1	Mass Balance .....	127
4.1.3.2	Flow Proportionality .....	127



4.1.3.3	Time Series Flow Rate and Pressure Measurements.....	129
4.1.3.4	Time Series Flow Rate, Pressure and Image Comparison at P1 .....	131
4.1.3.5	Time Series Flow Rate, Pressure and Image Comparison at P2 .....	132
4.1.3.6	Time Series Flow Rate, Pressure and Image Comparison at P3 .....	134
4.1.4	Tests Completed at 80% of the Design Flow Rate .....	136
4.1.4.1	Mass Balance .....	136
4.1.4.2	Flow Proportionality .....	136
4.1.4.3	Time Series Flow Rate and Pressure Measurements.....	138
4.1.4.4	Time Series Flow Rate, Pressure and Image Comparison at P1 .....	139
4.1.4.5	Time Series Flow Rate, Pressure and Image Comparison at P2 .....	141
4.1.4.6	Time Series Flow Rate, Pressure and Image Comparison at P3 .....	143
4.1.5	Tests Completed at the Design Flow Rate.....	145
4.1.5.1	Mass Balance .....	145
4.1.5.2	Flow Proportionality .....	145
4.1.5.3	Time Series Flow Rate and Pressure Measurements.....	147
4.1.5.4	Time Series Flow Rate, Pressure and Image Comparison at P1 .....	149
4.1.5.5	Time Series Flow Rate, Pressure and Image Comparison at P2 .....	151
4.1.5.6	Time Series Flow Rate, Pressure and Image Comparison at P2 .....	152
4.1.6	Tests Completed at the Ultimate Flow Rate .....	154
4.1.6.1	Mass Balance .....	154
4.1.6.2	Flow Proportionality .....	154
4.1.6.3	Time Series Flow Rate and Pressure Measurements.....	156
4.1.6.4	Time Series Flow Rate, Pressure and Image Comparison at P1 .....	157
4.1.6.5	Time Series Flow Rate, Pressure and Image Comparison at P2 .....	158
4.1.6.6	Time Series Flow Rate, Pressure and Image Comparison at P3 .....	159
4.1.7	Tests Completed at 120% of the Design Flow Rate .....	161
4.1.7.1	Mass Balance .....	161
4.1.7.2	Flow Proportionality .....	161
4.1.7.3	Time Series Flow Rate and Pressure Measurements.....	163
4.1.7.4	Time Series Flow Rate, Pressure and Image Comparison at P1 .....	165
4.1.7.5	Time Series Flow Rate, Pressure and Image Comparison at P2 .....	166
4.1.7.6	Time Series Flow Rate, Pressure and Image Comparison at P3 .....	167
4.2	Key Findings and Discussion.....	169
4.2.1	Quantified Measurement of the Flow Proportionality within a Multi-Outlet Siphonic Roof Drainage Test Facility.....	170
4.2.1.1	Comparison to Previous Research and Practice .....	173
4.2.2	Relative Flow Proportionality within a Multi-Outlet Siphonic Roof Drainage Test Facility .....	184
4.2.2.1	Comparison to Previous Research and Practice .....	185
4.2.3	Comparison Between Measured System Flow Rates and Pressure to the Calculated Values using the Model Based Design Software.....	187

4.2.3.1	Measured Pressure and Flow Comparison .....	192
4.2.3.2	Comparison to Previous Research and Practice .....	193
4.2.4	Observed Flow Regimes within the Multi-Outlet Siphonic Roof Drainage Test Facility .....	196
4.2.4.1	Comparison to Previous Research and Practice .....	198
4.2.5	Observed Air Entrainment During Steady Flow Tests within the Multi-Outlet Siphonic Roof Drainage Test Facility.....	202
4.2.5.1	Comparison to Previous Research and Practice .....	203
4.2.6	Measured Flow Velocity During Steady Flow Tests within the Multi-Outlet Siphonic Roof Drainage Test Facility.....	205
4.3	Practical Implications of the Research on Design Practice .....	208
4.3.1	Hydraulic Design .....	208
4.3.2	Design Criteria .....	209
4.3.3	System Balancing.....	209
4.3.4	Minimum Flow Velocities .....	210
4.3.5	Speed of Priming.....	210
4.3.6	Minimum Allowable Pressures.....	211
4.3.7	Air within Siphonic Systems .....	212
4.4	Results and Discussion Close .....	214
5	Conclusions and Recommendations for Further Research .....	215
5.1	Flow Measurement within a Multi-Outlet Siphonic Roof Drainage System.....	216
5.2	Flow Proportionality .....	217
5.3	Measured and Calculated System Flow Rate and Pressure .....	218
5.4	Flow Regimes .....	220
5.5	Air Entrainment .....	221
5.6	Flow Velocity.....	222
5.7	Recommendations for Further Research.....	223
5.7.1	Hydraulic Design .....	223
5.7.2	Design Criteria .....	223
5.7.3	System Balancing.....	223
5.7.4	Minimum Flow Velocities .....	223
5.7.5	Speed of Priming.....	223
5.7.6	Minimum Allowable Pressures.....	224
5.7.7	Air within Siphonic Systems .....	224
6	Summary Conclusions .....	225
	References.....	227
	Appendix 1 - Commercial System Software Design .....	229

Appendix 2 - Steady State Hydraulic Equations of the Experimental Test Facility.....	232
Appendix 3 - Pump Calibration Results .....	234
Appendix 4 - Pressure Transducer Calibration Results .....	237
Appendix 5 - Flourometer Calibration Results.....	239
Appendix 6 - Published Papers .....	243
Appendix 7 - Details of Equipment Used.....	257

## List of Figures

Figure 1.1 Conventional Roof Drainage System .....	1
Figure 1.2 Siphonic Roof Drainage Systems .....	2
Figure 1.3 Diagram of a Typical Siphonic System.....	3
Figure 2.1 Simple Siphon Arrangement Showing Two Example Reference Points .....	9
Figure 2.2 A Conventional Roof Drainage System .....	10
Figure 2.3 Conventional Gutter Outlet and Downpipe (Lucke et al. 2007) .....	11
Figure 2.4 A Siphonic Roof Drainage System.....	13
Figure 2.5 Principal Components of a Siphonic Roof Drainage System (BSI 2007).....	14
Figure 2.6 Siphonic Drainage Outlet with a Solid Anti-vortex Plate and Baffle Vanes (Bramhall, 2004).....	15
Figure 2.7 Flow Patterns in Full-Bore Flow Systems (May and Escarameia 1996).....	16
Figure 2.8 The Priming Procedure within a Siphonic System.....	17
Figure 2.9 The Cavitation Bubble Collapse Process (Lucke and Beecham 2009) .....	27
Figure 2.10 Cast Iron Siphonic Roof Drainage Outlet .....	31
Figure 2.11 Schematic View of the HWU Siphonic Roof Drainage Test Rig .....	34
Figure 2.12 Magnetic Induction Flowmeters and Collection Tank .....	34
Figure 2.13 The HWU Siphonic Test Rig Rear Supply Trough and Sloping Roof.....	35
Figure 2.14 Pressure Transducer within the Crown of the Horizontal Carrier Pipe.....	35
Figure 2.15 The Geberit Test Facility (Öngören and Materna 2006) .....	44
Figure 2.16 Method of Measuring Average Pressure within a Pipe (Öngören and Materna 2006) .....	44
Figure 2.17 The UniSA Siphonic Drainage Test Facility (Lucke et al. 2007) .....	46
Figure 2.18 The UniSA Cavitation Rig Setup (Lucke and Beecham 2009).....	48
Figure 2.19 University of South Australia Full Scale Siphonic Test Facility .....	51
Figure 2.20 Air Measurement Apparatus (Lucke and Beecham, 2010) .....	51
Figure 2.21 Velocity Measurement Techniques (Lucke and Beecham 2010).....	52
Figure 2.22 Experimental Test Facility Configuration (Qu et al. 2011).....	53
Figure 2.23 Image of the Propeller-Type Current Meter and Pressure Transducer within the Horizontal Carrier Pipe (Qu et al. 2011).....	54
Figure 2.24 Calibration Curves Reported by Qu et al. 2011 .....	55
Figure 2.25 Reported Comparison of Measured and Estimated Flows (Qu et al. 2011).....	55
Figure 3.1 Schematic of the Experimental Test Facility (not to scale).....	61
Figure 3.2 Plan View of the Experimental Test Facility .....	62
Figure 3.3 Side Elevation of the Experimental Test Facility.....	62
Figure 3.4 Dimensions of the Test Facility Framework (not to scale) .....	63
Figure 3.5 Image of the Submersible Pumps within the Sump.....	63
Figure 3.6 Dimensions of the Test Facility Water Supply Reservoir (not to scale) .....	64
Figure 3.7 Image of the Experimental Test Facility .....	64
Figure 3.8 Dimensions of the Test Facility Gutter (not to scale).....	65
Figure 3.9 Siphonic Outlet Installed within the Gutter.....	67
Figure 3.10 Outlet A Tailpipe Design.....	68
Figure 3.11 Image of Outlet A Tailpipe Configuration .....	68

Figure 3.12 Outlet B Tailpipe Design .....	69
Figure 3.13 Image of Outlet B Tailpipe Configuration .....	69
Figure 3.14 Outlet C Tailpipe Design .....	70
Figure 3.15 Image of Outlet C Tailpipe Configuration .....	70
Figure 3.16 Digital Depth Micrometer and Frame .....	74
Figure 3.17 Plan View of Gutter Measurement Points (not to scale) .....	74
Figure 3.18 Plan View of Outlet Midpoint Water Depth Measurements (not to scale) .....	75
Figure 3.19 Plan View of Gutter End Water Depth Measurement Points (not to scale) .....	75
Figure 3.20 The Pressure Transducer Collar Pre-Installation.....	76
Figure 3.21 Pressure Transducer Collar In-Situ .....	77
Figure 3.22 Pressure Transducer PT4 Configuration .....	78
Figure 3.23 Configuration of the Pressure Transducer Negative Range Calibration Apparatus .....	79
Figure 3.24 Feasibility Tests Dye Injection Apparatus Configuration .....	82
Figure 3.25 Dye Injection into Outlet A .....	83
Figure 3.26 Image of the Camera Configuration .....	87
Figure 3.27 Image of the Seeded Flow within the Horizontal Carrier Pipe .....	89
Figure 3.28 Image used for PIV Analysis.....	89
Figure 3.29 PIV Analysis Interrogation Areas (not to scale).....	90
Figure 3.30 Example of a Vector Analysis Plot .....	90
Figure 3.31 Detailed Image of a Vector Analysis Plot .....	91
Figure 3.32 Vector Analysis Plot with Range Validation.....	91
Figure 3.33 PIV Vector Statistics Plot .....	92
Figure 4.1 Mass Balance Comparison for Tests Completed at 20% of the Design Flow Rate .....	108
Figure 4.2 Radar Plot Showing Flow Proportionality (%) at 20% of the Design Flow Rate	109
Figure 4.3 Flow Proportionality at a Design Flow Rate of 20% with Standard Deviation shown by the Error Bars .....	110
Figure 4.4 Flow Measurement within the Horizontal Carrier Pipe during Test 2 .....	110
Figure 4.5 Pressure Measurement within the Horizontal Carrier Pipe during Test 2.....	111
Figure 4.6 Flow Rate Measured within the Horizontal Carrier Pipe during Test 22.....	111
Figure 4.7 Pressure Measured within the Horizontal Carrier Pipe during Test 22.....	112
Figure 4.8 Flow Rate and Pressure Measurements within the Horizontal Carrier Pipe during Test 22.....	112
Figure 4.9 Flow Rate and Pressure Measurements within the Horizontal Carrier Pipe during Test 3 (444.28 to 454.28 seconds) .....	113
Figure 4.10 Image at P1 at 444.28 seconds .....	113
Figure 4.11 Image at P1 at 445.28 seconds .....	113
Figure 4.12 Image at P1 at 446.91 seconds .....	113
Figure 4.13 Flow Rate at P1 and Pressure Measurements within the Horizontal Carrier Pipe during Test 3 (444.28 to 454.28 seconds).....	114
Figure 4.14 Flow Rate and Pressure Measurements within the Horizontal Carrier Pipe during Test 22 (583.78 to 593.78 seconds) .....	114
Figure 4.15 Image at P2 at 583.78 seconds .....	115

Figure 4.16 Image at P2 at 586.11 seconds .....	115
Figure 4.17 Image at P2 at 586.20 seconds .....	115
Figure 4.18 Image at P2 at 587.42 seconds .....	115
Figure 4.19 Image at P2 at 590.02 seconds .....	115
Figure 4.20 Image at P2 at 593.78 seconds .....	115
Figure 4.21 Flow Rate and Pressure Measurements within the Horizontal Carrier Pipe during Test 44 (348.91 to 358.91 seconds) .....	116
Figure 4.22 Image at P3 at 348.91 seconds .....	116
Figure 4.23 Image at P3 at 349.10 seconds .....	116
Figure 4.24 Image at P3 at 350.51 seconds .....	116
Figure 4.25 Image at P3 at 353.81 seconds .....	116
Figure 4.26 Image at P3 at 355.36 seconds .....	116
Figure 4.27 Image at P3 at 355.88 seconds .....	116
Figure 4.28 Mass Balance Comparison for Tests Completed at 40% of the Design Flow Rate .....	118
Figure 4.29 Radar Plot Showing Flow Proportionality (%) at 40% of the Design Flow Rate .....	119
Figure 4.30 Flow Proportionality at a Design Flow Rate of 40% with Standard Deviation shown by the Error Bars .....	120
Figure 4.31 Flow Measurement within the Horizontal Carrier Pipe during Test 4 .....	121
Figure 4.32 Pressure Measurement within the Horizontal Carrier Pipe during Test 4 .....	121
Figure 4.33 Flow Rate and Pressure Measurement within the Horizontal Carrier Pipe during Test 4 .....	122
Figure 4.34 Flow Rate and Pressure Measurement within the Horizontal Carrier Pipe during Test 4 (222.20 to 232.20 seconds) .....	122
Figure 4.35 Image at P1 at 220.20 seconds .....	123
Figure 4.36 Image at P1 at 224.84 seconds .....	123
Figure 4.37 Image at P1 at 225.00 seconds .....	123
Figure 4.38 Image at P1 at 226.25 seconds .....	123
Figure 4.39 Image at P1 at 226.65 seconds .....	123
Figure 4.40 Flow Rate and Pressure Measurement within the Horizontal Carrier Pipe during Test 27 (248.39 to 258.39 seconds) .....	124
Figure 4.41 Image at P2 at 248.39 seconds .....	125
Figure 4.42 Image at P2 at 249.33 seconds .....	125
Figure 4.43 Image at P2 at 249.65 seconds .....	125
Figure 4.44 Image at P2 at 250.38 seconds .....	125
Figure 4.45 Image at P2 at 251.85 seconds .....	125
Figure 4.46 Image at P2 at 253.38 seconds .....	125
Figure 4.47 Image at P2 at 257.78 seconds .....	125
Figure 4.48 Flow Rate and Pressure Measurement within the Horizontal Carrier Pipe during Test 46 (289.61 to 299.61 seconds) .....	126
Figure 4.49 Image at P3 at 289.61 seconds .....	126
Figure 4.50 Image at P3 at 290.70 seconds .....	126
Figure 4.51 Image at P3 at 291.37 seconds .....	126

Figure 4.52 Image at P3 at 295.46 seconds .....	126
Figure 4.53 Mass Balance Comparison for Tests Completed at 60% of the Design Flow Rate .....	127
Figure 4.54 Radar Plot Showing Flow Proportionality (%) at 60% of the Design Flow Rate .....	128
Figure 4.55 Flow Proportionality at a Design Flow Rate of 60% with Standard Deviation shown by the Error Bars .....	129
Figure 4.56 Flow Measurement within the Horizontal Carrier Pipe during Test 7 .....	129
Figure 4.57 Pressure Measurement within the Horizontal Carrier Pipe during Test 7 .....	130
Figure 4.58 Flow Rate and Pressure Measurement within the Horizontal Carrier Pipe during Test 7 .....	130
Figure 4.59 Flow Rate and Pressure Measurement within the Horizontal Carrier Pipe during Test 8 (367.71 to 377.71 seconds) .....	131
Figure 4.60 Image at P1 at 368.59 seconds .....	132
Figure 4.61 Image at P1 at 370.26 seconds .....	132
Figure 4.62 Image at P1 at 370.64 seconds .....	132
Figure 4.63 Image at P1 at 375.24 seconds .....	132
Figure 4.64 Image at P1 at 375.39 seconds .....	132
Figure 4.65 Flow Rate and Pressure Measurement within the Horizontal Carrier Pipe during Test 29 (319.89 to 329.89 seconds) .....	133
Figure 4.66 Image at P2 at 328.01 seconds .....	133
Figure 4.67 Image at P2 at 328.33 seconds .....	133
Figure 4.68 Image at P2 at 328.39 seconds .....	133
Figure 4.69 Image at P2 at 328.59 seconds .....	133
Figure 4.70 Image at P2 at 328.89 seconds .....	133
Figure 4.71 Flow Rate and Pressure Measurement within the Horizontal Carrier Pipe during Test 50 (400.08 to 410.08 seconds) .....	134
Figure 4.72 Image at P3 at 400.08 seconds .....	135
Figure 4.73 Image at P3 at 401.35 seconds .....	135
Figure 4.74 Image at P3 at 403.60 seconds .....	135
Figure 4.75 Image at P3 at 404.27 seconds .....	135
Figure 4.76 Image at P3 at 404.86 seconds .....	135
Figure 4.77 Image at P3 at 409.09 seconds .....	135
Figure 4.78 Mass Balance Comparison for Tests Completed at 80% of the Design Flow Rate .....	136
Figure 4.79 Radar Plot Showing Flow Proportionality (%) at 80% of the Design Flow Rate .....	137
Figure 4.80 Flow Proportionality at a Design Flow Rate of 80% with Standard Deviation shown by the Error Bars .....	138
Figure 4.81 Flow Measurement within the Horizontal Carrier Pipe during Test 11 .....	138
Figure 4.82 Pressure Measurement within the Horizontal Carrier Pipe during Test 11 .....	139
Figure 4.83 Flow Rate and Pressure Comparison During Test 11 .....	139
Figure 4.84 Flow Rate and Pressure Measurement within the Horizontal Carrier Pipe During Test 11 (279.07 to 289.07 seconds) .....	140

Figure 4.85 Image at P1 at 279.07 seconds .....	141
Figure 4.86 Image at P1 at 280.59 seconds .....	141
Figure 4.87 Image at P1 at 280.87 seconds .....	141
Figure 4.88 Image at P1 at 282.56 seconds .....	141
Figure 4.89 Image at P1 at 283.83 seconds .....	141
Figure 4.90 Image at P1 at 285.25 seconds .....	141
Figure 4.91 Image at P1 at 287.69 seconds .....	141
Figure 4.92 Image at P1 at 288.24 seconds .....	141
Figure 4.93 Flow Rate and Pressure Measurement within the Horizontal Carrier Pipe during Test 33 (317.41 to 327.41 seconds) .....	142
Figure 4.94 Image at P2 at 317.66 seconds .....	142
Figure 4.95 Image at P2 at 317.87 seconds .....	142
Figure 4.96 Image at P2 at 318.10 seconds .....	142
Figure 4.97 Image at P2 at 318.16 seconds .....	142
Figure 4.98 Image at P2 at 320.60 seconds .....	142
Figure 4.99 Image at P2 at 320.96 seconds .....	142
Figure 4.100 Flow Rate and Pressure Measurement within the Horizontal Carrier Pipe during Test 54 (325.05 to 335.05 seconds) .....	143
Figure 4.101 Image at P3 at 325.20 seconds .....	144
Figure 4.102 Image at P3 at 325.38 seconds .....	144
Figure 4.103 Image at P3 at 333.17 seconds .....	144
Figure 4.104 Image at P3 at 334.04 seconds .....	144
Figure 4.105 Image at P3 at 335.05 seconds .....	144
Figure 4.106 Mass Balance Comparison for Tests Completed at the Design Flow Rate .....	145
Figure 4.107 Radar Plot Showing Flow Proportionality (%) at the Design Flow Rate .....	146
Figure 4.108 Flow Proportionality at the Design Flow Rate with Standard Deviation shown by the Error Bars .....	147
Figure 4.109 Flow Rate Measurement within the Horizontal Carrier Pipe during Test 13 .....	148
Figure 4.110 Pressure Measurement within the Horizontal Carrier Pipe during Test 13 .....	148
Figure 4.111 Flow Rate and Pressure Comparison during Test 13 .....	149
Figure 4.112 Flow Rate and Pressure Measurement within the Horizontal Carrier Pipe during Test 13 (240.20 to 250.20 seconds) .....	150
Figure 4.113 Image at P1 at 248.23 seconds .....	150
Figure 4.114 Image at P1 at 248.47 seconds .....	150
Figure 4.115 Image at P1 at 249.14 seconds .....	150
Figure 4.116 Image at P1 at 249.41 seconds .....	150
Figure 4.117 Image at P1 at 249.54 seconds .....	150
Figure 4.118 Flow Rate and Pressure Measurements within the Horizontal Carrier Pipe during Test 36 (361.48 to 371.48 seconds) .....	151
Figure 4.119 Image at P2 at 363.06 seconds .....	152
Figure 4.120 Image at P2 at 363.18 seconds .....	152
Figure 4.121 Image at P2 at 363.32 seconds .....	152
Figure 4.122 Image at P2 at 363.84 seconds .....	152
Figure 4.123 Image at P2 at 364.09 seconds .....	152



Figure 4.124 Flow Rate and Pressure Measurement within the Horizontal Carrier Pipe during Test 57 (239.87 to 249.87 seconds) .....	153
Figure 4.125 Image at P3 at 239.98 seconds .....	153
Figure 4.126 Image at P3 at 240.53 seconds .....	153
Figure 4.127 Image at P3 at 241.39 seconds .....	153
Figure 4.128 Mass Balance Comparison for Tests Completed at the Ultimate Flow Rate ...	154
Figure 4.129 Radar Plot Showing Flow Proportionality (%) at the Ultimate Flow Rate .....	155
Figure 4.130 Flow Proportionality at the Ultimate Flow Rate with Standard Deviation shown by the Error Bars .....	156
Figure 4.131 Flow Rate Measurement within the Horizontal Carrier Pipe during Test 16...	156
Figure 4.132 Pressure Measurement within the Horizontal Carrier Pipe during Test 16.....	157
Figure 4.133 Flow Rate and Pressure Measurement within the Horizontal Carrier Pipe during Test 16 (255.49 to 265.49 seconds) .....	158
Figure 4.134 Image at P1 at 263.23 seconds .....	158
Figure 4.135 Image at P1 at 264.22 seconds .....	158
Figure 4.136 Image at P1 at 264.67 seconds .....	158
Figure 4.137 Flow Rate and Pressure Measurement within the Horizontal Carrier Pipe during Test 37 (164.87 to 174.87 seconds) .....	159
Figure 4.138 Image at P2 at 166.65 seconds .....	159
Figure 4.139 Image at P2 at 167.45 seconds .....	159
Figure 4.140 Image at P2 at 170.93 seconds .....	159
Figure 4.141 Flow Rate and Pressure Measurement within the Horizontal Carrier Pipe during Test 58 (235.69 to 245.69 seconds) .....	160
Figure 4.142 Image at P3 at 235.69 seconds .....	160
Figure 4.143 Image at P3 at 237.22 seconds .....	160
Figure 4.144 Image at P3 at 244.19 seconds .....	160
Figure 4.145 Mass Balance Comparison for Tests Completed at 120% of the Design Flow Rate .....	161
Figure 4.146 Radar Plot Showing Flow Proportionality (%) at 120% of the Design Flow Rate .....	162
Figure 4.147 Flow Proportionality at 120% of the Design Flow Rate with Standard Deviation shown by the Error Bars .....	163
Figure 4.148 Flow Rate Measurement within the Horizontal Carrier Pipe during Test 19...	164
Figure 4.149 Pressure Measurement within the Horizontal Carrier Pipe during Test 19.....	164
Figure 4.150 Flow Rate and Pressure Comparison During Test 19 .....	165
Figure 4.151 Flow Rate and Pressure Measurement within the Horizontal Carrier Pipe during Test 19 (225.89 to 235.89 seconds) .....	165
Figure 4.152 Image at P1 at 227.39 seconds .....	166
Figure 4.153 Image at P1 at 229.52 seconds .....	166
Figure 4.154 Image at P1 at 235.12 seconds .....	166
Figure 4.155 Flow Rate and Pressure Measurement within the Horizontal Carrier Pipe during Test 40 (275.69 to 285.69 seconds) .....	166
Figure 4.156 Image at P2 at 278.50 seconds .....	167
Figure 4.157 Image at P2 at 281.82 seconds .....	167

Figure 4.158 Image at P2 at 284.62 seconds .....	167
Figure 4.159 Flow Rate and Pressure Measurement within the Horizontal Carrier Pipe during Test 61 (198.31 to 208.31 seconds) .....	167
Figure 4.160 Image at P3 at 198.31 seconds .....	168
Figure 4.161 Image at P3 at 203.31 seconds .....	168
Figure 4.162 Image at P3 at 207.37 seconds .....	168
Figure 4.163 Measured Flow at F3 relative to the Calibrated Pumped Inflow and Volumetric Drop Test Comparison.....	172
Figure 4.164 Scatter Plot Showing the Difference between the Measured Flow at F3 and the Calibrated Pumped Inflow .....	172
Figure 4.165 Minimum, Mean and Maximum Flow Rate Comparison for Outlet A.....	175
Figure 4.166 Minimum, Mean and Maximum Flow Rate Comparison for Outlet B .....	175
Figure 4.167 Minimum, Mean and Maximum Flow Rate Comparison for Outlet C .....	176
Figure 4.168 Time Series Flow Rate Measurements from Test 4 .....	177
Figure 4.169 Time Series Data Measured by F1 during Test 4 and Comparison to a Sampling Method .....	178
Figure 4.170 Time Series Data Measured by F2 during Test 4 and Comparison to a Sampling Method.....	179
Figure 4.171 Time Series Data Measured by F3 during Test 4 and Comparison to a Sampling Method.....	180
Figure 4.172 Image Showing Flow Conditions and Corresponding PIV Analysis .....	181
Figure 4.173 Examples of Complex Flow Conditions.....	182
Figure 4.174 Proportionality of Flow through each Outlet.....	184
Figure 4.175 Plot Comparing System Pressure and Flow Rate .....	192
Figure 4.176 Siphonic System Theory Pressure Characteristics (May, 1997) .....	193
Figure 4.177 Image at P1 during Test Reference 13 .....	197
Figure 4.178 Image at P2 during Test Reference 36 .....	197
Figure 4.179 Image at P3 during Test Reference 57 .....	197
Figure 4.180 Image at P1 during Test Reference 19 .....	197
Figure 4.181 Image at P2 during Test Reference 40 .....	197
Figure 4.182 Image at P3 during Test Reference 61 .....	197
Figure 4.183 Flow Measured through each Outlet during Test Reference 22.....	198
Figure 4.184 Aerated Flow Observed at P3 during a Test Completed at 40% of the Design Capacity (Test Reference 46).....	199
Figure 4.185 Full-bore Flow at P1 at 60% of the Design Flow Rate.....	200
Figure 4.186 Free Surface Flow at P2 at 60% of the Design Flow Rate .....	200
Figure 4.187 Aerated Two-Phase Flow at P3 at 60% of the Design Flow Rate.....	200
Figure 4.188 Time Series Data during Test Reference 22.....	202
Figure 4.189 Air Entrainment within the Horizontal Carrier Pipe at P3 .....	203
Figure 4.190 Flow Velocity Results for Feasibility Tests Downstream of Outlet A (P1).....	205
Figure 4.191 Flow Velocity Results for Feasibility Tests Downstream of Outlet B (P2).....	206
Figure 5.1 Flow Proportionality as a Function of the System Flow Rate.....	217

## List of Tables

Table 2.1 Change in System Capacity due to Gutter Flow Depth .....	22
Table 2.2 Change in System Capacity due to Pipe Roughness (Arthur and Wright 2007) .....	23
Table 2.3 HWU Gutter and Tail Pipe Configurations (Wright et al. 2006b).....	37
Table 2.4 Calculation Method to Define the Hydraulic Jump for SIPHONET .....	38
Table 2.5 Comparison of Measured Pressure Results to those Derived by PrimaCalc Software adapted from Bramhall (2004).....	41
Table 2.6 Flow Rate Measurements Recorded by Bramhall (2004).....	42
Table 2.7 Comparison of Measured Flow Rate Results and those derived from Theoretical Models (BS EN 12056-3:2000 and PrimaCalc) adapted from Bramhall (2004).....	43
Table 3.1 Key to Figure 3.2 and Figure 3.3 .....	61
Table 3.2 Summary of Outlet Inflows and Reserves .....	65
Table 3.3 Summary of Gutter Sole Level Measurements.....	71
Table 3.4 Summary of the Control Valve Calibration used for the Feasibility Tests.....	73
Table 3.5 Summary of the Control Valve Calibration used for the Full Test Program.....	73
Table 3.6 Pressure Transducer Calibration Summary for the Range -10 m to 5 m H <sub>2</sub> O.....	79
Table 3.7 Summary of the Flourometer Calibration Results .....	84
Table 3.8 Mass Balance Measured using Flourometry.....	86
Table 4.1 Full Test Program Schedule.....	97
Table 4.2 Flow Measurement Analysis for Tests Completed at 20% of the Design Flow Rate .....	100
Table 4.3 Flow Measurement Analysis for Tests Completed at 40% of the Design Flow Rate .....	100
Table 4.4 Flow Measurement Analysis for Tests Completed at 60% of the Design Flow Rate .....	101
Table 4.5 Flow Measurement Analysis for Tests Completed at 80% of the Design Flow Rate .....	101
Table 4.6 Flow Measurement Analysis for Tests Completed at the Design Flow Rate .....	102
Table 4.7 Flow Measurement Analysis for Tests Completed at the Ultimate Flow Rate .....	102
Table 4.8 Flow Measurement Analysis for Tests Completed at 120% of the Design Flow Rate .....	103
Table 4.9 Pressure Measurement Analysis for Tests Completed at 20% of the Design Flow Rate .....	104
Table 4.10 Pressure Measurement Analysis for Tests Completed at 40% of the Design Flow Rate .....	104
Table 4.11 Pressure Measurement Analysis for Tests Completed at 60% of the Design Flow Rate .....	105
Table 4.12 Pressure Measurement Analysis for Tests Completed at 80% of the Design Flow Rate .....	105
Table 4.13 Pressure Measurement Analysis for Tests Completed at the Design Flow Rate .....	106
Table 4.14 Pressure Measurement Analysis for Tests Completed at the Ultimate Flow Rate .....	106

Table 4.15 Pressure Measurement Analysis for Tests Completed at 120% of the Design Flow Rate .....	107
Table 4.16 Maximum, Minimum and Average Flow Proportionality for Tests Completed at 20% of the Design Flow Rate .....	109
Table 4.17 Maximum, Minimum and Average Flow Proportionality for Tests Completed at 40% of the Design Flow Rate .....	119
Table 4.18 Maximum, Minimum and Average Flow Proportionality for Tests Completed at 60% of the Design Flow Rate .....	128
Table 4.19 Maximum, Minimum and Average Flow Proportionality for Tests Completed at 80% of the Design Flow Rate .....	137
Table 4.20 Maximum, Minimum and Average Flow Proportionality for Tests Completed at the Design Flow Rate.....	146
Table 4.21 Maximum, Minimum and Average Flow Proportionality for Tests Completed at the Ultimate Flow Rate .....	155
Table 4.22 Maximum, Minimum and Average Flow Proportionality for Tests Completed at 120% of the Design Flow Rate .....	162
Table 4.23 Summary of the Measured Flow at F3 Compared to the Calibrated Flow Rate and Volumetric Drop Test .....	170
Table 4.24 Measurement Analysis Comparison to Bramhall (2004) for Outlet A.....	174
Table 4.25 Measurement Analysis Comparison to Bramhall (2004) for Outlet B .....	174
Table 4.26 Measurement Analysis Comparison to Bramhall (2004) for Outlet C .....	174
Table 4.27 Test 4 Comparative Analysis .....	177
Table 4.28 Analysis of Time Series Data Measured by F1 during Test 4 and Comparison to a Sampling Method.....	178
Table 4.29 Analysis of Time Series Data Measured by F2 during Test 4 and Comparison to a Sampling Method.....	179
Table 4.30 Analysis of Time Series Data Measured by F3 during Test 4 and Comparison to a Sampling Method.....	180
Table 4.31 Comparison Between Measured and Calculated System Pressure at the Design Flow Rate .....	187
Table 4.32 Comparison Between Measured and Calculated System Pressure at the Ultimate Flow Rate .....	188
Table 4.33 Comparison between Commercially Available Software and Steady State Theory at the Design Inflow.....	190
Table 4.34 Comparison between Commercially Available Software and Steady State Theory at the Ultimate Inflow .....	190
Table 4.35 Observed Flow Regimes .....	196
Table 5.1 Average Flow Proportionality Relative to System Flow Rate.....	217
Table 5.2 Comparison Between Measured and Calculated System Pressure at the Design Flow Rate.....	218
Table 5.3 Comparison Between Measured and Calculated System Pressure at the Ultimate Flow Rate .....	218
Table 5.4 Observed Flow Regimes .....	220

## Notation

$A$	cross-sectional area
$A_a$	cross-sectional area of air entrainment
$A_f$	cross-sectional area of flow
$A_p$	cross-sectional area of the pipe
$B$	surface width
$C$	Chezy coefficient
$C_{F1}$	concentration of dye at F1
$C_{F2}$	concentration of dye at F2
$C_{F3}$	concentration of dye at F3
$C_{FB}$	concentration of the background solute level
$C_{in}$	concentration of dye injected
$c$	propagation velocity
$D$	diameter
$D_f$	depth of flow at an outlets optimum position
$D_{sp}$	depth of flow around an outlet
$E$	modulus of elasticity
$E$	energy gains
$E_{cr}$	creep modulus
$e$	base of natural log
$F$	Froude number
$F_r$	fluorescent reading at the reference temperature
$F_s$	observed fluorescence reading at the time of reading the sample temperature
$g$	gravitational acceleration
$H$	static pressure head
$h$	static pressure head
$h_f$	frictional head
$h_f$	losses
$h_v$	vapour pressure of the liquid
$i_{1,2}$	energy gradient of the flow
$K_{1,2}$	non-dimensional loss coefficient
$K_f$	bulk modulus of the fluid
$K_g$	bulk modulus of the gas
$k_s$	hydraulic roughness value of the pipe
$L$	length of pipe
$n$	temperature coefficient of the dye
$P$	wetted perimeter of the pipe
$P_{buc}$	critical pressure of a long pipe
$P_{cr}$	critical buckling pressure
$p$	pressure
$p_a$	absolute value of the atmospheric pressure
$p_v$	vapour pressure of the liquid
$Q$	discharge

$Q_{F1}$	flow rate at F1
$Q_{F2}$	flow rate at F2
$Q_{F3}$	flow rate at F3
$Q_i$	flow rate entering the outlet
$Q_{in}$	initial flow rate of water entering the collector pipe during priming
$q_{in}$	dye injection rate
$R$	hydraulic radius
$R_D$	distance ratio
$Re$	Reynolds number
$S_o$	invert gradient (dimensionless)
$T$	flow surface width
$T_F$	time to fill siphonic pipework
$T_r$	reference temperature
$T_s$	sample temperature
$t$	wall thickness of the pipe
$t$	time period
$u$	velocity
$V$	mean velocity of the liquid
$V_P$	total volume of collector pipes and downpipes to the point of discharge
$\nu$	Poisson's ratio (dimensionless)
$\nu$	kinematic viscosity of the water
$x$	length of travel of the particle pattern along the x axis
$y$	depth of water
$y$	length of travel of the particle pattern along the y axis
$y_c$	critical depth
$z$	height above discharge point
$\Delta$	change in a quantity
$\lambda$	Darcy-Weisbach friction factor
$\rho$	density/vapour pressure of liquid
$\rho_A$	average density
$\sigma$	non-dimensional cavitation index

## **Acknowledgements**

This study was only possible with the help and support from a number of people. I would like to acknowledge and thank everyone who helped me and contributed in any way during this journey.

Particular thanks must go to my supervisor, Professor Adrian Saul for his friendship, guidance and patience.

The experimental research was only made possible by the assistance, diligence and expertise of the technical staff from the Department of Civil and Structural Engineering at the University of Sheffield. In particular I would like to extend my gratitude to Mr Paul Osbourne and Mr Glen Brawn.

I would like to thank Dr Martyn Bramhall for his time, help, support and guidance.

I am very grateful to Rory Brown for his help and diligence.

I would like to extend my gratitude to Professor Simon Tait for his friendship and support.

I would like to thank my friends and colleagues, in particular Professor Pete Skipworth for his trust and support.

Finally, I would like to most sincerely thank my wife, Clare, my two daughters and my family for the sacrifices they have made and encouragement and inspiration they have given me.

Kieran Williams

## **Declaration**

Except where specific reference has been made to the work of others, this thesis is the result of my own work. No part of it has been submitted to any university for a degree, diploma or other qualifications.

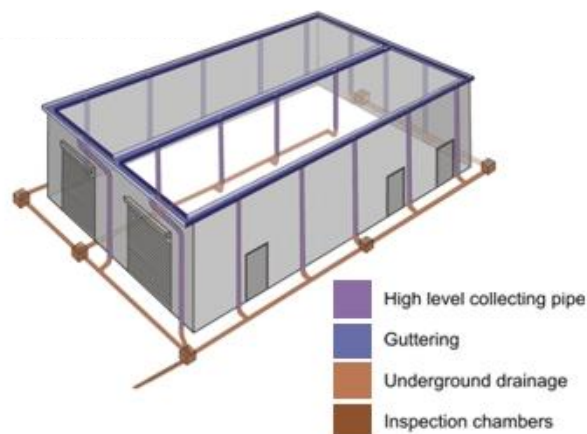


# 1 Introduction

Recent trends in the development of our urban landscape have seen the introduction of larger buildings with vast roof areas especially in localised business and industry parks. It is anticipated that the onset of climate change will see increased intensities and volumes of rainfall which will place significant pressures on the roof drainage systems for these buildings potentially leading to failure and major flooding. There is an urgent need to examine alternative forms of roof drainage and a potential future solution is the adoption of siphonic roof drainage systems. However, it has been identified that there is a universal lack of understanding of the hydraulic performance of siphonic systems, particularly with regard to multi-outlet systems. This project aims to address this shortfall in knowledge by completing an extensive and robust programme of sophisticated experimental research.

## 1.1 Background

Conventionally, roof drainage systems have been designed to safely convey the rainfall that runs off roof surfaces to the below ground drainage system. It is usual for the rainfall to be collected in a gutter or open outlets and then conveyed via a vertical downpipe, or series of downpipes, that are used to transfer the water from roof level to ground level (Figure 1.1).



**Figure 1.1 Conventional Roof Drainage System**  
(Fullflow Group Ltd (2016) "Syphonic Explained")

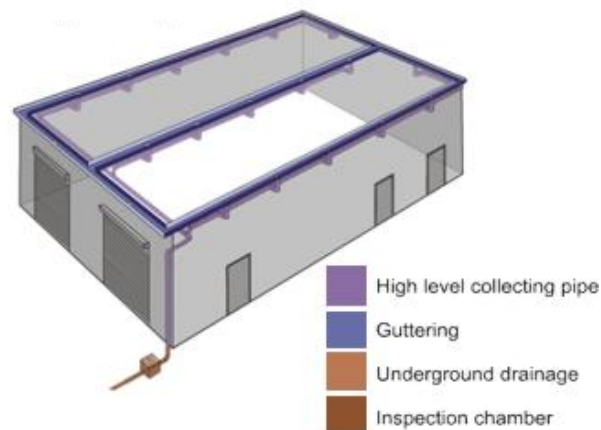
<http://www.fullflow.com/pages/syphonic-explained/> [accessed 23 Jan 2016]

Pipe diameters are sized to ensure annular flow through the downpipes with a continuous central air path operating at atmospheric pressure. These gravity driven systems have worked well for many years and, in the UK, their design is based on methodologies outlined in BS EN 12056-3: 2000 Part 3: 'Gravity Roof Drainage, Layout and Calculation' (BSI 2000).

However, in recent years the footprint of many buildings, particularly industrial units, stadia, schools, hospitals, prisons and airports has increased significantly leading to large buildings with vast roof areas. Similarly architectural practice has changed significantly with the use of

new materials and exterior surface finishes which provide elegance and intricate aesthetic appearance that incorporates concealed roof drainage systems. The use of conventional roof drainage for such buildings requires large gutters and a large number of downpipes and associated pipework. An additional consideration is that the receiving network needs to be designed to ensure sufficient capacity in which self-cleansing flow velocities can be maintained.

As a consequence the worldwide construction industry has seen the introduction of siphonic roof drainage systems. These have the advantage that their capacity is significantly greater than that of conventional systems and hence can drain much larger volumes of rainfall in a shorter period of time. They also require less pipework as a single carrier is used to drain several outlets within the gutter (Figure 1.2). Siphonic systems can be more easily upgraded or retro-fitted onto existing buildings to accommodate future increases in the frequency and severity of extreme rainfall events with the onset of climate change.



**Figure 1.2 Siphonic Roof Drainage Systems**  
**(Fullflow Group Ltd (2016) "Syphonic Explained"**

**<http://www.fullflow.com/pages/syphonic-explained/> [accessed 23 Jan 2016]**

The effective operation of siphonic roof drainage systems restrict the ingress of air entering the system inducing full-bore flow conditions at pressures lower than atmospheric. Figure 1.3 provides a simple overview of a siphonic system.



**Figure 1.3 Diagram of a Typical Siphonic System  
(Fullflow Group Ltd (2016) "Syphonic Explained"**

**<http://www.fullflow.com/pages/syphonic-explained/> [accessed 23 Jan 2016])**

The special design of the gutter outlets and small diameter pipework results in the priming of the system and full bore siphonic action. Factors critical for the successful priming of any siphonic system include the ability of roof outlets to prevent air infiltration, the design of the pipework to ensure that the air held within the system is quickly removed as well as good installation practice and an effective maintenance program (Arthur and Swaffield 1999).

Previous research has reported the benefits of siphonic systems (May and Escarameia 1996; Arthur and Swaffield 2001; Wright et al. 2002; Wearing 2004):

- Fewer outlets are required and these may be connected to a single vertical discharge pipe;
- Smaller diameter pipework may be specified which has less of an architectural impact and can be incorporated into the building fabric;
- Full-bore, de-pressurised flow enables much more flexibility of pipe routing allowing horizontal collection pipework to be located below roof level, significantly reducing the cost of underground drainage networks;
- Obtaining self-cleansing velocities is less of a concern; and,
- The reduced overall system size means that significant time and material savings can be obtained.

However, to achieve these benefits, the system must prime. Priming refers to the mechanism by which air is expelled from the system allowing full bore water flow conditions. The priming mechanism is an extremely complex process (Arthur and Swaffield 2001a; Arthur et al. 2005; Arthur and Wright 2007) dominated by four phases; free surface gravity driven flow to the outlet; unsteady flow when a mixture of air and water enters the outlet; drowning out of the outlet with the creation of negative pressures; and ultimately, siphonic conditions leading to full-bore-flow. As the flow subsides the system de-primed. Although the priming and de-priming mechanisms are understood (May and Escarameia 1996 and Arthur and Swaffield 2001a for example), existing design standards (BSI 2000; BSI 2007) recognise that there is no available analytical method that satisfactorily describe these processes.

Weaknesses in the current design approach and installation problems have resulted in a number of operational failures (Arthur and Swaffield 2001a). The severity of these failures

can range from minor operational problems including noise, vibration and gutter overtopping to severe system failure, for example pipe implosion and continual gutter overtopping.

More serious issues can compromise the integrity of the building, contents and functionality. It is recognised that despite siphonic gutter outlets incorporating vortex reducing elements, turbulent conditions of the flow within the gutter result in air entering the system, typically up to 10% (May 1997). It has been reported that the predominant failure mechanism of any siphonic system occurs during the design phase due to a lack of understanding of the basic priming process (Arthur and Swaffield 2001a). Due to limited experimental testing, results are extrapolated from small-scale studies which can result in severe design errors. In particular, the use of larger diameter vertical downpipes is common as a result of the perceived increased frequency of severe rainfall events. However, these large diameter pipes can often fail to prime with the system never operating siphonically. Guidance is given in Section 8.8 of BS 8490:2007, 'Guide to Siphonic Roof Drainage Systems', but this has been demonstrated to be based on a number of fallacies (Arthur and Wright 2007). More specifically, this focussed on the time it takes the primed tail pipes to fill the system. For certain hydraulic conditions, the tail pipes are assumed to prime instantly and the authors identified that the approach can lead to a significant underestimation of the actual priming time.

## **1.2 Research Aim and Objectives**

Experimental research to date has primarily focussed on idealised, steady state, single outlet systems and it is recognised that outlet conditions are key to understanding how a system will perform (Arthur et al. 2005; Bramhall 2004). Previous experimental research, for example Bramhall (2004), has identified that more robust, accurate and repeatable measurement techniques are essential to further the understanding of the hydraulic performance and interaction of flow within multi-outlet siphonic roof drainage systems. More specifically, a non-intrusive approach to enable the continuous measurement of flow through each outlet without affecting the hydraulic performance or generating additional, uncalculated losses during both flow conditions below, at and above the system design criteria is a necessity.

Qu et al. (2011) reported that experimental research to date has developed a good understanding of the theory and hydraulic performance of pipe-full, steady-state siphonic systems. However, there is a lack of understanding associated with the flow conditions that occur as the system 'primes' to become 'siphonic' and subsequently 'de-primes' when the inflow to the gutter outlet becomes less than the operating capacity of the pipework. Lucke et al. (2014) stated that "a complete understanding of how the flow is distributed between the individual gutter outlets and pipework during all anticipated rainfall events is required. This will improve knowledge of the priming process in particular and the overall performance of siphonic roof drainage systems in general."

Current British Standard assumes that all outlets operate at the same capacity. However, experimental research in pipe networks under surcharge has illustrated that at pipe junctions this is clearly not the case (Unwin 2008). Similarly, there is no understanding on how the priming mechanism interacts between multiple outlets as to the behaviour of the 'transient switch' from gravity to siphonic flow translates along the system.

Commercially available software used in the design of siphonic roof drainage systems is based on steady-state hydraulic theory, namely the Bernoulli and Colebrook White resistance equation. Previous experimental research, for example Bramhall (2004) and Wright et al (2005), has identified differences in the performance of experimental systems to those predicted using design tools and software.

### **1.2.1 Aim**

To develop and refine new and novel approaches to enable the continuous and simultaneous measurement of system pressure, discharge and flow velocity within an experimental siphonic roof drainage system with multiple outlets during steady flow tests below, at and above the design criteria.

### 1.2.2 Objectives

- Enhance the existing full-scale siphonic roof drainage experimental test facility at the University of Sheffield using commercially available design software based on steady-state hydraulic theory.
- Design, develop and refine experimental techniques specifically:
  - The measurement of system pressure;
  - A non-intrusive method of flow rate measurement through each outlet using flourometry;
  - Image data capture of the flow using high speed image velocimetry;
  - A non-intrusive method of flow velocity measurement using particle image velocimetry.
- Complete a series of performance evaluations under steady flow conditions below, at, and above the system design capacity to enable the simultaneous and high-resolution measurement of system pressure, flow rate and collation of image data within the horizontal carrier pipe.
- Quantify the proportionality of flow through each outlet during steady flow tests below, at, and above the system design capacity.
- Classify the flow regimes within the horizontal carrier pipe during steady flow tests below, at, and above the system design capacity.
- Examine the performance of the experimental system within the context of key network components and the interaction between multiple outlets.
- Apply the products of the research and compare with commercially available design software, steady state hydraulic theory, previously reported experimental research, methodologies and appropriate tools to predict siphonic system performance.
- Make recommendations to enhance the research into design practice.

### **1.3 Thesis Contents**

Chapter 2 of this thesis provides a concise, critical review of the evolution of siphonic roof drainage from when it was first developed in the 1960's. The chapter sets out the fundamental principles, design standards and a detailed appraisal of experimental research completed to date. The literature review concludes with a summary that identifies the specific areas of practical research that is required to further understanding and address the reported shortfall in knowledge.

Chapter 3 describes the experimental test facility used at the University of Sheffield as well as the approach, methodology and equipment used as part of the experimental study in four key phases: Enhancement and configuration of the experimental test facility; Calibration of the experimental test facility; Feasibility tests; and, Full test program.

Chapter 4 presents the results, key findings and discussion from a series of 63 steady flow tests completed using three outlets within a gutter draining to a single horizontal carrier pipe. The range of flow tests were selected to allow measurement of the experimental test facility operating in sub-prime and primed siphonic action to quantify for the first time, the measurement of flow through key components within the multi-outlet siphonic drainage test facility. Key findings from the experimental research program are presented and critically reviewed to reported results and conclusions from previous experimental research.

Conclusions are presented in Chapter 5 of this thesis specific to the aims and objectives of the study and corresponding to the key findings of this experimental research. Recommendations for further research are identified corresponding to the practical implications of this study on current design practice and system performance. Chapter 6 provides a concise summary of the conclusions from the experimental research study.

## 2 Literature Review

This chapter provides a concise, critical review of the evolution of siphonic roof drainage from when it was first developed in the 1960's and sets out the fundamental principles, design standards and a detailed appraisal of experimental research completed to date. The literature review concludes with a summary that identifies the specific areas of practical research that is required to further understanding and address the reported shortfall in knowledge.

### 2.1 Introduction

The principles of siphonic roof drainage were developed by Finnish consulting engineer Ovali Ebeling in the late 1960's with the first commercial application installed in 1972 in conjunction with Per Sommerhein (May and Escarameia 1996; Ross 2006). More recently, the design of such systems has been encapsulated in a number of British Standards including the most recent BS 8490:2007 'Guide to Siphonic Roof Drainage Systems' (BSI 1974; BSI 1983; BSI 2000; BSI 2007).

### 2.2 Siphons

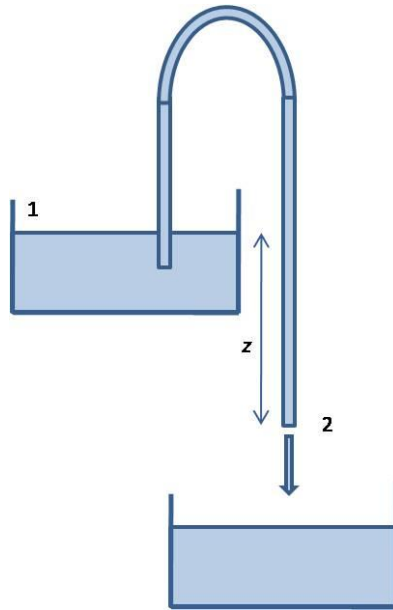
Siphonic action can be understood by considering the conservation of energy where liquid will flow under the influence of gravity to a lower energy state. Within a siphon, the liquid must first rise over a crest resulting in an increase in potential energy before flowing to a lower level than the original starting point resulting in an overall reduction in energy. Once a siphon is primed and flow is initiated, it requires no additional energy to maintain the flow of liquid. The siphon will continue until the level of liquid at the outlet equals the level at the inlet or the level of liquid at the starting point falls below the level of the inlet causing air to be drawn into the system subsequently breaking the siphonic action. The maximum height of the crest where siphonic action can be achieved is determined by atmospheric pressure and the density and vapour pressure of the liquid. When the pressure within the liquid falls below the liquids vapour pressure, vapour bubbles form at the crest of the siphon in a process called cavitation. This introduction of air within the system results in an end to the siphonic action.

Bernoulli's equation in conjunction with the continuity equation can be used to determine the discharge and pressure at two points (indicated by subscripts 1 and 2) within a frictionless siphon according to the following equation (Chadwick and Morfett 1993):

$$\frac{p_1}{\rho g} + \frac{u_1^2}{2g} + z_1 = \frac{p_2}{\rho g} + \frac{u_2^2}{2g} + z_2 = \text{constant}$$

Where  $p$  is pressure ( $\text{N/m}^2$ ),  $\rho$  is the density of liquid ( $\text{kg/m}^3$ ),  $g$  is the gravitational acceleration ( $\text{m/s}^2$ ),  $u$  is the velocity ( $\text{m/s}$ ) and  $z$  is the height above datum ( $\text{m}$ ).





**Figure 2.1 Simple Siphon Arrangement Showing Two Example Reference Points**

As the pressure at points 1 and 2 is atmospheric, and the velocity at point 1 is negligible (Figure 2.1), the equation can be simplified to (Chadwick and Morfett 1993):

$$z_1 - z_2 = \frac{u_2^2}{2g}$$

After the velocity at point 2 ( $u_2$ ) has been calculated, the continuity equation can be used to determine the discharge (Chadwick and Morfett 1993):

$$Q = uA$$

Where  $Q$  is the discharge ( $\text{m}^3/\text{s}$ ) and  $A$  is the cross-sectional area ( $\text{m}^2$ ). However, in practice, energy gains ( $E$ ) and losses ( $h_f$ ) exist within siphons. For example, energy may be added to a system using a pump or lost through friction due to the pipe roughness and through fittings. Therefore, Bernoulli's equation may be rewritten to incorporate these energy gains and losses (Chadwick and Morfett 1993):

$$\frac{p_1}{\rho g} + \frac{u_1^2}{2g} + z_1 + E = \frac{p_2}{\rho g} + \frac{u_2^2}{2g} + z_2 + h_f$$

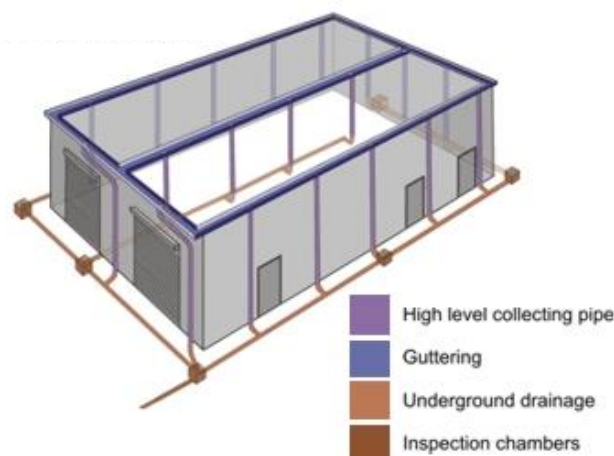
Siphons and siphonic systems have numerous wide-ranging uses. Within agriculture, siphons are utilised for irrigation; siphons have a range of uses within industry in particular the water

industry and can also be found in a range of commercial applications including toilets, plumbing and more specific to this study, siphonic roof drainage.

Since the first commercial application of siphonic roof drainage in 1972, adoption of the technology and the development of the international siphonic roof drainage industry has been widespread despite a fundamental lack of knowledge particularly concerning the mechanisms of the priming of systems. In the following section, conventional roof drainage is first described preceding a comprehensive review of current siphonic roof drainage understanding, applications, limitations and a critical review of previous, relevant experimental research.

### 2.3 Conventional roof drainage

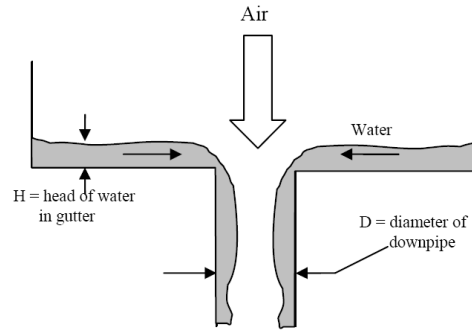
Conventional roof drainage systems are designed to safely convey the rainfall that runs off roof surfaces to the below ground drainage system. It is usual for the rainfall to be collected in a gutter from where it is conveyed to a downspout, or series of downspouts, that are used to transfer the water from roof level to ground level (Figure 2.2). These systems operate under gravity and have worked well for many years. Their design is based on methodologies outlined in British Standard EN 12056-3: 2000 Part 3: 'Gravity Roof Drainage, Layout and Calculation' (BSI 2000).



**Figure 2.2 A Conventional Roof Drainage System  
(Fullflow Group Ltd (2016) "Syphonic Explained")**

**<http://www.fullflow.com/pages/syphonic-explained/> [accessed 23 Jan 2016]**

Pipe diameters are sized to ensure annular flow through the downpipes with a continuous central air path operating at atmospheric pressure. Figure 2.3 shows a conventional gutter outlet and downpipe (Lucke et al. 2007).



**Figure 2.3 Conventional Gutter Outlet and Downpipe (Lucke et al. 2007)**

Conventional systems rely on gravity and the dimensions of the pipes are designed to operate at atmospheric pressure with only one quarter to one third of the cross-sectional area occupied by water (May 1997; Sommerhein 1999). Sommerhein (1999) recognised that these low flow rates provide reserve capacity and a wide safety of margin within a conventional roof drainage design. The volume of water able to enter a conventional outlet is dependent on the depth of water in the gutter ( $H$ ) and the outlet diameter ( $D$ ) highlighted in Figure 2.3 (Lucke et al. 2007). As the pressure within a conventional downpipe is atmospheric, the effective head is equal to the depth of water within the gutter which is typically no more than 100 mm (May 1997). This results in relatively low flows throughout the system and inefficient use of pipework requiring a significant number of large diameter downpipes connected to an underground drainage network. An additional consideration is that the receiving network needs to be designed to ensure sufficient capacity in which self-cleansing flow velocities can be maintained.

May (1997) identified that the maximum capacity of a conventional gutter is when the outlet is large enough for flow to discharge freely at its downstream end, conditions which can be described in terms of the Froude number ( $F$ ):

$$F = \left( \frac{BQ^2}{gA^3} \right)^{\frac{1}{2}}$$

Where  $B$  is the surface width corresponding to the downstream flow depth ( $y$ );  $A$  is the corresponding cross-sectional area;  $Q$  is the flow rate in the gutter; and  $g$  is the acceleration due to gravity.

At maximum capacity, the downstream flow depth is equal to the critical depth ( $y_c$ ) with a Froude number of 1 (May 1997). However, May (1997) identifies that if the head ( $H$ ) exceeds the critical depth ( $y_c$ ), the flow capacity will be reduced as the gutter is no longer able to discharge freely. From a practical perspective, it may not be possible to size the outlet large enough to ensure free discharge. The number and under-design of outlets is regarded as the most common cause of flooding within conventional roof drainage designs (May 1997). To prevent this problem, designers frequently implement a box-receiver where the gutters can

discharge into providing sufficient head required by the outlets. May (1997) identified the following advantages of using box-receivers:

1. The hydraulic design is simplified;
2. Gutters can achieve maximum flow capacity;
3. The head provided allows the use of smaller outlets and rainwater pipes.

The sizing of outlets was originally specified in British Standard 6367 (BSI 1983) following experimental research by the British Hydromechanics Research Association and more recently in British Standard BS EN 12056-3:2000 (BSI 2000). May (1997) stated that for small depths, 'weir-type' flow dominates with the critical depth upstream of the outlet perimeter. As the depth increases the flow develops into an 'orifice-type' as the flow chokes and is controlled by the throat area of the outlet. Dimensional equations for the two flow types are given in British Standard 6367 (BSI 1983):

Weir-flow:

$$Q_i = \frac{Dy^{1.5}}{7500}, \text{ for } y \leq \frac{D}{2}$$

Orifice-flow:

$$Q_i = \frac{D^2y^{0.5}}{1500}, \text{ for } y > \frac{D}{2}$$

Where  $Q_i$  (l/s) is the flow rate entering the outlet;  $D$  (mm) is the top diameter; and  $y$  (mm) is the depth of water above the outlet.

May (1997) identified that within a conventional system operating at atmospheric pressure, intermittent siphonic action may develop in the section of pipe immediately downstream of the outlet. Full-bore flow conditions continue until gravity causes the flow within the pipe to accelerate until it no longer occupies the cross-sectional area of the pipe (May 1997).

### 2.3.1 Limitations of Conventional Roof Drainage Systems

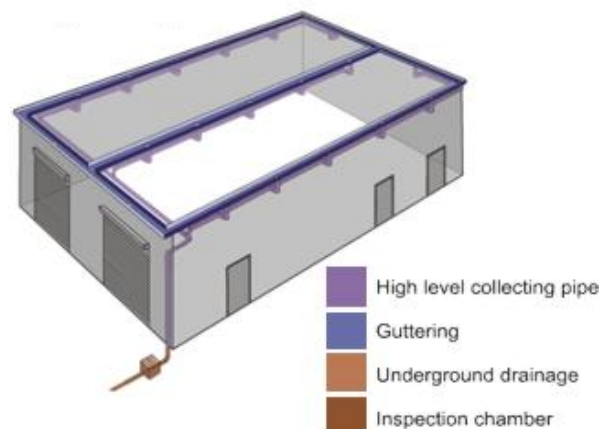
The operating capacity of a conventional system is determined by the size of the outlets and the limited depth of water within the gutter. The design of such systems are a careful balance to ensure that the expected return period storm flow can be drained efficiently from the roof surface whilst not over-engineering the solution so that self-cleansing velocities are not achieved for the majority of precipitation events.

Despite conventional roof drainage systems providing a wide safety margin and a reserve capacity this cannot necessarily be utilised. Sommerhein (1999) recognised that when the flow within a gravity system is greater than the one-third capacity design, there is a greater risk of air pockets forming. These air pockets could cause overtopping within the gutter as the flow within the vertical downpipe is trapped resulting in flooding.

In recent years the footprint of many buildings, particularly industrial units, stadia, schools, hospitals, prisons and airports has changed significantly with the construction of extremely large buildings with vast roof areas. Similarly architectural practice has changed with the use of new materials and exterior surface finishes that provide elegance and intricate aesthetic appearance which enables roof drainage systems to be hidden from view. The use of conventional roof drainage for such buildings requires large gutters and a large number of downspouts and associated pipework. As a consequence, the worldwide construction industry has seen the introduction of siphonic roof drainage systems.

## 2.4 Siphonic Roof Drainage

In contrast to a conventional roof drainage system, a siphonic system typically consists of specifically designed outlets fed by a vertical tail pipe typically 0.2 metres to 0.5 metres long (Arthur and Swaffield 1999a) to a horizontal carrier pipe leading to a single discharge point at ground level. A simple schematic demonstrates this in Figure 2.4.



**Figure 2.4 A Siphonic Roof Drainage System**  
 (Fullflow Group Ltd (2016) "Syphonic Explained")

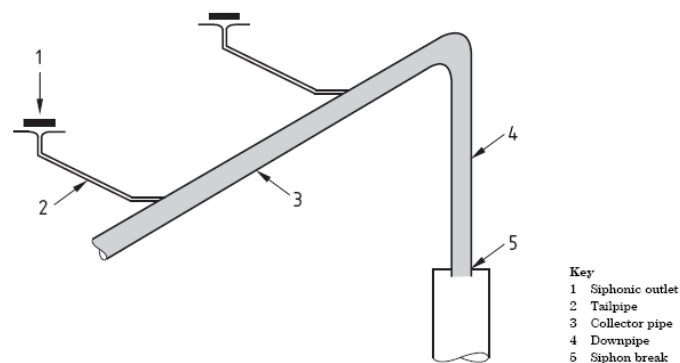
<http://www.fullflow.com/pages/syphonic-explained/> [accessed 23 Jan 2016]

May (1997) outlined the principle advantage of siphonic drainage compared to a conventional system:

‘The head acting on the outlet and pipework is equal to the difference in level between the water in the gutter and the discharge point.’

Therefore in practical terms, the available head could typically be 10 metres, much greater than the corresponding value of 100 mm for a conventional system. Hence, a siphonic system may be able to accommodate in the region of ten times the flow rate of an equivalent conventional system (May 1997)

Figure 2.5 shows the principal components of a siphonic roof drainage system (BSI 2007).



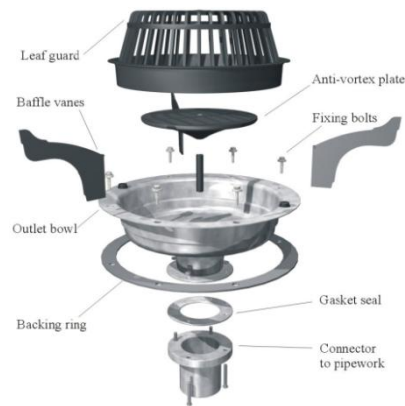
**Figure 2.5 Principal Components of a Siphonic Roof Drainage System (BSI 2007)**

Siphonic roof drainage systems are designed to function in both part-full (conventional) and full bore flow conditions (Bowler and Arthur 1999). The transition phase between these two states involves priming or de-priming of the flow throughout the system. Lucke (2009) provided a definition of the priming process:

‘Priming is the term used to describe the process where resistance to flow is sufficient to cause the pipe system to become full of water. It is the friction and form losses which are present in every pipe flow which resists the movement of the water and assists in the development of pipe-full flow conditions.’

The diameter and arrangement of the pipework is essential in ensuring the system can prime and generate siphonic action. Siphonic outlets are designed to restrict air entering the pipe system thereby inducing full-bore conditions at pressures lower than atmospheric.

May and Escarameia (1996) identified that the depth of the outlet bowl affects air being drawn into the tailpipe. A greater bowl depth produces a smoother entrance to the tailpipe, preventing air from being drawn in and reducing the amount of head loss caused by the outlet (May and Escarameia 1996). Siphonic outlets typically employ a horizontal baffle plate configuration to restrict the formation of a vortex preventing air from being drawn into the system (Lucke et al. 2007). Two designs of air baffle are recognised; a solid plate with vanes and a perforated design (May and Escarameia 1996). Within the first design, flow enters the bowl through openings between the bowl and the baffle with the vanes helping to prevent swirling of the water, thus preventing air from being drawn into the system shown in Figure 2.6.



**Figure 2.6 Siphonic Drainage Outlet with a Solid Anti-vortex Plate and Baffle Vanes (Bramhall, 2004)**

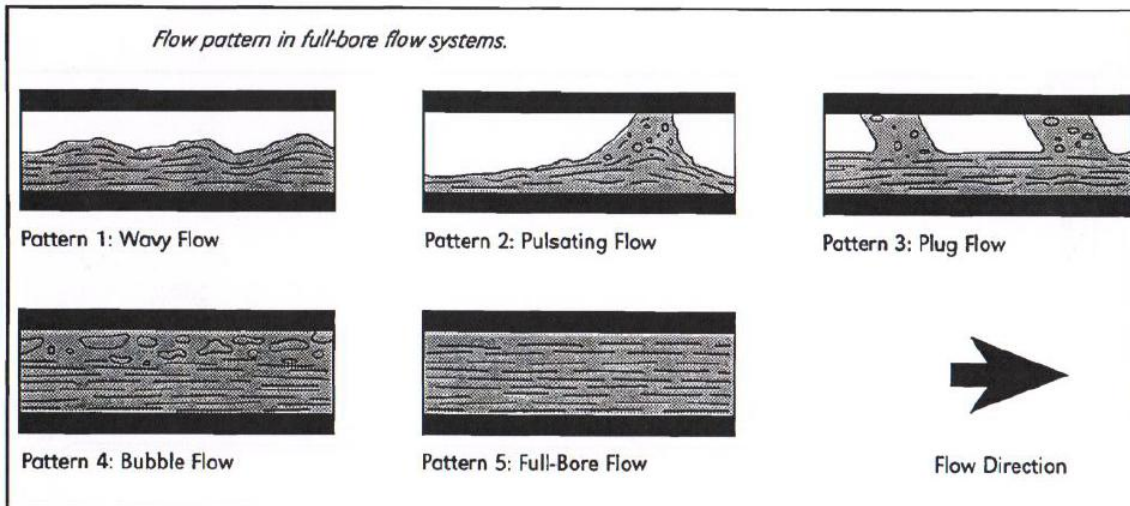
The perforated design may be in the form of a plate or an inverted cup. The benefits of this design are that at low flow rates the water depth in the bowl is increased preventing air from entering the system. Furthermore, May and Escarameia (1996) identified that this design disrupts the formation of air-entraining vortices as well as preventing surging of the flow.

Siphonic roof drainage has a number of benefits over conventional systems (May and Escarameia 1996; Arthur and Swaffield 2001a; Wright et al. 2002; Wearing 2004):

- Siphonic systems have a considerably higher capacity compared to conventional systems;
- Fewer outlets are required;
- Smaller diameter pipework may be specified which has less of an architectural impact and can be incorporated into the building;
- Several outlets may be connected to each vertical discharge pipe;
- Full-bore, de-pressurised flow provides much more flexibility concerning pipe routing allowing horizontal collection pipework to be located below roof level significantly reducing costly underground drainage networks;
- Self-cleansing velocities are less of a concern; and
- Significant savings can be made in terms of time and money.

#### **2.4.1 Siphonic System Priming**

At low flows, a siphonic system performs the same as a conventional system with the capacity determined by the size of the roof outlets and the head of water (Arthur and Swaffield 2001a). As flow increases, some pipes begin to flow full while others remain only partially filled depending on the air within the system. May and Escarameia (1996) report five air-water flow patterns consistent with full bore flow systems shown in Figure 2.7.



**Figure 2.7 Flow Patterns in Full-Bore Flow Systems (May and Escarameia 1996)**

It is recognised that the behaviour of the air is dependent on the velocity and turbulence of the inflow (Arthur and Swaffield 2001a). Air can either be drawn along above the water surface or entrained within the flow as bubbles. If air continues to be drawn into the system, priming will be prevented and the system will not be able to operate at its designed capacity. The special design of the gutter outlets and small diameter pipework means that air is displaced from the system quicker than it is entrained through the outlets.

The result is a bubbly two-phase mixture as the pipes throughout the system begin to flow full. As the depth of water surrounding each outlet increases, air is prevented from entering the system and full-bore flow is achieved. Therefore, the priming process occurs in three distinct phases recognised by Arthur and Swaffield (2001a):

1. Free surface flow.
2. Unsteady two-phase flow.
3. Full-bore flow.

Factors critical for the successful priming of any siphonic system include the ability of roof outlets to prevent air infiltration, the design of the pipework to ensure that the air held within the system is quickly removed as well as good installation practice and an effective maintenance program (Arthur and Swaffield 1999). Sommerhein (1999) identifies four factors that influence the priming of siphonic systems:

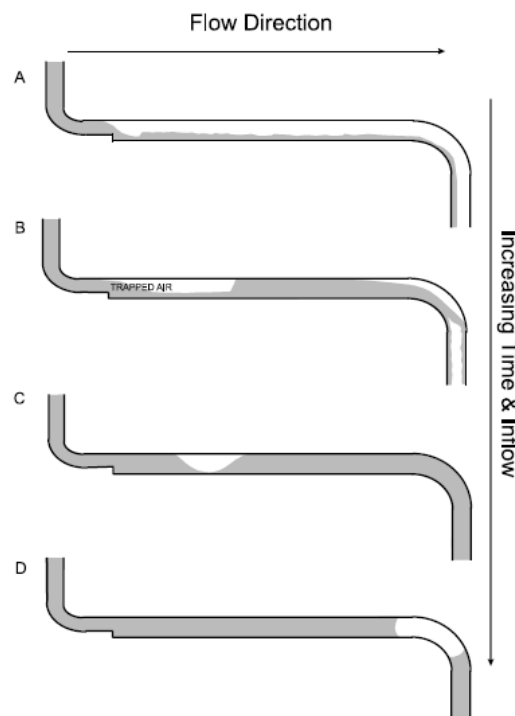
1. Correctly designed tailpipes;
2. Correctly designed downpipes;
3. Appropriate calculation model for the proposed roof type;
4. Main surface water sewer discharge condition.

Previous experimental and numerical research has identified that recognising the complexity of the priming process is fundamental in understanding how siphonic systems perform. Experimental research has identified the following sequence of events (Wright et al. 2002; Arthur et al. 2005; Arthur and Wright 2007):



1. Initial gutter inflow;
2. Outlet tail pipe priming;
3. Formation and movement of hydraulic jumps;
4. Formation and propagation of full bore flow;
5. Depressurisation of flow;
6. Partial re-pressurisation of flow;
7. Fully primed system.

Arthur and Swaffield (1999a) provided an overview of the priming procedure within a siphonic system (Figure 2.8).



**Figure 2.8 The Priming Procedure within a Siphonic System  
(Arthur and Swaffield 1999a)**

#### 2.4.1.1 Initial gutter inflow

During the first stage of the priming process, pressure within the system is equal to ambient atmospheric pressure. Flow within the vertical pipework is annular as in a conventional system, and sub-critical within the horizontal pipework (Figure 2.8A). As the flow increases within the gutter, super-critical flow develops within the horizontal carrier pipe forming a hydraulic jump further downstream.

#### 2.4.1.2 Outlet tail pipe priming

A short length of vertical pipe runs from the siphonic outlet, known as a tail pipe, which connects via a bend to the horizontal carrier pipe within the siphonic system. The tail pipe is essential in providing sufficient hydraulic resistance to generate the development of full bore

flow. The design of the tail pipe is critical in the priming of the system and four considerations are recognised (Arthur and Wright 2007):

1. The tail pipe diameter should not exceed the outlet diameter by more than 10-20%. Oversized pipes have been shown not to fill sufficiently preventing siphonic action (Sommerhein 1999; Arthur and Swaffield 1999a);
2. Tail pipes should not consist of a single pipe but include bends to generate hydraulic resistance required for hydraulic jumps;
3. A suitable vertical length is required to ensure a sufficient discharge rate;
4. The tail pipe horizontal length provides hydraulic resistance which therefore determines priming times affecting outlet and therefore system performance.

May and Escarameia (1996) recognised that the outlet and tail pipe can operate independently of the rest of the system and state:

‘Rapid priming of this mini-system can be achieved if the water dropping down the tail pipe accelerates sufficiently to produce a strong hydraulic jump sealing the entry to the collector pipe.’

The force of the hydraulic jump removes air very quickly from the tail pipe and also prevents it from being replaced with air from the carrier pipe generating a strong suction effect at the outlet.

#### 2.4.1.3 Formation and Movement of Hydraulic Jumps

As the flow to the gutter continues to increase, the hydraulic jump moves further downstream along the length of the horizontal carrier pipe as the downstream sub-critical depth of the jump increases (Arthur and Swaffield 2001a). Full bore flow develops in the horizontal pipework where the downstream depth of the hydraulic jump is equal to the pipe diameter (Figure 2.8B). As a result of this, air becomes trapped between the hydraulic jump and the upstream end of the horizontal pipe above the supercritical flow (Arthur and Swaffield 2001a).

#### 2.4.1.4 Formation and Propagation of Full Bore Flow

As full bore conditions continue downstream reaching the second bend, the main vertical pipe begins to fill and full bore flow develops along the carrier pipe.

#### 2.4.1.5 Depressurisation of Flow

De-pressurisation of the flow occurs in the carrier pipe causing inflow to the system through the outlet to increase. This increase in flow causes full bore flow to develop at the upstream end of the carrier pipe (Arthur and Swaffield 2001a).

#### 2.4.1.6 Partial Re-pressurisation of Flow

The continued increase in inflow causes the trapped air pocket to move downstream along the carrier pipe at the ambient velocity of the flow (Figure 2.8C). Partial re-pressurisation of the entire system occurs when the air pocket passes into the vertical section of the system (Arthur and Swaffield 2001a). Experimental research completed by Wright et al. (2002) observed that the re-pressurisation wave was generated at the downstream end of the horizontal carrier pipe and propagated upstream.

#### 2.4.1.7 Fully Primed System

The siphonic system becomes fully primed when the air pocket has moved along the vertical section of the pipework and leaves the system via the discharge point. Once a siphonic system has become fully primed, the pressures decrease and remain constant (Arthur and Wright 2007).

### 2.4.2 Current Design Practice

Increasing proportions of UK commercial roof space specifically portal frame distribution and industrial facilities are being designed using siphonic drainage (Bramhall and Wearing 2008). Ross (2006) identified that it is those projects with a roof space in excess of 10,000 square feet that provide benefits in terms of build costs and space. However, there are weaknesses in the current design approach and installation problems have resulted in a number of operational failures (Arthur and Swaffield 2001b). The severity of these failures can range from minor operational problems including noise, vibration and gutter overtopping to severe system failure, for example pipe implosion and continual gutter overtopping. More serious issues can compromise the integrity of the building, contents and functionality. It is recognised that despite siphonic gutter outlets incorporating vortex reducing elements, turbulent conditions of the flow within the gutter result in air entering the system, typically up to 10% (May and Escarameia 1996). The predominant failure mechanisms of any siphonic system occurs during the design phase due to a lack of understanding of the basic priming process, poor material specification, installation defects and a poor maintenance programme (Arthur et al. 2005). Although only a very small percentage of the many thousands of installed siphonic roof drainage systems worldwide have failed, blockages are identified as the predominant cause of operational problems and system failures which are avoidable with an effective maintenance programme (Arthur et al. 2005).

Due to limited experimental testing, results are extrapolated from small-scale studies which can result in severe design errors. In particular, the use of larger diameter vertical downpipes is common as a result of the perceived increased frequency of severe rainfall events. However, these large diameter pipes can often fail to prime with the system never operating siphonically.

Existing design standards (BSI 2000; BSI 2007) and recent research (Arthur and Swaffield 2001a; Arthur and Wright 2007) have identified seven key areas essential to the design of siphonic roof drainage systems:

1. Hydraulic design;
2. Design criteria;
3. System balancing;
4. Minimum flow velocities;
5. Speed of priming;
6. Minimum allowable pressures;
7. Air within siphonic systems;

#### 2.4.2.1 Hydraulic Design

Siphonic systems are designed to accommodate a specified design storm which will fill and prime the system (Arthur and Swaffield 2001a). Therefore, it is accepted that steady-state hydraulic relationships may be used to design a siphonic system using the steady flow energy equation (May and Escarameia 1996; May 1997; Slater et al. 1999; Arthur and Swaffield 1999). The pressure drop between two points within a siphonic system can be determined using Bernoulli's energy equation (May 1997):

$$(h_1 - h_2) + (z_1 - z_2) + \frac{Q^2}{2g} \left( \frac{1}{A_1^2} - \frac{1}{A_2^2} \right) = K_{1,2} \frac{Q^2}{2gA_2^2} + i_{1,2}L_{1,2}$$

Where  $h$  is the static pressure head,  $z$  is the height above the discharge point,  $Q$  is the discharge,  $g$  is the acceleration due to gravity,  $A$  is the cross-sectional area,  $K$  is the non-dimensional loss coefficient,  $i$  the energy gradient of the flow and  $L$  the length of pipe between two points.

May (1999) identifies that the three bracketed terms on the left side of the equation correspond to the changes in the three components of total energy possessed by the flow:

1. The pressure energy represented by the static pressure head;
2. The potential energy represented by the height;
3. The kinetic energy corresponding to the speed of water.

The two terms on the right side of the equation relate to the loss of total energy between the two points. The first element corresponds to point losses at fittings while the second relates to the frictional resistance of the length of pipe.

The Colebrook-White equation is used by siphonic roof drainage designers to estimate the energy gradient between two points in terms of  $i_{1,2}$  as a result of hydraulic resistance in head loss in metres per metre length of pipe (May 1997; Arthur and Swaffield 2001a):

$$i = \frac{Q^2}{8gA^2D} \left\{ \log_{10} \left( \frac{k_s}{3.7D} + \frac{2.51\nu}{D\sqrt{2gDi}} \right) \right\}^{-2}$$

Where:  $D$  is the diameter of the pipe;  $k_s$  is the hydraulic roughness value of the pipe; and  $\nu$  is the kinematic viscosity of the water.

The following equation is used to estimate losses across bends and fittings (Arthur and Swaffield 2001a):

$$\Delta H = \frac{KQ^2}{2gA^2}$$

It is recognised that inaccuracies in head losses as a result of individual fittings is likely to be small, the cumulative error throughout the whole system may be more significant (Arthur and Swaffield 2001a). However, May and Escarameia (1996) identified that the head loss generated by the outlet baffle should not be too large as this could reduce inflow capacity when the system is operating in a non-primed state subsequently increasing the time needed for the system to fill and prime.

Although small quantities of air are present in fully primed systems, previous research has identified that this method provides an acceptable level of accuracy (May and Escarameia 1996; Arthur and Swaffield 1999a; Arthur and Swaffield 2001a; Wright et al. 2002). However, Arthur et al. (2005) identify that steady state design methods are not applicable for rainfall events below the design criteria or with time varying rainfall intensity. Therefore, these design methods may not be suitable for determining the diurnal performance characteristics of siphonic roof drainage systems (Arthur et al. 2005). However, Sommerhein (1999) recognised that these equations provide a theoretical model with their associated limitations and exceptions.

More recent experimental research completed by Lucke (2009) found that the friction factor used in the Darcy-Weisbach equation ( $\lambda$ ) decreased as the degree of air entrainment within the flow increased, and can be expressed in the form (Chadwick and Morfett 1993):

$$h_f = \frac{\lambda LV^2}{2gD}$$

Where  $h_f$  is the frictional head (m).

The Darcy-Weisbach friction factor ( $\lambda$ ) can be derived using an iterative process after being substituted in to the Colebrook-White equation (Chadwick and Morfett 1993):

$$\frac{1}{\sqrt{\lambda}} = -2 \log \left( \frac{k_s}{3.7D} + \frac{2.51}{Re\sqrt{\lambda}} \right)$$

Where  $Re$  is the Reynolds number.

Lucke (2009) recommends using a friction factor ( $\lambda$ ) of 0.016 for the plastic pipework used in siphonic drainage systems for air entrainment of 10%. Furthermore, the author suggests that, based on the results of the experimental research, to use a safety factor of 1.2 for systems designed using Bernoulli's energy equation. To account for losses derived by the effects of air entrainment, the simplest method was to multiply the calculated losses by 1.2.

The British Standard BS EN 12056-3:2000 'Gravity drainage systems inside buildings' provided two equations for calculating the depth of water above a circular outlet for a given flow rate which are accepted in current industry practice (BSI 2000). Similar to conventional roof drainage, the application of either the weir flow equation or the orifice flow is dependent on the head of water at the outlet. Where  $h \leq D/2$ , the weir flow equation is used, and where  $h > D/2$ , the orifice flow equation is used. Application of these equations assumes an even flow rate through each outlet within a common gutter (Bramhall 2004). However it was concluded by Bramhall (2004) that when siphonic rainwater outlets were equally spaced within a common gutter, the weir flow equation was only applicable at low flow rates and the orifice flow equation was not applicable at all for siphonic rainwater outlets.

Although changes in gutter water level do not affect a fully primed siphonic system (May and Escarameia 1996; Arthur and Swaffield 2001a), it is recognised that they play an important role during the priming process itself (Arthur and Wright 2007). Table 2.1 shows the change in system capacity as a result of variations in gutter flow depth (Arthur and Wright 2007).

**Table 2.1 Change in System Capacity due to Gutter Flow Depth**

Gutter flow depth (mm)	System capacity (l/s)	Change (%)
50	7.59	-11.5
100	7.94	-7.5
150	8.27	-3.7
200	8.58	benchmark
250	8.89	3.6
300	9.18	6.9

Previous research has also identified that pipe roughness has a significant effect on system capacity (Arthur and Wright 2007). Table 2.2 provides an example of the change in system capacity due to pipe roughness.

**Table 2.2 Change in System Capacity due to Pipe Roughness (Arthur and Wright 2007)**

Pipe roughness (mm)	System capacity (l/s)	Change (%)
0.06	10.04	+4.9
0.15	9.57	benchmark
0.30	8.30	-13.3
0.60	8.05	-15.9

#### 2.4.2.2 Design Criteria

Due to the nature of siphonic roof drainage systems, there is very little spare capacity above the design storm to which they were designed. By increasing the design capacity of a system by 10% corresponded to a subsequent increase of 20% to 40% in the design rainfall return period (Arthur and Wright 2007). This may mean that the system may not operate in a fully primed state.

#### 2.4.2.3 System Balancing

May (1997) stated that a principal design objective is that the flow through each outlet within a siphonic system is balanced. Slater et al. (1999) defined three parameters consistent with siphonic system balancing:

1. The quantity of water to be discharged;
2. The resistance to flow provided by the network of pipes;
3. The head provided by the height of the building.

The American Society of Plumbing Engineers (ASPE) design standard states that (ASPE 2006):

‘An ideal siphonic system will have a total calculated energy loss through the piping system precisely equal to the available head for each branch in the system.’

Where siphonic systems are not balanced there is the potential for tail pipes to drain thereby drawing air into the system and breaking the siphon (Sommerhein 1999; Ross 2006). Lucke et al. (2007) identified the significance of dynamic balancing within a siphonic system and stated that friction and form losses within the pipework are proportional to the square of the velocity of the fluid. Therefore, energy is lost the further downstream the flow travels meaning lower volumes of flow are subsequently transported. To achieve balanced flows through siphonic outlets, smaller diameter tail pipes are selected to restrict downstream flow

volumes compared to those flows upstream (Ross 2006; Lucke et al. 2007). A value of  $\pm 2.5\%$  is suggested as an acceptable level of variation within the design of a siphonic system (Arthur and Wright 2007), however, the ASPE (2006) recommends a maximum imbalance of 0.5m or 10% of the available head. The design of any siphonic system will have a number of restrictions which consequently affect balancing and a number of limitations are identified (ASPE 2006):

- Pipes sizes are only available in nominal diameters;
- The type and placement of fittings are limited;
- The number of iterations to the energy loss calculations are excessive and unreasonable to achieve perfect balance;
- Flow variation caused by random and transient air entrainment.

#### 2.4.2.4 Minimum Flow Velocities

May and Escarameia (1996) identified that if flow velocities are too low, air will not be prevented from rising to form air pockets along the pipe soffit. Experimental research on flow in steep pipes identified that air entrainment does not occur according to the following equation (Volkart 1982):

$$V > 6.0 \left( \frac{gA}{P} \right)^{\frac{1}{2}}$$

Where  $V$  is the mean velocity of the liquid;  $g$  is the acceleration due to gravity;  $A$  is the cross-sectional area of the flow; and  $P$  is the wetted perimeter of the pipe. May and Escarameia (1996) stated:

‘Siphonic systems will prime and run full much more quickly if the air in the pipes is entrained in the form of bubbles than if it is dragged along by the surface of the flowing water.’

The authors suggest that a design velocity of 1 m/s or less as adopted by manufacturers and suppliers may not always be sufficient to ensure rapid priming. Experimental research suggests that a minimum velocity of 2 m/s may be more appropriate to ensure good air entrainment and the rapid removal of air (May and Escarameia 1996).

For the system to prime, flow velocities must be sufficient to generate hydraulic jumps and sustain super-critical flow (Arthur and Wright 2007). Rather than a minimum flow velocity stated by May and Escarameia (1996), a minimum Froude number of 1.50 is accepted as this considers pipe diameter (Arthur and Wright 2007) where:



$$F = \sqrt{\frac{BV^2}{gA}} \geq 1.50$$

#### 2.4.2.5 Speed of Priming

A significant area of uncertainty concerning the operation of siphonic systems is the speed of priming. It is recognised that factors controlling the rate of air entrainment are complex and no analytical method is available to determine how long or even if a system will prime (May 1997; Arthur and Wright 2007). Section 8.8 of British Standard 8490:2007 ‘Guide to Siphonic Roof Drainage Systems’ provides a formula to be adhered to by siphonic system designers:

$$T_F = \frac{1.2V_P}{Q_{in}}$$

Where:  $T_F$  is the time to fill siphonic pipework (s);  $V_P$  is the total volume of collector pipes and downpipes to the point of discharge (l);  $Q_{in}$  is the initial flow rate of water entering the collector pipe during priming (l/s).

This formula assumes that tail pipes and carrier pipes are empty prior to priming and does not take into account that they will be partially filled and therefore part-primed at the onset of a rainfall event. The most recent British Standard, BS 8490:2007 ‘Guide to Siphonic Roof Drainage Systems’, assumes that the tail pipes should prime instantly and fill the system within 60 seconds. However, since siphonic system within the UK are designed for two minute storm events, May and Escarameia (1996) identify that is not feasible to specify the 60 second priming requirement due to the unavailability of a quantitative method of predicting the speed of priming. Therefore in practice, siphonic systems are typically designed with tail pipes that are oversized to meet this specification.

Previous experimental research using full scale test facilities have typically been small in size and the relative diameter pipework has therefore primed rapidly. Data from these tests have therefore provided a considerable underestimation of actual priming times (Arthur and Wright 2007). Furthermore, limited data is available on the performance of installed systems particularly when primed (Arthur and Swaffield 2001). However, the limited data has indicated that priming times have exceeded 120 seconds and when partially primed, rainfall took 60 seconds to move from the roof into the siphonic system (Arthur and Wright 2007). Sommerhein (1999) recognised that large pipe systems may need a considerable time period to fill during which the siphonic system will not be operating at peak capacity.

Experimental testing reported by Bramhall and Wearing (2008) examined the effect on priming using a range of tailpipe and carrier pipe diameters within a full-scale test facility. The research concluded that for siphonic outlets with a diameter of 75 mm, tailpipes with a

diameter greater than 110 mm may adversely affect system priming and should be avoided particularly with short drop tailpipes (less than 1.8 m). Furthermore, if the 110 mm diameter tailpipe is used in conjunction with a carrier pipe diameter greater than 110 mm, priming stability is not guaranteed. It is suggested that where a 125 mm diameter carrier pipe is used, it is selected in combination with a 90 mm tailpipe (Bramhall and Wearing 2008).

#### 2.4.2.6 Minimum Allowable Pressure

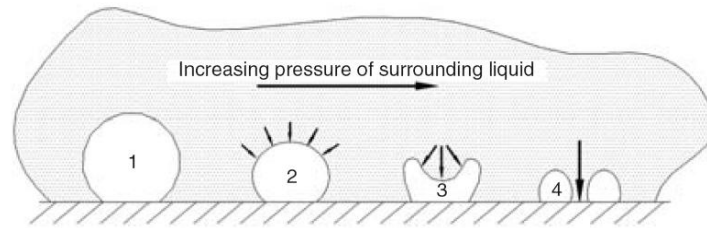
Negative pressures within siphonic systems need to be considered firstly regarding the structural strength of the pipes to resist collapse and secondly the risk of cavitation damage affecting the internal walls of the pipes. A minimum allowable pressure of -9m H<sub>2</sub>O is adopted by designers. However, existing British and EU standards recommend a more conservative minimum pressure of -7.8m H<sub>2</sub>O (BSI 2000; BSI 2007). This is because methods used to estimate pressures do not consider localised turbulence (Arthur and Wright 2007). System pressures can vary and increase due to a number of factors including (Arthur and Swaffield 2001a):

- Interaction with the underground system;
- Partial or total blockage of an outlet;
- Changes in pipework configuration from the original design during installation;
- Volumes of air entering the system.

This would result in system pressures falling below their design levels which could cause system failure by cavitation and/or pipe deformation (May and Escarameia 1996; Sommerhein 1999; Arthur and Swaffield 1999a; Wright et al. 2002). May and Escarameia (1996) identified that cavities form in a liquid when the pressure at a specific point falls close to the vapour pressure of the liquid. Lucke and Beecham (2009) stated that:

‘Cavitation is a phenomenon that can occur when the local pressure in a fluid falls below vapour pressure. The vapour pressure of a liquid is the absolute pressure at which the liquid vaporises or converts into a gas at a specific temperature.’

May and Escarameia (1996) reported that cavitation damage is not caused by the formation of these cavities, but by their collapse. Figure 2.9 shows the cavitation bubble collapse process (Lucke and Beecham 2009).



**Figure 2.9 The Cavitation Bubble Collapse Process (Lucke and Beecham 2009)**

May and Escarameia (1996) suggested a non-dimensional cavitation index ( $\sigma$ ) to identify the conditions needed for cavitation. The higher the cavitation index, the more easily the pipe or fitting will cavitate. The cavitation index can be expressed as (May and Escarameia 1996):

$$\sigma = \frac{p + p_a - p_v}{\frac{1}{2}\rho V^2}$$

Where  $p$  is the mean static pressure at which cavitation first occurs;  $p_a$  is the absolute value of the atmospheric pressure;  $p_v$  is the vapour pressure of the liquid,  $\rho$  is the vapour pressure of the liquid; and  $V$  is the mean velocity of the liquid.

As water is the liquid, the equation can be expressed in terms of pressure head (May and Escarameia 1996):

$$\sigma = 2g \left( \frac{h + h_a - h_v}{V^2} \right)$$

Where:  $g$  is the acceleration due to gravity;  $h$  is the mean static pressure head at which cavitation first occurs;  $h_a$  is the absolute value of the pressure head; and  $h_v$  is the vapour pressure of the liquid.

May and Escarameia (1996) identified four factors that can cause an increase in the cavitation index:

- An increase in flow velocity;
- An increase in temperature;
- A reduction in the mean static pressure;
- A reduction in the value of atmospheric pressure.

Further to this, excess negative pressures are regarded as a possible problem in buildings taller than fifteen metres (May and Escarameia 1996). Experimental research using a full scale test facility has been completed to examine this problem at the University of South Australia and is discussed in more detail in Section 2.4.4.4.

#### 2.4.2.7 Air within Siphonic Systems

Air is able to enter a siphonic system via three mechanisms (Arthur and Swaffield 2001a; Arthur and Swaffield 2001b):

1. Air already within the system prior to any inflow;
2. Air held within the inflowing rainwater;
3. Air entrained into the system through the siphonic outlet.

It is recognised that prior to any inflow, the entire system will be filled with air (Arthur and Swaffield 2001a; Arthur and Swaffield 2001b). Within a well designed system this is removed via the roof outlet and via the discharge point, however, the presence of this air significantly affects the hydraulic conditions and more significantly the priming process within a siphonic system. As the inflow to the system increases, the turbulent nature of the inflow entrains large quantities of air due to partial unsteady de-pressurisation within the system (Arthur and Swaffield 2001a; Arthur and Swaffield 2001b). This de-pressurisation has been shown in some circumstances to exceed the volume of water entering the system (Arthur and Swaffield 2001b). The unsteady flow regime which has been observed as cyclic, can result in noise generation and structural vibration throughout the siphonic system (Arthur and Swaffield 2001b).

Siphonic outlets are designed to prevent air from being drawn into the system, however, air is able to enter as a result of small vortices, reduced flow depths or by turbulent mixing within the gutter (Arthur and Swaffield 2001a; Arthur and Swaffield 2001b). Existing siphonic roof drainage design is completed on the assumption that no air is present when the system is fully primed and operating at full bore. However, air can be easily entrained into the system via the three identified mechanisms (Arthur and Swaffield 2001a; Arthur and Swaffield 2001b) typically up to 10% of the system volume (May and Escarameia 1996) although Arthur and Swaffield (1999) reported a value of less than 5%. May (1997) identified that two-phase flow formed as a result of the introduction of air is complex and it is very difficult to predict accurately how siphonic systems perform under part-full conditions.

The presence of air within a siphonic system has three identified effects (Arthur and Swaffield 1999):

1. System operating pressure;
2. Propagation velocity;
3. Friction losses.

The steady flow energy equation used in the design of siphonic systems is dependent on the density of the inflow. Therefore, any air within the system will cause a change in local pressure which may be transmitted through the whole system causing a reduction in system capacity (Arthur and Swaffield 2001a).

Air within a siphonic system can influence local transient propagation velocity ( $c$ ) according to the following equation (Wylie and Streeter 1978):

$$c = \sqrt{\left( \left\{ \frac{1-y}{K_f} + \frac{y}{K_g} \right\} \div \rho_A \right)}$$

Where  $c$  is the propagation velocity (m/s),  $K_f$  is the bulk modulus of the fluid ( $\text{kg ms}^{-2}$ ),  $K_g$  is the bulk modulus of the gas ( $\text{kg ms}^{-2}$ ) and  $\rho_A$  is the average density ( $\text{kg m}^{-3}$ ).

According to the equation the influence of pipe wall thickness and Young's modulus is disregarded as the effect of the gas content dominates (Wylie and Streeter 1978).

### 2.4.3 Limitations of Siphonic Roof Drainage

A number of failures of siphonic roof drainage installations have been reported (Bowler and Arthur 1999; Sommerhein 1999). However, following a number of high profile failures in the 1990's, it was recognised that it is not the fault of the siphonic system as a concept, but due to design, installation inadequacies or a lack of maintenance of the system (Wearing 2004).

Bowler and Arthur (1999) suggest five key factors for a risk analysis in terms of the inability of a system to meet its expectations derived from investigations of siphonic system failures:

1. Interaction between the above and below ground systems.
2. System operating and design pressures.
3. Mechanical failure of pipework.
4. Inadequate capacity.
5. Inadequate maintenance.

#### 2.4.3.1 Interaction between the Above and Below Ground Systems

Bowler and Arthur (1999) identified that the underground infrastructure is not necessarily designed and installed at the same time as the roof water drainage system. This can lead to lead to flooding of paved areas, roads and car parks if the capacity of the underground system is exceeded. Of greater consequence, overtopping of the gutter and flooding within the building can be caused if the free discharge required for the operation of a siphonic system is not achieved due to the interaction between the above and below ground system. May (1997) identifies that under-capacity of the underground drainage may result in flow backing up within the vertical downpipes, subsequently reducing the available head and hence, the performance of the system. There are examples of buildings flooding where siphonic downpipes have been connected directly into the underground drainage system (Bowler and Arthur 1999). To prevent this problem, a siphon break can be incorporated by increasing the diameter of the vertical downpipe so that the two systems operate independently.

#### 2.4.3.2 System Operating and Design Pressures

Pressures within the system can vary from the specified design as a result of four main factors identified by Bowler and Arthur (1999):

1. Partial blockages of the outlets.
2. Interactions with the underground system.
3. Changes in pipework configuration from the original design.
4. Air entering the system.

Excessive pressures could result in the system not performing to its peak capacity or the development of noise and structural vibration which could lead to physical failure of components.

Slater et al. (1999) also identified that pipes and fittings are only commercially available in a limited range of sizes which generate limitations for system designers. Furthermore, hydraulic resistance data is not always available for the components selected leading to increased uncertainty in the system design.

#### 2.4.3.3 Mechanical Failure of Pipework

Although extensive testing is available for the characteristics of pipework operating under positive pressures, there is no corresponding data for negative pressures (May and Escarameia 1996; Bowler and Arthur 1999). May and Escarameia (1996) stated that:

‘Under positive pressures, the walls of a pipe tend to deform symmetrically until the tensile strength of the material is exceeded. Under negative pressures, the walls tend to deflect inwards asymmetrically, leading to localised overloading and failure at considerable lower pressure differentials than apply under positive pressures.’

Consequently, there are no recognised international standards for siphonic drainage pipework operating under negative pressure. Bowler and Arthur (1999) provided an equation to determine the critical pressure of a long pipe ( $P_{buc}$ ):

$$P_{buc} = 2.2E_{cr} \left( \frac{t}{D} \right)^3$$

Where:  $E_{cr}$  is the Creep Modulus;  $t$  is the wall thickness of the pipe; and  $D$  is the pipe diameter.

A range of materials are used for siphonic system pipes and fittings including high-density polyethylene (HDPE), unplasticized polyvinyl chloride (uPVC) and acrylonitrile butadiene styrene (ABS). Furthermore, cast iron pipes and outlets shown in Figure 2.10 are also used but are more common in Germany (May and Escarameia 1996).



**Figure 2.10 Cast Iron Siphonic Roof Drainage Outlet**  
(Thorne Rainwater Systems (2016) "Syphonic Cast Iron System"  
[http://thornerws.com/trws\\_syphonic\\_cast\\_iron.html](http://thornerws.com/trws_syphonic_cast_iron.html) [accessed Jan 23 2016])

Bowler and Arthur (1999) identified five key functions that determine the ability of pipes to accept negative pressures:

1. Elastic behaviour of the pipe material;
2. Ratio of wall thickness to pipe diameter;
3. Temperature;
4. Temporal effects;
5. Load history.

Furthermore, significant limitations of the HDPE pipe used extensively within siphonic roof drainage particularly within the UK are identified by Bowler and Arthur (1999):

‘Some manufacturers and siphonic designers are aware of the limitations of pipes under negative pressures and restrict use of low pressure rated pipework or limit design pressures in systems to that which the pipes will accept. This information readily available or universally appreciated, consequently systems have failed due to the use of inadequately rated pipes. Comprehensive impartial testing is required under a variety of regimes to give designers and specifiers adequate information on the long-term performance of different types and sizes of pipe.’

Bowler and Arthur (1999) completed negative pressure testing on HDPE pipe and reported that a 200mm diameter PN3.2 rated pipe buckled at a short term loading of  $-86\text{kN/m}^2$ . According to the equation used to calculate the buckling pressure ( $P_{buc}$ ) PN3.2 pipe produces a buckling value of  $-28\text{kN/m}^2$ . Lucke and Beecham (2009) identified that the use of these pipes within siphonic systems could lead to failure. Furthermore, Lucke and Beecham (2009) recognised that a 100mm diameter PVC (PN6) would buckle at a differential pressure on  $150\text{kN/m}^2$  which suggests using a factor of safety of 1.5 against failures instigated by sudden blockages.

#### 2.4.3.4 Inadequate Capacity

The capacity of a siphonic system is fixed and when operating at its design capacity will not increase as the head within the gutter increases as it would do in a conventional system (Bowler and Arthur 1999). Therefore, flows in excess of the design capacity can only be accommodated if a separate overflow or secondary system is incorporated within the design, otherwise overtopping of the gutter may occur.

#### 2.4.3.5 Inadequate Maintenance

Gutters are prone to blockage from a range of detritus. Within conventional systems, this material reduces the operating capacity of the system. However, within a siphonic system, blockages are more severe. The blockage of one or more outlets disturbs the flow balancing resulting in overloading of the roof outlets which may result in air being entrained within the system effectively breaking the siphon and significantly reducing the performance of the system (Sommerhein 1999).

Bowler and Arthur (1999) suggested six inspections within the first year of installation and a subsequent maintenance programme developed from the results. However, from a practical perspective, maintenance, CCTV surveys and gutter cleaning is frequently difficult due to access restrictions and can only be carried out if sufficient access is incorporated within the design of the building. Frequently, maintenance of siphonic system is neglected which can result in reduced performance and more critically system failure.



#### **2.4.4 Previous Experimental Research**

There have been several experimental research studies focussing on improving the understanding of siphonic roof drainage systems from institutions including Heriot Watt University (UK), The University of Sheffield (UK), Geberit International (Switzerland) and the University of South Australia. The following section provides a review of relevant experimental research to date.

##### **2.4.4.1 Heriot-Watt University (HWU), Edinburgh, Scotland**

Since 1996 research has been underway at HWU investigating siphonic roof drainage systems (Wright et al. 2006a). The primary objectives of the research were sub-divided into three phases (Arthur and Swaffield 2001b):

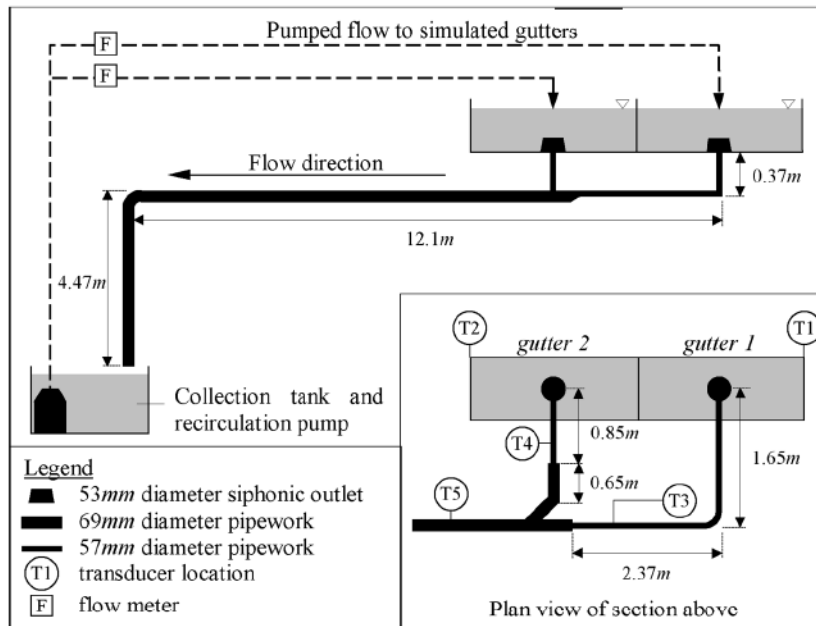
1. An experimental study to investigate pressure transient generation and propagation within a siphonic system during priming;
2. Establish stationary and moving boundary conditions consistent with developing a numerical model;
3. The development of a computer based design tool to provide design guidance to system designers and building operators.

The research programme was furthered by Wright et al. (2006a) to achieve two primary objectives:

1. Experimental research to investigate the performance of multi-outlet siphonic systems, including the effects of system imbalance, different types of sewer connection and outlet blockages;
2. To enhance the numerical model to simulate the operation of multi-outlet siphonic drainage systems under various scenarios.

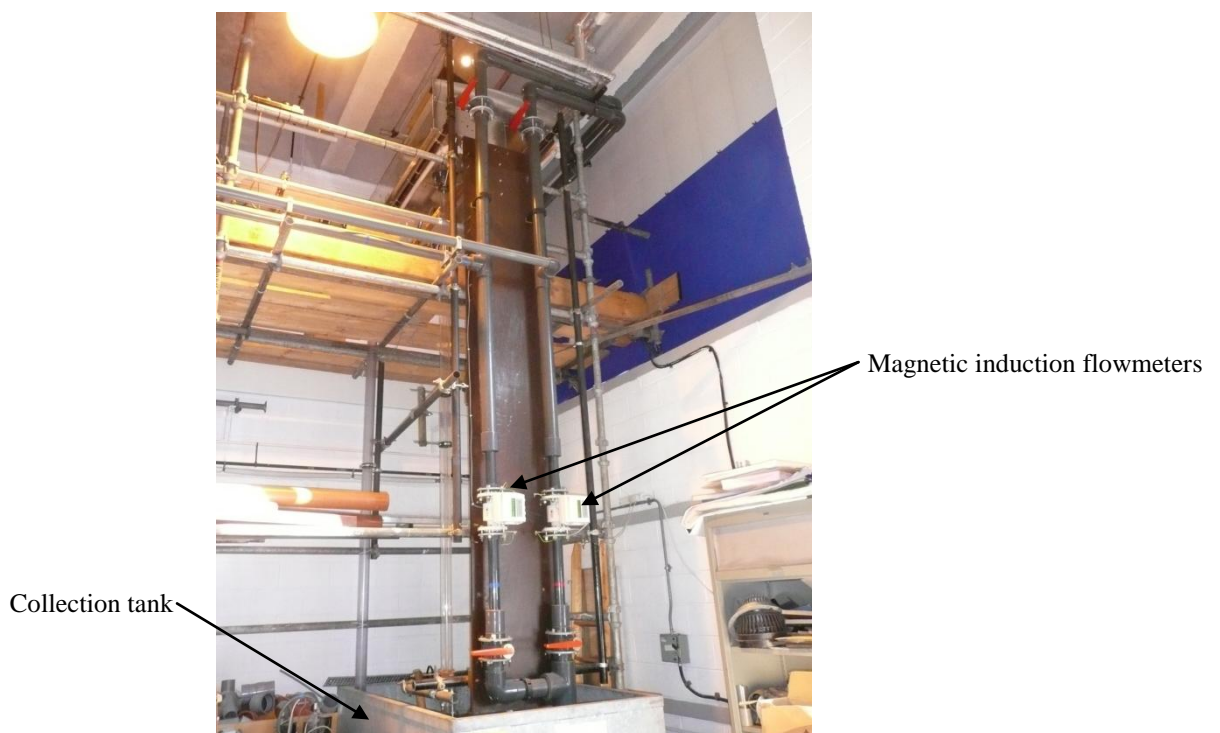
##### **2.4.4.1.1 HWU Experimental Study**

An experimental study was completed at HWU using a laboratory test facility shown in Figure 2.11 (Wright et al. 2002).



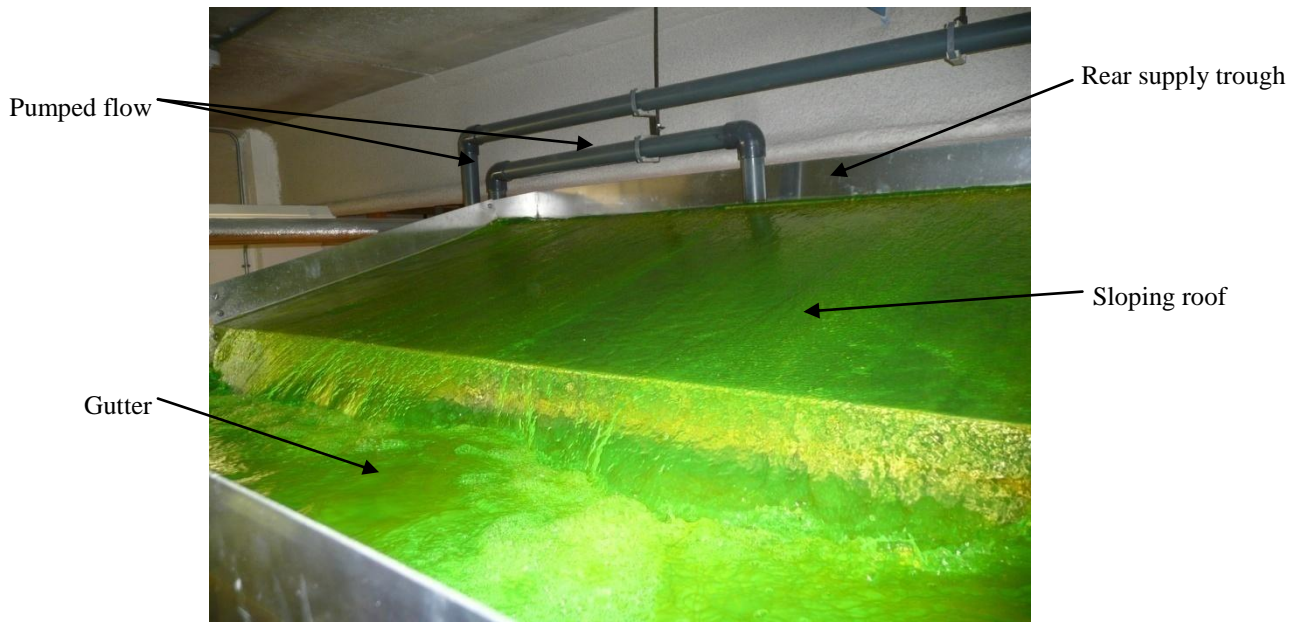
**Figure 2.11 Schematic View of the HWU Siphonic Roof Drainage Test Rig (Wright et al. 2002)**

Magnetic induction flowmeters were used to record the flow rate to each of the independent gutters shown in Figure 2.12.



**Figure 2.12 Magnetic Induction Flowmeters and Collection Tank**

Flow to the gutter was fed into a rear supply trough and then a sloping gutter (Figure 2.13).



**Figure 2.13 The HWU Siphonic Test Rig Rear Supply Trough and Sloping Roof**

Pressure measurements were recorded using transducers installed in the base of the gutters to record flow depths and in the crown of the horizontal carrier pipe (Figure 2.14) to measure system pressures (Wright et al. 2002).



**Figure 2.14 Pressure Transducer within the Crown of the Horizontal Carrier Pipe**

The laboratory tests facility was used to investigate five scenarios (Wright et al. 2002):

1. Steady state design criteria rainfall events (where the system is fully primed);
2. Rainfall events below the design criteria;
3. Design criteria rainfall event varying gutter inflows (where the system is fully primed);
4. Rainfall events above the design criteria;
5. Total blockage of one of the outlets.

#### *2.4.4.1.1.1 Steady State Design Criteria Rainfall Event (Fully Primed System)*

Priming within gutter 1 was observed at 5.85 l/s and 7.78 l/s within gutter 2 (Wright et al. 2002). This difference was accounted for solely as a result of the pipework configuration of the test facility (Wright et al. 2002). The observed priming procedure was consistent with the order of events outlined in section 2.4.1. Wright et al. (2006a) observed that priming within a multi-outlet system is similar to a single outlet system however flow conditions were more complex as a result of inherent inter-relationships particularly the formation and movement of trapped air pockets.

#### *2.4.4.1.1.2 Rainfall Events below the Design Criteria*

Experimental testing was undertaken according to three flow regimes (Wright et al. 2002):

1. Between 15% and 40% of the design criteria inflows – Results showed highly unsteady flow regimes with cyclical periods of positive and negative pressures with siphonic action sustained for only very short periods. (Wright et al. 2002);
2. Between 40% and 60% of the design criteria inflows – During these conditions the levels of inflow resulted in oscillating, constantly negative system pressure above those within fully primed systems. Limited gutter flow depths led to continuous siphonic action but with large amounts of air being entrained causing lower flow rates and higher pressures compared to a fully primed system (Wright et al. 2002);
3. Above 60% of the design criteria inflow – Initial pressures were similar to those within a fully primed system, however, the limited inflow resulted in oscillating, negative system pressures similar to the previous regime. Gutter flow depths were again insufficient to sustain a fully primed state and large quantities of air continued to be entrained throughout the system (Wright et al. 2002);

#### *2.4.4.1.1.3 Design Criteria Rainfall Event Varying Gutter Inflows (Fully Primed System)*

During testing at this regime, gutter inflows gradually increased throughout each test up to the design threshold. Similar to those tests completed at constant gutter inflows, siphonic action was initiated, however, it took longer for system pressures and gutter flow depths to purge air from the system and achieve a fully primed state (Wright et al. 2002).

#### *2.4.4.1.1.4 Rainfall Events above the Design Criteria*

System pressures at gutter inflows above the design criteria were observed to be identical to those at the design criteria (Wright et al. 2002). However, the increased flow to the system resulted in rising gutter levels that eventually resulted in overtopping. From the experimental research, Wright et al. (2002) stated that:

‘System pressures occurring once a siphonic system has become primed are the minimum possible, and the capacity is the maximum possible, for that particular system.’

#### 2.4.4.1.1.5 Total Blockage of one of the Outlets

The experimental research identified that when one outlet was blocked, the test facility performed as a single-outlet siphonic system (Wright et al. 2002). However, system pressures were recorded considerably lower than at the design criteria producing a negative pressure wave that propagated and reflected throughout the whole system (Wright et al. 2002; Wright et al. 2006a). This raised a significant concern as if a system was designed to achieve low system pressures, the blockage on an outlet would result in the system pressure reducing further which may result in the onset of pipe deformation or cavitation.

Further experimental research was completed by Wright et al. (2006b) to examine flow conditions by altering gutter and tail pipe configurations. Three different gutter configurations were used according to Table 2.3.

**Table 2.3 HWU Gutter and Tail Pipe Configurations (Wright et al. 2006b)**

Gutter	Cross- sectional shape	Sole width (mm)	Top width (mm)	Depth (mm)	Tail pipe diameter (mm)
A	Trapezoidal	80	112	60	64
B	Half-round	N/A	150	75	110
C	Rectangular	600	600	300	64 and 110

The normal experimental setup involved the gutter being directly connected to the tail pipe, however, further experiments were completed with alternative standard system elements connected immediately downstream of the gutter outlet including (Wright et al. 2006b):

- A collection hopper;
- A minor offset of two 45° bends in series;
- A major offset of two 45° bends connected by a short length of pipework.

Testing completed using Gutter A and Gutter B showed that flow conditions were not affected by a collection hopper or by the presence of either offset (Wright et al. 2006b). However, Gutter C using both tail pipes showed the flow conditions were influenced by the downstream pipework. The collection hopper significantly reduced system capacity and both offsets reduced system flow rates (Wright et al. 2006b). During full bore flow conditions within Gutter C, large quantities of air were observed to be entrained possibly as a result that the configurations had a greater capacity than the available laboratory pumping capacity (Wright et al. 2006b).

#### 2.4.4.1.2 HWU Numerical Model

A numerical model, termed SIPHONET, was developed by HWU to simulate the transitory flow conditions within siphonic roof drainage systems and a method of characteristic based solutions was used to simulate free surface and full bore flow condition (Arthur and

Swaffield 1999a; Wright et al. 2006a). The model addressed three components of siphonic action: the formation of the hydraulic jump within the upstream section; the subsequent development of full bore flow and the priming of the system as well as tracking the movement of discrete pockets of air and their influence on the internal pressure regime (Arthur and Swaffield 1999a).

To determine the formation of the hydraulic jump, four equations were used shown in Table 2.4 (Arthur and Swaffield 1999a). These equations determined the flow rate at which full bore flow is developed, the position where the condition is reached and the volume of air upstream of the hydraulic jump.

**Table 2.4 Calculation Method to Define the Hydraulic Jump for SIPHONET (Arthur and Swaffield 1999a)**

Application	Equation
Determination of depth immediately downstream of bend 1	$H_e = \frac{Q^2}{2gA^2} - \frac{Q^2}{2gA_e^2}$
Calculation of the upstream conjugate depth	$f(H) = 1 - \frac{Q}{CA_n\sqrt{R_nS_o}} = 0$
Calculation of the upstream conjugate depth	$\rho A_1 \left( g\bar{H}_1 + \frac{Q^2}{A_1^2} \right) = \rho A_2 \left( g\bar{H}_2 + \frac{Q^2}{A_2^2} \right)$
Position of the hydraulic jump along the horizontal carrier pipe	$\Delta x_{H_e-H_1} = \int_{H_e}^{H_1} \frac{1 - Q^2T/gA^3}{S_0 - Q^2/A^2RC^2}$

To complete the data required for the numerical section of SIPHONET, initial pressures were then calculated assuming homogenous flow using the following equation (Arthur and Swaffield 1999a):

$$\bar{\rho} = \frac{V_g\rho_g + V_f\rho_f}{V_{stack}}$$

The numerical model could then compute the hydraulics within the siphonic system using the quasi-linear hyperbolic partial differential equations of continuity and momentum in terms of velocity and pressure head (Arthur and Swaffield 1999a). Once full bore flow had been established within the model, any further inflow was assumed to contain 0.1% air (Arthur and Swaffield 1999a). This value is a significant underestimate in comparison to the value of 10% suggested by May and Escarameia (1996).

Arthur et al. (2005) reported that the numerical model SIPHONET can accurately simulate the priming of a siphonic system, steady siphonic conditions and complex operating conditions.

Wright et al (2006b) identified that the numerical model incorporated three elements; a roof flow module, a gutter flow module and a pipe flow module. The roof flow module employed a kinematic approach combining the continuity and momentum equations rather than the more accurate dynamic approach due to unfeasibly long computer run times associated with the latter (Wright et al. 2006b). Wright et al. (2006b) stated that the roof flow module can account for different roof geometries and the effect of wind-driven rain. The gutter flow module is based on momentum equations of one-dimensional, unsteady flow in open channels with lateral inflow which are hyperbolic partial differential equations which cannot be solved directly (Wright et al. 2006b). For the gutter flow module, the method of characteristics was used adopting three types of boundary conditions: the upstream/downstream ends of a gutter, an open gutter outlet and a fully/partially closed gutter outlet. For the pipe flow module a two-step approach was used. Under free surface conditions, flow was assumed to be annular within the downpipes. During full-bore flow conditions, a method of characteristics solution technique was again used to solve the continuity and momentum equations similar to the gutter flow module (Wright et al. 2006b). Boundary conditions were also applied to the pipe flow module including a blocked outlet, a 90° bend, a diameter change, a three-pipe change and a system exit. Wright et al. (2006b) recognised that the two-step approach can not accurately simulate all aspects of a siphonic system, however, the errors involved are not regarded as particularly significant and conclude that the modelling method accurately simulated siphonic systems under extreme events.

The experimental research completed by Wright et al. (2006a) was used to enhance the numerical model to develop SIPHONET2. Wright et al. (2006a) identified that the method of characteristics based solution technique used in SIPHONET was not suited to the simulation of moving hydraulic jumps within complex multi-outlet systems. Instead, the MacCormack method was used to simulate initial free surface flow conditions using the original characteristics based solution technique for the simulation of full bore flow conditions (Wright et al. 2006a). Wright et al. (2006a) provided a synopsis of the MacCormack method:

‘The MacCormack solution technique relies on the hyperbolic nature of the governing equations, which leads to spontaneous discontinuities that have real physical meanings, e.g. hydraulic jumps.’

However, the author recognised that by using these two methods, oscillations occur when the model switches from the MacCormack method to the method of characteristics. The enhancement of the numerical model enabled the simulation of the following phenomenon (Wright et al. 2006a):

- System priming including partial re-pressurisation;
- Rainfall events below the design condition;
- Variable rainfall conditions;
- Outlet blockages;
- Submergence of the system exit.

Despite the enhancement of the model, Wright et al. (2006a) recognised that numerical stability problems and extended computational run times restrict its general applicability.

#### 2.4.4.2 The University of Sheffield, UK

A detailed experimental study was completed at the University of Sheffield using a test gutter facility measuring 35m in length with a 600mm wide by 170mm deep gutter (Bramhall 2004). The research focussed on five key areas:

1. The interaction of primary and secondary siphonic rainwater outlets;
2. The validity of a theoretical methodology for siphonic roof drainage design;
3. The prediction of water depths around siphonic rainwater outlets;
4. The effect of sub-atmospheric pressure;
5. Flow measurement.

##### *2.4.4.2.1 The Interaction of Primary and Secondary Siphonic Rainwater Outlets*

The research summarised that the hydraulic performance of a secondary system is comparable to that of the primary system. When both systems operate simultaneously within a shared gutter, the primary system dictates the flow profile at flow depths lower than the secondary outlet upstand (Bramhall 2004). However, when the flow depth exceeded the secondary outlet upstand, the secondary system dominated.

##### *2.4.4.2.2 The Validity of a Theoretical Methodology for Siphonic Roof Drainage Design*

The results highlighted that when adopting a theoretical methodology for siphonic roof drainage design, there is discrepancy between the upstream water depths generated by the theoretical model (BSI 1983) and experimental research (Bramhall 2004). The experimental research completed by Bramhall (2004) identified that when the outlets were equally spaced within the gutter, the theoretical model specified in BS 6367 (1983) 'Code of practice for the drainage of roofs and paved areas' became less accurate as the flow increased. However, the research also concluded that further work is required to understand the influence of negative pressures on the flow through each outlet (Bramhall 2004).

##### *2.4.4.2.3 The Prediction of Water Depths around Siphonic Rainwater Outlets*

When considering water depths around siphonic outlets, the flow rate through each outlet is affected by the position within the gutter. Outlets located at the extreme ends of the gutter required a greater head of water to achieve the same flow compared to outlets positioned equidistant within the gutter at their optimum position. Flow depths were observed to increase by up to 47% to achieve the same flow rate (Bramhall 2004). Furthermore, flow depths were shown to increase as the width of the gutter sole reduced.



An equation is specified to determine the depth of flow around an outlet by Bramhall (2004):

$$D_{sp} = AR_D + D_f$$

Where  $D_{sp}$  is the depth of flow around an outlet (accounting for gutter sole, width and position),  $R_D$  the distance ratio,  $D_f$  the depth of flow at an outlets optimum position and  $A$  a constant (equivalent to 23.38).

The research identified the potential for operational problems to occur concerning the group of secondary outlets near to the end of a gutter which has the potential to cause the gutter to overtop. Recommended practice is for both the primary and secondary outlets to be positioned equidistant along the length of the gutter and the operational depth of water within the primary system calculated to ensure that it is shallower than the height of the upstand of the secondary outlet (Bramhall 2004).

Observations during the experimental study showed that water depths within the gutter became constant and uniform as the system reached the maximum design capacity with a redistribution of flows within the gutter (Bramhall 2004). It was concluded that the capacity of outlets was dependent on a number of factors, specifically, the resistance to flow within individual pipe sections. As a result, there was a balancing out of the water profile within the gutter reaching a uniform state (Bramhall 2004).

#### 2.4.4.2.4 *The Effects of Sub-Atmospheric Pressure*

Analysis of the experimental results completed by Bramhall (2004) identified areas of negative pressure and a varying pressure distribution during the operation of a siphonic system. Furthermore, in comparison with a theoretical model used by system manufacturers (PrimaCalc) based on the application of Bernoulli's energy equation combined with the Colebrook-White equation, the experimental results showed a significant difference highlighted in Table 2.5 (Bramhall 2004).

**Table 2.5 Comparison of Measured Pressure Results to those Derived by PrimaCalc Software adapted from Bramhall (2004)**

	Pressure (bar)		
	Outlet 1	Outlet 2	Outlet 3
PrimaCalc theoretical model	-0.007	-0.045	-0.420
Measured results	-0.010	-0.116	-0.372
Difference between the measured results and the PrimaCalc theoretical model	6%	16%	4%

Further research was identified to investigate the validity of these theoretical calculations in more detail.

#### 2.4.4.2.5 Flow Measurement

An off-line dye dilution technique was developed to investigate the flow rates through an experimental test facility with three outlets within a common gutter. An injection pump was used to inject dye of a known concentration into the upstream outlet. Dilution samples were retrieved from three sample points at the furthest possible point downstream of each outlet. The positioning of the sample points was selected to allow mixing of the dye and water due to the turbulent nature of the flow. Each sample was collected using a number of adapted syringe arrangements. The samples were placed in clean sample tubes and analysed using a flourometer. Samples were also taken periodically of the supply water and analysed to account for any residual dye entering the system. Five samples were taken from each of the three sample points and an average concentration determined for each point. This average value was then used to determine the average flow of water through the individual outlets.

This methodology was applied to one flow test at a constant inflow to the system of 36 l/s. This flow rate was selected as it was close to the calculated theoretical maximum capacity of the system (ultimate flow rate). The results are summarised in Table 2.6.

**Table 2.6 Flow Rate Measurements Recorded by Bramhall (2004)**

Sample Point	Flow Rate (l/s)								
	Test 1	Test 2	Test 3	Test 4	Test 5	Average	Max	Min	$\sigma$
1	9.12	9.12	9.17	9.36	9.40	9.28	9.40	9.12	0.14
2	23.28	23.18	23.22	23.31	23.22	23.24	23.31	23.18	0.05
3	35.46	35.33	35.49	35.27	35.99	35.37	35.99	35.27	0.29

Bramhall (2004) reported that analysis of the flow rate measurements obtained using this method closely matched the inflow to the experimental test facility.

The average flow rates measured using this method were compared with values derived using British Standard theoretical models as well as using commercially available design software, PrimaCalc. Table 2.7 shows the difference in flow rates and between the measured results and those derived from the models, adapted from Bramhall (2004).

**Table 2.7 Comparison of Measured Flow Rate Results and those derived from Theoretical Models (BS EN 12056-3:2000 and PrimaCalc) adapted from Bramhall (2004)**

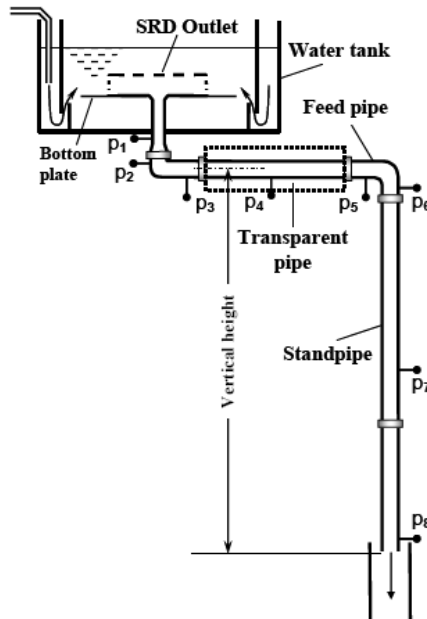
	Flow Rate (l/s)		
	Outlet 1	Outlet 2	Outlet 3
BS EN 12056-3:2000 theoretical model (weir equation)	10.97	11.15	11.05
PrimaCalc theoretical model	9.86	16.65	11.68
Measured results using flourometry	9.28	13.97	12.17
Difference between the measured results and the BS EN 12056-3:2000 theoretical model	10.6%	33.0%	5.4%
Difference between the measured results and the PrimaCalc theoretical model	17.5%	20.0%	10.0%

The results show that compared to the measured data, neither the BS EN 12056-3:2000 theoretical model or the PrimaCalc software provided an accurate representation of flow rate or pressure within a siphonic system. It was recognised that for the PrimaCalc software, the flow rate was derived from the energy loss, pipe diameter, pipe length and pipe direction which it is not always possible to accurately determine (Bramhall 2004). As a result, a factor of safety of 12% was suggested within the software to account for this difference.

Conclusions from the research identified that outlets within a siphonic system do not accept equal amounts of flow and the depth of water within the gutter was observed to become deeper and redistribute toward the outlet with the greatest capacity (Bramhall 2004). This was a significant observation regarding the design of siphonic systems as current design codes assume that an equal flow rate is transferred through each outlet.

#### 2.4.4.3 Geberit International A.G., Switzerland

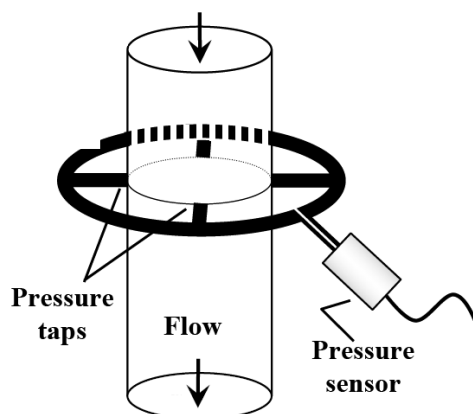
Geberit are an international supplier of sanitary, supply and drainage systems as well as specific siphonic roof drainage designers and installers. Experimental research was reported by Öngören and Materna (2006) to generate a data set to inform design criteria for both primed and multi-phase flow. Testing was completed within a water tank using a single siphonic outlet, a 2.8m horizontal pipe termed the ‘feed pipe’ and a vertical ‘stand pipe’ varying in length between 5 and 10m to vary the capacity of the system allowing a range of flow conditions shown in Figure 2.15 (Öngören and Materna 2006).



**Figure 2.15 The Geberit Test Facility (Öngören and Materna 2006)**

Tests were completed at flow rates ranging from 0 to 16 l/s. During each test, pressure measurements were made along the ‘feed pipe’ and ‘standpipe’ shown in Figure 2.16 according to the following method (Öngören and Materna 2006):

‘Four equally spaced pressure taps drilled around the periphery of the SRD pipe are connected to the same transducer by means of miniature tubes in order to determine the average local pressure at each selected location. The use of such a method is necessary since the systems examined in this study operate mostly under partly filled conditions which cause a spatially varying pressure distribution at the pressure tap locations.’



**Figure 2.16 Method of Measuring Average Pressure within a Pipe (Öngören and Materna 2006)**

An image velocimetry technique was undertaken to examine local velocities within a transparent section of the horizontal carrier pipe using a high speed camera at a rate of 640 frames per second. Customised particle tracking software was used to determine flow velocity by marking and tracking fine air bubbles recorded in the sequence of images. Öngören and Materna (2006) identified that siphonic systems predominantly operate under design capacity at unprimed part load conditions and the technique was used to study the transition from multi-phase flow under part load conditions to single phase fully primed flow. The research concluded (Öngören and Materna 2006):

‘One of the most important results of this study is the observation of a flow regime where the effective flow velocity in the piping remains constant for a relatively wide range of flow rates. It is assumed that the breaking-up of large air pockets into small size dispersed bubbles and their transition to a homogenously distributed regime is the cause of this unique flow phenomenon.’

The authors reported that at low flows there was a clear air/water interface with a turbulent free surface. With increasing flow rates the air entrainment became augmented and exhibited a ‘bubbly zone’ between the air/water interface (Öngören and Materna 2006). This bubbly layer was observed to increase in depth with increasing flow rates until it occupied the upper section of the carrier pipe. At flow rates in excess of this hydraulic regime, the amount of bubbles reduced until almost disappearing.

This was consistent with other reported experimental research which identified three distinct hydraulic regimes including free surface flow, unsteady two-phase flow and full bore flow (Arthur and Swaffield 2001).

However, the experimental research may only be applicable to single outlet applications and images were only recorded from a short section of the horizontal carrier pipe. The camera positioning was selected as it was assumed that the flow structures induced by multi-phase flow would have fully developed by this point. However, at three metres long, the carrier pipe was relatively short and the unreported position of the camera may also be affected by the proceeding pipe configuration. Furthermore, the research did not report any temporal or spatial variation but instead identified a typical flow regime as a function of flow rate. It has already been discussed that as flow increases, some pipes begin to flow full while others remain only partially filled depending on the air within the system. Significantly, these observations may not be representative of the performance of multi-outlet systems and flow characteristics are a function of temporal and spatial variation and vary along the length of the carrier pipe.

#### 2.4.4.4 University of South Australia (UniSA), Melbourne, Australia

Experimental research is on-going at UniSA in collaboration with Syfon Systems of Melbourne. A full scale testing facility was constructed measuring 32m long by 6m high by 3m wide shown in Figure 2.17 (Lucke et al. 2007).



**Figure 2.17 The UniSA Siphonic Drainage Test Facility (Lucke et al. 2007)**

The pipework throughout the rig was constructed of Perspex to be able to observe flow patterns. A commercially available software package was used to determine the hydraulic calculations for the rig at a maximum expected flow rate of 69 l/s equivalent to a 1 in 300 year storm event (Lucke et al. 2007). The research has shown consistency between the experimental data and the software recording a maximum flow rate of 70l/s. The research was successfully defended as a PhD entitled ‘The role of air entrainment in the performance of siphonic roof drainage systems’ and focussed on four aspects of air entrainment in siphonic roof drainage systems (Lucke 2009):

1. The influence of air entrainment on maximum system capacity and on friction and form losses;
2. How air entrainment can limit negative pressured in tall siphonic systems, and whether this can control the onset of cavitation in vertical downpipes;
3. How air entrainment is affected by varying the number of operational siphonic outlets within the same gutter;
4. The effects of air entrainment on the gutter water depths required for the effective operation of primary and overflow outlets.

##### *2.4.4.4.1 The Effects of Air Entrainment on System Capacity*

The experimental research concluded that the maximum system capacity of siphonic drainage systems was affected by air entrainment in the flow although the reduction in capacity was not directly proportional to the increasing degree of air entrainment (Lucke 2009). This capacity loss was greater than the volume occupied by the air bubbles alone which may be caused by the significant expansion of the air bubbles in aerated flows subjected to sub-

atmospheric pressures. The air bubbles therefore occupy a greater pipe volume, subsequently reducing the flow rate (Lucke 2009). From a practical, quantifiable perspective, the design of a siphonic system not considering system capacity loss due to aeration in full flow conditions would result in an over-estimation in system capacity of 16% when the flow contains 10% of air. This would therefore have significant consequences on the performance of a siphonic system and could potentially result in failure and flooding.

Tests undertaken using a single outlet system concluded that flow containing 10% of air resulted in system pressures rising by approximately 20% (Lucke 2009). Pressure head fluctuations of between 1% and 58% of the measured mean pressures were observed under siphonic flow conditions (Lucke 2009). However, the results are not necessarily transferable to a multi-outlet system and further experimental research may be necessary to determine the extent of pressure head fluctuations for a number of outlets sharing the same carrier pipe.

Three different techniques were used to measure average flow velocities for a range of air/water ratios; volumetric flow measurement producing repeatable results to an accuracy of  $\pm 0.8\%$ ; a current meter which despite not performing well in aerated flows was repeatable to an accuracy of  $\pm 0.7\%$  at air/water ratios up to 30% and; flow visualisation using a video camera at a frequency of 50Hz producing repeatable results to an accuracy of  $\pm 5\%$ . The results concluded that for all air/water ratios the flow velocities were significantly higher than the corresponding average velocities calculated using the continuity equation:

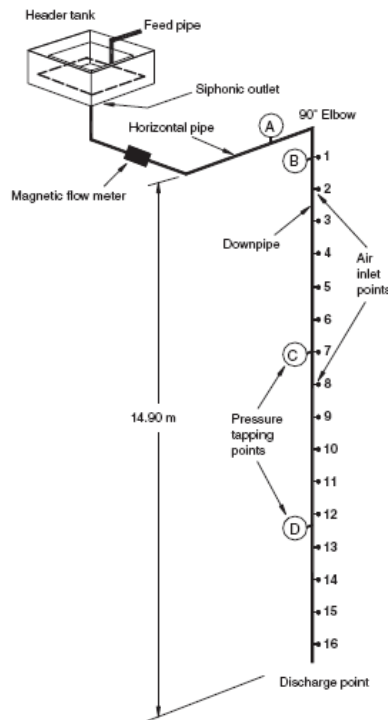
$$\sum_1 \rho VA = \sum_2 \rho VA$$

However, it was observed that the two phase flow resulting from air entrainment travelled at a lower velocity than single phase flow and the continuity equation used to predict the two phase flow does not consider the volume of air and therefore underestimated the measured velocities in the pipes (Lucke 2009). With a flow containing 10% of air, the continuity equation could underestimate the flow velocity by 16% compared to the measured results (Lucke 2009).

#### 2.4.4.4.2 *Controlling Negative Pressures within Siphonic Roof Drainage Systems using Air Entrainment*

Experimental research was completed at UniSA to investigate cavitation and its propagation, aeration and negative pressures within a prototype scale siphonic system. More specifically, the study focussed on the negative pressure transients generated within the pipework of tall buildings and the implications of pipe-wall collapse and cavitation.

Experimental research was conducted within a sixteen metre high siphonic roof drainage rig shown in Figure 2.18. The diagram highlights the magnetic flow meter used to measure flow rate between the siphonic outlet and the top of the downpipe, the position of four pressure tapping points (labelled A-D) and the location of sixteen air inlet points within the downpipe.



**Figure 2.18 The UniSA Cavitation Rig Setup (Lucke and Beecham 2009)**

Contrary to the design ethos of siphonic systems, air was introduced at locations that did not affect the priming process or the ensuing development of siphonic flow conditions (Lucke and Beecham 2009). The purpose of this was to control the negative pressures within the vertical downpipe by breaking the siphonic action. The study involved four phases of testing including aeration testing, cavitation testing, cavitation endurance testing and pressure surge testing.

#### 2.4.4.4.2.1 Aeration Testing

Aeration testing was completed within four different lengths of an 80mm diameter polyvinyl chloride (PVC) downpipe at 9.44m, 11.26m, 13.08m and 14.90m. The pressure and flow rate within the system was recorded when different quantities of air were introduced into the downpipe through three different size air hole diameters of 2mm, 5mm and 10mm at the locations highlighted in Figure 2.15.

Pressures within the 9.44m and 11.26m downpipes were above the recommended limit of  $-90\text{kN/m}^2$  so no further testing was conducted. Within the 13.08m downpipe, the maximum recorded pressure was  $-96\text{kN/m}^2$ . The introduction of air through a 10mm diameter hole approximately every 10 metres limited the minimum pressure within the downpipe to  $-70\text{kN/m}^2$  with a decrease in flow capacity of less than 2% (Lucke and Beecham 2009). Within the 14.08m downpipe, air needs to be introduced every 8.7m to limit the minimum pressure to  $-70\text{kN/m}^2$ , less than within the 13.08m downpipe suggesting that aeration is affected by the length of the downpipe (Lucke and Beecham 2009). However, further



research at different downpipe lengths was suggested to examine this hypothesis. The authors identified that a limitation of this approach is the risk of the air vents surcharging as a result of blockages or non-siphonic flows and suggests a breather pipe with an outlet at the ground level discharge pit.

#### *2.4.4.4.2.2 Cavitation Testing*

Cavitation testing was conducted to observe the flow conditions using three different downpipe diameters; 50mm, 80mm and 100mm. Similar to the aeration testing, air was introduced into the vertical downpipe to examine the effect on cavitation. Furthermore, with the 80mm diameter downpipe, the 90° elbow identified in Figure 2.18 was replaced with a long radius, swept bend to examine localised form losses on cavitation (Lucke and Beecham 2009). During testing the cavitation zone was observed within the clear PVC downpipe and its position and length recorded.

Despite the end of the cavitation zone being audible, cavitation within the 50mm diameter downpipe could not be observed due to the pipe material. Furthermore, vibration of the downpipe was recorded approximately 100mm below the 90° elbow shown in Figure 2.18, however, no pressure tapping points were fitted within the 50mm diameter downpipe.

Within the 80mm diameter downpipe the cavitation effects increased with a corresponding decrease in pressure as the downpipe length increased at an approximately linear rate with all of the air inlets closed (Lucke and Beecham 2009). The results showed that cavitation effects were initiated at downpipe pressures around  $-44\text{kN/m}^2$  and full cavitation occurred at pressures below  $-64\text{kN/m}^2$  (Lucke and Beecham 2009). When the 90° elbow was replaced with a long radius swept bend cavitation was not evident and the maximum flow rate increased. However, Lucke and Beecham (2009) identified that further testing is required to investigate whether these observations are consistent for other downpipe diameters.

Similar to the 50mm diameter downpipe, the cavitation zone within the 100mm diameter downpipe was audible but could not be observed due to the pipe material. Vibration was detected at the end of the cavitation zone, 7.15m below the 90° elbow shown in Figure 2.18 (Lucke and Beecham 2009). Conclusions from the research identified that cavitation within the 100mm diameter downpipe was more pronounced than in the 80mm and 50mm diameter pipes which suggests that the effects of cavitation increase with increasing pipe diameter (Lucke and Beecham 2009). However, further experimental research was proposed to examine this relationship in more detail.

#### *2.4.4.4.2.3 Cavitation Endurance Testing*

Cavitation endurance testing was completed to examine the long-term effects on pipe-walls of three different diameter downpipes; 50mm, 80mm and 100mm. The system was operated so that the system was subjected to cavitation for more than eight hours following which the affected sections of pipe were removed and inspected under a microscope. However, a 40x

magnification revealed no signs of pitting, scarring or deterioration of any of the downpipe sections (Lucke and Beecham 2009).

#### 2.4.4.4.2.4 Pressure Surge Testing

Pressure surge testing was undertaken to examine the resistance of a 100mm diameter PVC (PN6) downpipe to withstand a negative pressure surge generated by blocking the gutter outlet. During the study the maximum pressure that was induced in the downpipe was -99 kN/m<sup>2</sup>, close to absolute zero (vacuum) pressure. Inspection of the downpipe after testing did not show any signs of being affected by the surge pressures (Lucke and Beecham 2009).

Lucke and Beecham (2009) stated that many pipe manufacturers use the following equation to calculate pipe knuckling capacities due to negative pressure effects:

$$P_{cr} = \frac{2E}{1 - \nu^2} \left( \frac{t}{D} \right)^3$$

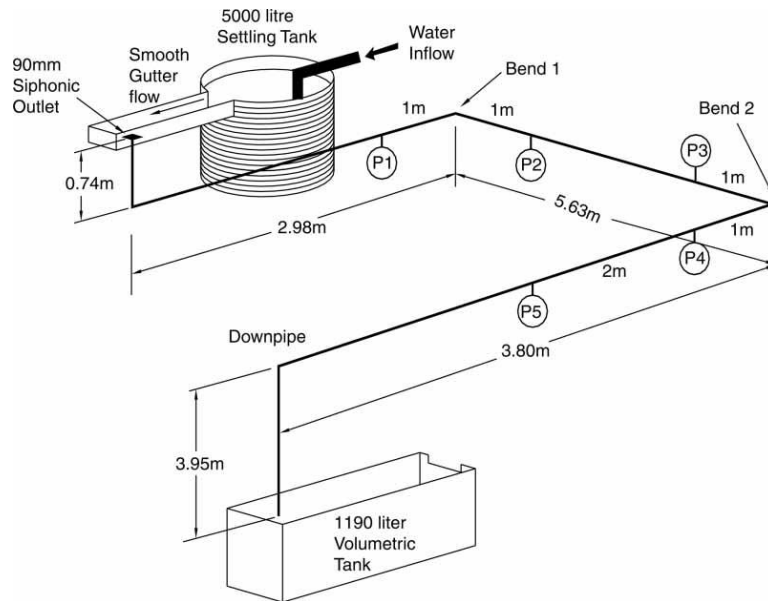
Where  $P_{cr}$  is the critical buckling pressure (N/m<sup>2</sup>).  $E$  is the modulus of elasticity,  $\nu$  is Poisson's ratio (dimensionless),  $t$  is mean pipe wall thickness (m) and  $D$  is mean pipe diameter (m).

Based on this equation, a 100mm diameter PVC (PN6) pipe would buckle when a pressure differential of 150 kN/m<sup>2</sup> develops between the internal and external pipe walls. From the experimental results observed by Lucke and Beecham (2009), a PN6 pressure rated pipe would provide a factor of safety of 1.5 against failures by sudden blockages. These results are compared to negative pressure testing completed by Bowler and Arthur (1999) using 200 mm diameter PN3.2 rated pipe. Based on the same equation, a theoretical buckling value of -28 kN/m<sup>2</sup> is calculated while pipe collapse was observed at -86 kN/m<sup>2</sup>. Lucke and Beecham (2009) concluded that the use of PN3.2 rated pipe in siphonic systems could potentially result in system failure.

#### 2.4.4.4.3 Capacity Loss in Siphonic Systems due to Aeration

Further experimental research was reported by Lucke and Beecham (2010) on the influence of aerated flows on the capacity of siphonic drainage systems. The objectives of the experimental research was to measure and predict capacity loss in siphonic drainage systems due to aeration and quantify the effects on friction and form losses. The reported research focussed on the effects that increasing air/water ratios have on friction and form losses within a primed siphonic system and the affect on system capacity.

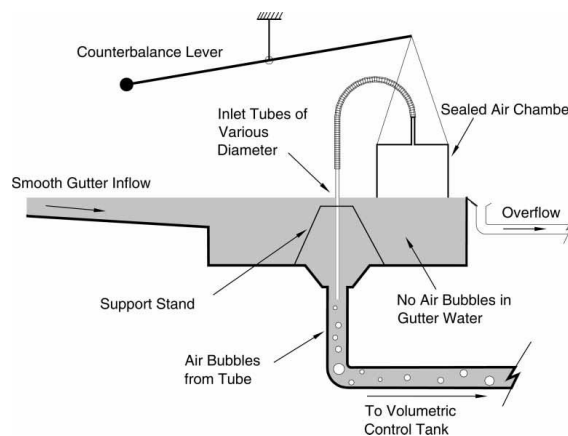
A schematic of the full scale test facility is shown in Figure 2.19.



**Figure 2.19 University of South Australia Full Scale Siphonic Test Facility (Lucke and Beecham 2010)**

The experimental setup consisted of a single 90 mm diameter siphonic outlet within a gutter. All pipework was constructed from 82.5 mm internal diameter Perspex with a 3 mm wall thickness. Pressure within the horizontal carrier pipe was measured at five positions along the length of the horizontal carrier pipe to determine the friction losses within the pipework and form losses caused by bends.

Air measurement apparatus shown in Figure 2.20 utilised a stand designed to hold tubes of various diameters above the outlet. During operation, air at atmospheric pressure was drawn through the tubes at a constant, measurable rate.

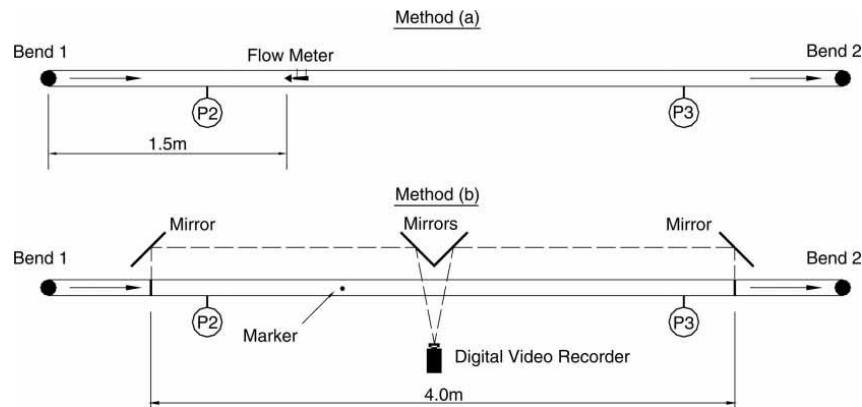


**Figure 2.20 Air Measurement Apparatus (Lucke and Beecham, 2010)**

To measure the average velocity of the varying air/water flows within the pipes three different techniques were used:

1. Volumetric flow measurement using a 1190 litre tank;

2. Current flow meter inserted into the centre of the pipe flow and the average number of propeller revolutions per minute recorded shown in Figure 2.21;
3. Flow visualisation recording the time taken for a marker to travel 4 m using a digital video recorded and an arrangement of mirrors demonstrated in Figure 2.21.



**Figure 2.21 Velocity Measurement Techniques (Lucke and Beecham 2010)**

Key conclusions from the experimental research are reported by the authors specifically (Lucke and Beecham, 2010):

- Reduction in system capacity was not directly proportional to the increase in air content;
- Pressure within the system increased with increasing air/water ratios;
- Cyclic pressure head fluctuations were observed which increased in terms of time and range as the air content increased;
- The velocity of two phase flow was lower than single phase water flow;
- Using the continuity equation to estimate the velocity of two-phase flow underestimated flow velocities;
- The friction factor ( $f$ ) decreased as the air/water ratio increased;
- Bend loss coefficients decreased slightly as the air/water ratio increased and differed indicatin that they are affected by system pressures;
- Current siphonic design procedures that do not consider aeration may produce unreliable predictions leading to operational problems and/or system failure.

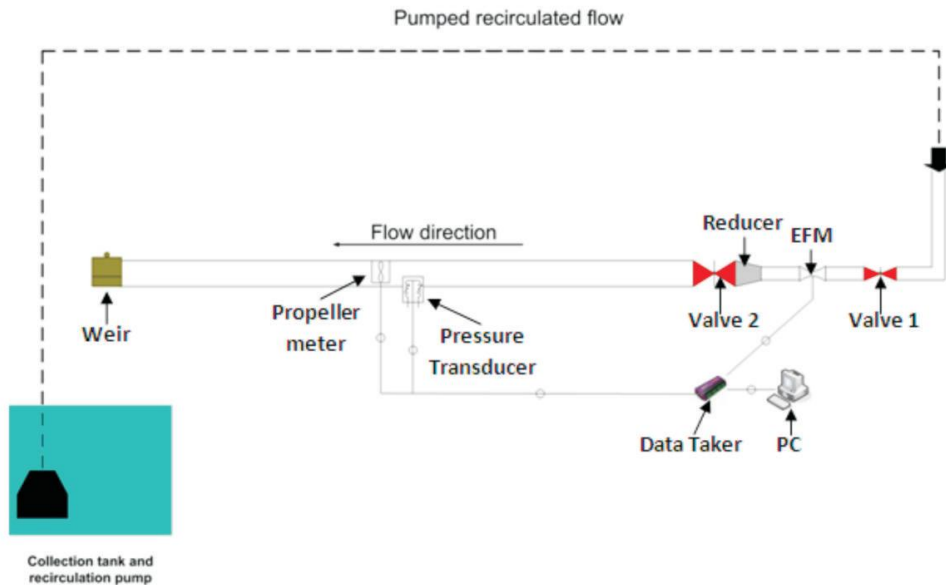
It is clear from this reported experimental study that further research is required to increase the understanding of air entrainment within siphonic systems to inform and improve current design practice.

#### 2.4.4.4.4 *Measurement of Flows in Partially Filled Pipes in Siphonic Roof Drainage Systems*

Experimental research was reported by Qu et al. (2011) using the experimental test facility at the University of South Australia to determine flows within partially filled pipes. A propeller-type current meter was used to measure flow velocity and a pressure transducer to measure flow depth and discharge calculated using a modified version of the continuity equation. As

an output of the research a computational model was developed which estimated unsteady flows passing through partially filled pipework.

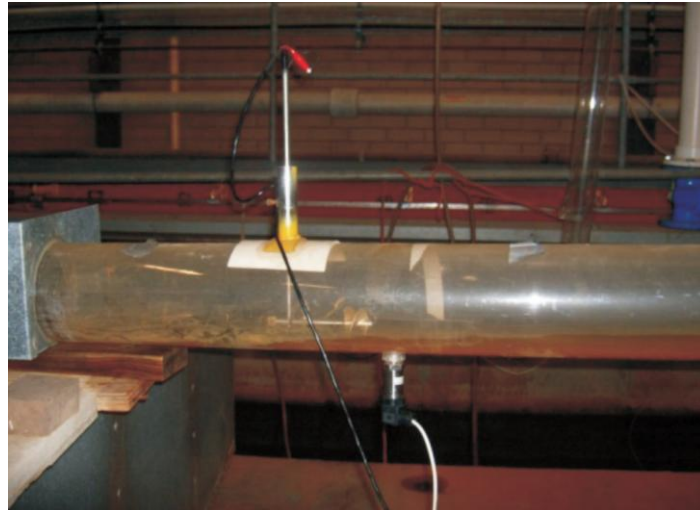
The reported experimental research was undertaken using a variable slope testing rig within a 150mm diameter 4400mm long acrylic pipe. A schematic of the experimental test facility used is shown in Figure 2.22.



**Figure 2.22 Experimental Test Facility Configuration (Qu et al. 2011)**

The current meter was selected as it was able to measure low and high velocities within variable flow depths. This eliminated the option to specify electromagnetic Doppler flow meters as often the limiting of the measurement range is 0.1 m/s and flow depths of 25mm. The author identified that the introduction of a device into the flow stream will cause disturbance of the flow resulting in a backing-up effect upstream and subsequently increased flow depths. Disturbance testing was undertaken to quantify the effect of the current meter within the flow. Water level differences of up to 14% were measured across a range of flow conditions when the current meter was in the flow stream. The author reported that despite these measured differences these effects do not significantly influence the measured flows.

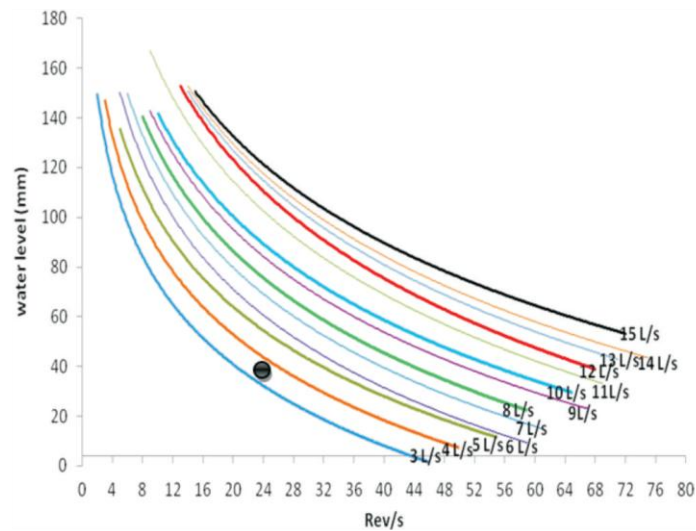
The configuration of the apparatus within the carrier pipe is shown in Figure 2.23.



**Figure 2.23 Image of the Propeller-Type Current Meter and Pressure Transducer within the Horizontal Carrier Pipe (Qu et al. 2011)**

The current meter was installed 1mm above the invert of the test pipe to capture low levels and flow velocity in the immediate vicinity. To calibrate the experimental setup, the apparatus was exposed to a discharge from  $0.003 \text{ m}^3/\text{s}$  to  $0.015 \text{ m}^3/\text{s}$  in  $0.001 \text{ m}^3/\text{s}$  increments. The flow rate was verified by the electromagnetic flow meter (EFM) shown in Figure 2.22. As part of the calibration process, a range of flow depths were generated using the tilting mechanism of the flume and a weir positioned downstream (Figure 2.22). This was to create sub-critical and super-critical flow conditions for each flow rate. Flow conditions where a hydraulic jump was created upstream of the measurement apparatus was avoided. Flow velocity was measured by average number of revolutions by the current meter for each flow test.

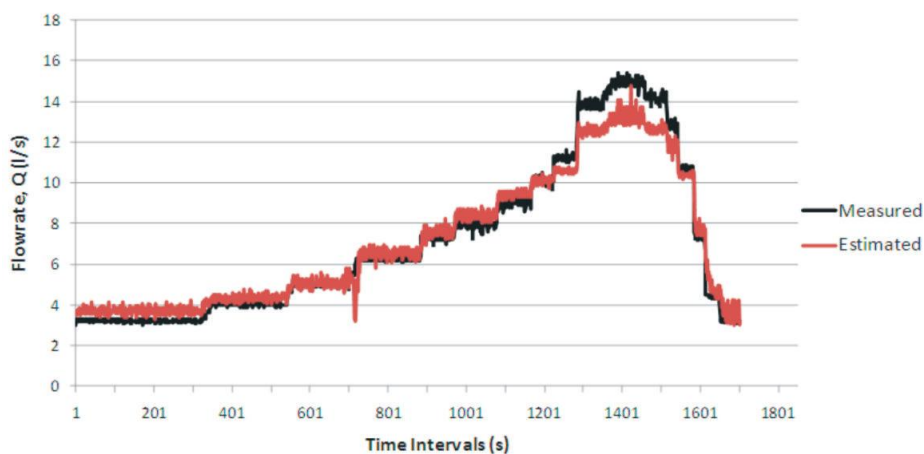
The water level and current meter revolutions were plotted and a modified log function trend line added. These trend lines formed a set of calibration curves based on the measured experimental data from the test facility. The author reported that the agreement between the measured data and trend line was generally very close with the lowest regression value of 0.83. The reported calibration curves are shown in Figure 2.24.



**Figure 2.24 Calibration Curves Reported by Qu et al. 2011**

A numerical model was developed based on the calibration curves to estimate instantaneous flow as a function of the outputs generated by the current meter and pressure transducer. At a frequency of one second the model would record the number of revolutions from the current meter and water level from the pressure transducer and determine the flow rate. Interpolation would be used if the recorded values were between two calibration curves.

The performance of the numerical model was then compared against a range of flows recorded by the EFM shown in Figure 2.25. The main variation was noted where the flows were low or reaching the maximum measured values.



**Figure 2.25 Reported Comparison of Measured and Estimated Flows (Qu et al. 2011)**

Lucke et al. (2011) reported results of the use of the experimental approach and numerical model within the full-scale siphonic roof drainage rig at the University of South Australia described in Section 2.4.4.4. Calibration testing results revealed cyclic and fluctuating flow conditions for each of the steady state flow tests. This caused different readings in the system

at the same flow rate. The authors identified that these observed fluctuations were caused by negative pressures from localised siphonic action.

Lucke et al. (2011) stated that a method of measuring water level within pipes that is not affected by fluctuating pressures is needed and such a methodology would significantly improve the accuracy of numerical models used to predict unsteady flow rates.

Analysis of the experimental data showed cyclic pressure fluctuations categorised as either high or low. The low pressure was understood to be caused by siphonic action (May and Escarameia, 1996) and associated with a corresponding increase in current meter propeller revolutions measuring flow velocity. High pressure trends were recognised as being caused by cessation of siphonic action and re-pressurisation of the system (Wright et al. 2002). Reduced flow velocity measured by the current meter propeller was generally recorded during the higher pressure periods.

A "lookup-data" computer model was developed comparing the instantaneous readings from the pressure transducer and current meter. The flow rate values associated with each tail pipe were estimated assuming an equal distribution of the gutter flow between the outlets. The author states that this is possibly erroneous and verification of this assumption is required. Results presented show a reasonable relationship between the measured and predicted flow rates using the computer model despite this uncertainty.

Lucke et al (2014) reported the results from an experimental study using this measurement technique on a full scale, multi-outlet (4) siphonic system. The testing procedure covered a flow range of 0 to 13 l/s through each outlet, equivalent to an overall system flow rate of 0 to 52 l/s for the 4 outlet experimental test facility. During low flow rates, free surface flow conditions were observed although the flow conditions were not steady despite the flow supplied to the test rig being constant. These observations support previous research reported by Arthur and Swaffield (2001), Wright, Swaffield and Arthur (2002 and 2006a).

Lucke et al (2014) reported that backwater effects were recorded at low flow rates although did not appear to affect the flow velocity in the tailpipe where the instrumentation was installed. At larger flow rates an oscillating pressure phenomenon was observed. Low pressure recorded within the tailpipe was reported to be accompanied by an increase in flow velocity. High pressure was reportedly due to cessation of the siphonic action and the corresponding repressurisation of the system, an observation also reported by Wright et al (2002). Low velocities measured within the tail pipe corresponded to periods of high water level.

The flow rate value for the downstream outlet (Outlet 4) was estimated to be an equal proportion of flow relative to the overall system flow rate. However, the author recognised that equal distribution of flow between the outlets may not be the case for all flow rates. The predicted flow rates through Outlet 4 was overestimated and a factor of 0.795 was applied to optimise the fit between measured and predicted flow rates.



Lucke et al (2014) identified the methodology developed to measure flow through outlets was suitable. However, it was understood that the instrumentation used does contribute to the error and uncertainty in the results particularly as the pressure transducers produced highly variable results.

## 2.5 Literature Review Summary

A considerable threat to the performance of roof drainage systems is changing precipitation intensity and duration associated with climate change. As well as more intense rainfall increasing the risk of flooding, long periods of low precipitation may result in flow levels insufficient to attain self-cleansing velocities (Arthur and Wright 2005). However, it is recognised that there are weaknesses in the current design approach of siphonic roof drainage systems (Arthur and Swaffield 2001b; Öngören and Materna 2006; Wright et al. 2006a). More specifically Arthur et al. 2005 and Arthur and Swaffield 2001b identified that the steady state methods used to design siphonic systems are not accurate when the system contains substantial quantities of air. Lucke and Beecham (2010) identified that the steady-state energy equation used universally for the design of siphonic systems is dependent on the water density which changes with aeration. Therefore, current design methods may not be suitable for the performance characteristics of siphonic roof drainage systems particularly when they are operating in sub-primed conditions.

Despite no analytical method being available regarding the priming of siphonic systems (Arthur et al. 2005), existing design is conducted using current understanding and knowledge. For a system to operate successfully, it is imperative that rapid priming occurs. However, there is no existing method to predict the rate at which a system will prime, and even if it will prime at all, and existing experimental research has so far been inaccurate (Arthur et al. 2005; Arthur and Wright 2007). Further research is required to improve the understanding of system priming with respect to the evacuation of air from horizontal pipework and the precise mechanisms controlling the filling of vertical downpipes (Arthur and Wright 2007).

Experimental research to date has primarily focussed on idealised, steady state, single outlet systems and it is recognised that outlet conditions are key to understanding how a system will perform (Arthur et al. 2005; Bramhall 2006). Qu et al. (2011) reported that experimental research to date has developed a good understanding of the theory and hydraulic performance of pipe-full, steady-state siphonic systems. However, there is a lack of understanding associated with the flow conditions that occur as the system 'primes' to become 'siphonic' and subsequently 'de-primed' when the inflow to the gutter outlet becomes less than the operating capacity of the pipework.

Lucke and Beecham (2010) acknowledged that the performance of drainage systems at very, high, steady, rainfall intensities is well known, however, how they perform at lower varying rainfall intensities is less certain. In addition, the current British Standard assumes that all outlets operate at the same capacity. However, recent research in pipe networks under surcharge has illustrated that at pipe junctions this is clearly not the case (Unwin 2008). Similarly, there is no understanding on how the priming mechanism interacts between multiple outlets as to the behaviour of the 'transient switch' from gravity to siphonic flow translates along the system. The problem is likely to be further compounded if the future anticipated uplifts in urban rainfall due to climate change are observed and the fact that the peakedness (ratio of peak rainfall intensity to average rainfall intensity) of storm events may

increase, giving rise to the need for the systems to prime much more quickly. There is also the potential for the transients and their interactions to become more violent.

Recent research (Lucke et al. 2014) stated that "a complete understanding of how the flow is distributed between the individual gutter outlets and pipework during all anticipated rainfall events is required. This will improve knowledge of the priming process in particular and the overall performance of siphonic roof drainage systems in general."

The authors go further to report that an improved understanding of flow measurement within multi-outlet siphonic systems "will enable designers to move from the commonly used steady-state, peak-flow design techniques to a more comprehensive full-hydrograph simulation that can model important siphonic phenomena such as time to priming".

A number of specific areas of essential research have been identified to further understanding of siphonic systems including (May and Escarameia 1996; Arthur and Swaffield 2001a; Bramhall 2006; Bramhall and Wearing 2008; Lucke and Beecham 2010; Lucke et al. 2011):

- The priming of multi-outlet systems;
- The operation of multi-outlet systems at inflow rates below the design consideration;
- Time-varying flow conditions in roof gutters;
- Predicting the distribution of pressures within a siphonic system;
- Understanding the role of aeration;
- Capacity losses due to air entrainment;
- Investigation of the relationship between bend loss coefficients and system pressures;
- A method of measuring water level within pipes that is not affected by fluctuating pressures; and,
- Accurate measurement of the relative flow component through each outlet within a common gutter.

This experimental research project seeks to address this shortfall in knowledge and to provide new design guidance that enhances the scope of current practice. A comprehensive experimental study is therefore required to identify the concepts and processes associated with sub-prime and primed flow mechanisms at individual outlets. Furthermore a robust programme of research will improve current understanding of the way in which systems with multiple outlets and associated pipework interact and influence the flow mechanisms within siphonic roof drainage systems.

### 3 Experimental Study

To test the research hypothesis and objectives, the experimental study was completed in four phases:

- Phase 1 - Enhancement and configuration of the experimental test facility
- Phase 2 - Calibration of the experimental test facility
- Phase 3 - Feasibility tests
- Phase 4 - Full test program

Four methods of measurement were designed during the experimental research programme including:

1. Water depth measurement within the gutter detailed in Section 3.3
2. Pressure measurement at four locations within the horizontal carrier pipe detailed in Section 3.4
3. Flow rate measurement within the horizontal carrier pipe downstream of each gutter outlet using flourometry detailed in Section 3.5
4. Flow velocity measurement within the horizontal carrier pipe downstream of each gutter outlet using high speed image velocimetry detailed in Section 3.6.

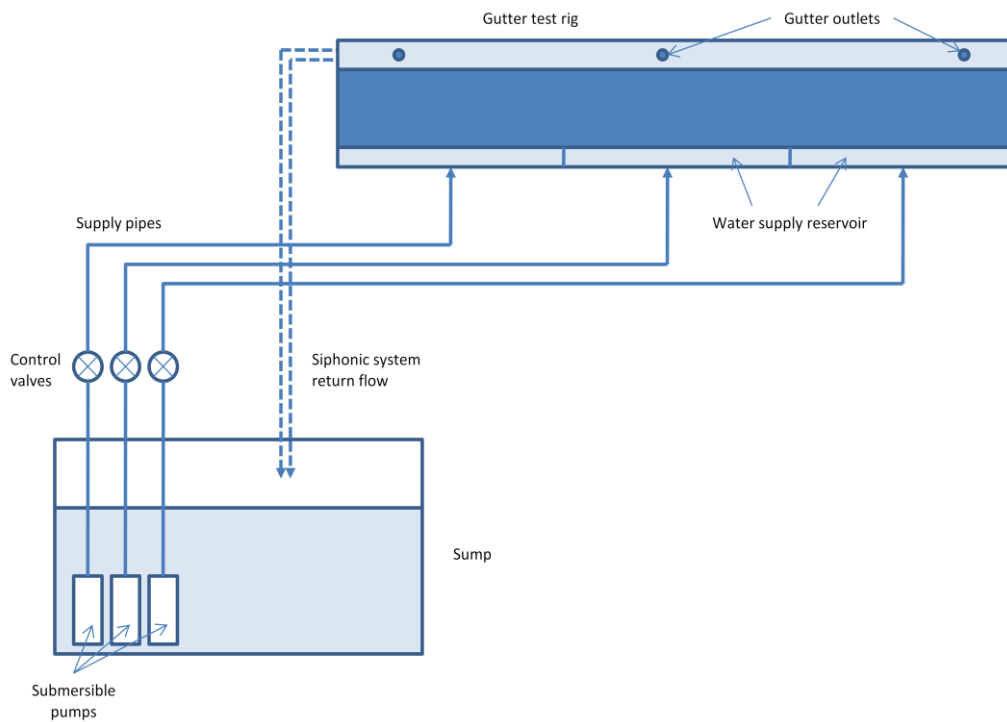
A series of feasibility tests were undertaken to independently assess, review and refine the methods of measurement. Steady flow tests were completed using three outlets within the gutter where flow rates in the range of 2 l/s to 14 l/s in 1 l/s increments were pumped into each water supply reservoir. This was equivalent to a total flow rate through the system of 6 l/s to 42 l/s in 3 l/s increments equivalent to 20% to 140% of the system design flow rate in 10% increments. It was important to examine and understand the hydraulic performance over this flow range as siphonic systems predominantly perform at sub-prime conditions (Öngören and Materna 2006). Sub-prime in this study was regarded as a flow rate to the system less than the design flow rate of 30 l/s.

As part of the full test program, a series of 63 steady flow tests were completed using three outlets within the gutter. Tests were completed at an overall system flow rate of 6 l/s, 12 l/s, 18 l/s, 24 l/s, 30 l/s (design rate), 35.12 l/s (ultimate design) and 36 l/s. This was equivalent to 20%, 40%, 60%, 80%, 100%, 117.07% and 120% of the systems design flow rate respectively. The following data sets were collected simultaneously and analysed for each steady flow test:

1. System pressure measurement at four positions within the horizontal carrier pipe according to Section 3.4;
2. Flow rate measurement using flourometry at three positions within the horizontal carrier pipe according to Section 3.5; and
3. Images of the flow using high speed image velocimetry at three positions within the horizontal carrier pipe outlet according to Section 3.6.

### 3.1 Phase 1 - Enhancement and Configuration of the Experimental Test Facility

The full scale experimental test facility was positioned on the mezzanine roof of the structures laboratory of the Sir Frederick Mappin Building at the University of Sheffield. Figure 3.1 provides a schematic of the experimental test facility.

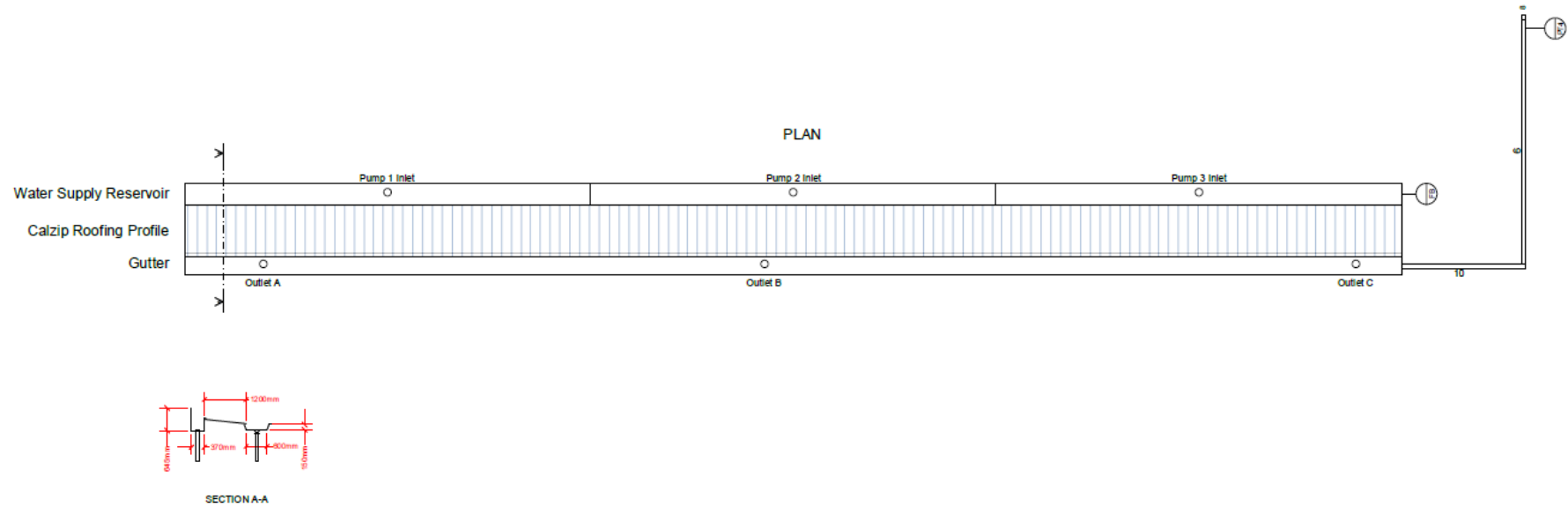


**Figure 3.1 Schematic of the Experimental Test Facility (not to scale)**

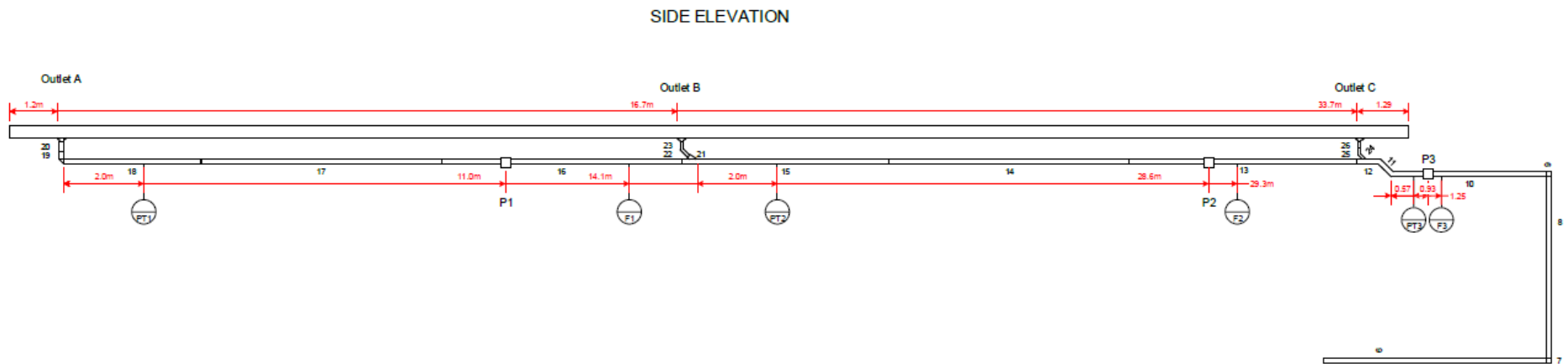
A detailed scale plan and side elevation of the experimental test facility is shown in Figure 3.2 and Figure 3.3 respectively. The configuration of the instrumentation used during this study is labelled and a key provided in Table 3.1. Details of the equipment, calibration and methodology used throughout this experimental research are described in Sections 3.3, 3.4, 3.5, 3.6 and 3.7 of this chapter and in Appendix 7.

**Table 3.1 Key to Figure 3.2 and Figure 3.3**

Reference	Description	Thesis Section
PT1, PT2, PT3, PT4	Pressure Transducers	3.4
F1, F2, F3, FB	Flourometers	3.5
P1, P2, P3	Camera positions	3.6

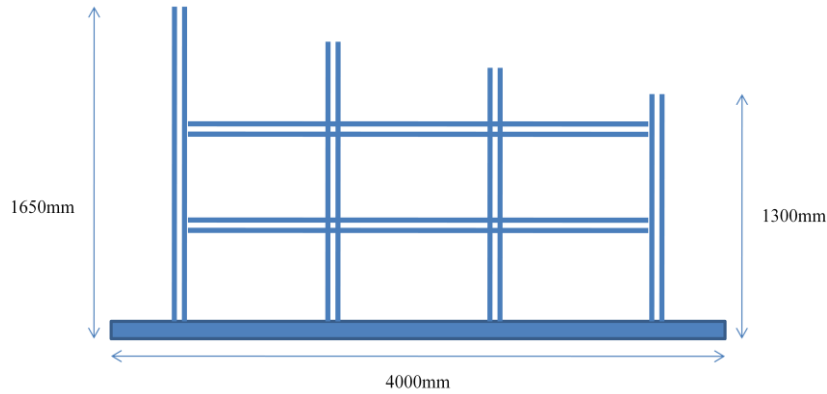


**Figure 3.2 Plan View of the Experimental Test Facility**



**Figure 3.3 Side Elevation of the Experimental Test Facility**

The test facility had a gutter length of 35 metres and a working head of 9.5 metres. The gutter, water supply box, roof section and pipework was fitted to a framework made of galvanised mild steel. Figure 3.4 shows the major dimensions of the framework.



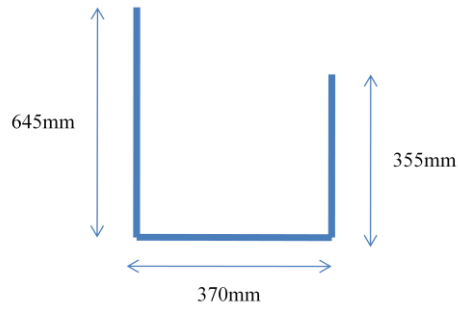
**Figure 3.4 Dimensions of the Test Facility Framework (not to scale)**

The supply of water to the test facility was transferred from a 272 m<sup>3</sup> sump via three independent, submersible pumps shown in Figure 3.5.



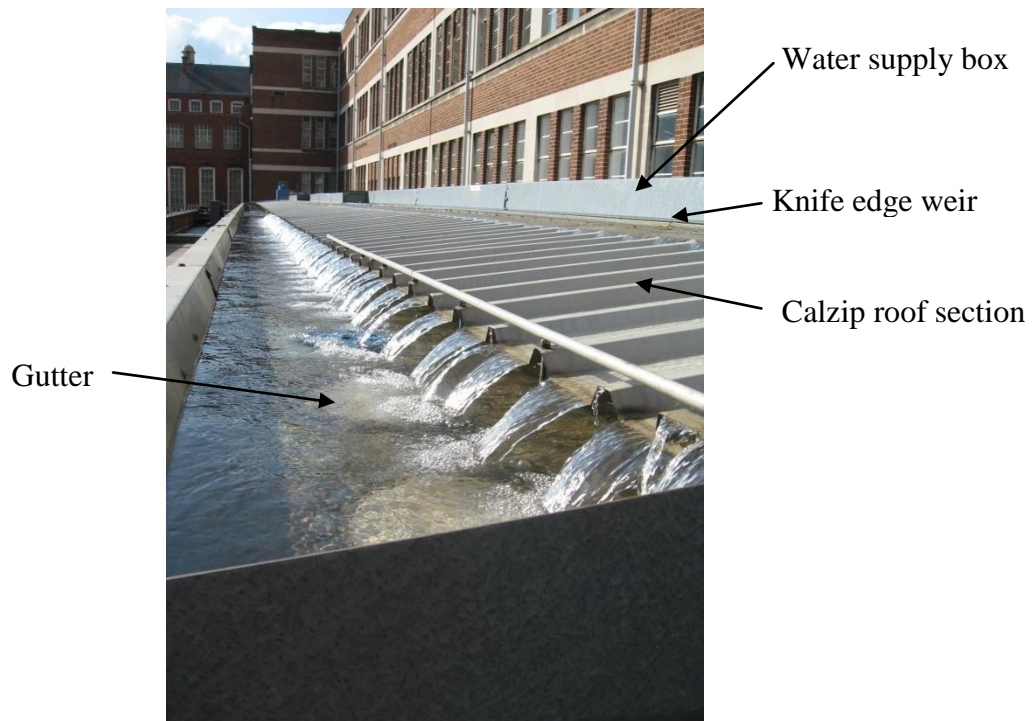
**Figure 3.5 Image of the Submersible Pumps within the Sump**

Each supply pipe was configured with a computer controlled butterfly valve that was controlled using real time control software. Water to the test facility was supplied from each supply pipe into three supply reservoirs (Figure 3.6) from where it spilled over a knife-edged weir and onto the Calzip roof section. The flow then discharged from the roof section into the gutter. This configuration is highlighted in Section A-A in Figure 3.2.



**Figure 3.6 Dimensions of the Test Facility Water Supply Reservoir (not to scale)**

Figure 3.7 shows the experimental test facility highlighting the water supply box, Calzip roof section and gutter.

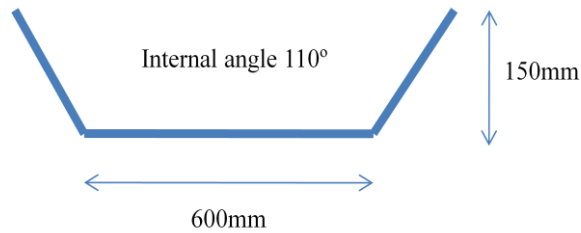


**Figure 3.7 Image of the Experimental Test Facility**

The gutter dimensions were 600 mm wide by 150 mm deep with a 1.2 metre wide roof section constructed from Calzip profiled roofing sheet at a pitch of  $6^\circ$ . Both the roof and gutter were fitted according to standard construction industry practice (Bramhall 2006).

Figure 3.8 shows the dimensions of the gutter within the experimental test facility.





**Figure 3.8 Dimensions of the Test Facility Gutter (not to scale)**

The sizing and configuration of the pipework was completed using commercially available software described in Appendix 1 - Commercial System Software Design. The system was designed as a primary system with three siphonic outlets fitted within the gutter sole shown in Figure 3.9. Design flow and operating pressure of the system was 30 l/s and -3.23 mH<sub>2</sub>O respectively with an ultimate flow of 35.12 l/s and ultimate operating pressure of -4.67 mH<sub>2</sub>O. The output from the design software relative to each outlet is summarised in Table 3.2.

**Table 3.2 Summary of Outlet Inflows and Reserves**

Outlet	Design inflow (l/s)	Reserve		Ultimate inflow (l/s)	Reserve	
		m	%		m	(%)
A	10.00	2.69	27	11.74	0.000	0
B	10.00	2.60	26	11.25	-0.025	0
C	10.00	2.70	27	12.14	0.024	0

Bramhall (2004) stated that:

"The design inflow value is assigned to each individual siphonic roof outlet determined from the basic design information on catchment areas and rainfall intensities, in accordance with the principles of BS EN 12056-3:2000 Gravity Drainage Inside Buildings."

The reserve values are how well the resistance presented by the piping network calculated by the software has been matched to the available working head. The pressure reserve is calculated according to the following equation:

$$\text{Pressure Reserve} = R_T - L$$

$$\text{Reserve Capacity (\%)} = 1 - \frac{L}{R_T} \times 100$$

Where  $R_T$  is the height of the outlet minus height of the discharge point and  $L$  is the sum of all losses between the outlet and the discharge point including the discharge loss.

This value is also an indication of how much extra rainwater can be accommodated by the system as designed.

The ultimate inflow utilises the fully available pressure reserve of the system design and represents the maximum capacity of the system design and the most severe operating condition.

### **3.1.1 Principles of the Commercially Available Siphonic Roof Drainage Design Software**

The commercially available software used to design the experimental test facility and define the flow and pressure through the system is based on basic fluid mechanics, specifically the Bernoulli Energy Equation and the Colebrook White Equation set out in Section 2.4.2.1. Bernoulli's energy equation is used to determine the change in flow conditions between two points in the system. The method uses the loss values obtained using the Colebrook White formula to predict the other parameters such as operational pressure. The Colebrook White formula is used to determine the loss factor for the flow through the piping network. The formula is solved using iterative techniques to establish the loss for each section of pipe. The losses through fittings are calculated by means of a loss factor applied to the kinetic energy of the flow through the fitting. The source of the empirical loss factors is not specified, however, Bramhall (2004) stated:

"The value for the loss factor are dependent upon the geometry of each component and may also vary on the severity of the change in velocity or direction. Loss factors have been derived from available text books, research documents, manufacturer's published data and validated as far as possible on test rigs."

The primary activity of the software is to determine the energy losses associated with the flow of water through the piping network. The principal objective of the design software is to match as closely as possible the resistance to flow provided by the pipe network (from outlet to discharge point) to the height of the building. The secondary objective is to produce the most cost effective design by minimising pipe diameters.

The design of any siphonic drainage system using this software commences at the discharge point and builds up the pipework system toward each of the gutter outlets. Design inflow is then assigned according to the design and specification of each gutter outlet. Following the selection of a suitable piping material, the software carries out a survey to determine initial available pipe diameters and suitable connections and fittings.

The software then calculates flow velocity, reserve head at each outlet, the hydraulic losses in each pipe and the system pressure at each node. Software checks ensure that at the design flow rate, velocity is greater than 1 m/s, the operating pressure is within acceptable limits (i.e. greater than -8 mH<sub>2</sub>O), there is a positive pressure reserve at each gutter outlet and that these reserves are within 1 metre or 10% of each other. Corrective changes can be made by a designer before the final design is produced and a technically acceptable solution is obtained.

The ultimate flow feature performs further iterations by incrementing the inflow and recalculating the system losses until the range of pressure reserve converges or the iteration limit set by the designer is exceeded. The condition of ultimate flow represents the maximum capacity of the system design and the most severe operating condition.

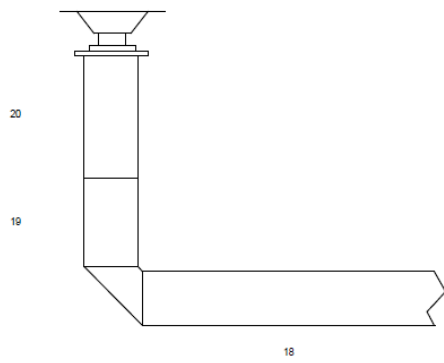
### **3.1.2 Gutter Outlets and Tailpipe Configuration**

Three commercially available siphonic drainage outlets supplied by a UK manufacturer shown in Figure 3.9 were installed within the gutter.

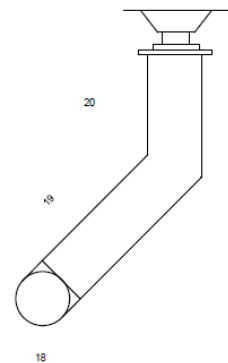


**Figure 3.9 Siphonic Outlet Installed within the Gutter**

Flow passing through each outlet (termed Outlet A, B and C) entered a tailpipe configuration specific to each outlet before joining a horizontal carrier pipe shown in more detail in Figure 3.10 to Figure 3.15. The tailpipes and carrier pipe were manufactured from annealed cast acrylic with a wall thickness of 5mm.



SIDE ELEVATION

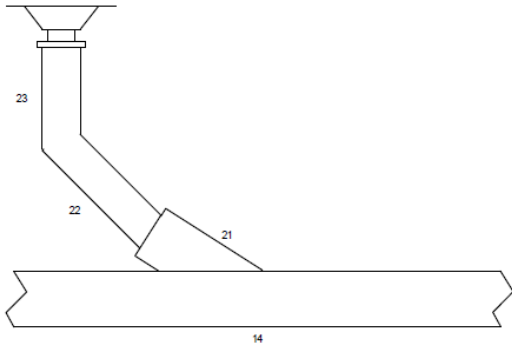


END ELEVATION

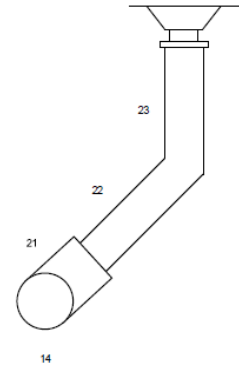
**Figure 3.10 Outlet A Tailpipe Design**



**Figure 3.11 Image of Outlet A Tailpipe Configuration**



SIDE ELEVATION

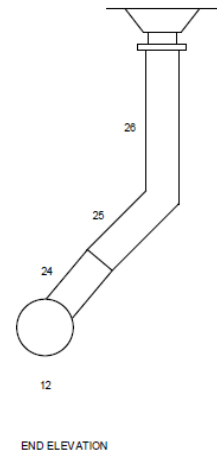
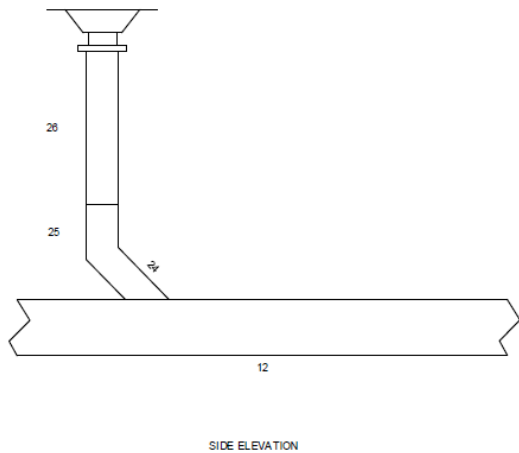


END ELEVATION

**Figure 3.12 Outlet B Tailpipe Design**



**Figure 3.13 Image of Outlet B Tailpipe Configuration**



**Figure 3.14 Outlet C Tailpipe Design**



**Figure 3.15 Image of Outlet C Tailpipe Configuration**

From the horizontal carrier pipe, flow entered a vertical pipe which returned to the sump via a volumetric measuring tank installed above the water supply reservoir. The measuring tank could only be used for calibration and verification when the water within the sump was not being used by others. When the measuring tank was not required, the drain was opened fully allowing flow to pass directly through the tank. During periods of high flow when the water could not drain quickly enough from the measuring tank, a high level overflow returned the water to the sump.

## 3.2 Phase 2 - Calibration of the Experimental Test Facility

### 3.2.1 Levelling of the Gutter Sole

The gutter sole was levelled using a Wild Heerbrugg NA20 optical level at thirteen points (every 2.9 metres) along the length of the gutter to an accuracy of  $\pm 1$  mm. At each of these points, the level of the gutter was recorded at the front, centre and rear of the gutter sole. Following an initial survey, modification to the height of the framework and consequently the gutter sole was completed using galvanised steel shims. Following this intervention, the gutter sole was measured four further times prior to the feasibility tests and full test program. A summary of the gutter sole measurements are shown in Table 3.3.

**Table 3.3 Summary of Gutter Sole Level Measurements**

	Intervention Test				
	Pre	Post 1	Post 2	Post 3	Post 4
Range (mm)	19	6	7	7	6
Standard deviation (mm)	4.3	1.6	1.6	2.0	1.3
Sample variance (mm)	18.9	2.5	2.5	4.0	1.8

Table 3.3 shows that following intervention, the level measurements within the gutter sole produced a mean standard deviation of 1.6 mm and sample variance between 1.8 mm and 4.0 mm.

### 3.2.2 Levelling of the Knife-Edged Weir

The knife-edge weir was constructed in 1.5 metre sections along the length of the test rig in-between the water supply reservoir and the Calzip roof section. The level of the weir was measured using the Wild Heerbrugg NA20 optical level at five points along the length of each 1.5 metre section and adjusted to a reference datum level to an accuracy of  $\pm 1$  mm.

### 3.2.3 Levelling of the Horizontal Carrier Pipe

The level of the crown of the carrier pipe was measured using the Wild Heerbrugg NA20 optical level at 1 metre intervals and adjusted to a reference datum level to an accuracy of  $\pm 1$  mm.

### 3.2.4 Calibration of the Butterfly Control Valve

It was necessary to control three butterfly valves to operate the systems to ensure an equal proportion of flow to the roof section of the experimental test facility from each water supply pipe.

The butterfly valve that controlled the flow rate to the test facility was calibrated by establishing the relationship between the angle of valve opening and the flow rate discharged to the rig measured volumetrically.

Before calibration, each valve was opened and closed across the full operational range in 10% increments. The three water supply reservoirs were then filled to ensure all pumped flow passed over the knife-edged weir and onto the roof section.

For each calibration test, the valve being calibrated was opened to a specified percentage and the flow left to establish for a minimum of 15 minutes. A drain within the measuring tank was then closed so no flow discharged to the sump. The time taken to fill a measured volume in the tank was repeated a minimum of four times on different days and the flow rate calculated from the average of the readings.

Following each calibration test, the valve was fully closed before being opened to the next increment. Each valve calibration was completed to fully open and then repeated in descending order.

The flow rate relative to each percentage opening was then plotted to determine the percentage opening required for each test flow rate.

A summary of the calibration results for the Feasibility Tests is shown in Table 3.4. The system flow rate was achieved from equal proportions of flow from each supply pipe. i.e. for a system flow rate of 6 l/s each supply pipe contributed 33.33% each or 2 l/s.



**Table 3.4 Summary of the Control Valve Calibration used for the Feasibility Tests**

Control Valve Opening (%)	Control Valve Opening (%)		
	Pump 1	Pump 2	Pump 3
5	N/A	0.86	N/A
6	N/A	1.06	N/A
8	N/A	2.02	N/A
10	N/A	3.28	N/A
12	0.70	4.79	0.65
15	1.32	6.74	1.67
18	1.97	8.40	2.62
20	2.53	9.43	3.53
25	4.09	12.13	4.92
30	5.68	15.10	6.83
35	7.57	18.52	9.44
40	9.43	20.98	11.95
45	11.23	22.82	14.50
50	13.03	24.03	16.80
55	14.65	25.71	19.35
60	15.74	27.05	21.54
70	18.03	28.01	23.40
80	19.78	28.69	25.04
90	21.37	28.31	26.26
100	22.70	N/A	N/A

Following the feasibility tests, Pump 2 failed and could not be repaired. The water supply box was modified to two reservoir sections by removing the divide in the water supply box that separated the supply from Pumps 2 and 3. Control valves 1 and 3 were recalibrated in accordance with the methodology described in this section of the thesis with Pump 1 supplying one third of the supply and Pump 3 two thirds. A summary of the calibration results for the Full Test Program is shown in Table 3.5 and detailed in Appendix 3.

**Table 3.5 Summary of the Control Valve Calibration used for the Full Test Program**

Control Valve Opening (%)	Flow Rate (l/s)	
	Pump 1	Pump 3
12	0.53	0.97
15	0.96	2.92
18	1.41	N/A
20	1.79	5.98
25	3.12	8.75
30	4.44	11.43
35	5.51	14.75
40	7.38	18.00
45	8.95	21.55
50	10.36	23.97
55	11.82	N/A
60	13.25	26.35
70	14.79	28.62
80	16.49	30.58

### 3.3 Water Depth Measurement within the Gutter

Water depth measurements within the gutter were made using a digital depth micrometer fitted to a frame that could be moved along the gutter shown in Figure 3.16.



Figure 3.16 Digital Depth Micrometer and Frame

#### 3.3.1 Calibration of the Digital Depth Micrometer

Before use, the micrometer was referenced to the same datum point and the water depth and gutter level in relation to this datum recorded.

#### 3.3.2 Methodology

Water depth measurements were made 150 mm either side of each outlet in accordance with Section B.2.6 of BS 8490:2007 Guide to Siphonic Roof Drainage Systems (BSI 2007). Two further depth measurements were made at 50 mm around the perimeter of the outlet to monitor the effect of draw down. Water depth measurements either side of the outlet are shown in Figure 3.17.

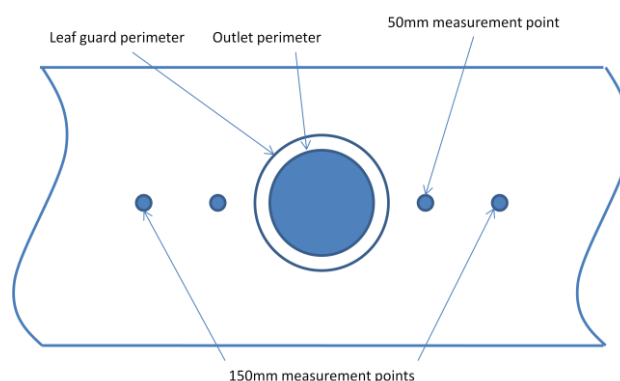
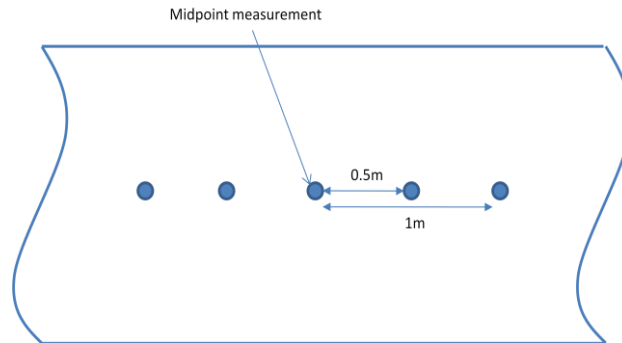


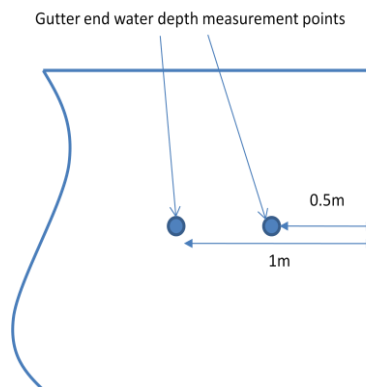
Figure 3.17 Plan View of Gutter Measurement Points (not to scale)

Five water depth measurements were also made between each outlet including the midpoint, 0.5 metres and 1 metre either side of the midpoint according to Figure 3.18. This was to measure the maximum depth of water within the gutter between the outlets.



**Figure 3.18 Plan View of Outlet Midpoint Water Depth Measurements (not to scale)**

Two further water depth measurements were also made 0.5 metres and 1 metre from each gutter end shown in Figure 3.19. This was to completed to understand the water depth profile along the gutter and the effect of changes in flow rate relative to gutter position.



**Figure 3.19 Plan View of Gutter End Water Depth Measurement Points (not to scale)**

### 3.3.3 Summary

Water depth measurements, recorded manually, were completed during the feasibility tests and were used to understand the hydraulic profile of the flow within the gutter relative to the system flow rate. This method of measurement was not included as part of the full test program as it could not be undertaken simultaneously when combined with the other methods of measurement. To achieve continuous water depth measurement within the gutter, a series of pressure transducers could have been used and integrated with the data acquisition system. This would have provided a more refined and detailed data set for analysis and comparison. However these measurements provided an accurate measure of the water depth during the feasibility tests.

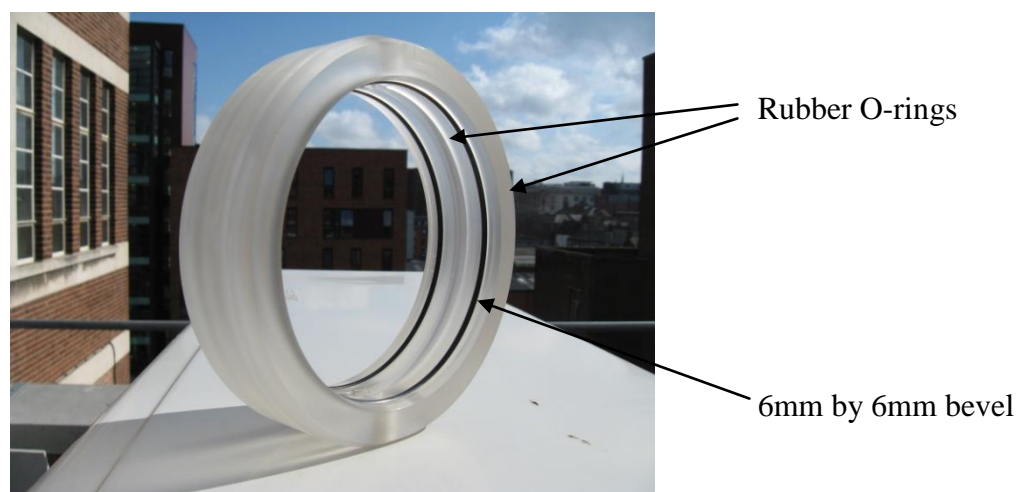
### 3.4 Pressure Measurement within the Horizontal Carrier Pipe

Four Gems 2200 series pressure transducers with an analogue 4-20mA output were installed within the horizontal carrier pipe to measure pressure with a range of -1 Bar to 0.6 Bar (equivalent to -10 mH<sub>2</sub>O to 6 mH<sub>2</sub>O) with an accuracy of 0.15%, equivalent to 0.0024 Bar or 2.4 cm. Further details on the pressure transducers used during this study is included in Appendix 7.

The signal from each pressure transducer was recorded using Labview software at a frequency of 5 Hz through a National Instruments SC-2345 Data Acquisition Module and the transducers excited using a Kingshill stabilised power supply set at 10 Amps. Calibration of the pressure transducers is described in Section 3.4.1 and included in more detail in Appendix 4 - Pressure Transducer Calibration Results.

Three transducers were positioned downstream of where each tail pipe entered the horizontal carrier pipe (termed PT1, PT2 and PT3). The fourth transducer was installed at the end of the horizontal carrier pipe, termed PT4. Within the horizontal carrier pipe the pressure transducers were positioned 2 metres downstream of where the tail pipe entered the horizontal carrier pipe. The transducer after the third tail pipe was positioned 2 metres after a short change in the configuration of the carrier pipe. The position of each pressure transducer within the horizontal carrier pipe was selected to provide a minimum of fifteen pipe diameters downstream of any fitting to reduce the risk of high pressure fluctuations closer to any changes in the pipework. The configuration of the pressure transducers within the experimental test facility are shown in Figure 3.2 and Figure 3.3 at the beginning of this chapter.

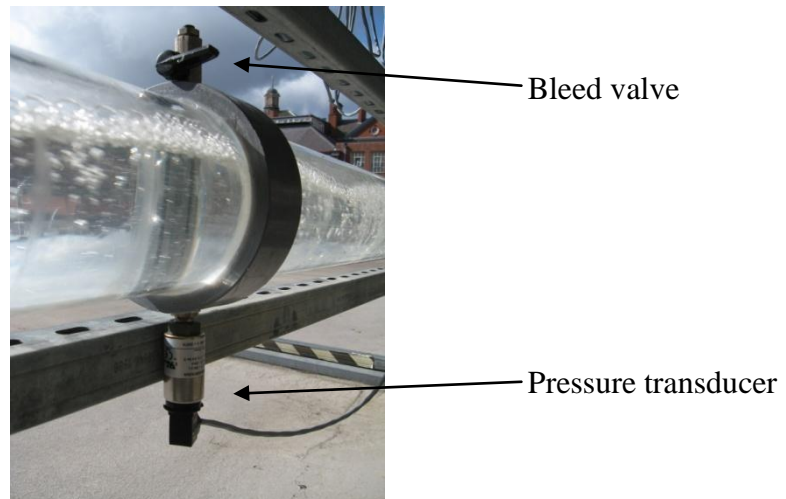
To record average pressure around the circumference of the pipe, a collar was designed and manufactured shown in Figure 3.20.



**Figure 3.20 The Pressure Transducer Collar Pre-Installation**

The collar featured two rubber o-rings either side of a 6 mm by 6 mm bevel. Four equidistant 4 mm holes were drilled into the carrier pipe at the crown, invert and horizontal sides of the pipe wall and the collar slid over the pipe so the holes were positioned in the bevel. Sealant was then applied between the edge of the collar and the carrier pipe to create an airtight seal.

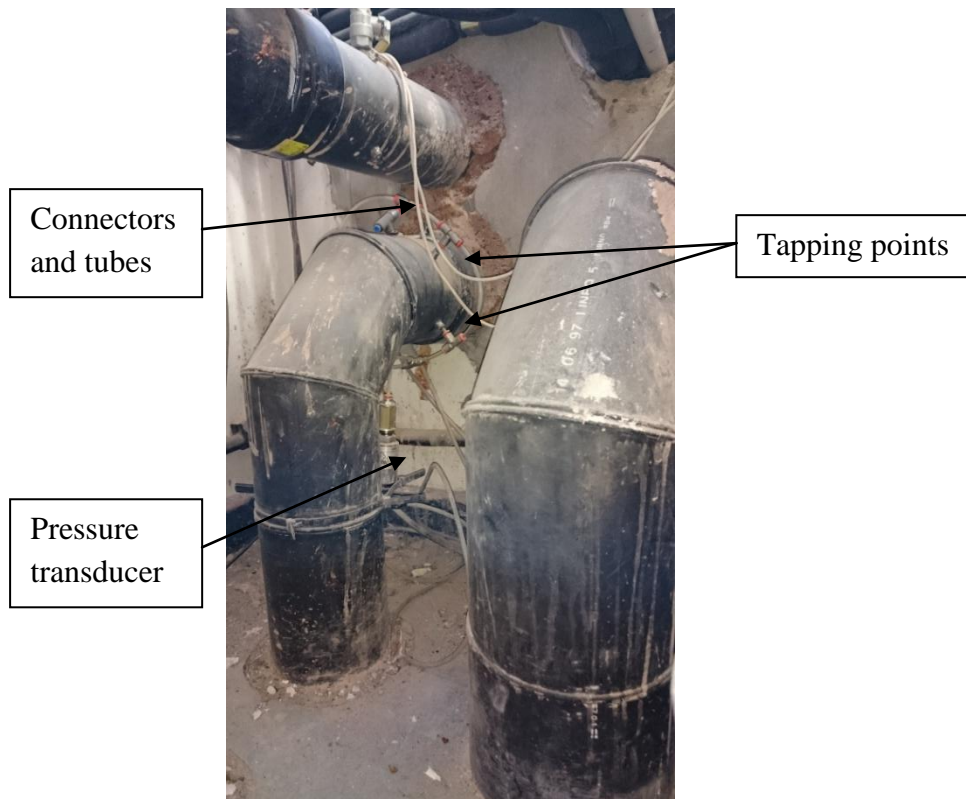
Each pressure transducer was positioned at the invert of the collar and a simple bleed valve attached to the crown shown in Figure 3.21. The bleed valve was incorporated within the design to enable the removal of any air blocks should they occur.



**Figure 3.21 Pressure Transducer Collar In-Situ**

This configuration enabled the pressure around the circumference of the carrier pipe to be measured via the four holes and the bevel within the collar.

The pressure transducer positioned immediately before the vertical downpipe (PT4) had a different measurement configuration due to access limitations. Rather than a collar, four equidistant holes were drilled through the horizontal carrier pipe to provide tapping points. A series of tubes and connectors were then configured to provide a common circuit all the way around the carrier pipe. The pressure transducer was then fitted to this circuit to allow the measurement of pressure from these four tapping points. The configuration of the installed pressure transducer PT4 is shown in Figure 3.22.

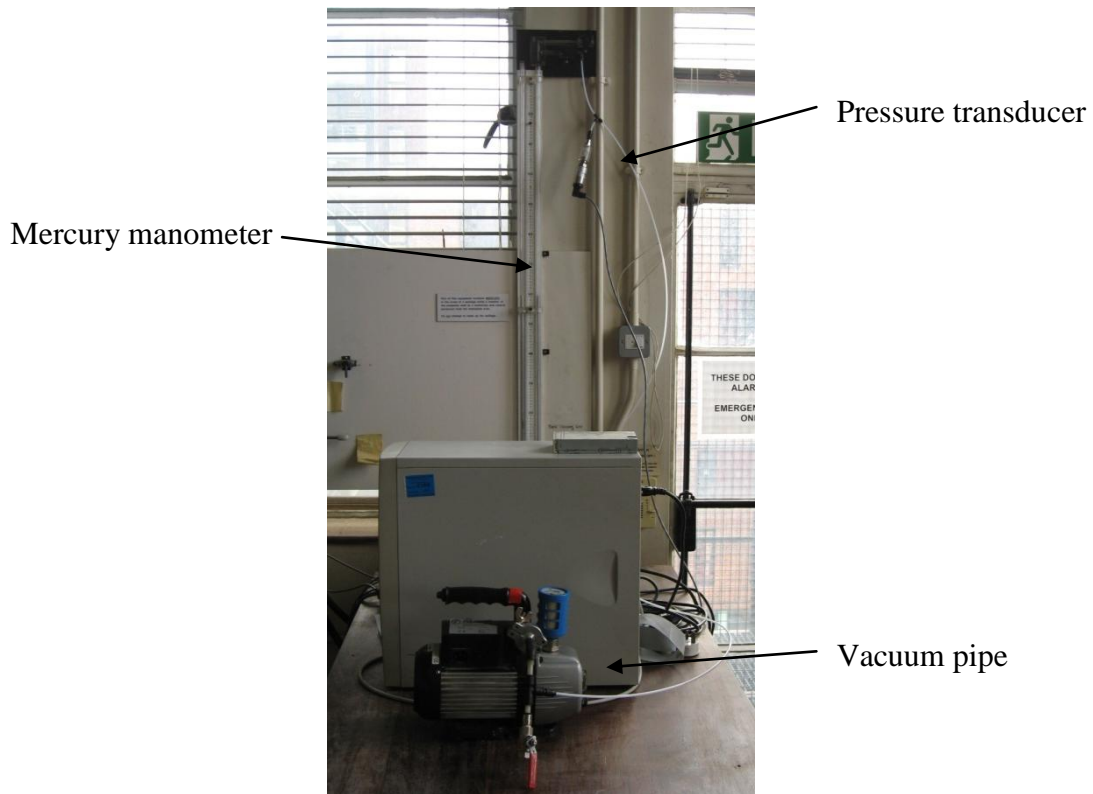


**Figure 3.22 Pressure Transducer PT4 Configuration**

### **3.4.1 Calibration of the Pressure Transducers**

The pressure transducers were calibrated over a positive and negative range separately. For the positive range, each transducer was calibrated using a Budenberg Dead Weight Tester supplied with nitrogen to a maximum of 60 KPa in ascending and descending increments of 0, 10, 15, 20, 25, 30, 35, 40, 45, 50, 55 and 60 KPa. For each increment the amplitude generated by the pressure transducer was recorded at a frequency of 5 Hz for a ten second period and an average taken. The frequency was used to match the frequency of data collection used during the Feasibility Tests and Full Test Program. The calibration methodology was repeated three times for each pressure transducer.

For the negative range, each pressure transducer was calibrated using a vacuum pump and mercury manometer. The configuration of the calibration apparatus is shown in Figure 3.23.



**Figure 3.23 Configuration of the Pressure Transducer Negative Range Calibration Apparatus**

Six increments of decreasing pressure were applied to each pressure transducer from 0 KPa to a maximum negative pressure of 100 KPa and then back up to 0 KPa. For each increment the amplitude generated by the pressure transducer was recorded at a frequency of 10 Hz for a ten second period and an average of the readings taken. This methodology was repeated three times for each pressure transducer.

The calibration results were plotted for each pressure transducer with pressure (KPa) against amplitude (mA). The amplitude generated by each pressure transducer only remained linear to a maximum positive pressure of 50 KPa (equivalent to 5 mH<sub>2</sub>O). Hence, the calibration results in excess of 50 KPa were not considered.

The calibration plots for each pressure transducer are set out in Appendix 4 - Pressure Transducer Calibration Results and Table 3.6 provides a summary of the results.

**Table 3.6 Pressure Transducer Calibration Summary for the Range -10 m to 5 m H<sub>2</sub>O**

Pressure transducer	Equation	Regression
PT1	$y = 0.00010x + 0.01404$	0.99999
PT2	$y = 0.00010x + 0.01404$	0.99988
PT3	$y = 0.00010x + 0.01404$	0.99934
PT4	$y = 0.00010x + 0.01403$	0.99997

These relationships were used throughout the feasibility tests and full test program for the analysis of the recorded pressure data.

### **3.4.2 Summary**

Refinement of the pressure measurement technique during the feasibility tests showed that at the upstream monitoring position (PT1), there was minimal change in pressure irrespective of the flow rate through the system. A maximum pressure of  $-0.2 \text{ mH}_2\text{O}$  was recorded during the tests completed at 21 l/s and 30 l/s. The system pressure after the second tailpipe (PT2) steadily decreased from a positive pressure of  $1 \text{ mH}_2\text{O}$  to less than  $0.1 \text{ mH}_2\text{O}$  at test flow rates greater than 36 l/s. The pressure transducer located downstream of the third tailpipe (PT3) showed a steady pressure decrease throughout the tests from  $-0.22 \text{ mH}_2\text{O}$  at 9 l/s to  $-2.59 \text{ mH}_2\text{O}$  at 42 l/s. The transducer located at the top of the downpipe (PT4) showed the most significant change in system pressure. The results decreased from  $-0.35 \text{ mH}_2\text{O}$  at 9 l/s to  $-4.44 \text{ mH}_2\text{O}$  at 42 l/s.

It was concluded from the feasibility tests that the method of pressure measurement and data resolution was appropriate for the experimental research and full test program.



### **3.5 Flow Rate Measurement within the Horizontal Carrier Pipe using Fluorometry**

To measure the flow rate through within the horizontal carrier pipe a novel approach using a fluorescein tracer was used to measure the flow component through each outlet. Three Turner Designs Cyclops-7 submersible fluorometers (termed F1, F2 and F3) were fitted within the horizontal carrier pipe such that the sensor was exposed to the main body of the flow, but with a minimum of disruption. A further fluorometer was fitted within the supply reservoir to record the background solute levels (termed FB). The configuration of the fluorometers within the experimental test facility are shown in Figure 3.2 and Figure 3.3 at the beginning of this chapter.

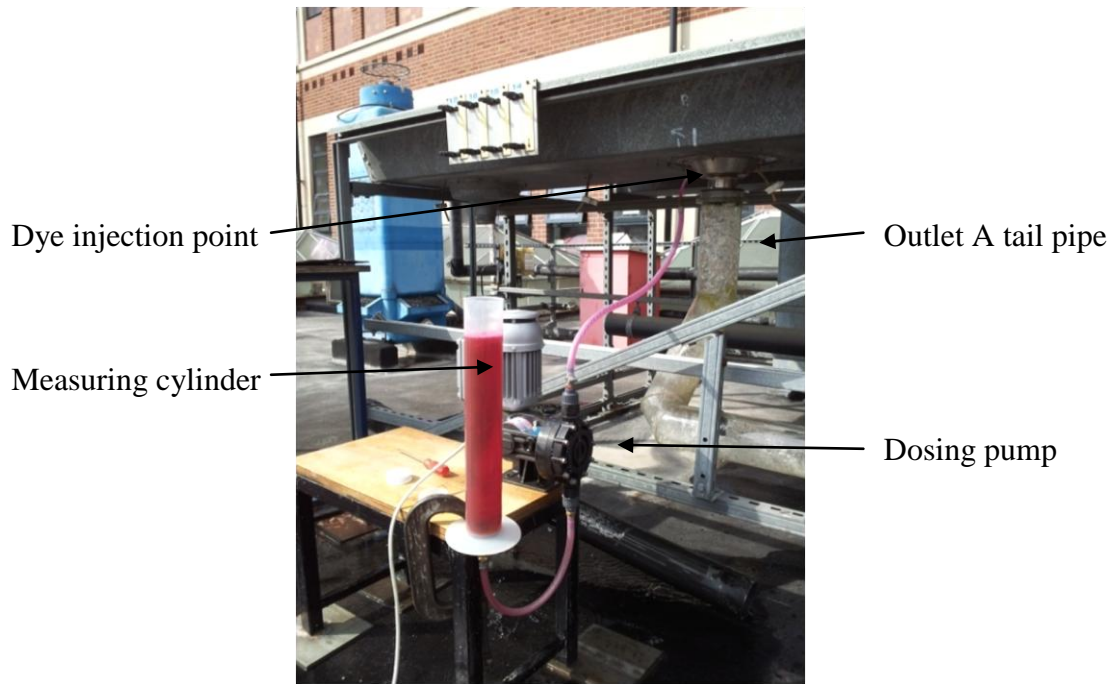
The fluorometers were able to detect a change in solute concentration of Rhodamine WT with a sensitivity of 4 ppb excited using a Kingshill stabilised power supply set at 12 Amps. Power to the fluorometers was maintained at this level to ensure all data collected was relative. Each fluorometer was operated using a gain setting of x10 to achieve the required sensitivity, range and resolution. The signal from each fluorometer was recorded using Labview software at a frequency of 5 Hz through a National Instruments SC-2345 Data Acquisition Module.

The horizontal pipe section immediately upstream, downstream and around fluorometers F1, F2 and F3 was covered in blackout material to eliminate any ambient light affecting the voltage response.

A wire mesh frame and cover was placed over the fluorometer installed within the supply reservoir (FB) 50mm above the sensor. This allowed the fluorometer to be exposed to the water but eliminated the ambient light affecting the voltage response.

A temperature probe with an accuracy of  $\pm 0.3^{\circ}\text{C}$  was used within the supply reservoir to allow for temperature correction required as part of the data analysis. Three measurements were made during each test and an average taken to determine the value.

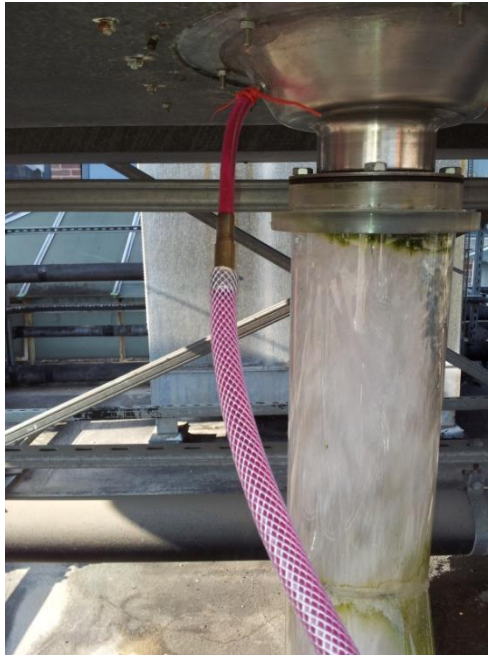
For the feasibility tests, Rhodamine WT dye was injected into the outlet bowl of the upstream outlet using a dosing pump. The configuration of the apparatus is shown in Figure 3.24.



**Figure 3.24 Feasibility Tests Dye Injection Apparatus Configuration**

An OBL MB.101 PP controlled volume reciprocating dosing pump was used to inject the dye from the measuring cylinder into the outlet bowl. Detailed information on the pump is included in Appendix 7. Adjustment of the pump diaphragm stroke rate was regulated using a control valve and the time taken to pump dye from the measuring cylinder into the outlet was used to calculate the dye injection rate. The concentration of Rhodamine and dye injection rate was refined so that the upstream flourometer was generating a signal as close to 4 volts as possible. This ensured that the diluted concentration of Rhodamine measured by the downstream flourometers was sufficient to generate a voltage response greater than 0.5 volts.

The dye was injected directly into the outlet bowl (Figure 3.25) so the turbulence of the flow passing through the outlet and tail pipe configuration mixed the dye as much as possible before reaching the first flourometer 14.12 metres (equivalent to 120 diameters) along the length of the horizontal carrier pipe.



**Figure 3.25 Dye Injection into Outlet A**

### **3.5.1 Calibration of the Fluorimeters**

The fluourometers were calibrated using a known volume of deionised water with increasing measured volumes of Rhodamine WT at a concentration of  $5 \times 10^{-4}$ . The fluourometers were calibrated to each new batch of solution according to the following methodology:

1. The fluourometers were placed within a black bucket and positioned at least 50 mm from the base and side;
2. Black lining material was then placed over the fluourometers to shield any ambient light;
3. As the Rhodamine was added to the bucket, the solution was stirred with a glass rod to ensure mixing;
4. The water temperature was recorded at each concentration;
5. The voltage response from each fluourometer was recorded over a ten second period at a frequency of 5 Hz;
6. The mean voltage value was then plotted against the Rhodamine WT concentration.

The fluourometer calibration results are summarised in Table 3.7 and described in more detail in Appendix 5.

**Table 3.7 Summary of the Fluorometer Calibration Results**

Date/Ref	F1		F2		F3		FB	
	Equation	Regression	Equation	Regression	Equation	Regression	Equation	Regression
Feasibility Tests	y = 1.22E+06x + 0.0032	0.9994	y = 1.20E+06x + 0.0033	0.9998	y = 1.15E+06x + 0.0041	0.9998	y = 1.14E+06x + 0.0032	0.9999
10.09.13	y = 1.27E+06x + 0.0083	0.9994	y = 1.24E+06x + 0.0081	0.9995	y = 1.27E+06x + 0.0091	0.9995	y = 1.33E+06x + 0.0087	0.9995
08.10.13	y = 1.21E+06x + 0.0077	0.9969	y = 1.24E+06x + 0.0078	0.9990	y = 1.25E+06x + 0.0085	0.9949	y = 1.22E+06x + 0.0090	0.9865
09.12.13	y = 1.29E+06x + 0.0115	0.9991	y = 1.31E+06x + 0.0125	0.9981	y = 1.36E+06x + 0.0134	0.9979	y = 1.31E+06x + 0.0138	0.9958

It was concluded that the fluorometers could be used with confidence to measure the changes in Rhodamine concentration observed in the experimental programme. These relationships were used throughout the feasibility tests and full test program for the measurement and analysis of flow rate within the horizontal carrier pipe.

### 3.5.2 Methodology

For each feasibility test, 1 litre of Rhodamine WT dye at a concentration of  $5 \times 10^{-4}$  ( $C_{in}$ ) was pumped from the measuring cylinder into the bowl of the upstream outlet. The dye injection rate ( $q_{in}$ ) was measured volumetrically recording the time taken to dose every 100 ml of dye. The dye injection rate was adjusted so that the data recorded by the upstream fluorometer (F1) was as close to 4 volts as possible. This ensured a response from the fluorometer downstream of Outlet C (F3) of no less than 0.5 volts. It was critical that all fluorometers were continuously detecting the dye being injected into the system otherwise the data would not be representative of the relative dilution.

The data recorded by each fluorometer was first resolved to a reference temperature of 20°C according to the following calculation (Wilson, 1968):

$$F_r = F_s e^{[n(T_s - T_r)]}$$

Where  $F_r$  is the calculated fluorescent reading at the reference temperature,  $F_s$  is the observed fluorescence reading of the sample at the time of reading the sample temperature,  $e$  is the base of natural log,  $n$  is the temperature coefficient of the dye used (0.026 for Rhodamine WT),  $T_s$  is the sample temperature at the time of reading  $F_s$  and  $T_r$  is the reference temperature.

The appropriate calibration was then applied to the resolved data values to calculate the concentration of dye at each measurement point.

The position of each of the flourometers within the test facility was selected to assess the flow rate through each outlet based on the measured dilution of the Rhodamine dye according to the following equation:

$$q_{in} C_{in} = Q_{F1} C_{F1}$$

Where  $q_{in}$  is the dye injection rate,  $C_{in}$  the concentration of dye injected,  $Q_{F1}$  the flow rate at flourometer point 1 and  $C_{F1}$  is the concentration of dye at F1. This equation can be rearranged to:

$$Q_{F1} = \frac{q_{in} C_{in}}{C_{F1}}$$

The background solute level was measured to accurately determine the flow rate at the location of each flourometer:

$$Q_{F1} = \frac{q_{in} C_{in}}{C_{F1} - C_{FB}}$$

$$Q_{F2} = \frac{q_{in} C_{in}}{C_{F2} - C_{FB}}$$

$$Q_{F3} = \frac{q_{in} C_{in}}{C_{F3} - C_{FB}}$$

Where  $C_{FB}$  the concentration of the background solute level,  $C_{F2}$  is the concentration of dye at F2,  $C_{F3}$  is the concentration of dye at F3,  $Q_{F2}$  the flow rate at flourometer point 2 and  $Q_{F3}$  the flow rate at flourometer point 3.

A series of feasibility tests were completed at each flow rate to refine the dye injection method. This was necessary to ensure that a response from each flourometer could be achieved over the range of flow rates using the selected concentration of dye and dye injection rate. The dye injection rate had to be regulated carefully to ensure that there was a measurable response from the downstream flourometer (F3) without the upstream flourometer (F1) becoming saturated.

For one feasibility test at each system flow rate, the response from each flourometer was observed and data recorded. This was completed to develop the analysis process using the equations set out in this section. The results from the analysis were then used to compare the mass balance measured using flourometry to the system flow rate pumped to the system using the control valve calibration. The mass balance was using flourometry was determined by the values measured by the downstream flourometer (F3) and hence the overall system flow passing through each outlet and tail pipe configuration. This was necessary to establish the suitability and accuracy of this method of flow measurement.

Table 3.8 shows the flow measured by the downstream flourometer (F3) for a minimum of 200 seconds and a volumetric comparison to the calibrated pumped flow to the test facility for each feasibility test flow rate.

**Table 3.8 Mass Balance Measured using Flourometry**

Flow Test (l/s)	Measured flow at F3 (l/s)	Volumetric Difference (%)
9	9.25	2.78
15	15.2	1.33
18	18.1	0.56
21	21.1	0.48
30	30.1	0.33
33	31.7	-3.94
36	34.9	-3.06
39	39.0	0.00
42	42.0	0.00

### 3.5.3 Summary

To measure the flow rate within the horizontal carrier pipe novel approach using flourometry was used to measure the flow component through each outlet. A series of feasibility tests were completed at each flow rate to refine the dye injection method. This was necessary to ensure that a response from each flourometer could be achieved over the range of flow rates using a known concentration of dye and dye injection rate.

Total flow through the system was measured using flourometry downstream of Outlet C (F3) and for all feasibility tests the measured flows were within 4% of the volumetrically calibrated flow input. It was concluded from the refinement of this method and the results from the feasibility tests that this approach to continuous flow measurement within the horizontal carrier pipe was appropriate, robust and accurate. Hence this methodology provided an appropriate approach to measure the overall system flow rate and individual flow component through each outlet.

### 3.6 Flow Velocity Measurement within the Horizontal Carrier Pipe using High Speed Image Velocimetry

The design and configuration of the experimental test facility provided the opportunity to utilise high speed image velocimetry as a method to measure flow velocity within the horizontal carrier pipe.

The feasibility tests were necessary to examine the quality of image produced within the test environment and the flow velocity results following particle image velocimetry (PIV) analysis. These tests were completed using a Photron Fastcam XLR high speed camera to record images of the flow within the horizontal carrier pipe.

To minimise distortion of the images as a result of the curvature of the pipe, a 240mm by 240mm glass fronted water box was designed, manufactured and installed at three points along the length of the carrier pipe (termed P1, P2 and P3). The water boxes were positioned 11m, 14.52m and 1.91m downstream of Outlets A, B and C respectively shown in Figure 3.2 and Figure 3.3 at the beginning of this chapter.

The position of each water box along the length of the horizontal carrier pipe was selected to be a minimum of 15 pipe diameters downstream and 11 diameters upstream of any fitting to reduce the effect of turbulence associated with changes in the horizontal pipework configuration. The position of P1 and P2 relative to any changes was far in excess of this. The position of P3 was much more limited due to the carrier pipe configuration and available access to instrument the experimental test facility.

The configuration of the apparatus is shown in Figure 3.26.



Figure 3.26 Image of the Camera Configuration

To enable PIV analysis to be completed, flow through the respective outlet was seeded with inert, white, plastic, spherical, particles with a diameter of 150  $\mu\text{m}$  and density of 1000  $\text{kg/m}^3$  detailed in Appendix 7. The particles were a critical part of the PIV system and were selected due to their size and density to match the fluid properties as closely as possible. Distribution and visibility of the particles throughout each image was essential to enable the PIV software to be successful.

Blackout material was fitted to the section of horizontal carrier pipe behind each water box to provide sufficient contrast for the particle seeding to be seen. Depending on the ambient light conditions, additional lighting shown in Figure 3.26 was used to highlight the seeding particles and create the quality of image required for PIV analysis.

For the full scale test program the Photon Fastcam was no longer available. A Southern Vision Systems Gigaview high speed camera was used with TCP/IP gigabit ethernet interface according to the following settings:

- Frame size (pixels) – 1280 x 1024
- Frame rate (fps) – 532
- Record time (s) – 10

Further information on the camera used during the Full Test Program is included in Appendix 7.

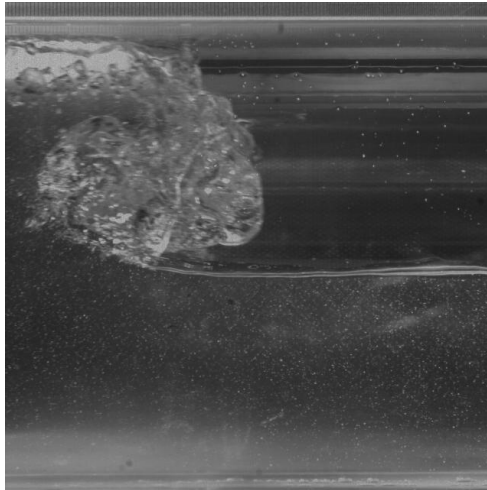
The image data was collected using an on-board memory card that was transferred to a computer following each test. This imaging system provided a reduced image frequency at the same resolution and quality of 532 Hz compared to 2000 Hz but an increased recording time of 10 seconds.

### **3.6.1 Methodology**

Prior to testing, the glass fronted water box (P1, P2 or P3) was cleaned and filled with water and a graduated steel rule placed along the crown of the pipe. The rule was required to be able to scale the images for analysis. The camera was positioned in front of the water box and the image field adjusted to include the full cross-section of the pipe focussed on the steel rule.

For each test, the seeding particles were added to the flow within the gutter immediately around the outlet directly upstream of the camera measurement position. For example when the camera was positioned at P1, the particles were added to the flow within the gutter surrounding Outlet A. Sufficient particles were applied to the system to ensure that the images remained seeded for the duration of the image measurement period. The quantity increased relative to the flow through the system. During the feasibility tests images were recorded by the camera using a sophisticated data acquisition system at a frequency of 2000 Hz and exported as .jpeg files. An example is shown in Figure 3.27.

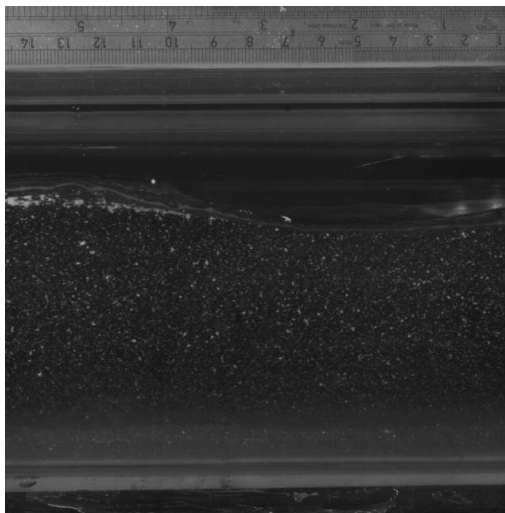




**Figure 3.27 Image of the Seeded Flow within the Horizontal Carrier Pipe**

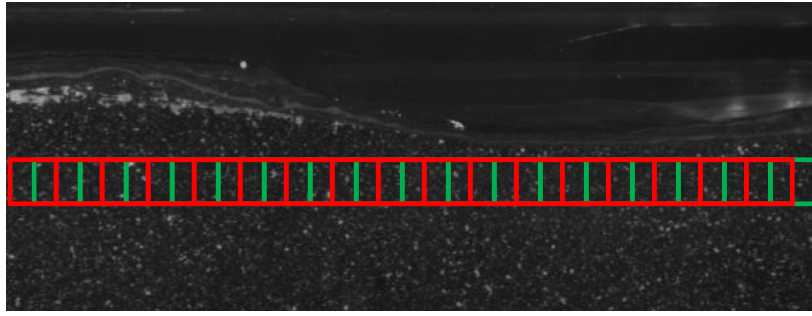
Analysis of the images collected during the feasibility tests was completed according to the following methodology:

10 consecutive images representing 1/200th of a second were selected and imported into the Dantec PIV software. An example is shown in Figure 3.28.



**Figure 3.28 Image used for PIV Analysis**

Each image was divided into 32 pixel interrogation areas with an overlap of 50% to provide the best resolution for the size of image and concentration of seeded particles. An example is shown in Figure 3.29 with the red boxes showing the overlap with the green boxes.



**Figure 3.29 PIV Analysis Interrogation Areas (not to scale)**

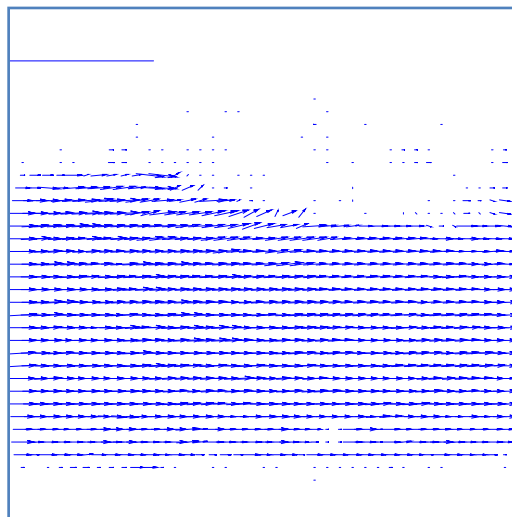
Cross-correlation analysis of the particle pattern within each interrogation area was then completed between each sequential image.

The velocity of the particle pattern between each interrogation area was determined according to the following simplified equation:

$$V = \frac{\sqrt{\Delta x^2 + \Delta y^2}}{\Delta t}$$

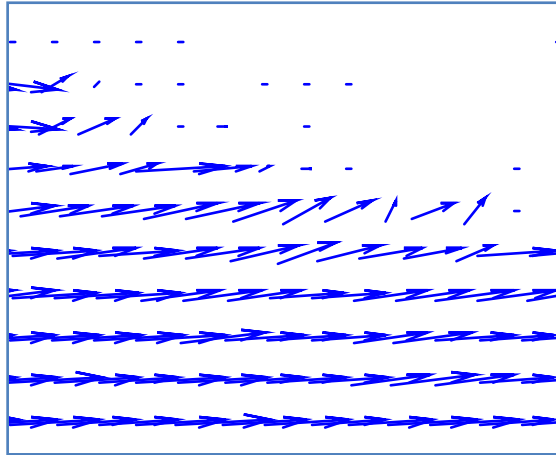
Where  $V$  is the velocity (mm/s),  $x$  is the length of travel of the particle pattern along the x axis (mm),  $y$  is the length of travel of the particle pattern along the y axis (mm) and  $t$  is the time period between each sequential image (s).

This produced nine vector analysis plots for each set of 10 images. An example of a vector analysis plot relative to the image shown in Figure 3.28 is shown in Figure 3.30.



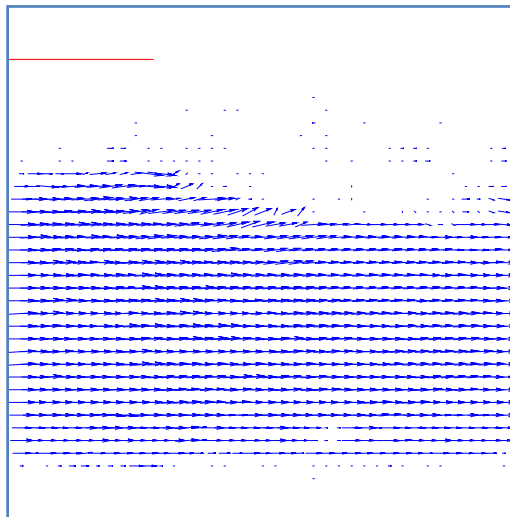
**Figure 3.30 Example of a Vector Analysis Plot**

A more detailed view of Figure 3.30 demonstrating the overlapping interrogation areas is shown in Figure 3.31.



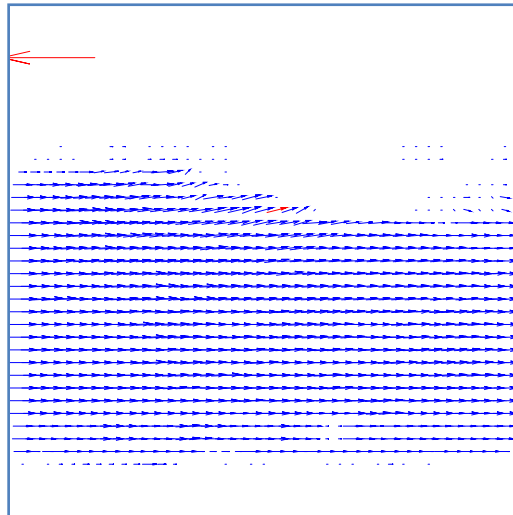
**Figure 3.31 Detailed Image of a Vector Analysis Plot**

Range validation was applied to each vector analysis plot to eliminate spurious readings detected outside of the flow field. An example is shown in Figure 3.32 where the red line demonstrates a spurious velocity value identified by the range validation.



**Figure 3.32 Vector Analysis Plot with Range Validation**

Vector statistics were then applied to produce an average velocity within each interrogation area for the series of 9 vector analysis plots. An example is shown in Figure 3.33.



**Figure 3.33 PIV Vector Statistics Plot**

The average velocity data from each interrogation area was then exported for analysis. The average velocity based on the velocity results from each interrogation area from the 9 validated, vector analysis plots was calculated. Any data point less than 0.01 m/s was excluded from the average so that stationary objects within the image did not skew the results.

This value represented the average velocity for a 1/200th of a second time period. This process was repeated for every 1,000 images to determine an average velocity value for each 1/200th of a second at 0.5 second intervals based on 2,000 frames per second. These data points were then plotted to provide time series data for the period that images were collected.

### **3.6.2 Summary**

The design and configuration of the experimental test facility provided the opportunity to utilise high speed image velocimetry as a method to measure flow velocity within the horizontal carrier pipe.

The feasibility tests were necessary to examine the quality of image produced within the test environment and the flow velocity results following particle image velocimetry (PIV) analysis.

The images captured during the feasibility tests were of sufficient quality to enable PIV analysis to be successfully completed. The application of the methodology generated time series data for approximately 7 seconds limited by the available storage capacity of the data acquisition system.

It was concluded from the refinement of the image capture methodology, results and analysis from the feasibility tests that this approach to continuous measurement of the flow velocity within the horizontal carrier pipe was also appropriate and accurate. However, the limitation

of this method and equipment used was the relatively short measurement period. The data captured using this approach only provided a limited snap shot of the flow velocity within the horizontal carrier pipe. Furthermore, without local measurement of the depth of water, discharge could not be determined experimentally using the continuity equation for example. Further analysis of the image data could be undertaken to estimate the depth of flow but this was not included within the scope of this experimental research. Therefore, PIV analysis of all the images captured during the full test program was not completed but the full complement of results are available for further research. Instead the images were used to describe and provide an observational record of the flow conditions within the horizontal carrier pipe in relation to the same time series data as the flow rate measured using flourometry.

### **3.7 Feasibility Test Summary and Introduction to the Full Test Program**

The refinement of the measurement methods, analysis and interpretation of the results completed during the feasibility tests was essential to design the scope and focus of Phase 4 of this experimental research - the Full Test Program.

The strategy for the full test program was to complete a series of measurements refined during the feasibility tests simultaneously rather than in isolation for a series of steady flow tests. The aim of the full test program was to develop a comprehensive data set based on robust and repeatable experimental measurement techniques to enable a detailed understanding of the interaction of flow and pressure within the experimental test facility.

Water depth measurements were not included as part of the full test program as they could not be undertaken simultaneously when combined with the other methods. The methods of pressure measurement, flow rate using flourometry and image capture using high speed image velocimetry were all appropriate, robust and accurate to achieve the aim of the experimental research study.

A series of 63 steady flow tests were completed using three outlets within a common gutter at 20%, 40%, 60%, 80%, 100%, ultimate and 120% of the calculated system design flow rate. These were equivalent to overall system flow rates of 6 l/s, 12 l/s, 18 l/s, 24 l/s, 30 l/s (design flow), 35.12 l/s (ultimate flow) and 36 l/s. These steady flow rates were selected to allow measurement of the experimental test facility operating in sub-prime (i.e. flow tests less than the design flow rate) and primed (flow tests at or above the design flow rate) siphonic action. Each steady flow test was repeated three times for each of the three positions that the camera was used along the length of the horizontal carrier pipe.

The methodology for the full test program combining the measurement techniques is set out in the following section of this chapter.

### 3.7.1 Full Test Program Methodology

During Phase 4, the strategy was to simultaneously complete a series of measurements for the series of 63 steady flow tests. This was completed according to the following methodology;

1. The water supply to the experimental test facility was set to the required test flow rate according to the butterfly control valve calibration and allow to stabilise for 15 minutes;
2. A 2 litre measuring cylinder was filled with Rhodamine solution at a concentration of  $5 \times 10^{-4}$ ;
3. The data acquisition software was checked to confirm response from the 4 pressure transducers and 4 fluourometers;
4. The destination file to append the data from the flow test was created on the computer controlling the data acquisition system;
5. The temperature of the water in the water supply reservoir was recorded (pre-test temperature);
6. The outlet from the dosing pump was connected to the Outlet A injection point;
7. Dye was injected into the outlet and the dosing pump speed regulated until the voltage response from the upstream fluourometer (F1) was measuring a response of  $4 \text{ Volt} \pm 0.5 \text{ Volts}$ . The voltage from F2 and F3 was also checked to ensure a response to the dye being injected;
8. The dosing pump was stopped and the dye in the measuring cylinder refilled;
9. The append to file function on the data acquisition software was started at the same time as a stopwatch (termed stopwatch #1);
10. The dosing pump was started and dye injected the dye into Outlet A;
11. A second stopwatch (termed stopwatch #2) was started when the dye within the measuring cylinder reached the 2000 ml level;
12. The time taken to inject every 100 ml of dye was recorded using stopwatch #2. This was necessary to establish the dye injection rate relative to each steady flow test;
13. The seeding particles were fed into the gutter after 200 ml of dye had been injected into Outlet A according to the methodology outlined in Section 3.6.1;
14. The record function on the camera was started and the time on stopwatch #1 noted. This enabled the series of images to be time referenced relative to the pressure and fluourometer data recorded by the data acquisition system;
15. The dosing pump and collection of data by the data acquisition software was stopped after 1000 ml of Rhodamine dye had been injected into Outlet A;
16. The feed line from the dosing pump to Outlet A was disconnected,
17. The temperature of the water in the water supply reservoir was recorded (post-test temperature).

Application of this methodology for each of the 63 steady flow tests provided the following data:

- Time series pressure data recorded at a frequency of 5 Hz from the 4 pressure transducers installed within the horizontal carrier pipe;

- Time series data from the 3 flourometers installed within the horizontal carrier pipe and 1 flourometer installed within the water supply reservoir recorded at a frequency of 5 Hz;
- The dye injection rate;
- The temperature of the water within the water supply reservoir pre and post each steady flow test;
- Images of the flow at 3 positions within the horizontal carrier recorded at a frequency of 532 frames per second at a known time period relative to the pressure and flourometer data.

After completion of the experimental programme of tests, the extensive, time-series data set collected was analysed. The focus of the analysis was to investigate the relative proportionality of flow measured through each outlet within the experimental test facility for the series of steady flow tests. The relative pressure data and time series images were used to explore and understand the hydraulic performance and interaction of the system according to the analysis methodologies described in this chapter.

Chapter 4 of this thesis presents the analysis of the results from the series of 63 steady flow tests of the full test program as part of this experimental research study. Detailed results are presented in a consistent format with key findings summarised in the second part of this chapter. This section provides a detailed discussion exploring these key findings in the context of previous, relevant experimental research.



## 4 Results and Discussion

Having refined the experimental methods and established the methodology procedure, a full test program was developed to quantify for the first time, the measurement of flow through each component within the multi-outlet siphonic drainage test facility. Chapter 4 of this thesis presents the analysis of these results in a consistent format with key findings summarised in Section 4.2 of this chapter. This section provides a detailed discussion exploring these key findings in the context of previous, relevant experimental research.

A series of 63 steady flow tests were completed using three outlets within a common gutter at 20%, 40%, 60%, 80%, 100%, ultimate (117.7%) and 120% of the calculated system design flow rate. These were equivalent to overall system flow rates of 6 l/s, 12 l/s, 18 l/s, 24 l/s, 30 l/s (design flow), 35.12 l/s (ultimate flow) and 36 l/s. Each steady flow test was repeated three times with the camera positioned at three locations along the length of the horizontal carrier pipe termed P1, P2 and P3, highlighted in Figure 3.2 and Figure 3.3 of this thesis.

These steady flow tests were selected to allow measurement of the experimental test facility operating in sub-prime and primed siphonic action. A summary of the full test program schedule is shown in Table 4.1.

**Table 4.1 Full Test Program Schedule**

Test Reference	Flow Rate Relative to Design (%)	Flow Rate (l/s)	Repeat	Camera Position
1	20	6	1	P1
4	40	12	1	P1
7	60	18	1	P1
10	80	24	1	P1
13	Design	30	1	P1
16	Ultimate	35.12	1	P1
19	120	36	1	P1
2	20	6	2	P1
5	40	12	2	P1
8	60	18	2	P1
11	80	24	2	P1
14	Design	30	2	P1
17	Ultimate	35.12	2	P1
20	120	36	2	P1
3	20	6	3	P1
6	40	12	3	P1
9	60	18	3	P1
12	80	24	3	P1
15	Design	30	3	P1
18	Ultimate	35.12	3	P1
21	120	36	3	P1
22	20	6	1	P2
25	40	12	1	P2

28	60	18	1	P2
31	80	24	1	P2
34	Design	30	1	P2
37	Ultimate	35.12	1	P2
40	120	36	1	P2
<hr/>				
23	20	6	2	P2
26	40	12	2	P2
29	60	18	2	P2
32	80	24	2	P2
35	Design	30	2	P2
38	Ultimate	35.12	2	P2
41	120	36	2	P2
<hr/>				
24	20	6	3	P2
27	40	12	3	P2
30	60	18	3	P2
33	80	24	3	P2
36	Design	30	3	P2
39	Ultimate	35.12	3	P2
42	120	36	3	P2
<hr/>				
43	20	6	1	P3
46	40	12	1	P3
49	60	18	1	P3
52	80	24	1	P3
55	Design	30	1	P3
58	Ultimate	35.12	1	P3
61	120	36	1	P3
<hr/>				
44	20	6	2	P3
47	40	12	2	P3
50	60	18	2	P3
53	80	24	2	P3
56	Design	30	2	P3
59	Ultimate	35.12	2	P3
62	120	36	2	P3
<hr/>				
45	20	6	3	P3
48	40	12	3	P3
51	60	18	3	P3
54	80	24	3	P3
57	Design	30	3	P3
60	Ultimate	35.12	3	P3
63	120	36	3	P3

## **4.1 Summary of the Results**

The results from each steady flow test showing the measured flow rate and relative proportionality of the flow component through each outlet is presented in Table 4.2 to Table 4.8. The results from Test No. 1 and Test No. 43 have been noted as N/A as in these tests the data was corrupted by a malfunction of the data acquisition system. A volumetric comparison of the flow rate recorded using a drop test and that measured using flourometry at Outlet C is shown in the two right hand columns of each table.

A summary of the measured pressure results for the same steady flow tests over the same time series are shown in Table 4.9 to Table 4.15. Following the set of tabulated results, there is a detailed analysis of the tests completed at each steady flow rate. Key findings and discussion from the experimental research are then presented in Section 4.2.

**Table 4.2 Flow Measurement Analysis for Tests Completed at 20% of the Design Flow Rate**

Ref	Outlet A					Outlet B					Outlet C					Volumetric Comparison	
	Mean (l/s)	Proportionality (%)	Max (l/s)	Min (l/s)	SD (l/s)	Mean (l/s)	Proportionality (%)	Max (l/s)	Min (l/s)	SD (l/s)	Mean (l/s)	Proportionality (%)	Max (l/s)	Min (l/s)	SD (l/s)	Drop Test (l/s)	Difference (%)
1	N/A	N/A	N/A	N/A	N/A	N/A	N/A	N/A	N/A	N/A	N/A	N/A	N/A	N/A	N/A	6.02	N/A
2	1.74	28.76	2.22	1.52	0.12	4.10	39.01	5.43	2.24	0.67	6.05	32.23	9.79	2.89	1.27	5.73	5.58
3	1.66	29.09	2.06	1.42	0.11	3.87	38.86	5.19	2.10	0.55	5.70	32.05	9.75	2.79	1.02	6.22	-8.36
22	1.61	28.33	1.78	1.44	0.08	3.97	41.45	16.35	2.25	0.99	5.69	30.22	21.03	2.84	1.66	5.33	6.75
23	1.62	29.14	1.96	1.38	0.11	3.87	40.47	18.26	2.12	1.14	5.56	30.39	29.98	2.96	2.04	4.91	13.24
24	1.79	32.31	2.19	1.46	0.11	4.06	40.97	16.88	2.46	1.07	5.54	26.72	22.02	3.17	1.66	4.92	12.60
43	N/A	N/A	N/A	N/A	N/A	N/A	N/A	N/A	N/A	N/A	N/A	N/A	N/A	N/A	N/A	N/A	N/A
44	1.88	29.47	2.13	1.63	0.09	4.76	45.14	76.32	2.30	4.56	6.38	25.39	112.99	2.85	6.47	N/A	N/A
45	1.87	31.97	2.28	1.54	0.13	4.41	43.42	55.23	2.45	2.82	5.85	24.61	65.96	2.97	4.42	N/A	N/A

**Table 4.3 Flow Measurement Analysis for Tests Completed at 40% of the Design Flow Rate**

Ref	Outlet A					Outlet B					Outlet C					Volumetric Comparison	
	Mean (l/s)	Proportionality (%)	Max (l/s)	Min (l/s)	SD (l/s)	Mean (l/s)	Proportionality (%)	Max (l/s)	Min (l/s)	SD (l/s)	Mean (l/s)	Proportionality (%)	Max (l/s)	Min (l/s)	SD (l/s)	Drop Test (l/s)	Difference (%)
4	3.75	29.60	4.26	3.32	0.16	8.57	38.05	11.70	5.55	1.43	12.67	32.35	19.52	7.78	2.12	11.54	9.79
5	3.72	29.89	4.17	3.34	0.16	8.51	38.41	11.25	5.41	1.40	12.45	31.70	18.94	7.63	2.11	11.47	8.54
6	3.63	29.13	4.15	3.21	0.16	8.39	38.20	12.21	5.13	1.54	12.46	32.67	21.27	6.90	2.17	11.63	7.14
25	4.15	30.70	4.69	3.78	0.17	10.03	43.49	21.58	6.40	1.67	13.52	25.81	20.51	9.33	2.01	12.47	8.42
26	3.79	30.91	4.23	3.34	0.15	8.60	39.23	12.00	5.79	1.22	12.26	29.86	17.97	7.68	1.97	12.55	-2.31
27	3.84	31.60	4.37	3.55	0.14	8.72	40.17	12.22	5.91	1.18	12.15	28.23	18.65	7.54	1.84	12.40	-2.02
46	4.24	35.25	5.23	3.66	0.31	9.25	41.65	14.30	6.16	1.29	12.03	23.10	18.21	7.77	1.83	12.07	-0.33
47	4.24	35.75	5.98	3.35	0.49	9.10	40.98	13.48	5.60	1.42	11.86	23.27	20.24	6.92	1.88	11.40	4.04
48	4.03	36.01	4.83	3.09	0.38	8.62	41.02	12.61	5.29	1.24	11.19	22.97	17.68	7.37	1.58	11.51	-1.84

**Table 4.4 Flow Measurement Analysis for Tests Completed at 60% of the Design Flow Rate**

Ref	Outlet A					Outlet B					Outlet C					Volumetric Comparison	
	Mean (l/s)	Proportionality (%)	Max (l/s)	Min (l/s)	SD (l/s)	Mean (l/s)	Proportionality (%)	Max (l/s)	Min (l/s)	SD (l/s)	Mean (l/s)	Proportionality (%)	Max (l/s)	Min (l/s)	SD (l/s)	Drop Test (l/s)	Difference (%)
7	5.72	30.48	6.32	5.28	0.19	13.06	39.18	16.97	10.76	1.08	18.75	30.34	24.43	14.89	1.67	18.01	4.11
8	5.87	30.79	6.65	5.25	0.24	13.34	39.14	16.50	10.86	1.01	19.07	30.07	26.05	15.25	1.64	17.93	6.36
9	5.82	30.51	6.68	5.18	0.23	13.27	39.04	17.02	10.65	1.10	19.08	30.45	25.52	14.94	1.65	17.89	6.65
28	5.97	31.29	6.66	5.47	0.21	13.34	38.63	17.80	10.26	1.23	19.08	30.08	27.55	14.57	1.87	18.70	2.03
29	5.90	31.25	6.52	5.30	0.22	13.17	38.51	17.53	10.19	1.20	18.88	30.24	25.78	14.89	1.79	18.59	1.56
30	6.18	32.00	6.88	5.59	0.21	13.53	38.06	17.20	11.12	1.13	19.31	29.94	25.20	15.80	1.71	18.58	3.93
49	5.88	33.18	6.46	5.36	0.21	12.92	39.73	17.63	9.37	1.68	17.72	27.09	26.56	12.85	2.41	N/A	N/A
50	6.02	33.50	7.10	5.22	0.32	13.20	39.96	20.90	9.20	1.76	17.97	26.54	28.42	12.81	2.38	N/A	N/A
51	6.15	32.71	6.83	5.56	0.23	13.68	40.05	18.90	10.09	1.96	18.80	27.24	28.96	13.72	2.66	N/A	N/A

**Table 4.5 Flow Measurement Analysis for Tests Completed at 80% of the Design Flow Rate**

Ref	Outlet A					Outlet B					Outlet C					Volumetric Comparison	
	Mean (l/s)	Proportionality (%)	Max (l/s)	Min (l/s)	SD (l/s)	Mean (l/s)	Proportionality (%)	Max (l/s)	Min (l/s)	SD (l/s)	Mean (l/s)	Proportionality (%)	Max (l/s)	Min (l/s)	SD (l/s)	Drop Test (l/s)	Difference (%)
10	7.82	30.64	8.58	7.14	0.27	17.61	38.32	23.51	14.30	1.61	25.53	31.04	33.69	21.00	2.08	24.64	3.61
11	7.73	30.61	8.42	6.93	0.29	17.32	37.97	23.67	14.18	1.57	25.26	31.43	32.14	20.52	2.05	24.61	2.64
12	7.79	30.98	8.54	7.14	0.27	17.58	38.96	22.94	14.33	1.65	25.13	30.06	31.70	20.88	2.05	24.70	1.74
31	8.26	32.87	9.20	1.42	0.32	17.44	36.53	22.31	14.19	1.51	25.13	30.60	31.27	20.58	1.93	24.91	0.88
32	8.28	32.53	9.05	7.53	0.29	17.62	36.70	22.77	14.58	1.50	25.45	30.77	32.60	21.37	2.00	24.94	2.04
33	8.39	33.20	9.33	7.51	0.36	17.65	36.64	23.40	14.30	1.58	25.27	30.15	33.97	20.68	2.10	24.95	1.28
52	8.59	36.90	9.26	7.67	0.28	17.24	37.16	21.35	14.76	1.24	23.28	25.94	28.53	19.75	1.58	N/A	N/A
53	8.50	36.89	9.46	7.75	0.31	17.27	38.06	22.48	14.30	1.30	23.04	25.05	29.47	19.34	1.63	N/A	N/A
54	8.47	37.00	9.67	7.54	0.33	17.11	37.75	21.27	13.65	1.29	22.89	25.25	27.42	18.06	1.56	N/A	N/A

**Table 4.6 Flow Measurement Analysis for Tests Completed at the Design Flow Rate**

Ref	Outlet A					Outlet B					Outlet C					Volumetric Comparison	
	Mean (l/s)	Proportionality (%)	Max (l/s)	Min (l/s)	SD (l/s)	Mean (l/s)	Proportionality (%)	Max (l/s)	Min (l/s)	SD (l/s)	Mean (l/s)	Proportionality (%)	Max (l/s)	Min (l/s)	SD (l/s)	Drop Test (l/s)	Difference (%)
13	9.77	31.50	10.54	9.03	0.27	21.62	38.19	25.75	18.93	1.21	31.02	30.31	35.99	27.22	1.62	N/A	N/A
14	9.92	31.76	10.83	9.03	0.35	21.81	38.06	25.72	18.80	1.38	31.24	30.17	37.13	27.07	1.82	N/A	N/A
15	10.02	32.04	11.00	9.11	0.35	21.87	37.89	26.59	18.82	1.32	31.28	30.07	37.43	27.05	1.73	N/A	N/A
34	10.45	33.46	11.56	9.30	0.47	21.39	35.03	26.15	17.73	1.39	31.23	31.51	38.18	26.07	1.97	30.65	1.89
35	10.23	33.21	11.36	9.45	0.32	20.92	34.71	26.37	18.39	1.15	30.80	32.08	36.13	26.48	1.63	30.60	0.65
36	10.22	33.33	11.28	9.25	0.38	20.84	34.64	24.52	17.97	1.31	32.03	30.66	35.67	25.90	1.80	30.63	4.57
55	10.48	37.35	12.05	9.60	0.38	20.78	36.71	24.58	18.40	1.04	28.06	25.94	32.50	24.62	1.30	30.58	-8.24
56	10.75	37.50	12.07	9.75	0.41	21.16	36.31	26.48	18.61	1.23	28.67	26.19	35.33	24.57	1.64	30.45	-5.85
57	10.63	37.44	12.14	9.80	0.40	21.11	36.91	25.00	18.62	1.11	28.39	25.65	33.37	24.59	1.45	30.47	-6.83

**Table 4.7 Flow Measurement Analysis for Tests Completed at the Ultimate Flow Rate**

Ref	Outlet A					Outlet B					Outlet C					Volumetric Comparison	
	Mean (l/s)	Proportionality (%)	Max (l/s)	Min (l/s)	SD (l/s)	Mean (l/s)	Proportionality (%)	Max (l/s)	Min (l/s)	SD (l/s)	Mean (l/s)	Proportionality (%)	Max (l/s)	Min (l/s)	SD (l/s)	Drop Test (l/s)	Difference (%)
16	12.71	34.27	13.74	11.71	0.41	25.53	34.57	27.63	23.40	0.91	37.09	31.16	40.85	33.57	1.37	N/A	N/A
17	12.66	34.10	13.76	11.69	0.38	25.41	34.35	27.78	23.53	0.84	37.13	31.55	40.61	34.28	1.21	N/A	N/A
18	12.52	34.30	13.77	11.42	0.37	24.97	34.10	27.02	22.71	0.78	36.51	31.60	39.75	33.13	1.13	N/A	N/A
37	12.06	33.41	12.93	11.21	0.31	25.20	36.40	27.35	23.08	0.70	36.10	30.19	38.99	33.15	1.05	34.60	4.16
38	11.19	32.28	12.09	10.46	0.32	24.41	38.13	27.37	22.53	0.89	34.67	29.59	39.37	31.76	1.33	34.57	0.29
39	11.61	29.77	13.11	10.43	0.44	26.98	39.41	30.87	24.19	1.20	39.00	30.82	45.17	35.13	1.80	34.59	12.75
58	13.12	39.81	14.55	12.20	0.42	24.45	34.38	26.83	22.67	0.81	32.96	25.81	37.37	30.28	1.20	N/A	N/A
59	13.15	39.80	14.48	12.20	0.43	24.40	34.05	26.92	22.75	0.83	33.04	26.15	37.04	30.28	1.15	N/A	N/A
60	12.92	39.70	14.28	11.65	0.46	23.94	33.87	26.93	21.91	0.89	32.54	26.43	37.21	28.33	1.44	N/A	N/A

**Table 4.8 Flow Measurement Analysis for Tests Completed at 120% of the Design Flow Rate**

Ref	Outlet A					Outlet B					Outlet C					Volumetric Comparison	
	Mean (l/s)	Proportionality (%)	Max (l/s)	Min (l/s)	SD (l/s)	Mean (l/s)	Proportionality (%)	Max (l/s)	Min (l/s)	SD (l/s)	Mean (l/s)	Proportionality (%)	Max (l/s)	Min (l/s)	SD (l/s)	Drop Test (l/s)	Difference (%)
19	12.45	33.72	13.44	11.55	0.35	24.63	32.97	26.45	23.04	0.65	36.93	33.32	39.59	34.10	0.95	N/A	N/A
20	12.41	33.78	13.36	11.55	0.37	24.49	32.89	26.15	22.82	0.78	36.73	33.33	39.37	33.61	1.21	N/A	N/A
21	12.44	33.75	13.35	11.66	0.32	24.62	33.06	26.30	23.14	0.64	36.84	33.19	39.40	34.44	0.93	N/A	N/A
40	11.41	32.65	12.54	10.49	0.35	24.78	37.83	27.05	22.90	0.69	35.34	29.52	38.69	32.02	0.99	35.61	-0.76
41	11.43	32.32	12.54	10.46	0.40	24.73	37.60	27.76	22.60	0.96	35.37	30.08	39.62	31.90	1.42	35.71	-0.95
42	11.40	32.22	12.40	10.34	0.37	24.58	37.25	27.08	21.91	0.90	35.38	30.53	38.72	31.52	1.36	35.76	-1.06
61	13.37	39.47	14.55	12.42	0.39	24.66	33.33	26.60	22.75	0.76	33.87	27.20	36.52	31.38	1.03	N/A	N/A
62	13.36	39.22	14.57	11.89	0.43	24.54	32.82	26.84	22.00	0.81	34.06	27.96	37.08	30.52	1.17	N/A	N/A
63	13.14	38.50	14.46	12.02	0.43	24.72	33.93	27.27	22.73	0.86	34.13	27.57	39.01	30.86	1.24	N/A	N/A

**Table 4.9 Pressure Measurement Analysis for Tests Completed at 20% of the Design Flow Rate**

Ref	PT1 (mH <sub>2</sub> O)				PT2 (mH <sub>2</sub> O)				PT3 (mH <sub>2</sub> O)				PT4 (mH <sub>2</sub> O)			
	Mean	Max	Min	SD	Mean	Max	Min	SD	Mean	Max	Min	SD	Mean	Max	Min	SD
1	N/A	N/A	N/A	N/A	N/A	N/A	N/A	N/A	N/A	N/A	N/A	N/A	N/A	N/A	N/A	N/A
2	0.11	0.26	0.00	0.03	1.03	1.14	0.86	0.02	-0.04	0.17	-0.58	0.10	-0.06	0.26	-1.04	0.17
3	0.11	0.24	0.00	0.03	1.03	1.20	0.85	0.03	-0.02	0.21	-0.78	0.11	-0.05	0.30	-1.21	0.18
22	0.11	0.21	0.01	0.03	1.04	1.15	0.95	0.03	-0.07	0.14	-0.60	0.10	-0.04	0.25	-1.13	0.17
23	0.11	0.29	0.00	0.03	1.04	1.13	0.93	0.03	-0.07	0.21	-0.62	0.09	-0.03	0.24	-1.09	0.16
24	0.12	0.24	0.00	0.02	1.04	1.13	0.95	0.03	-0.06	0.16	-0.64	0.09	-0.03	0.24	-1.23	0.16
43	N/A	N/A	N/A	N/A	N/A	N/A	N/A	N/A	N/A	N/A	N/A	N/A	N/A	N/A	N/A	N/A
44	0.12	0.23	0.01	0.03	1.03	1.14	0.92	0.03	-0.05	0.21	-0.73	0.11	-0.06	0.24	-1.08	0.19
45	0.13	0.33	0.04	0.03	1.03	1.16	0.93	0.03	-0.04	0.47	-0.65	0.10	-0.05	0.22	-1.12	0.18

**Table 4.10 Pressure Measurement Analysis for Tests Completed at 40% of the Design Flow Rate**

Ref	PT1 (mH <sub>2</sub> O)				PT2 (mH <sub>2</sub> O)				PT3 (mH <sub>2</sub> O)				PT4 (mH <sub>2</sub> O)			
	Mean	Max	Min	SD	Mean	Max	Min	SD	Mean	Max	Min	SD	Mean	Max	Min	SD
4	0.03	0.15	-0.10	0.03	0.91	1.11	0.57	0.06	-0.42	0.12	-1.44	0.24	-0.63	0.27	-1.93	0.37
5	0.03	0.16	-0.09	0.03	0.92	1.10	0.66	0.06	-0.40	0.08	-1.39	0.22	-0.60	0.26	-1.82	0.34
6	0.04	0.21	-0.08	0.04	0.92	1.11	0.68	0.06	-0.38	0.09	-1.38	0.22	-0.57	0.26	-1.92	0.35
25	0.01	0.11	-0.10	0.03	0.89	1.04	0.60	0.07	-0.51	0.03	-1.62	0.27	-0.69	0.29	-2.37	0.44
26	0.07	0.16	-0.16	0.03	0.93	1.08	0.57	0.06	-0.42	0.09	-1.44	0.26	-0.60	0.32	-1.96	0.40
27	0.05	0.17	-0.05	0.03	0.93	1.06	0.65	0.06	-0.41	0.04	-1.45	0.25	-0.58	0.32	-1.85	0.39
46	0.03	0.10	-0.34	0.02	0.90	1.06	0.66	0.06	-0.46	0.01	-1.46	0.25	-0.66	0.29	-1.20	0.40
47	0.04	0.35	-0.05	0.04	0.91	1.12	0.66	0.06	-0.43	0.05	-1.62	0.24	-0.63	0.22	-2.12	0.39
48	0.03	0.39	-0.09	0.03	0.93	1.10	0.66	0.05	-0.40	0.08	-1.45	0.21	-0.58	0.26	-1.95	0.32



**Table 4.11 Pressure Measurement Analysis for Tests Completed at 60% of the Design Flow Rate**

Ref	PT1 (mH <sub>2</sub> O)				PT2 (mH <sub>2</sub> O)				PT3 (mH <sub>2</sub> O)				PT4 (mH <sub>2</sub> O)			
	Mean	Max	Min	SD	Mean	Max	Min	SD	Mean	Max	Min	SD	Mean	Max	Min	SD
7	-0.08	0.02	-0.18	0.03	0.71	0.87	0.50	0.05	-1.24	-1.00	-1.54	0.09	-1.31	-0.38	-2.24	0.24
8	-0.08	0.03	-0.21	0.03	0.71	0.87	0.47	0.05	-1.23	-0.94	-1.52	0.10	-1.32	-0.49	-2.10	0.24
9	-0.07	0.05	-0.18	0.03	0.72	0.88	0.52	0.05	-1.23	-0.99	-1.50	0.09	-1.30	-0.53	-2.01	0.24
28	-0.07	0.04	-0.18	0.03	0.69	0.91	0.49	0.05	-0.95	-0.47	-1.47	0.17	-1.36	-0.48	-2.09	0.24
29	-0.07	0.05	-0.18	0.03	0.69	0.84	0.51	0.05	-0.94	-0.39	-1.64	0.16	-1.36	-0.59	-2.22	0.24
30	-0.09	0.01	-0.22	0.03	0.66	0.82	0.47	0.05	-0.97	-0.48	-1.48	0.16	-1.42	-0.60	-2.77	0.24
49	-0.05	0.05	-0.14	0.03	0.70	0.92	0.51	0.05	-0.92	-0.38	-1.50	0.17	-1.38	-0.33	-2.50	0.27
50	-0.06	0.03	-0.16	0.03	0.70	0.90	0.52	0.06	-0.93	-0.28	-1.41	0.18	-1.38	-0.47	-2.35	0.27
51	-0.07	0.01	-0.17	0.03	0.69	0.92	0.46	0.06	-0.92	-0.36	-1.47	0.18	-1.39	-0.46	-2.26	0.27

**Table 4.12 Pressure Measurement Analysis for Tests Completed at 80% of the Design Flow Rate**

Ref	PT1 (mH <sub>2</sub> O)				PT2 (mH <sub>2</sub> O)				PT3 (mH <sub>2</sub> O)				PT4 (mH <sub>2</sub> O)			
	Mean	Max	Min	SD	Mean	Max	Min	SD	Mean	Max	Min	SD	Mean	Max	Min	SD
10	-0.13	0.02	-0.26	0.04	0.44	0.64	0.26	0.06	-1.42	-0.89	-1.93	0.16	-2.16	-1.32	-3.10	0.25
11	-0.13	0.02	-0.26	0.04	0.44	0.64	0.26	0.06	-1.42	-0.89	-1.93	0.16	-2.16	-1.32	-3.10	0.25
12	-0.14	0.01	-0.29	0.04	0.46	0.66	0.28	0.06	-1.40	-0.79	-1.88	0.17	-2.13	-1.25	-2.99	0.26
31	-0.13	0.22	-0.30	0.05	0.41	0.64	0.19	0.06	-1.47	-0.91	-2.17	0.17	-2.22	-1.30	-3.02	0.25
32	-0.13	0.02	-0.30	0.05	0.42	0.60	0.24	0.06	-1.47	-0.95	-2.03	0.16	-2.20	-1.30	-3.10	0.26
33	-0.13	0.13	-0.27	0.05	0.43	0.65	0.23	0.06	-1.47	-0.94	-1.98	0.17	-2.20	-1.36	-3.08	0.25
52	-0.05	0.15	-0.22	0.05	0.50	0.71	0.33	0.06	-1.39	-0.83	-1.90	0.16	-2.15	-1.27	-2.96	0.26
53	-0.06	0.11	-0.22	0.05	0.50	0.73	0.30	0.06	-1.40	-0.85	-1.91	0.16	-2.15	-1.07	-2.91	0.26
54	-0.06	0.15	-0.18	0.05	0.51	0.75	0.34	0.06	-1.38	-0.91	-1.83	0.16	-2.11	-1.02	-2.94	0.26

**Table 4.13 Pressure Measurement Analysis for Tests Completed at the Design Flow Rate**

Ref	PT1 (mH <sub>2</sub> O)				PT2 (mH <sub>2</sub> O)				PT3 (mH <sub>2</sub> O)				PT4 (mH <sub>2</sub> O)			
	Mean	Max	Min	SD	Mean	Max	Min	SD	Mean	Max	Min	SD	Mean	Max	Min	SD
13	0.00	0.14	-0.12	0.04	0.40	0.57	0.22	0.05	-1.73	-1.16	-2.14	0.14	-2.79	-1.95	-3.51	0.21
14	-0.01	0.11	-0.15	0.04	0.40	0.60	0.22	0.05	-1.71	-1.16	-2.16	0.14	-2.75	-1.99	-3.38	0.22
15	0.00	0.16	-0.14	0.04	0.39	0.59	0.22	0.05	-1.73	-1.16	-2.11	0.13	-2.79	-2.03	-3.45	0.22
34	0.00	0.12	-0.19	0.04	0.37	0.54	0.17	0.05	-1.78	-1.23	-2.18	0.12	-2.85	-2.09	-3.52	0.20
35	-0.01	0.10	-0.13	0.04	0.36	0.56	0.20	0.05	-1.77	-1.27	-2.12	0.13	-2.84	-2.04	-3.46	0.20
36	0.00	0.12	-0.15	0.04	0.37	0.52	0.15	0.05	-1.77	-1.29	-2.15	0.13	-2.84	-2.13	-3.48	0.20
55	0.03	0.17	-0.13	0.04	0.42	0.61	0.25	0.05	-1.72	-1.20	-2.15	0.13	-2.81	-2.13	-3.57	0.20
56	0.05	0.16	-0.04	0.03	0.42	0.59	0.24	0.05	-1.72	-1.22	-2.11	0.13	-2.85	-2.01	-3.46	0.21
57	0.04	0.17	-0.08	0.04	0.42	0.59	0.22	0.05	-1.72	-1.18	-2.09	0.12	-2.83	-2.05	-3.43	0.21

**Table 4.14 Pressure Measurement Analysis for Tests Completed at the Ultimate Flow Rate**

Ref	PT1 (mH <sub>2</sub> O)				PT2 (mH <sub>2</sub> O)				PT3 (mH <sub>2</sub> O)				PT4 (mH <sub>2</sub> O)			
	Mean	Max	Min	SD	Mean	Max	Min	SD	Mean	Max	Min	SD	Mean	Max	Min	SD
16	0.16	0.28	0.05	0.03	0.40	0.55	0.25	0.04	-1.84	-1.58	-2.11	0.06	-3.22	-2.76	-3.51	0.09
17	0.16	0.26	0.02	0.03	0.39	0.52	0.27	0.03	-1.85	-1.55	-2.14	0.07	-3.22	-2.74	-3.49	0.10
18	0.16	0.65	-0.01	0.04	0.39	0.53	0.23	0.04	-1.85	-1.39	-2.10	0.08	-3.20	-2.57	-3.58	0.11
37	0.15	0.22	0.04	0.03	0.40	0.55	0.29	0.03	-1.82	-1.52	-2.15	0.07	-3.21	-2.69	-3.61	0.11
38	0.14	0.24	0.03	0.03	0.40	0.52	0.26	0.04	-1.81	-1.48	-2.03	0.07	-3.20	-2.69	-3.57	0.11
39	0.12	0.23	-0.01	0.03	0.40	0.56	0.25	0.04	-1.81	-1.55	-2.07	0.07	-3.18	-2.64	-3.53	0.12
58	0.17	0.28	0.07	0.04	0.41	0.57	0.31	0.04	-1.82	-1.52	-2.11	0.08	-3.20	-2.59	-3.54	0.12
59	0.16	0.27	0.05	0.03	0.40	0.53	0.28	0.03	-1.83	-1.60	-2.20	0.08	-3.21	-2.64	-3.65	0.11
60	0.17	0.30	0.02	0.03	0.40	0.55	0.28	0.04	-1.82	-1.54	-2.15	0.08	-3.20	-2.71	-3.56	0.11

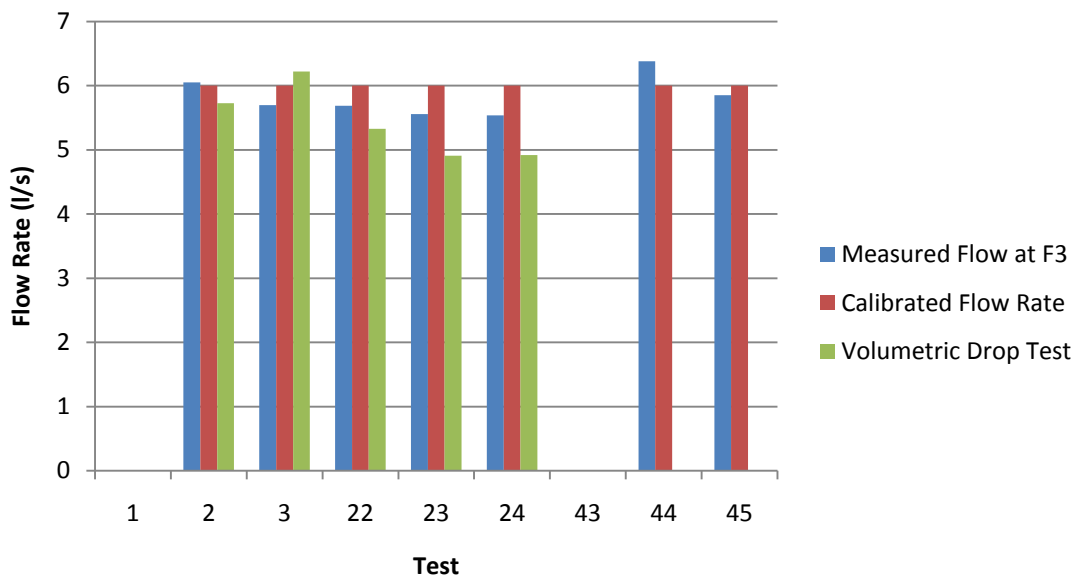
**Table 4.15 Pressure Measurement Analysis for Tests Completed at 120% of the Design Flow Rate**

Ref	PT1 (mH <sub>2</sub> O)				PT2 (mH <sub>2</sub> O)				PT3 (mH <sub>2</sub> O)				PT4 (mH <sub>2</sub> O)			
	Mean	Max	Min	SD	Mean	Max	Min	SD	Mean	Max	Min	SD	Mean	Max	Min	SD
19	0.19	0.29	0.09	0.03	0.43	0.52	0.32	0.03	-1.82	-1.65	-1.98	0.05	-3.23	-2.90	-3.42	0.07
20	0.19	0.34	0.07	0.03	0.43	0.56	0.31	0.03	-1.82	-1.62	-2.06	0.05	-3.24	-2.90	-3.42	0.07
21	0.19	0.28	0.05	0.03	0.43	0.52	0.34	0.03	-1.82	-1.60	-1.95	0.05	-3.24	-2.94	-3.46	0.06
40	0.18	0.86	0.04	0.06	0.41	0.52	0.29	0.04	-1.83	-1.66	-2.02	0.05	-3.26	-2.93	-3.45	0.07
41	0.17	0.36	-0.08	0.06	0.41	0.53	0.24	0.04	-1.84	-1.68	-1.99	0.05	-3.26	-2.95	-3.44	0.07
42	0.16	0.32	-0.04	0.05	0.40	0.53	0.28	0.04	-1.84	-1.71	-1.99	0.04	-3.28	-2.97	-3.48	0.07
61	0.18	0.30	0.08	0.03	0.41	0.53	0.34	0.03	-1.83	-1.69	-2.01	0.04	-3.27	-2.91	-3.49	0.06
62	0.19	0.25	0.12	0.02	0.42	0.49	0.32	0.02	-1.82	-1.71	-1.95	0.04	-3.28	-3.05	-3.43	0.06
63	0.19	0.29	0.07	0.03	0.42	0.54	0.27	0.03	-1.81	-1.66	-2.01	0.05	-3.25	-2.92	-3.47	0.08

### 4.1.1 Tests Completed at 20% of the Design Flow Rate

#### 4.1.1.1 Mass Balance

The 7 flow tests completed at 20% of the design flow rate showed an average difference between the mass balance measured using flourometry and the volumetric drop test of  $\pm 9.31\%$  and a maximum difference of  $+13.24\%$ . The measured mean flow rate varied between 5.54 l/s to 6.38 l/s and a comparison between the measured flow at F3, calibrated flow rate and volumetric drop test is shown in Figure 4.1.

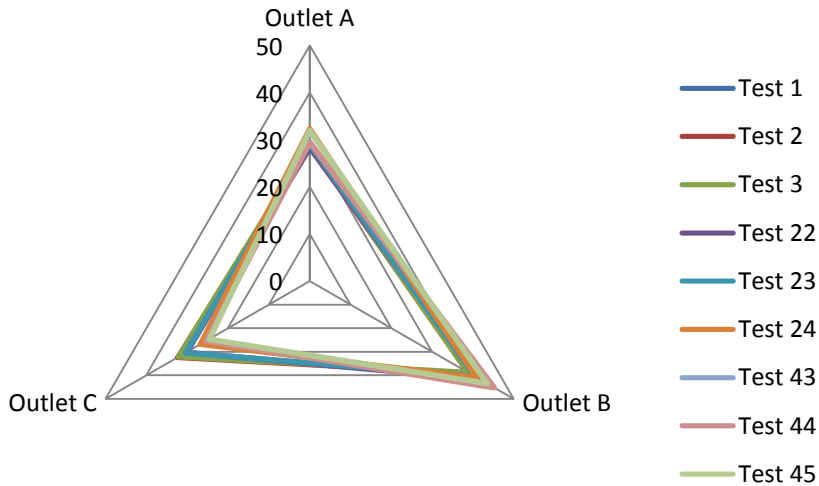


**Figure 4.1 Mass Balance Comparison for Tests Completed at 20% of the Design Flow Rate**

These results show that the refined measurement methodology demonstrates repeatability and provides confidence in measuring relatively low flow rates through the experimental test facility.

#### 4.1.1.2 Flow Proportionality

Figure 4.2 shows a radar plot demonstrating the relative proportionality of flow through each outlet during the tests reported in Table 4.2.



**Figure 4.2 Radar Plot Showing Flow Proportionality (%) at 20% of the Design Flow Rate**

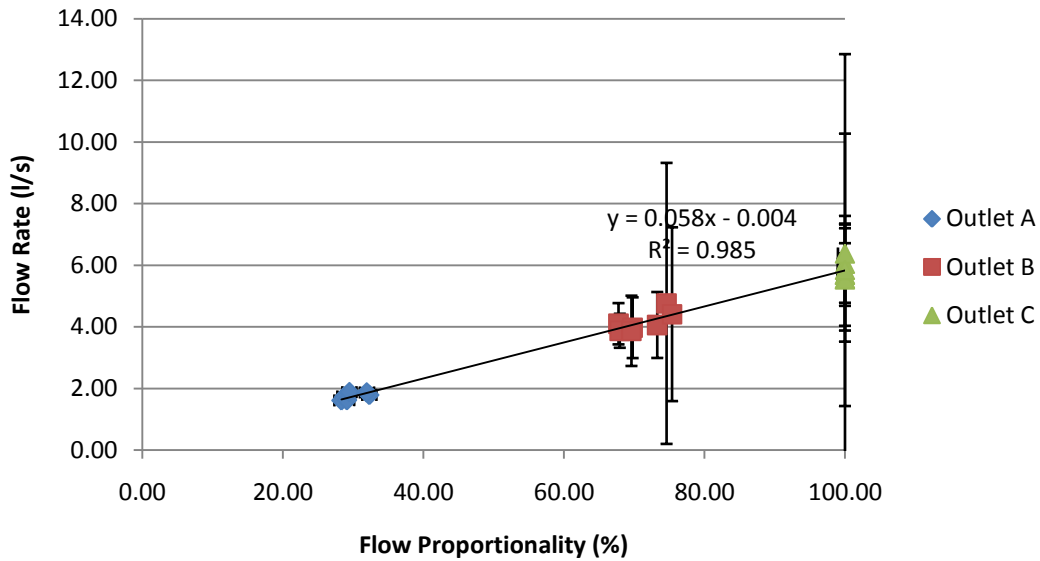
The radar plot demonstrates that for the tests completed at 20% of the design flow rate, flow through Outlet B dominated. This is consistent for all of the tests. The relative proportion between outlets A and C is very similar. Maximum, minimum and average flow proportionality for the series of tests is shown in Table 4.16.

**Table 4.16 Maximum, Minimum and Average Flow Proportionality for Tests Completed at 20% of the Design Flow Rate**

Outlet	Maximum (%)	Minimum (%)	Average (%)
A	32.31	28.76	29.87
B	45.14	38.86	41.33
C	32.23	24.61	28.80

It is clear that for these series of tests there is a consistent and repeatable imbalance in the magnitude of the flow through each outlet which is contradictory to the assumptions made in the hydraulic design of the system.

Figure 4.3 shows the measured component of flow through each outlet and relative standard deviation shown by the error bars for the same 7 tests.

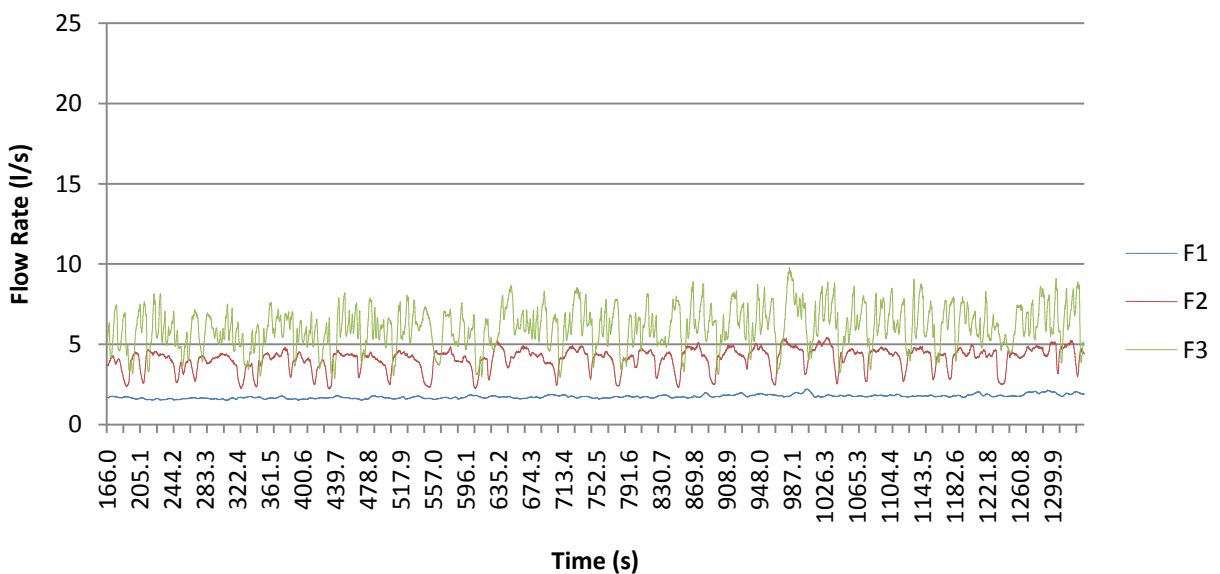


**Figure 4.3 Flow Proportionality at a Design Flow Rate of 20% with Standard Deviation shown by the Error Bars**

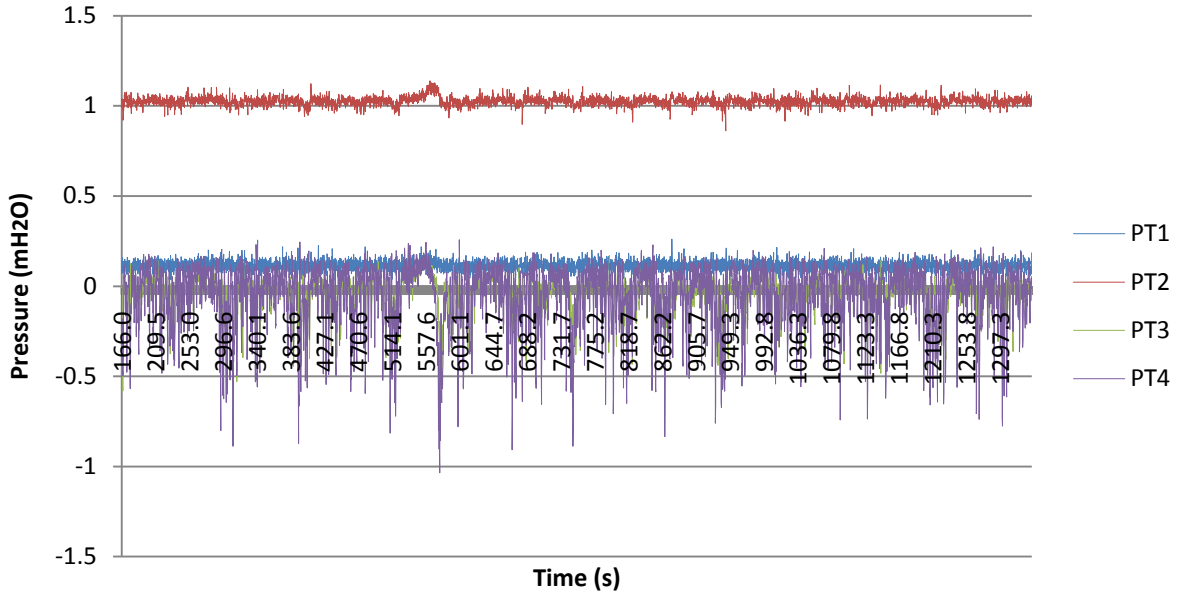
These results show that the standard deviation associated with the average flow rate measured through each outlet increased through the experimental test facility. This suggests greater fluctuations in the measured flow through Outlet B and C respectively.

#### 4.1.1.3 Time Series Flow Rate and Pressure Measurements

Figure 4.4 and Figure 4.5 show continuous flow data measured using flourometry through each outlet and system pressure within the horizontal carrier pipe during Test 2.

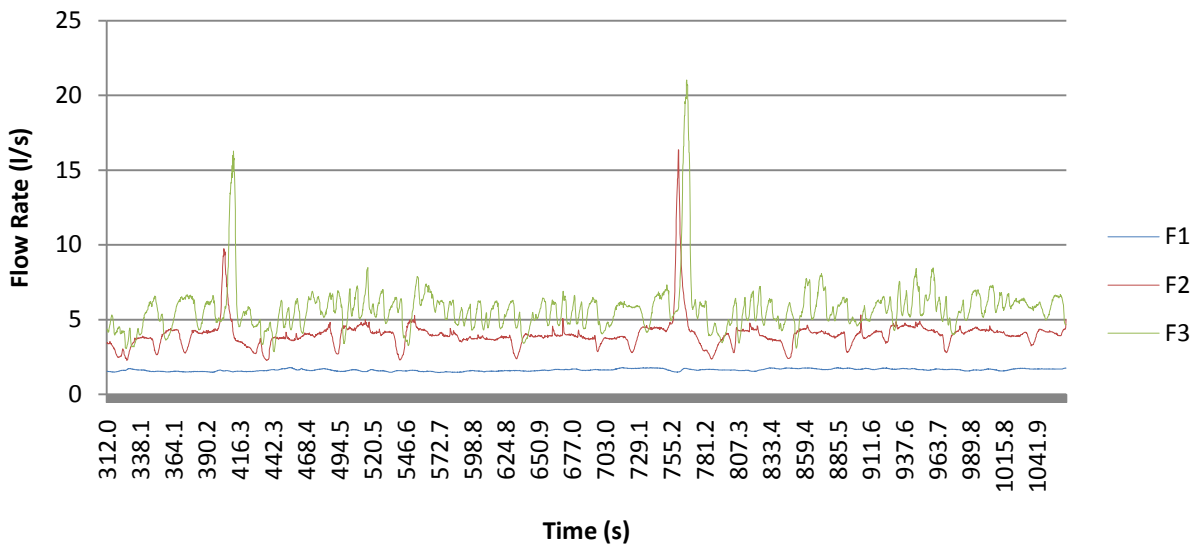


**Figure 4.4 Flow Measurement within the Horizontal Carrier Pipe during Test 2**

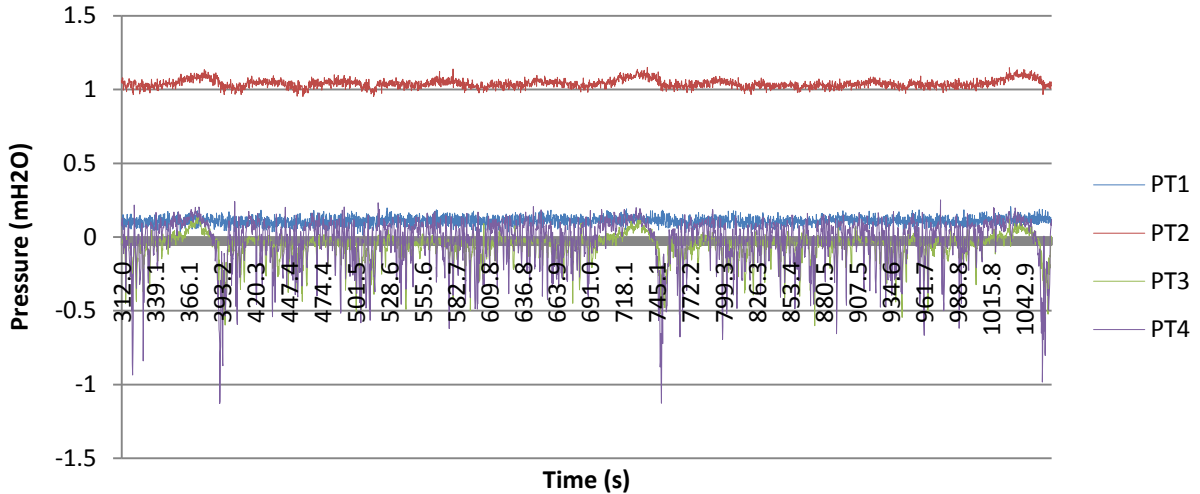


**Figure 4.5 Pressure Measurement within the Horizontal Carrier Pipe during Test 2**

In comparison to Test 2 and 3, Test 22 had a significantly higher maximum value recorded at Outlet B and C. A plot showing the measured flow rate and pressure is shown in Figure 4.6 and Figure 4.7 respectively.

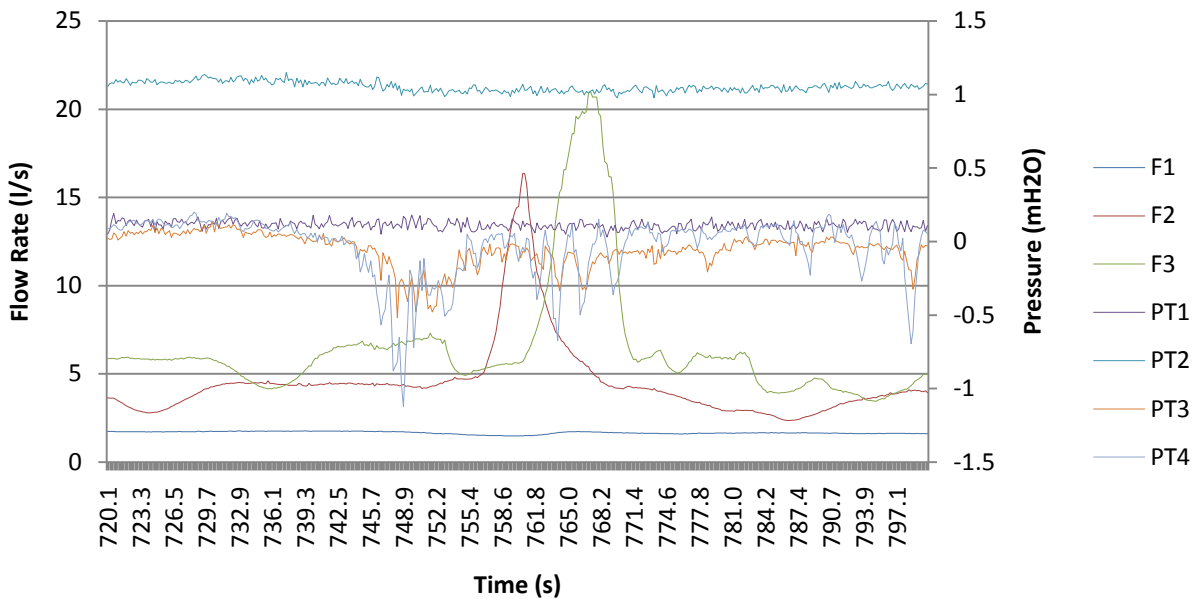


**Figure 4.6 Flow Rate Measured within the Horizontal Carrier Pipe during Test 22**



**Figure 4.7 Pressure Measured within the Horizontal Carrier Pipe during Test 22**

Two significant flow peaks were measured at Outlets B and C after 400 seconds and 760 seconds respectively. There was an associated decrease in pressure recorded by PT3 and PT4 shown in Figure 4.7. A more detailed plot of the flow rate and pressure results for the peak measured at 760 seconds is shown in Figure 4.8.



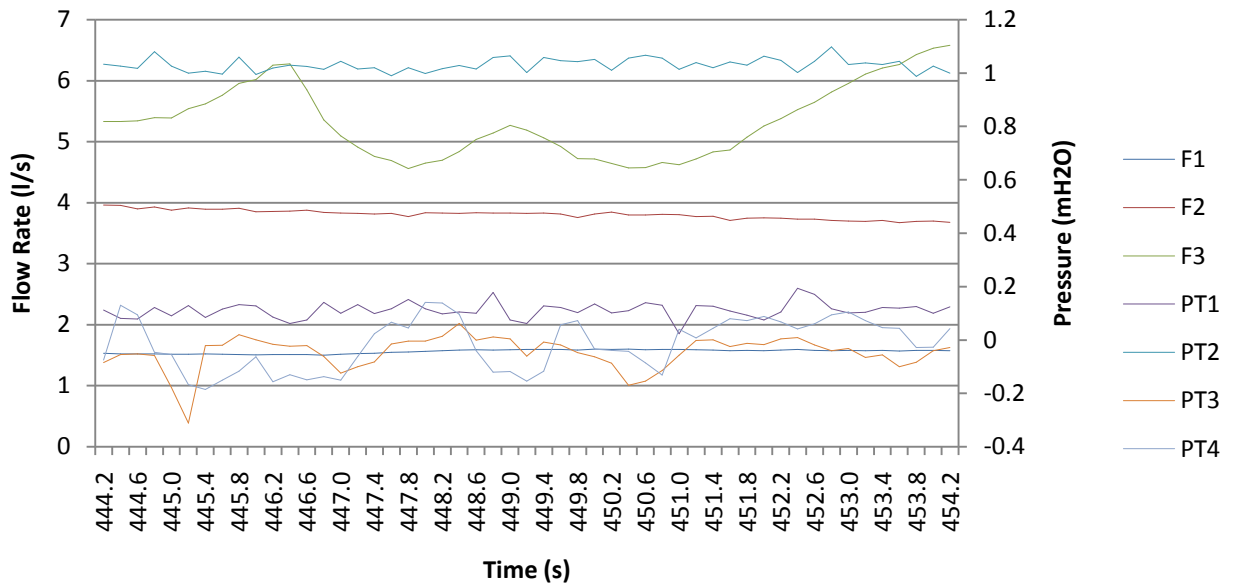
**Figure 4.8 Flow Rate and Pressure Measurements within the Horizontal Carrier Pipe during Test 22**

Figure 4.8 shows a decrease in pressure at PT4 and PT3 followed by a sharp increase in flow rate measured downstream of Outlets B and C. The pressure measured at PT1 and PT2 and the flow rate measured downstream of Outlet A were unaffected by these flow rate and pressure fluctuations.



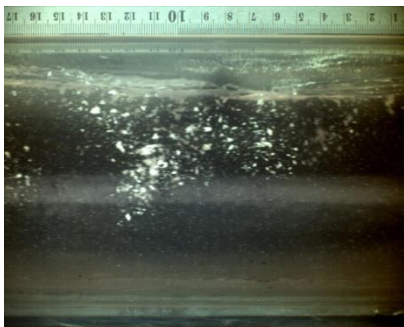
#### 4.1.1.4 Time Series Flow Rate, Pressure and Image Comparison at P1

To further highlight these changes in pressure and flow rate, Figure 4.9 shows the flow rate and pressure measurements for the corresponding 10 second period (444.28 seconds to 454.28 seconds) that images were collected at P1 (downstream of Outlet A and F1) during Test 3.

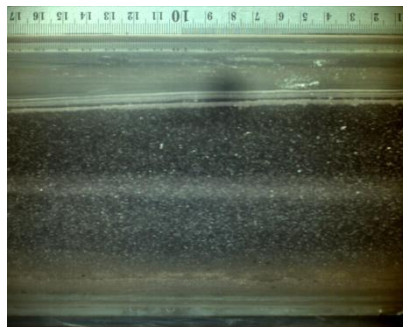


**Figure 4.9 Flow Rate and Pressure Measurements within the Horizontal Carrier Pipe during Test 3 (444.28 to 454.28 seconds)**

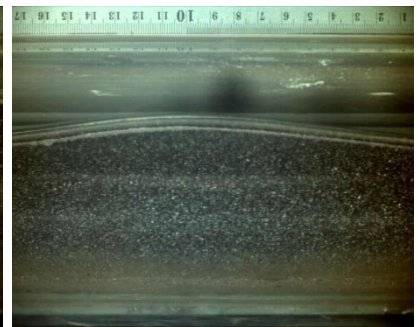
The following selected images correspond to the time series data shown in Figure 4.9.



**Figure 4.10 Image at P1 at 444.28 seconds**

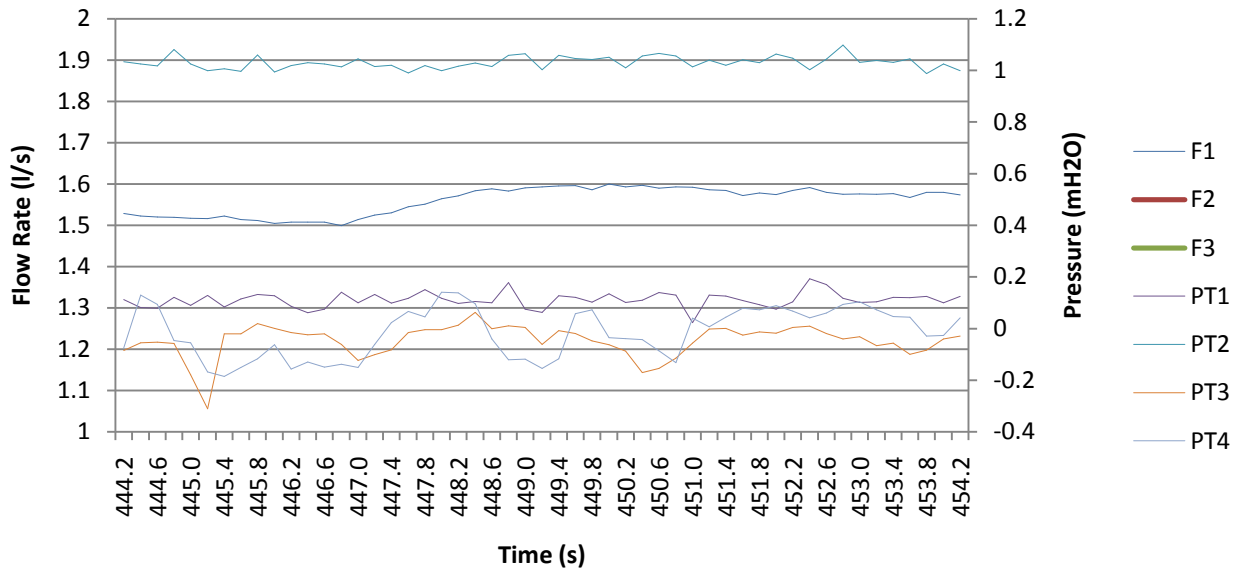


**Figure 4.11 Image at P1 at 445.28 seconds**



**Figure 4.12 Image at P1 at 446.91 seconds**

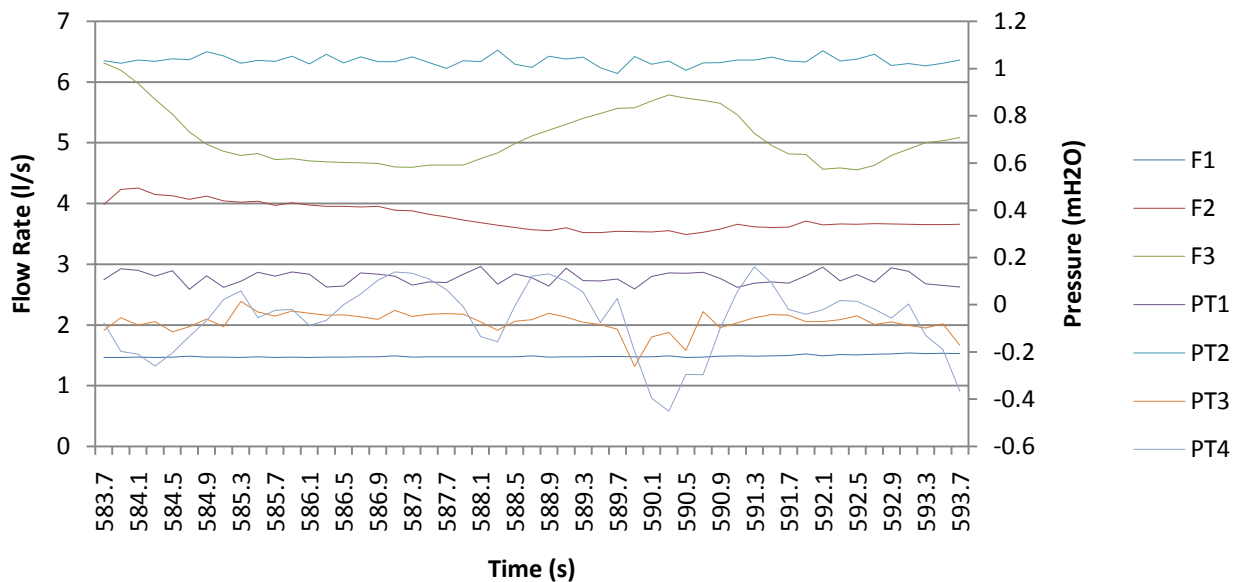
The images show free surface flow with an example of full bore flow with entrained air (Figure 4.10). Other than this one instance of full bore flow, free surface flow conditions dominated throughout the measurement period. The measured variations in the measured flow rate at P1 can be seen more clearly in Figure 4.13 where the scale of the flow rate has been adjusted to only include the flow measured at F1.



**Figure 4.13 Flow Rate at P1 and Pressure Measurements within the Horizontal Carrier Pipe during Test 3 (444.28 to 454.28 seconds)**

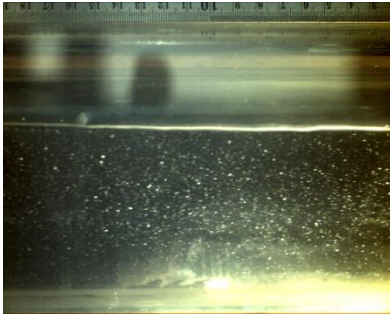
4.1.1.5 Time Series Flow Rate, Pressure and Image Comparison at P2

Figure 4.14 shows the flow rate and pressure measurements for the corresponding 10 second period (583.78 seconds to 593.78 seconds) that images were collected at P2 (downstream of Outlet B and F2) during Test 22.

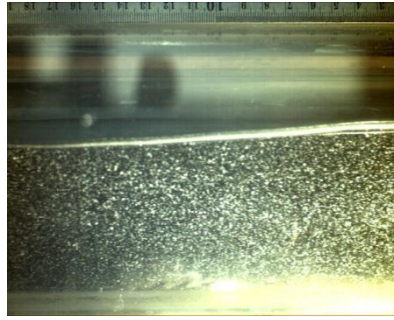


**Figure 4.14 Flow Rate and Pressure Measurements within the Horizontal Carrier Pipe during Test 22 (583.78 to 593.78 seconds)**

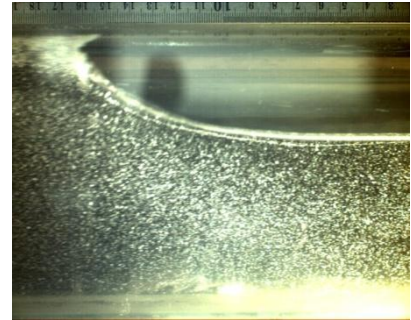
The following selected images correspond to the time series data shown in Figure 4.14.



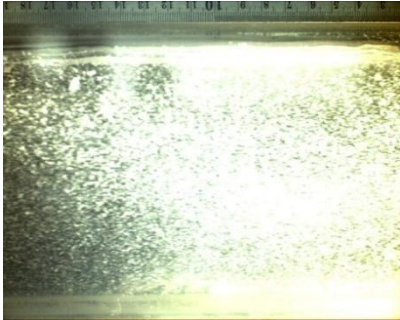
**Figure 4.15 Image at P2 at 583.78 seconds**



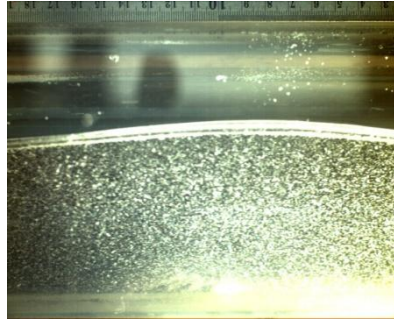
**Figure 4.16 Image at P2 at 586.11 seconds**



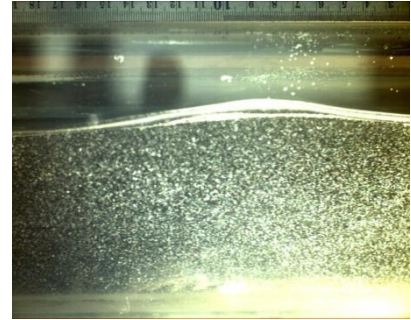
**Figure 4.17 Image at P2 at 586.20 seconds**



**Figure 4.18 Image at P2 at 587.42 seconds**



**Figure 4.19 Image at P2 at 590.02 seconds**

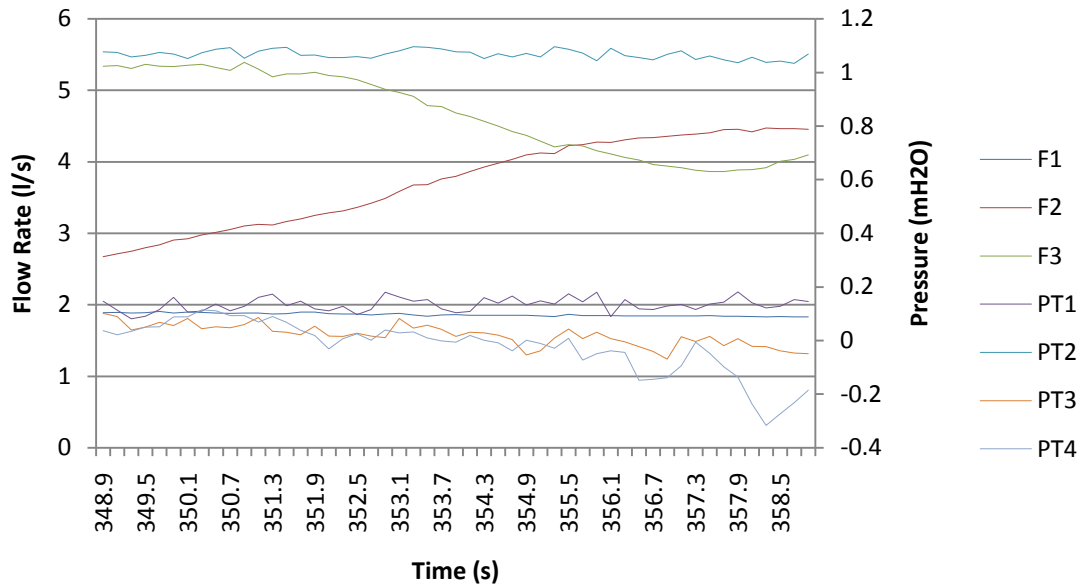


**Figure 4.20 Image at P2 at 593.78 seconds**

Analysis of the images showed an initial period of free surface flow (Figure 4.15) followed by an increase in flow depth (Figure 4.16). A period of pulsed or plug flow was observed following this increase in flow depth (Figure 4.17). The period of full bore flow lasted for approximately 1 second (586 seconds to 587 seconds) where the level then receded (shown in Figure 4.18) returning to free surface flow conditions (shown in Figure 4.19 and Figure 4.20).

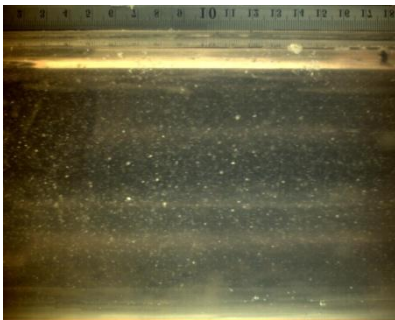
#### 4.1.1.6 Time Series Flow Rate, Pressure and Image Comparison at P3

Figure 4.21 shows the flow rate and pressure measurements for the corresponding 10 second period (348.91 to 358.91 seconds) that images were collected at P3 (downstream of Outlet C and F3) during Test 44.

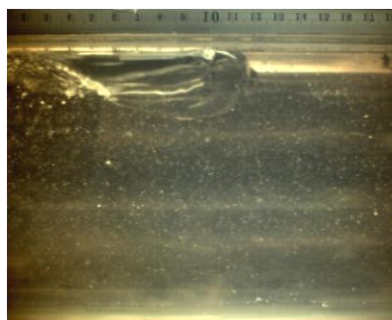


**Figure 4.21 Flow Rate and Pressure Measurements within the Horizontal Carrier Pipe during Test 44 (348.91 to 358.91 seconds)**

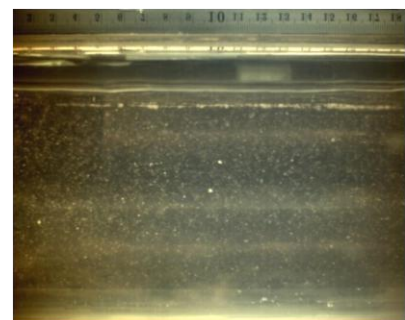
The following selected images correspond to the time series data shown in Figure 4.21.



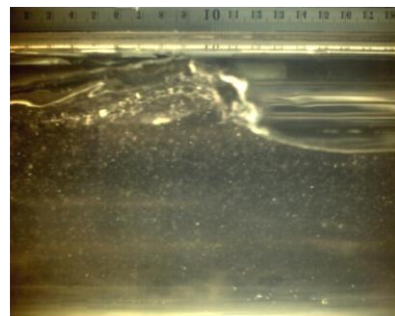
**Figure 4.22 Image at P3 at 348.91 seconds**



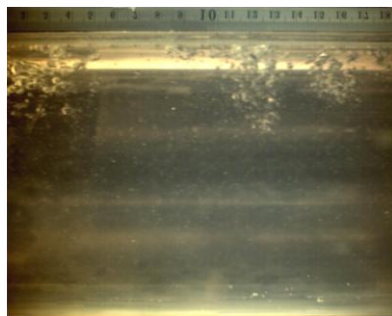
**Figure 4.23 Image at P3 at 349.10 seconds**



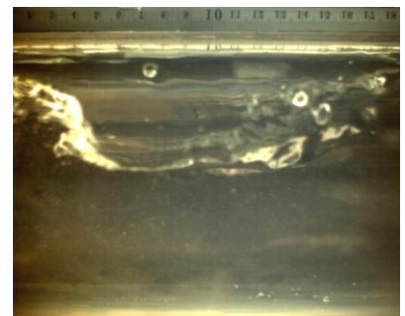
**Figure 4.24 Image at P3 at 350.51 seconds**



**Figure 4.25 Image at P3 at 353.81 seconds**



**Figure 4.26 Image at P3 at 355.36 seconds**



**Figure 4.27 Image at P3 at 355.88 seconds**

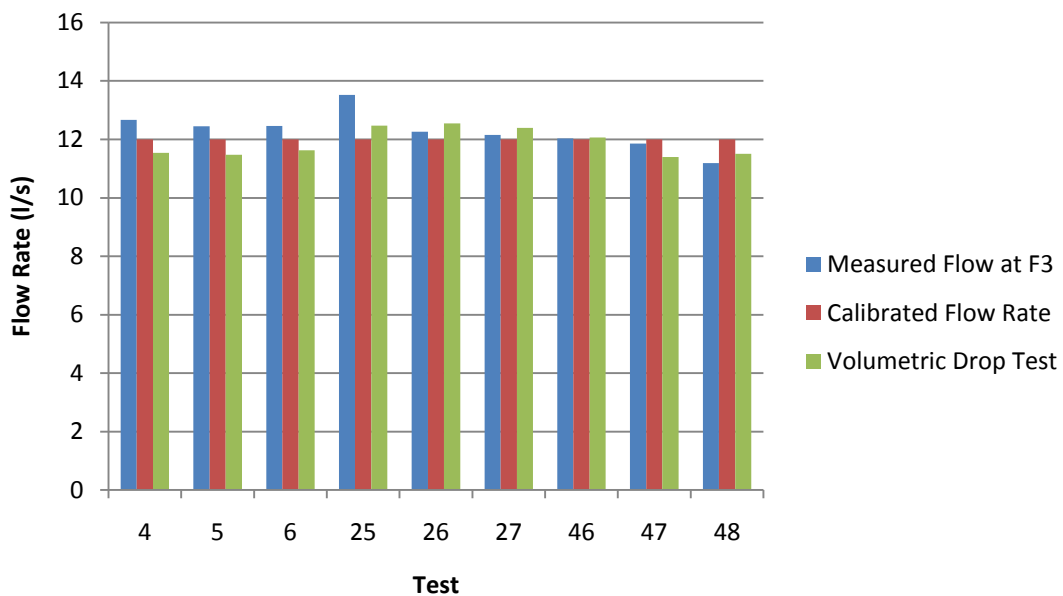
A range of flow conditions were observed at P3 throughout the 10 second measurement period. This included free surface flow (Figure 4.24), plug flow (Figure 4.23, Figure 4.25 and Figure 4.27), free surface flow with entrained air (Figure 4.26) and full bore flow conditions

(Figure 4.22). These varying conditions were observed repeatedly throughout this measurement period.

## 4.1.2 Tests Completed at 40% of the Design Flow Rate

### 4.1.2.1 Mass Balance

Flow tests completed at 40% of the design flow rate showed an average difference between the mass balance measured using flourometry and the volumetric drop test of  $\pm 4.94\%$  and a maximum difference of  $+9.79\%$ . The measured mean flow rate varied between 11.19 l/s to 13.52 l/s and a comparison between the measured flow at F3, calibrated flow rate and volumetric drop test is shown in Figure 4.28.

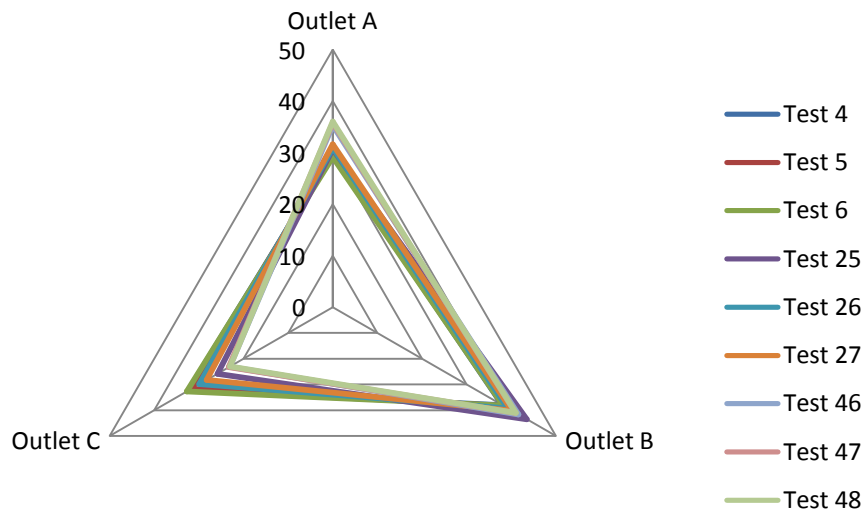


**Figure 4.28 Mass Balance Comparison for Tests Completed at 40% of the Design Flow Rate**

These results demonstrate repeatability and provide confidence in the application of this measurement technique for this series of tests.

### 4.1.2.2 Flow Proportionality

Figure 4.29 shows a radar plot demonstrating the relative proportionality of flow through each outlet during the tests reported in Table 4.3.



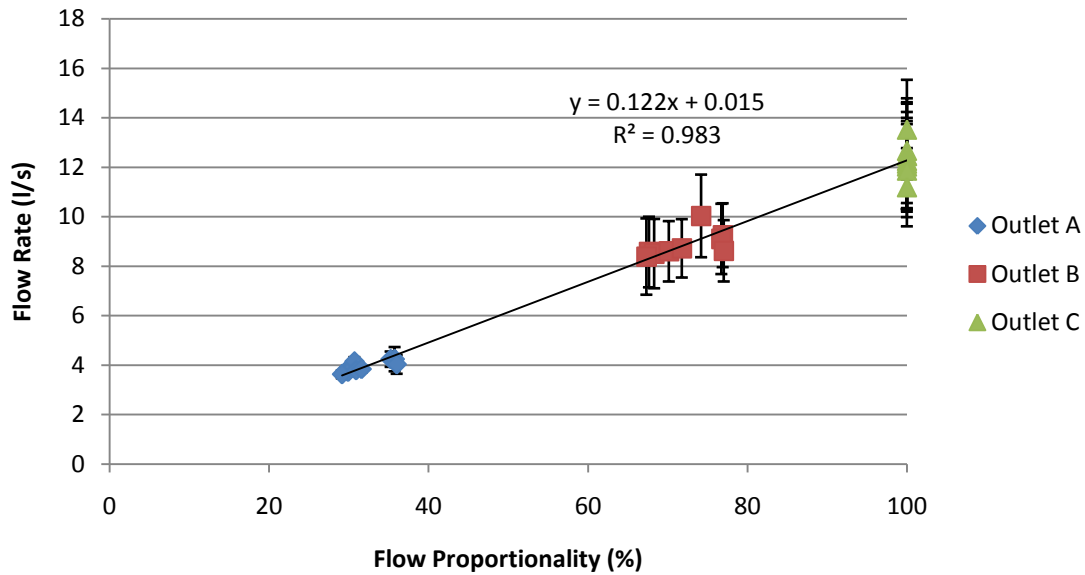
**Figure 4.29 Radar Plot Showing Flow Proportionality (%) at 40% of the Design Flow Rate**

The radar plot demonstrates that for the tests completed at 40% of the design flow rate, flow through Outlet B dominated, followed by Outlet A and finally Outlet C. This is a different trend compared to the tests completed at 20% of the design flow rate where although flow through Outlet B dominated, the proportionality between Outlet A and C was very similar. Maximum, minimum and average flow proportionality for the series of tests is shown in Table 4.17.

**Table 4.17 Maximum, Minimum and Average Flow Proportionality for Tests Completed at 40% of the Design Flow Rate**

Outlet	Maximum (%)	Minimum (%)	Average (%)
A	36.01	29.13	32.09
B	43.49	38.05	40.13
C	32.67	22.97	27.77

Figure 4.30 shows the measured component of flow through each outlet and relative standard deviation shown by the error bars for the series of flow tests.



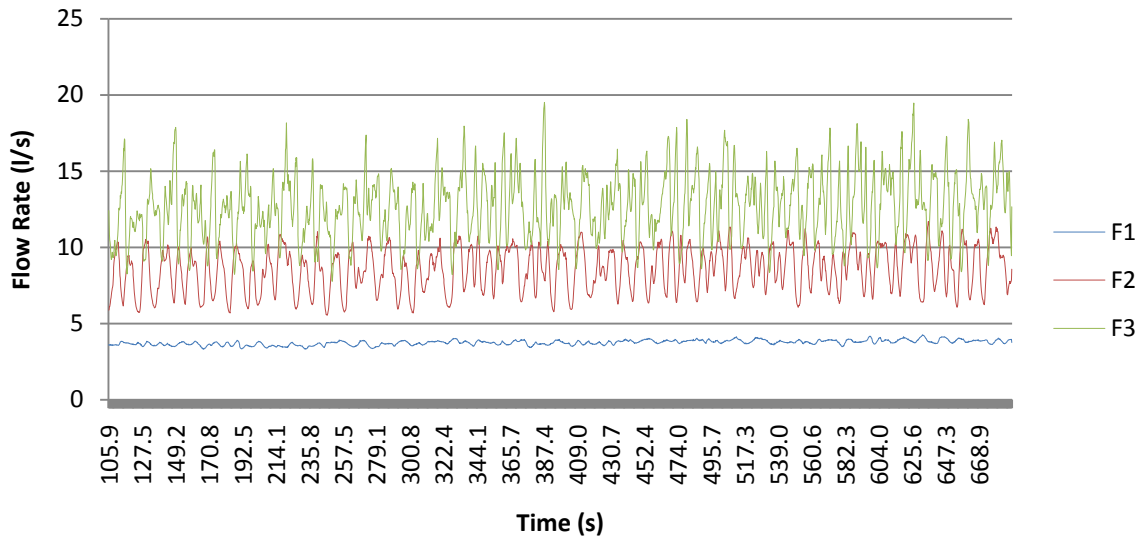
**Figure 4.30 Flow Proportionality at a Design Flow Rate of 40% with Standard Deviation shown by the Error Bars**

These results show that although the standard deviation of the flow proportionality increased through Outlets A, B and C, the range was significantly less when compared to the results from the tests completed at 20% of the design flow rate. This suggests that flow through Outlets B and C in particular is less variable in comparison.

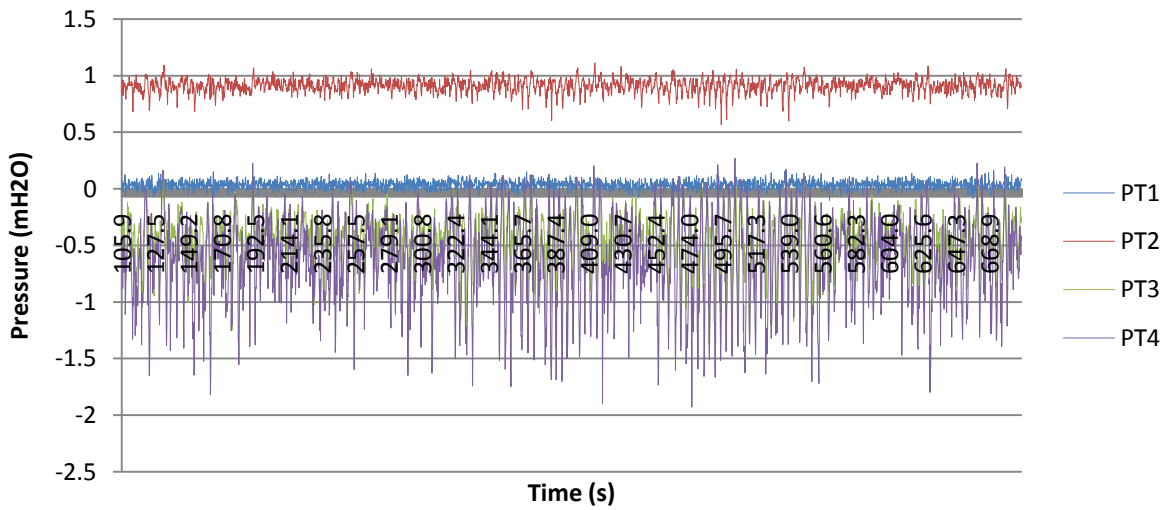
#### 4.1.2.3 Time Series Flow Rate and Pressure Measurements

Figure 4.31 and Figure 4.32 show continuous flow measurement measured using flourometry through each outlet and system pressure within the horizontal carrier pipe for the same time period during Test 4.



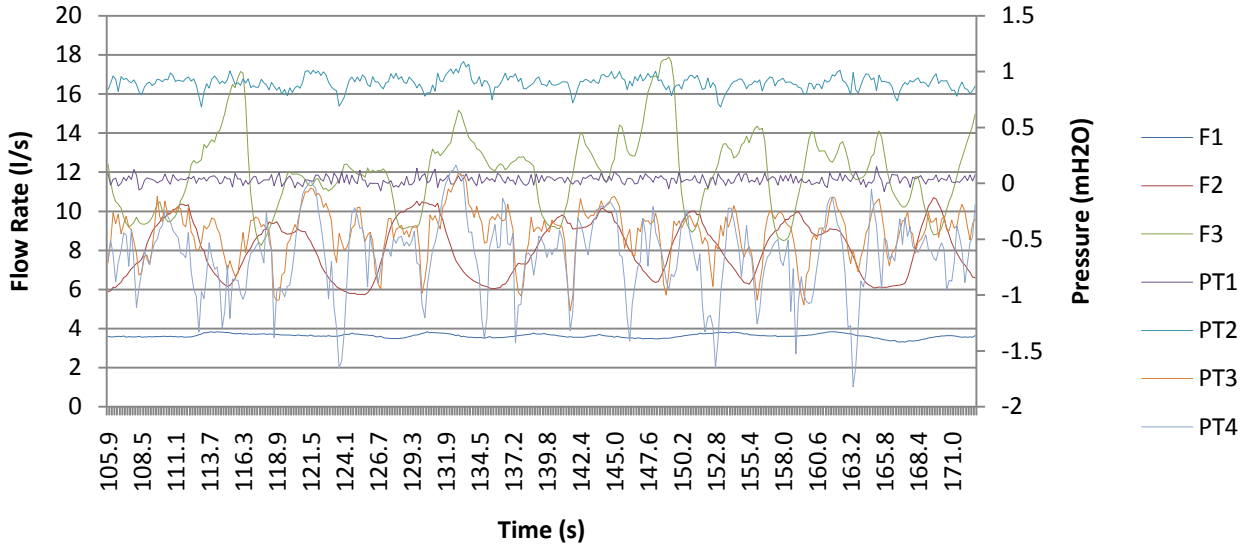


**Figure 4.31 Flow Measurement within the Horizontal Carrier Pipe during Test 4**



**Figure 4.32 Pressure Measurement within the Horizontal Carrier Pipe during Test 4**

Figure 4.33 shows the measured flow rate and pressure for a selected time period during Test 4.

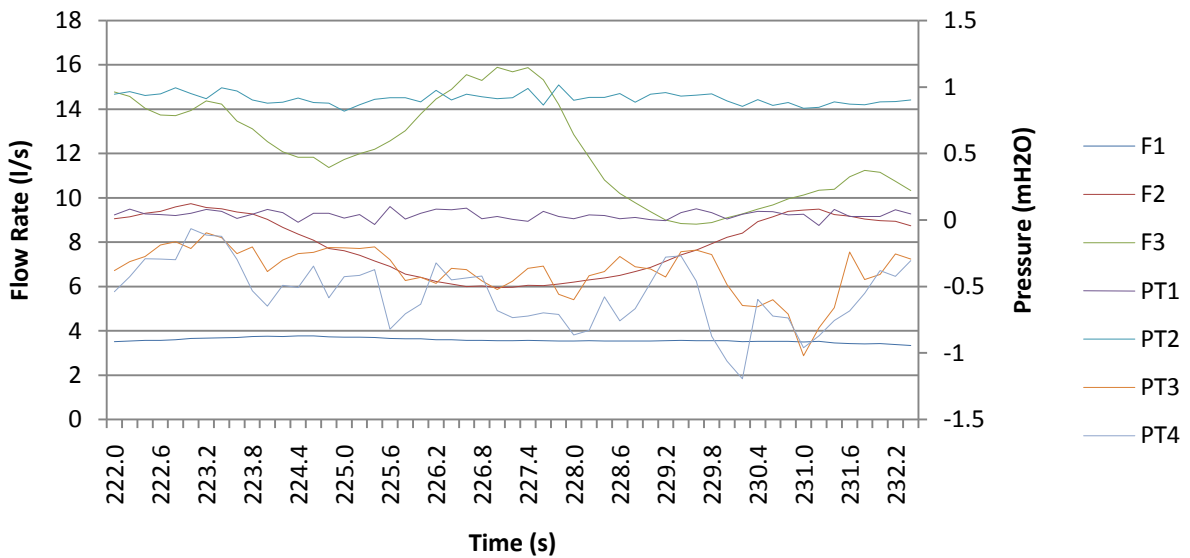


**Figure 4.33 Flow Rate and Pressure Measurement within the Horizontal Carrier Pipe during Test 4**

Figure 4.31, Figure 4.32 and Figure 4.33 demonstrated the flow profile through each outlet and the relative time series pressure data. The results showed that moving downstream through the system, both flow and pressure measurements became increasingly variable.

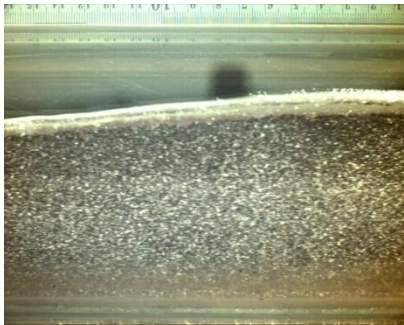
#### 4.1.2.4 Time Series Flow Rate, Pressure and Image Comparison at P1

Figure 4.34 shows the flow rate and pressure measurements for the corresponding 10 second period (222.20 seconds to 232.20 seconds) that images were collected at P1 (downstream of Outlet A and F1) during Test 4.

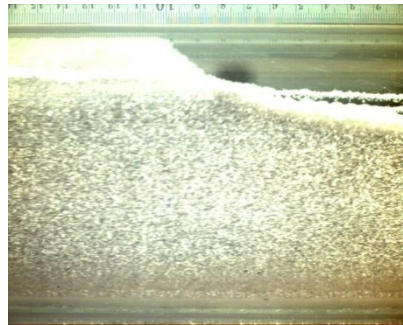


**Figure 4.34 Flow Rate and Pressure Measurement within the Horizontal Carrier Pipe during Test 4 (222.20 to 232.20 seconds)**

The following selected images correspond to the time series data shown in Figure 4.34.



**Figure 4.35 Image at P1 at 220.20 seconds**



**Figure 4.36 Image at P1 at 224.84 seconds**



**Figure 4.37 Image at P1 at 225.00 seconds**



**Figure 4.38 Image at P1 at 226.25 seconds**

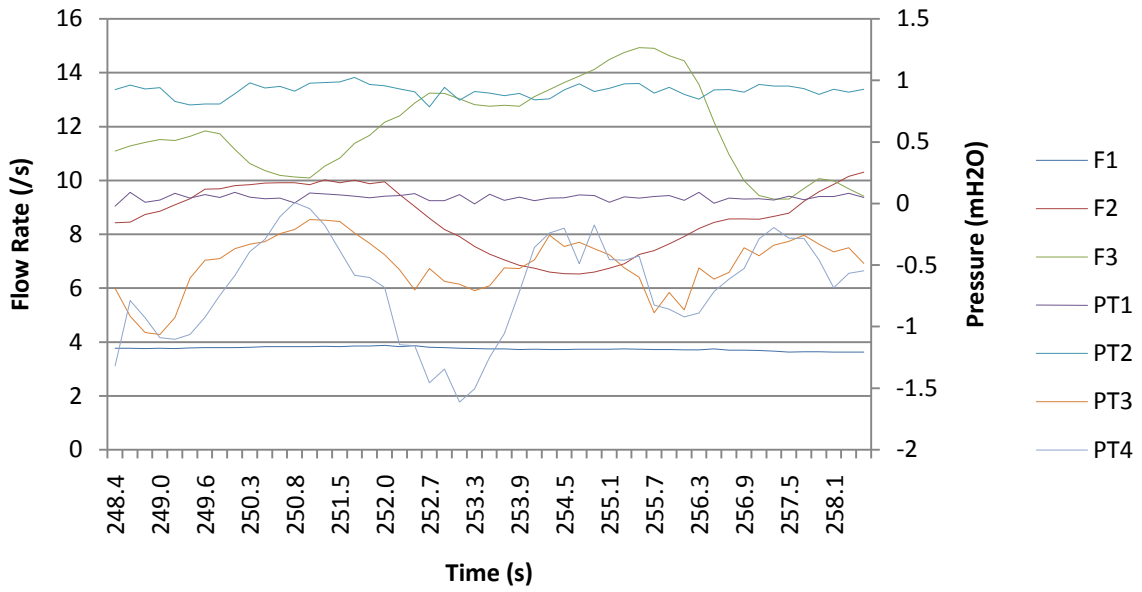


**Figure 4.39 Image at P1 at 226.65 seconds**

The images show free surface flow (Figure 4.35) with one observed period of plug flow (Figure 4.36) followed by full bore flow (Figure 4.37) lasting approximately 1 second (333 seconds to 334 seconds). Free surface flow conditions followed with a series of observed waves shown in Figure 4.39. The effect of this was recorded throughout the carrier pipe highlighted in Figure 4.34 where there is an measured increase in flow rate at F2 and F3 and decrease in pressure recorded by PT3 and PT4 after 228 seconds.

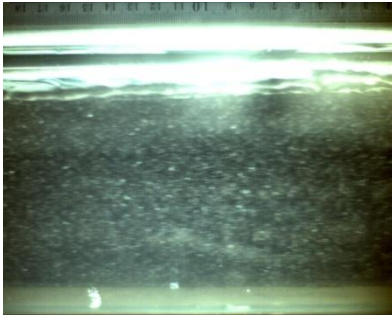
#### 4.1.2.5 Time Series Flow Rate, Pressure and Image Comparison at P2

Figure 4.40 shows the flow rate and pressure measurements for the corresponding 10 second period (248.39 to 258.39 seconds) that images were collected at P2 (downstream of Outlet B and F2) during Test 27.

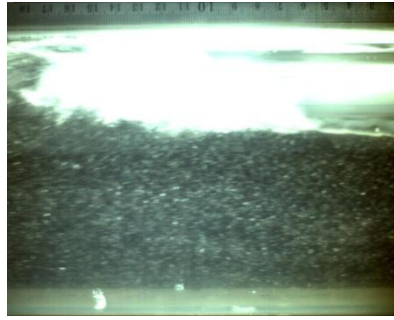


**Figure 4.40 Flow Rate and Pressure Measurement within the Horizontal Carrier Pipe during Test 27 (248.39 to 258.39 seconds)**

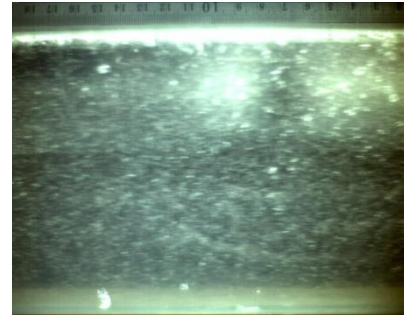
The following selected images correspond to the time series data shown in Figure 4.40.



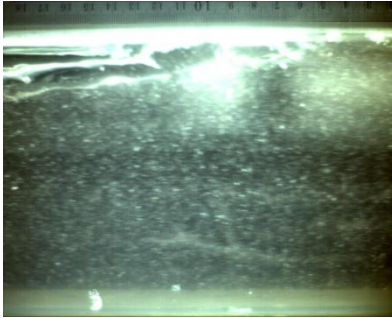
**Figure 4.41 Image at P2 at 248.39 seconds**



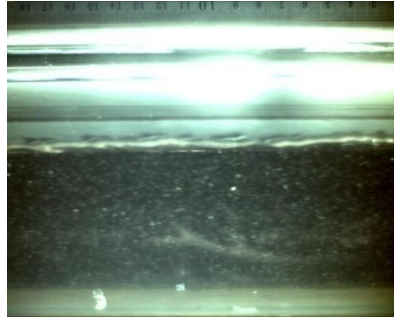
**Figure 4.42 Image at P2 at 249.33 seconds**



**Figure 4.43 Image at P2 at 249.65 seconds**



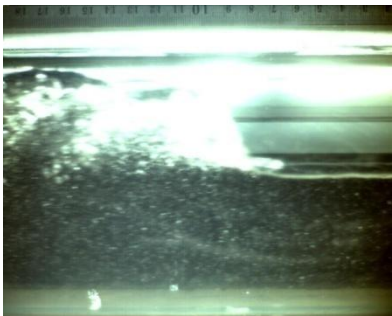
**Figure 4.44 Image at P2 at 250.38 seconds**



**Figure 4.45 Image at P2 at 251.85 seconds**



**Figure 4.46 Image at P2 at 253.38 seconds**

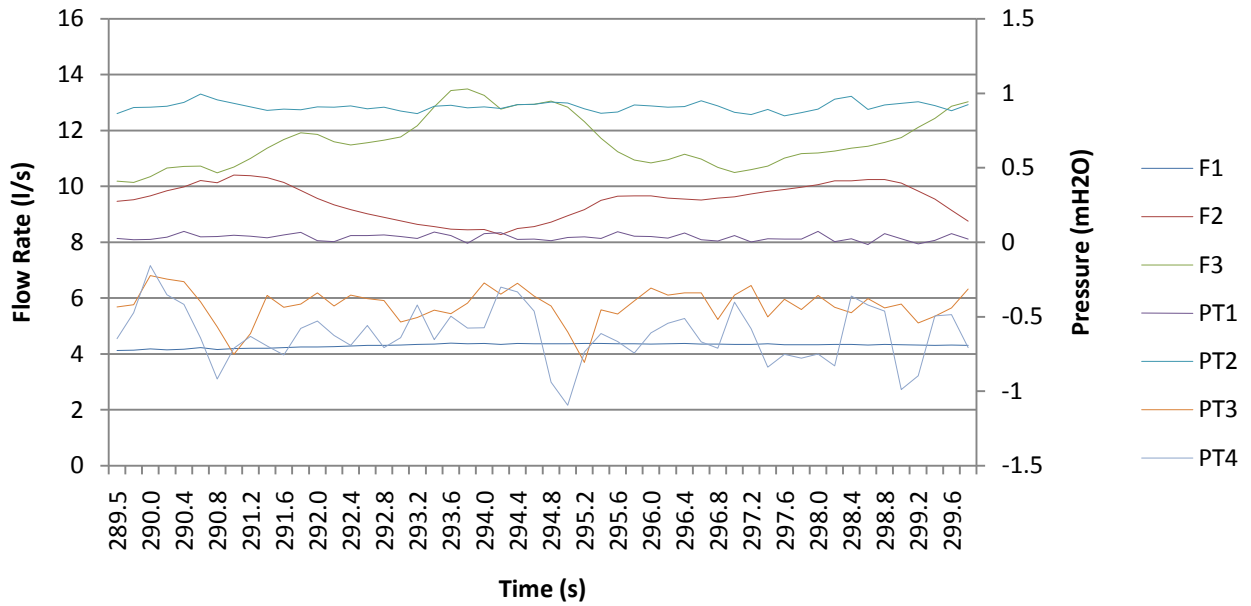


**Figure 4.47 Image at P2 at 257.78 seconds**

A range of flow conditions were observed during the measurement period including free surface flow (Figure 4.45), plug flow (Figure 4.42 and Figure 4.46) and full bore flow (Figure 4.43). A series of waves were recorded following which full bore flow (Figure 4.42) and free surface flow (Figure 4.47) conditions followed. Each period of full bore flow lasted approximately 1 second.

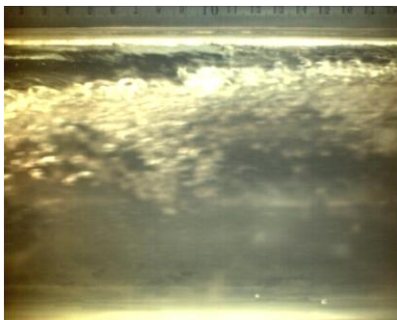
#### 4.1.2.6 Time Series Flow Rate, Pressure and Image Comparison at P3

Figure 4.48 shows the flow rate and pressure measurements for the corresponding 10 second period (289.61 to 299.61 seconds) that images were collected at P3 (downstream of Outlet C and F3) during Test 46.

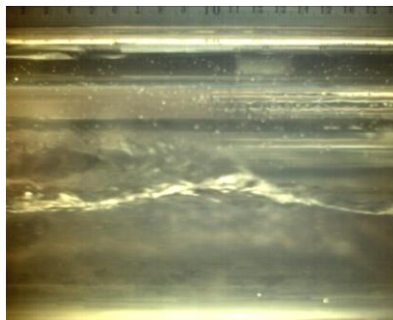


**Figure 4.48 Flow Rate and Pressure Measurement within the Horizontal Carrier Pipe during Test 46 (289.61 to 299.61 seconds)**

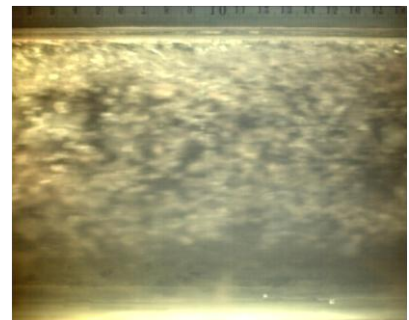
The following selected images correspond to the time series data shown in Figure 4.48.



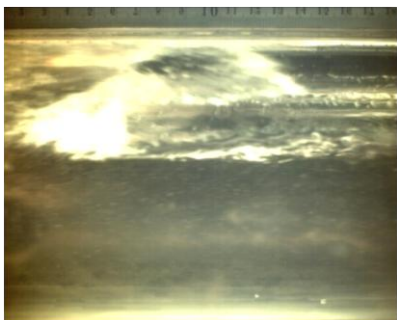
**Figure 4.49 Image at P3 at 289.61 seconds**



**Figure 4.50 Image at P3 at 290.70 seconds**



**Figure 4.51 Image at P3 at 291.37 seconds**



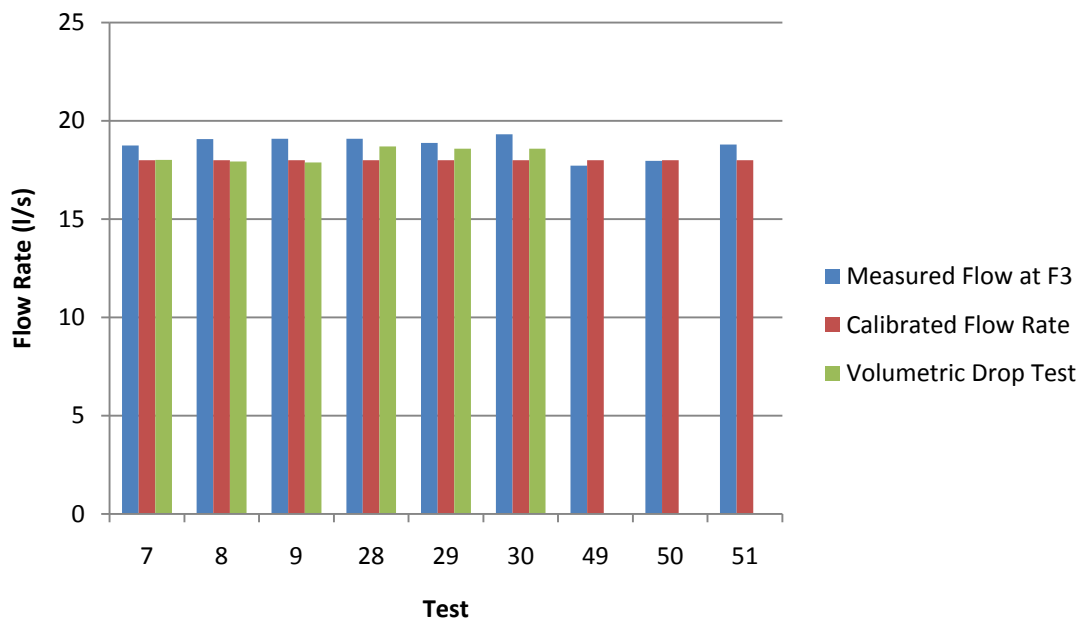
**Figure 4.52 Image at P3 at 295.46 seconds**

Flow at P3 during the steady flow tests completed at 12 l/s were dominated by free surface flow (Figure 4.50) and a series of waves (Figure 4.52) preceding periods of aerated two-phase flow (Figure 4.49 and Figure 4.51). There were no periods of plug flow or full bore flow observed at P3.

### 4.1.3 Tests Completed at 60% of the Design Flow Rate

#### 4.1.3.1 Mass Balance

Flow tests completed at 60% of the design flow rate showed an average difference between the mass balance measured using flourometry and the volumetric drop test of  $\pm 4.11\%$  and a maximum difference of  $+6.65\%$ . The measured mean flow rate varied between 17.72 l/s to 19.31 l/s and a comparison between the measured flow at F3, calibrated flow rate and the volumetric drop test is shown in Figure 4.53.

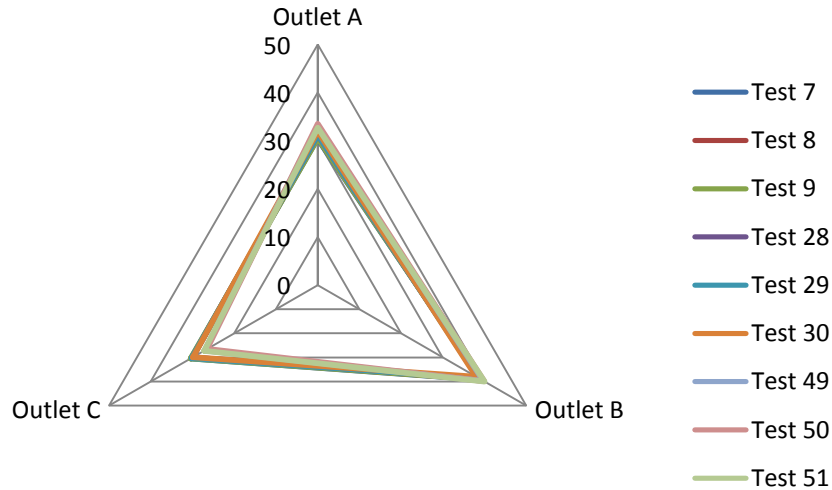


**Figure 4.53 Mass Balance Comparison for Tests Completed at 60% of the Design Flow Rate**

These results show a continued decrease in the difference between the measured average flow rate and the volumetric drop tests in comparison to the tests completed at 20% and 40% of the design flow rate.

#### 4.1.3.2 Flow Proportionality

Figure 4.54 shows a radar plot demonstrating the relative proportionality of flow through each outlet during the tests reported in Table 4.4.



**Figure 4.54 Radar Plot Showing Flow Proportionality (%) at 60% of the Design Flow Rate**

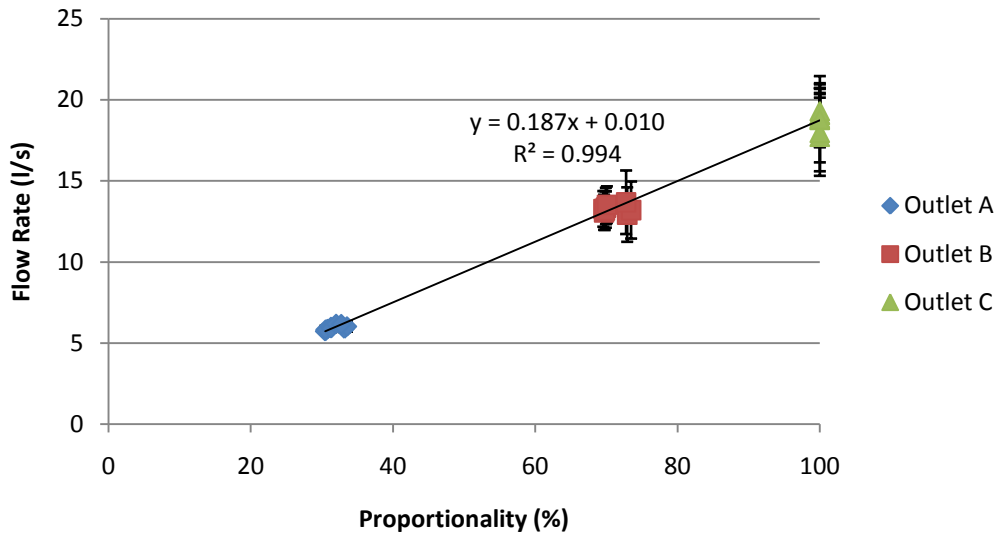
The radar plot shows that during the tests completed at 60% of the design flow rate, flow through Outlet B dominated, followed by Outlet A and finally Outlet C. These results are comparable to the trend observed in the flow tests completed at 40% of the design flow rate. However, flow proportionality through Outlet B is slightly lower and Outlet C slightly higher in comparison. Maximum, minimum and average flow proportionality for the series of tests is shown in Table 4.18.

**Table 4.18 Maximum, Minimum and Average Flow Proportionality for Tests Completed at 60% of the Design Flow Rate**

Outlet	Maximum (%)	Minimum (%)	Average (%)
A	33.50	30.48	31.75
B	40.05	38.06	39.14
C	30.45	26.54	29.11

Figure 4.55 shows the measured component of flow through each outlet and relative standard deviation shown by the error bars for the series of flow tests.



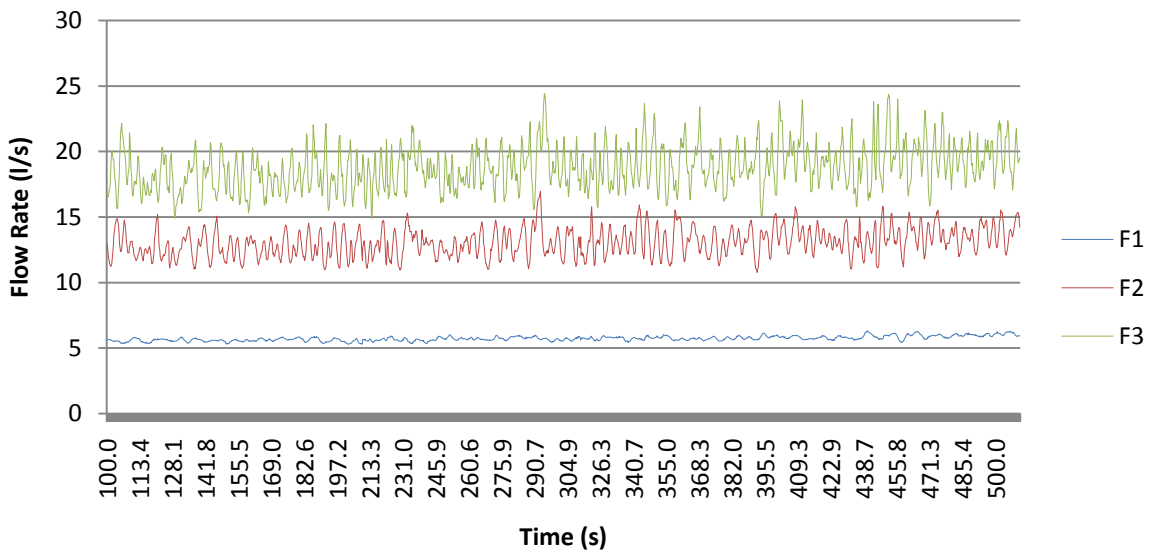


**Figure 4.55 Flow Proportionality at a Design Flow Rate of 60% with Standard Deviation shown by the Error Bars**

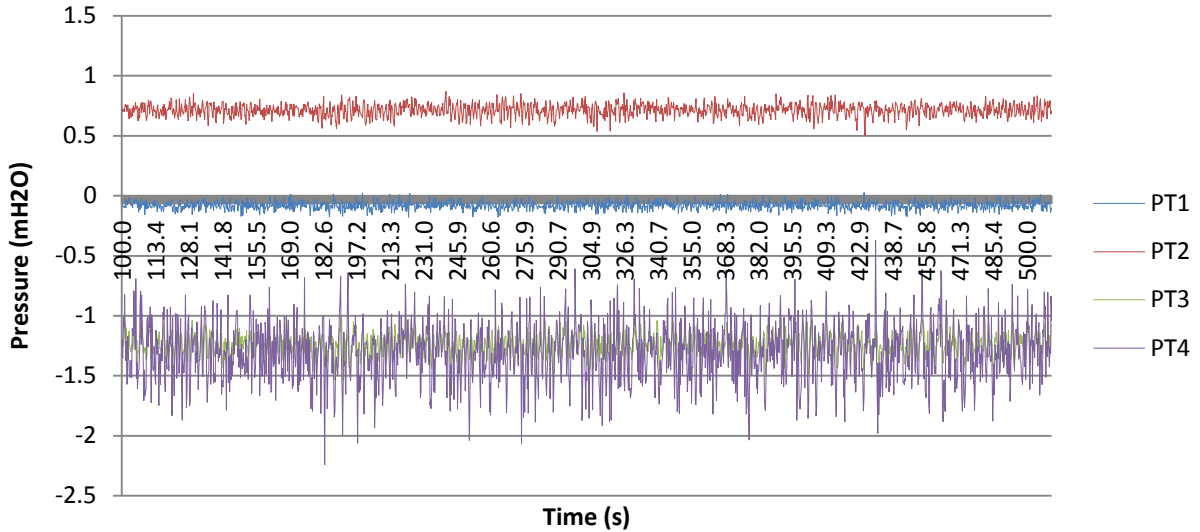
These results show that although the standard deviation increased through Outlets A, B and C, the range is comparable to the results measured during the tests completed at 40% of the design flow rate.

#### 4.1.3.3 Time Series Flow Rate and Pressure Measurements

Figure 4.56 and Figure 4.57 show continuous flow measurement measured using flourometry through each outlet and system pressure within the horizontal carrier pipe for the same time period during Test 7.

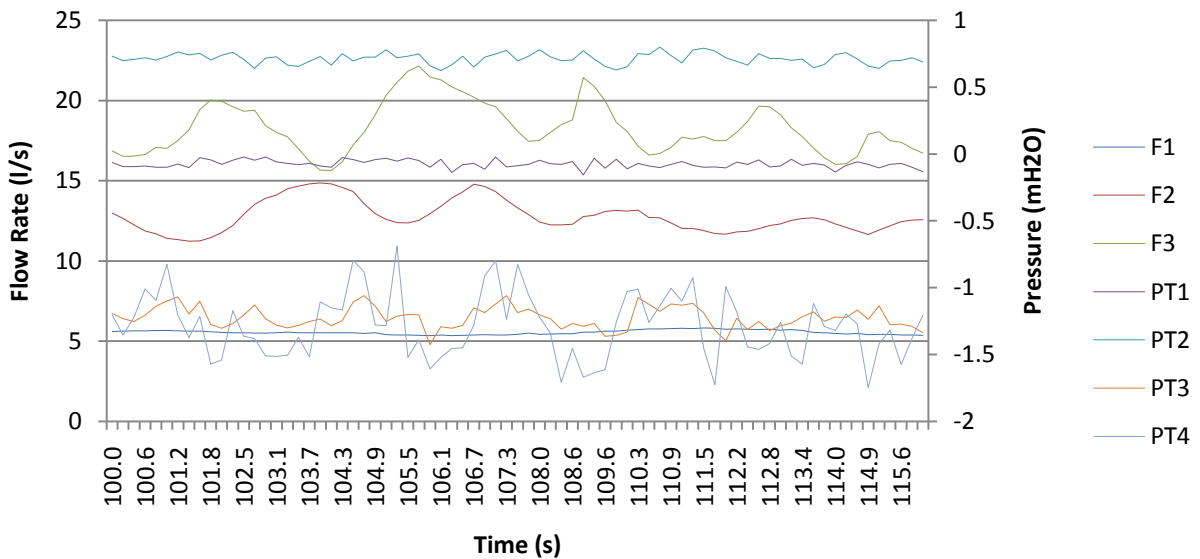


**Figure 4.56 Flow Measurement within the Horizontal Carrier Pipe during Test 7**



**Figure 4.57 Pressure Measurement within the Horizontal Carrier Pipe during Test 7**

Figure 4.58 shows the measured flow rate and pressure for a selected time period during Test 7.

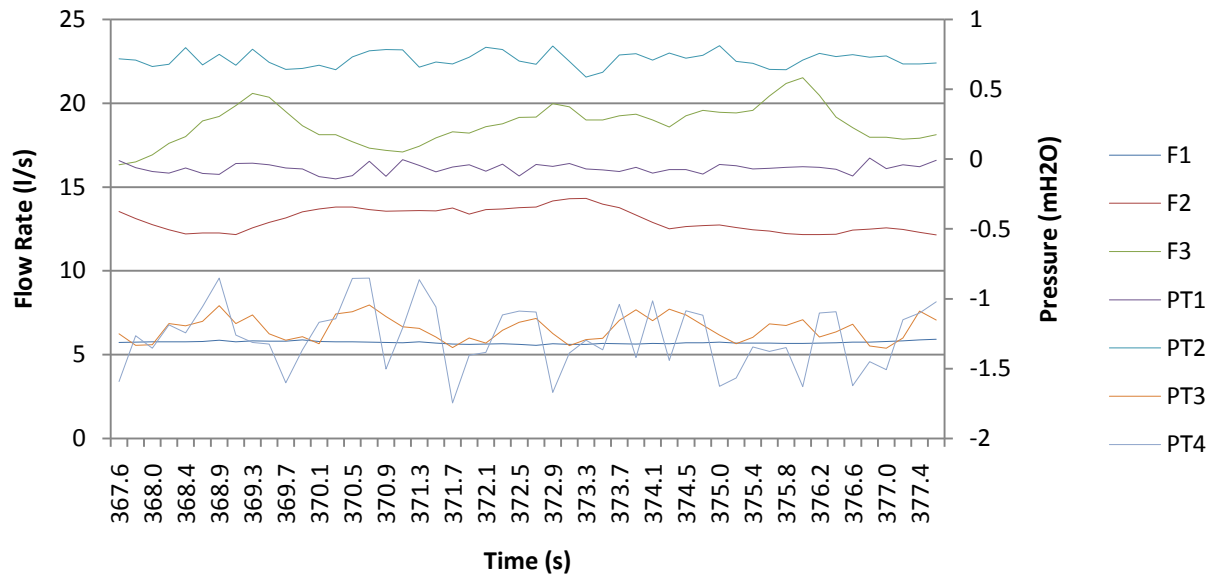


**Figure 4.58 Flow Rate and Pressure Measurement within the Horizontal Carrier Pipe during Test 7**

Figure 4.56, Figure 4.57 and Figure 4.58 demonstrate that similar to the flow tests completed at 40% of the design flow rate, the flow profile through each outlet and the relative time series pressure data became increasingly variable moving downstream through the experimental test facility.

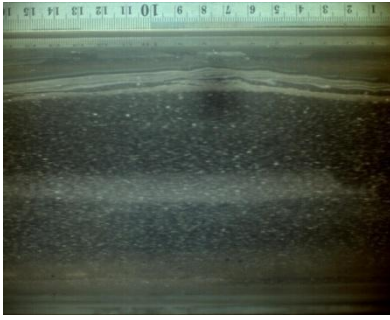
#### 4.1.3.4 Time Series Flow Rate, Pressure and Image Comparison at P1

Figure 4.59 shows the flow rate and pressure measurements for the corresponding 10 second period (367.71 seconds to 377.71 seconds) that images were collected at P1 (downstream of Outlet A and F1) during Test 8.

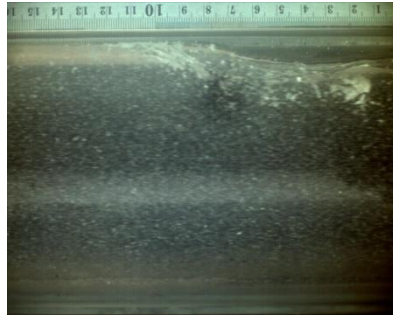


**Figure 4.59 Flow Rate and Pressure Measurement within the Horizontal Carrier Pipe during Test 8 (367.71 to 377.71 seconds)**

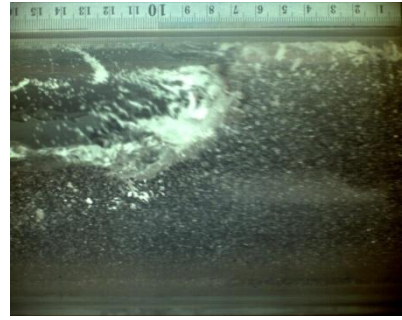
The following selected images correspond to the time series data shown in Figure 4.59.



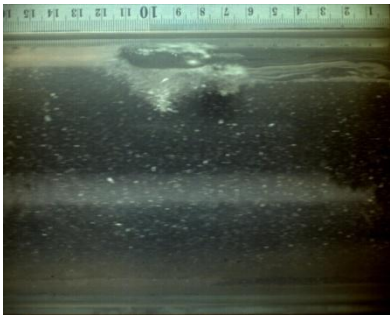
**Figure 4.60 Image at P1 at 368.59 seconds**



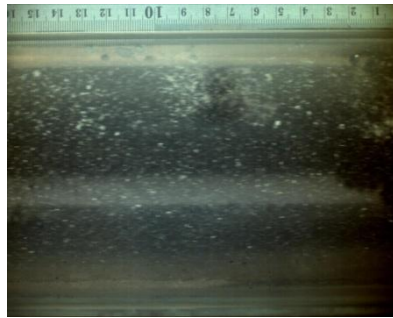
**Figure 4.61 Image at P1 at 370.26 seconds**



**Figure 4.62 Image at P1 at 370.64 seconds**



**Figure 4.63 Image at P1 at 375.24 seconds**

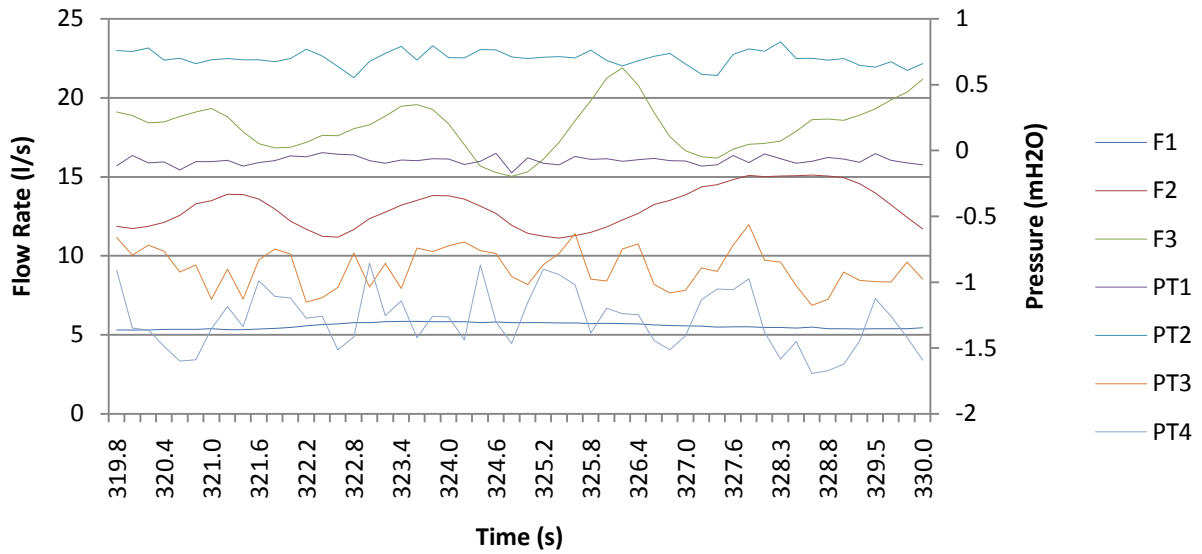


**Figure 4.64 Image at P1 at 375.39 seconds**

A series of free surface waves were observed at P1 (Figure 4.60). Where the water occupied the cross-sectional area of the carrier pipe (Figure 4.61 and Figure 4.63), full bore flow followed containing entrained air shown in Figure 4.64. These full bore conditions lasted approximately 0.4 seconds demonstrated by the time difference between the images in Figure 4.61 and Figure 4.62.

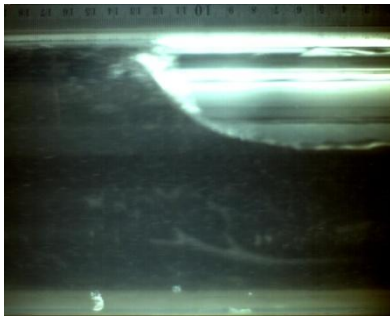
#### 4.1.3.5 Time Series Flow Rate, Pressure and Image Comparison at P2

Figure 4.65 shows the flow rate and pressure measurements for the corresponding 10 second period (319.89 to 329.89 seconds) that images were collected at P2 (downstream of Outlet B and F2) during Test 29.

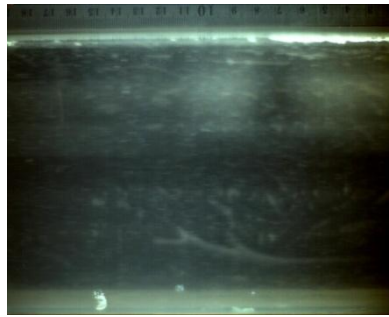


**Figure 4.65 Flow Rate and Pressure Measurement within the Horizontal Carrier Pipe during Test 29 (319.89 to 329.89 seconds)**

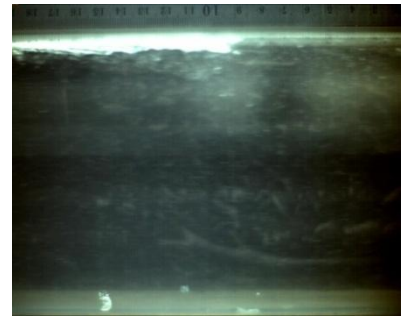
The following selected images correspond to the time series data shown in Figure 4.65.



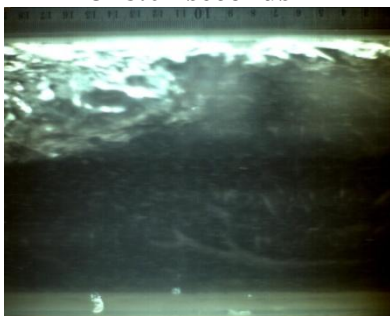
**Figure 4.66 Image at P2 at 328.01 seconds**



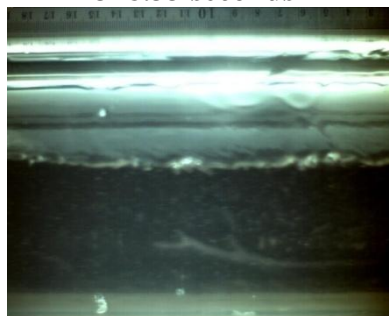
**Figure 4.67 Image at P2 at 328.33 seconds**



**Figure 4.68 Image at P2 at 328.39 seconds**



**Figure 4.69 Image at P2 at 328.59 seconds**



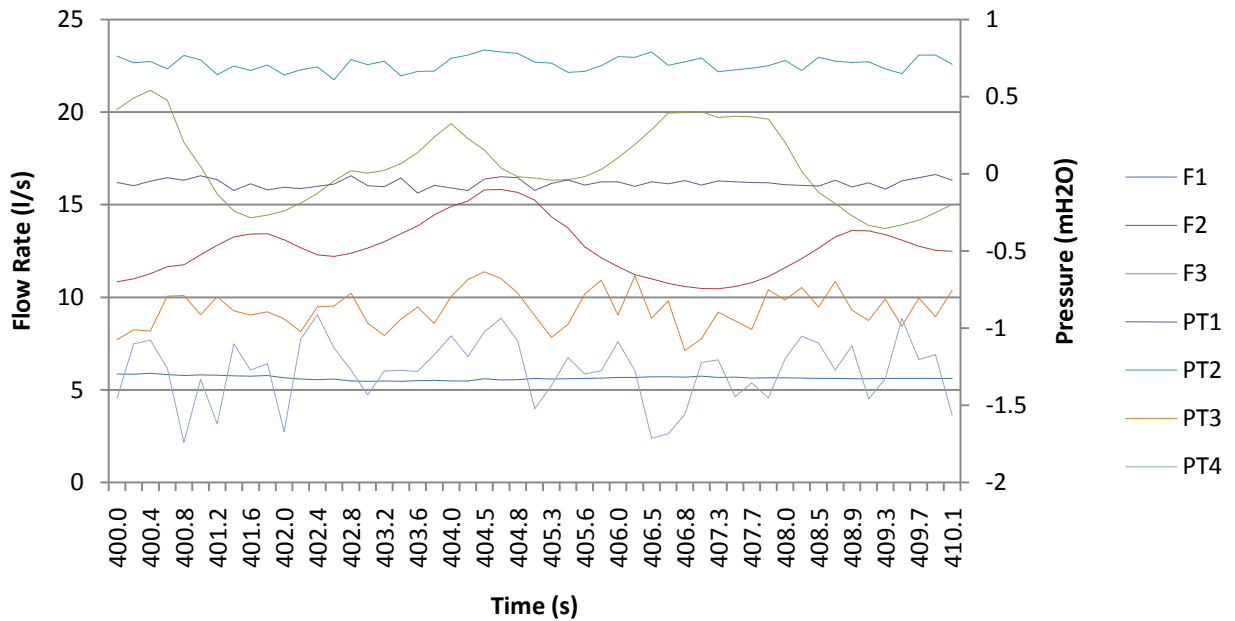
**Figure 4.70 Image at P2 at 328.89 seconds**

The images recorded at P2 showed frequent plug flow interspersed by free surface flow. Following the initial wave (Figure 4.66) full bore conditions follow (Figure 4.67). A series of air pockets along the crown of the pipe were observed (Figure 4.68) with little to no entrained air before the siphonic effect was broken (Figure 4.69). Each of the flow pulse or plug lasted

approximately 0.6 seconds demonstrated by the time between the images shown in Figure 4.66 and Figure 4.69.

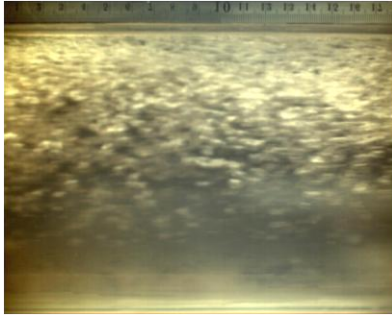
#### 4.1.3.6 Time Series Flow Rate, Pressure and Image Comparison at P3

Figure 4.71 shows the flow rate and pressure measurements for the corresponding 10 second period (400.08 to 410.08 seconds) that images were collected at P3 (downstream of Outlet C and F3) during Test 50.

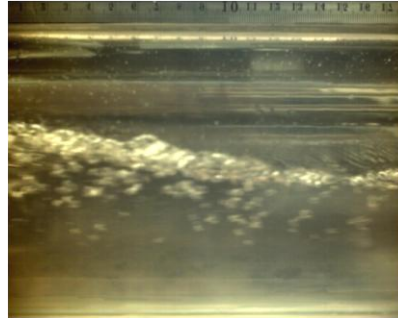


**Figure 4.71 Flow Rate and Pressure Measurement within the Horizontal Carrier Pipe during Test 50 (400.08 to 410.08 seconds)**

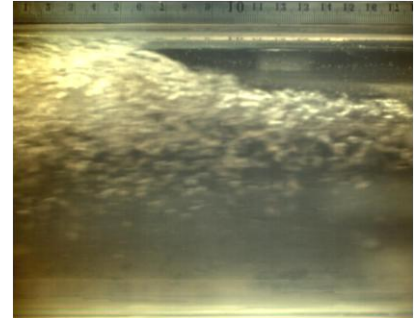
The following selected images correspond to the time series data shown in Figure 4.71.



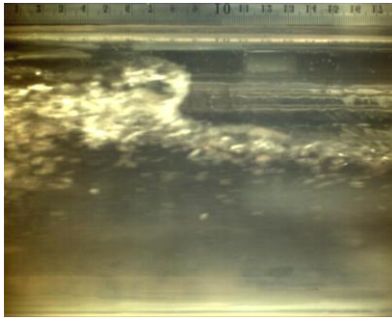
**Figure 4.72 Image at P3 at 400.08 seconds**



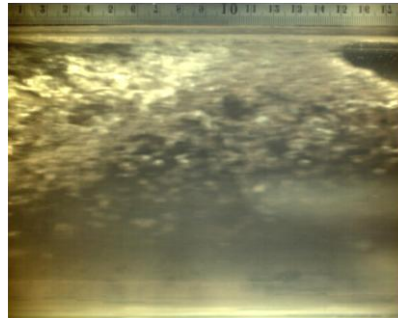
**Figure 4.73 Image at P3 at 401.35 seconds**



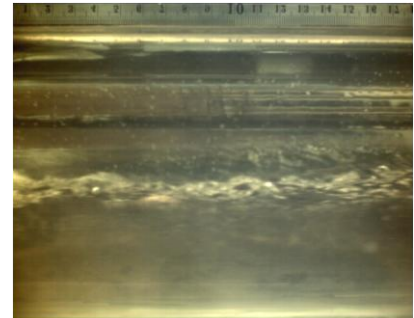
**Figure 4.74 Image at P3 at 403.60 seconds**



**Figure 4.75 Image at P3 at 404.27 seconds**



**Figure 4.76 Image at P3 at 404.86 seconds**



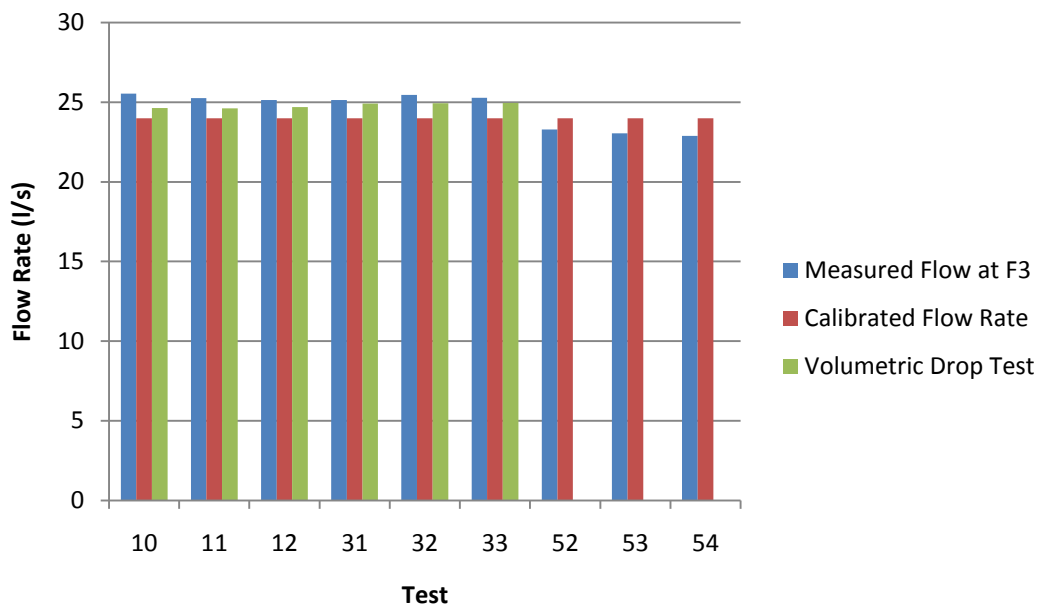
**Figure 4.77 Image at P3 at 409.09 seconds**

Flow at P3 during the steady flow tests completed at 18 l/s were dominated by aerated two phase flow (Figure 4.72) and a series of waves (Figure 4.74, Figure 4.75 and Figure 4.76) that both occupied and did not fully occupy the cross-sectional area of the pipe (Figure 4.72, Figure 4.73 and Figure 4.77). There were short periods of free surface flow with no entrained air (Figure 4.77) and no observed plug flow or full bore flow conditions observed at P3.

#### 4.1.4 Tests Completed at 80% of the Design Flow Rate

##### 4.1.4.1 Mass Balance

Flow tests completed at 80% of the design flow rate showed an average difference between the mass balance measured using flourometry and the volumetric drop test of  $\pm 2.03\%$  and a maximum difference of  $+3.61\%$ . The measured mean flow rate varied between 22.89 l/s to 25.53 l/s and a comparison between the measured flow at F3, calibrated flow rate and the volumetric drop test is shown in Figure 4.78.



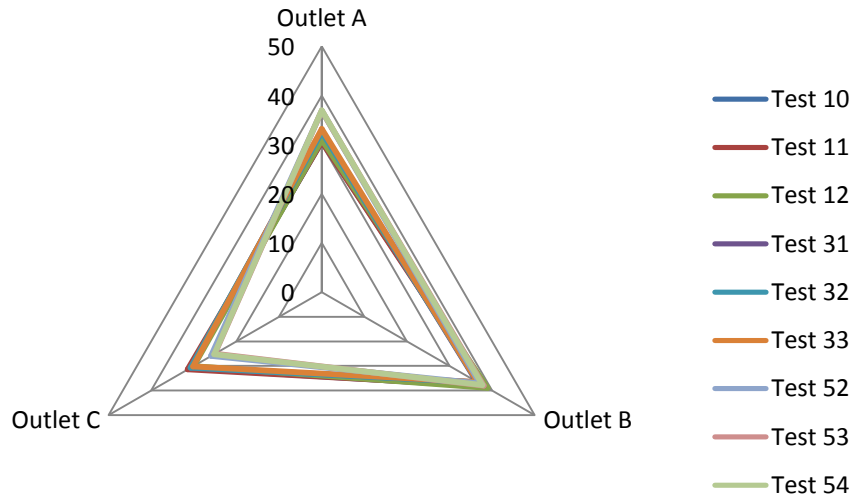
**Figure 4.78 Mass Balance Comparison for Tests Completed at 80% of the Design Flow Rate**

These results show a continued trend of a decrease in the difference between the measured average flow rate and the volumetric drop tests in comparison to the tests completed at 20%, 40% and 60% of the design flow rate.

##### 4.1.4.2 Flow Proportionality

Figure 4.79 shows a radar plot demonstrating the relative proportionality of flow through each outlet during the tests reported in Table 4.5.





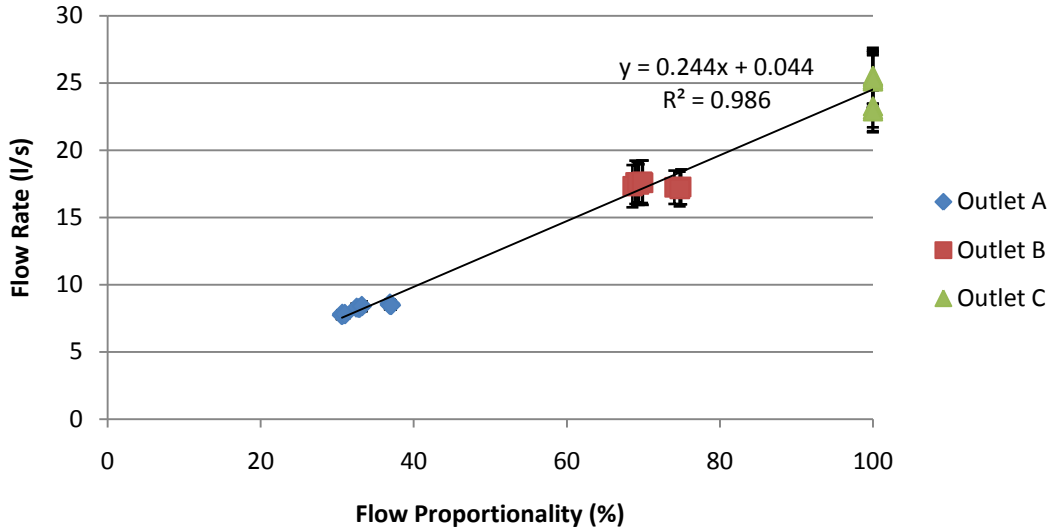
**Figure 4.79 Radar Plot Showing Flow Proportionality (%) at 80% of the Design Flow Rate**

These results show that at 80% of the design flow rate, flow through Outlet B dominated, followed by Outlet A and finally Outlet C. The average flow proportionality measured through Outlet C was very similar (0.65%) to the results observed at 60% of the design flow rate. Proportionality increased through Outlet A and decreased through Outlet B relative to the results measured during the flow tests at 20%, 40% and 60% of the design flow rate. Maximum, minimum and average flow proportionality for the series of tests is shown in Table 4.19.

**Table 4.19 Maximum, Minimum and Average Flow Proportionality for Tests Completed at 80% of the Design Flow Rate**

Outlet	Maximum (%)	Minimum (%)	Average (%)
A	37.00	30.61	33.51
B	38.96	36.53	37.57
C	31.43	25.05	28.92

Figure 4.80 shows the measured component of flow through each outlet and relative standard deviation shown by the error bars for the series of flow tests.

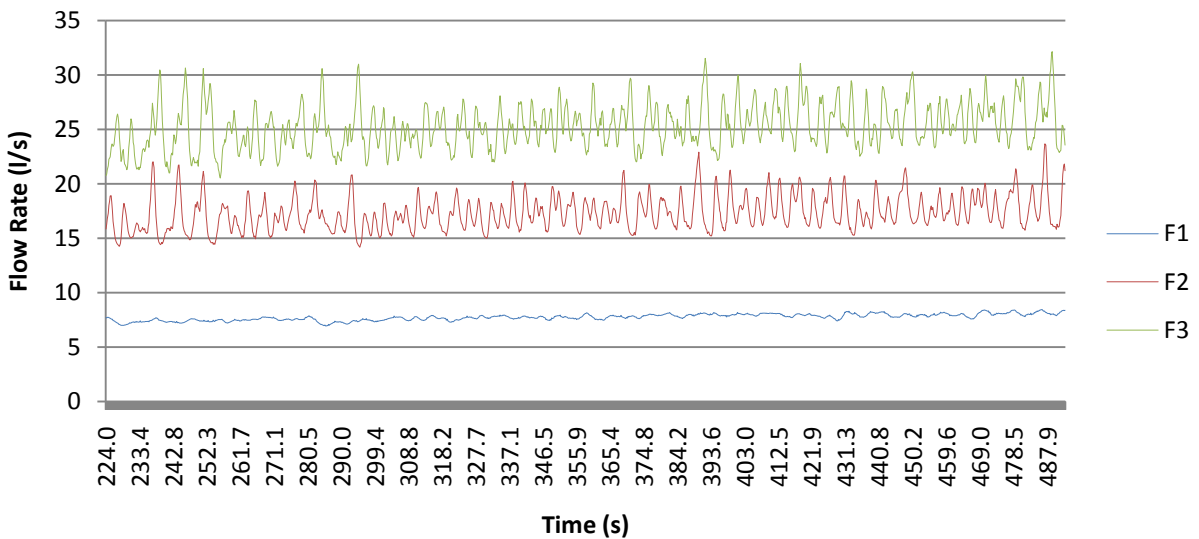


**Figure 4.80 Flow Proportionality at a Design Flow Rate of 80% with Standard Deviation shown by the Error Bars**

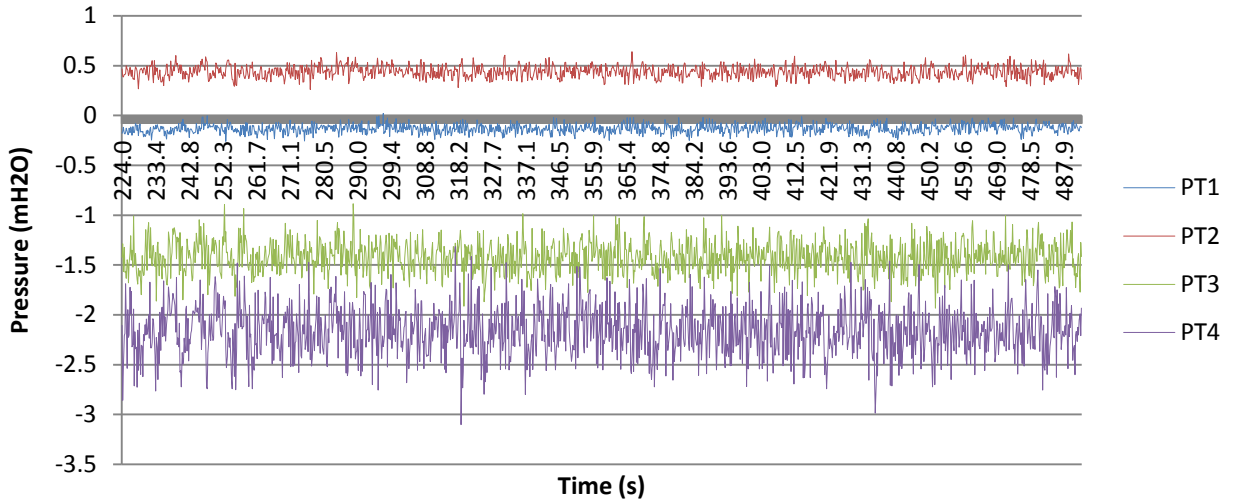
These results show that although the standard deviation increases through Outlets A, B and C, the range is comparable to the results measured during the tests completed at 40% and 60% of the design flow rate.

#### 4.1.4.3 Time Series Flow Rate and Pressure Measurements

Figure 4.81 and Figure 4.82 show continuous flow measurement measured using flourometry through each outlet and system pressure within the horizontal carrier pipe for the same time period during Test 11.

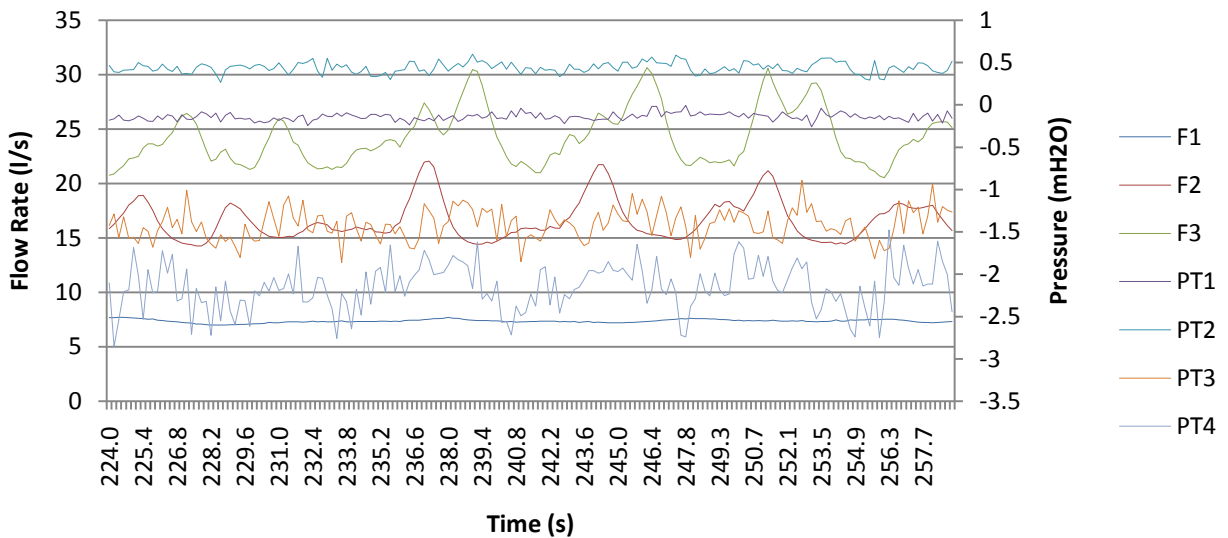


**Figure 4.81 Flow Measurement within the Horizontal Carrier Pipe during Test 11**



**Figure 4.82 Pressure Measurement within the Horizontal Carrier Pipe during Test 11**

Figure 4.83 shows the measured flow rate and pressure for a selected time period during Test 11.

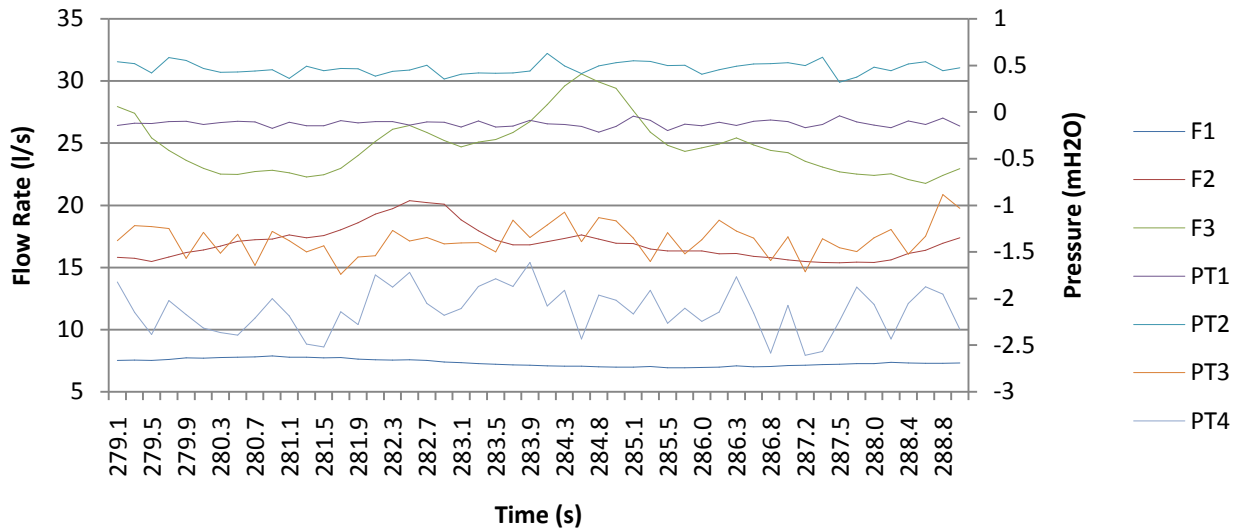


**Figure 4.83 Flow Rate and Pressure Comparison During Test 11**

Figure 4.81, Figure 4.82 and Figure 4.83 demonstrate that similar to the flow tests completed at 40% and 60% of the design flow rate, the flow profile through each outlet and the relative time series pressure data became increasingly variable moving downstream through the experimental test facility.

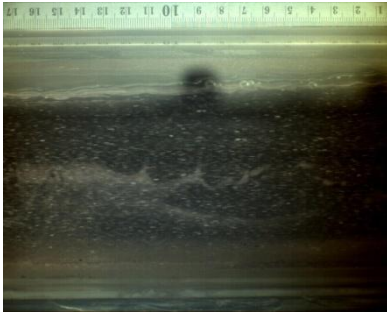
#### 4.1.4.4 Time Series Flow Rate, Pressure and Image Comparison at P1

Figure 4.84 shows the flow rate and pressure measurements for the corresponding 10 second period (279.07 seconds to 289.07 seconds) that images were collected at P1 (downstream of Outlet A and F1) during Test 11.



**Figure 4.84 Flow Rate and Pressure Measurement within the Horizontal Carrier Pipe During Test 11 (279.07 to 289.07 seconds)**

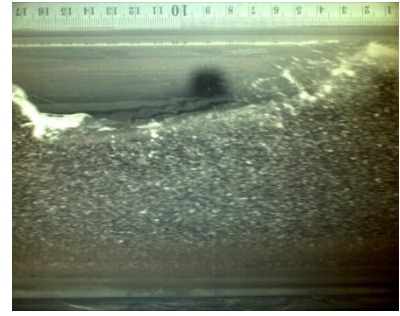
The following selected images were taken at P1 (downstream of Outlet A and F1) during Test 11 from 279.07 to 289.07 seconds.



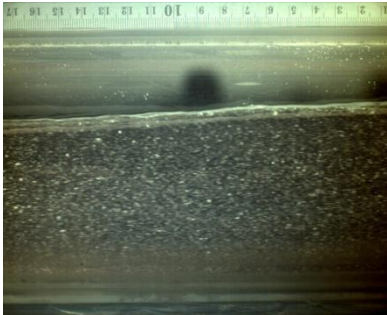
**Figure 4.85 Image at P1 at 279.07 seconds**



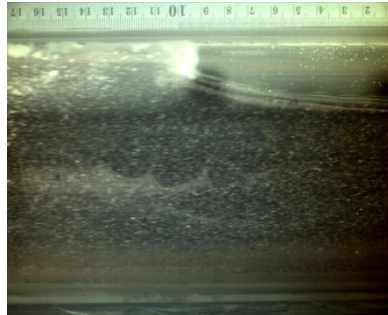
**Figure 4.86 Image at P1 at 280.59 seconds**



**Figure 4.87 Image at P1 at 280.87 seconds**



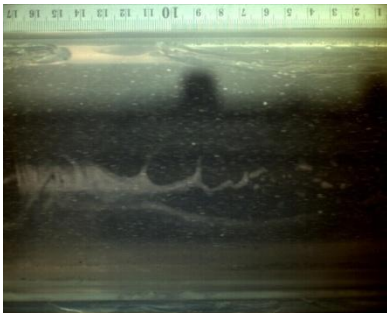
**Figure 4.88 Image at P1 at 282.56 seconds**



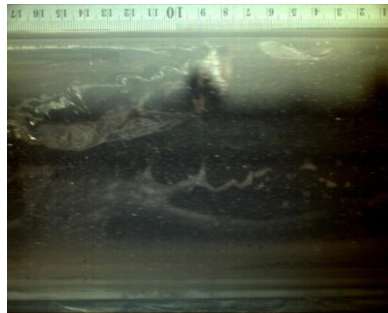
**Figure 4.89 Image at P1 at 283.83 seconds**



**Figure 4.90 Image at P1 at 285.25 seconds**



**Figure 4.91 Image at P1 at 287.69 seconds**

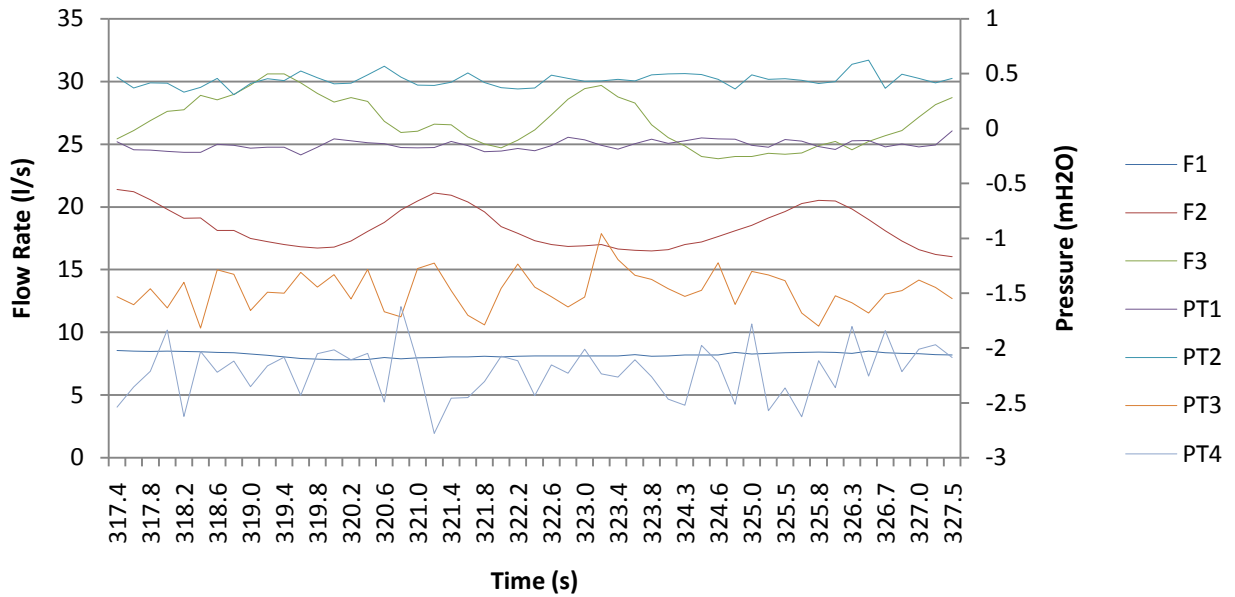


**Figure 4.92 Image at P1 at 288.24 seconds**

The images recorded at P1 showed plug flow conditions interspersed by free surface flow. Following the initial wave (Figure 4.89) full bore conditions follow until the siphonic effect is broken and free surface flow conditions resume (Figure 4.85 and Figure 4.88). A series of air pockets along the crown of the pipe were observed (Figure 4.86) with little to no entrained air before the siphonic effect was broken (Figure 4.90). Each of the flow pulses or plugs varied in time between 0.55 seconds (Figure 4.91 to Figure 4.92) and 1.4 seconds (Figure 4.89 to Figure 4.90).

#### 4.1.4.5 Time Series Flow Rate, Pressure and Image Comparison at P2

Figure 4.93 shows the flow rate and pressure measurements for the corresponding 10 second period (317.41 to 327.41 seconds) that images were collected at P2 (downstream of Outlet B and F2) during Test 33.



**Figure 4.93 Flow Rate and Pressure Measurement within the Horizontal Carrier Pipe during Test 33 (317.41 to 327.41 seconds)**

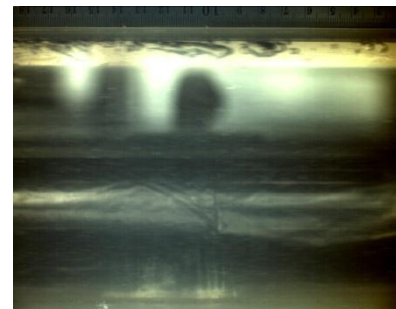
The following selected images correspond to the time series data shown in Figure 4.93.



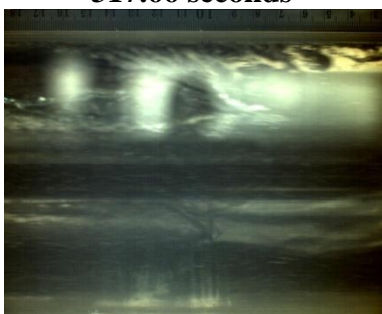
**Figure 4.94 Image at P2 at 317.66 seconds**



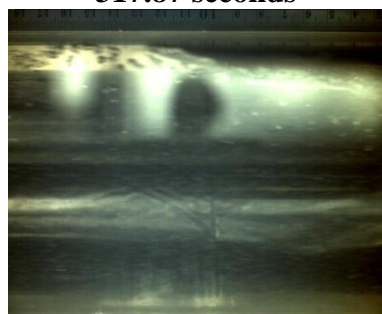
**Figure 4.95 Image at P2 at 317.87 seconds**



**Figure 4.96 Image at P2 at 318.10 seconds**



**Figure 4.97 Image at P2 at 318.16 seconds**



**Figure 4.98 Image at P2 at 320.60 seconds**



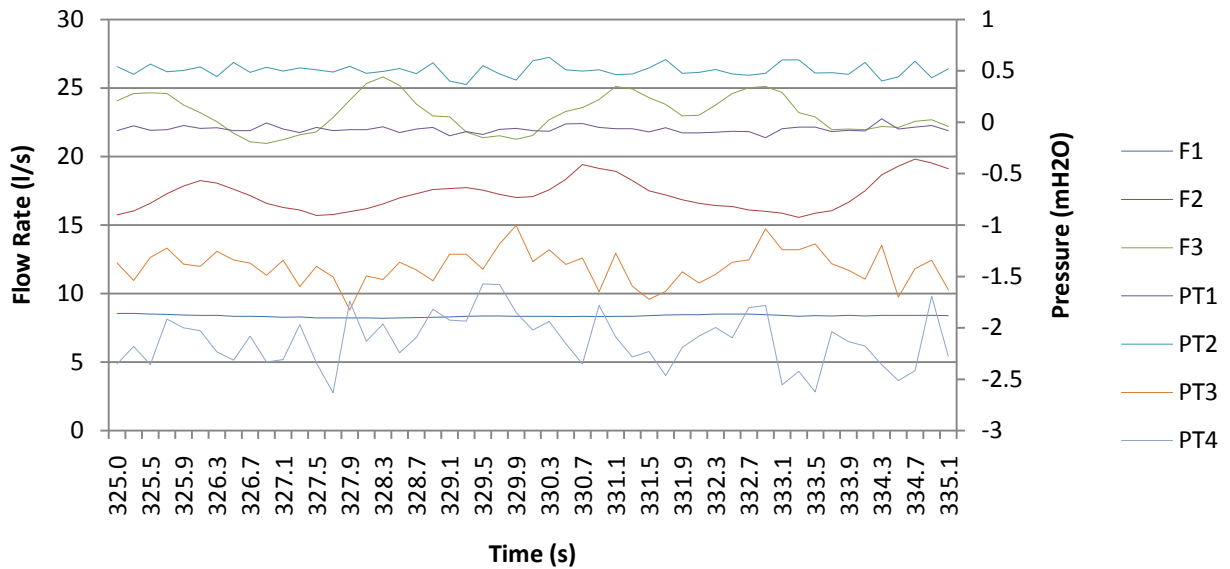
**Figure 4.99 Image at P2 at 320.96 seconds**

The images recorded at P2 show a series of short pulses or plugs of flow bore flow conditions interspersed by free surface flow shown in Figure 4.94. During full bore flow, a series of air pockets and small amounts of entrained air were observed along the crown of the pipe shown

in Figure 4.96. Each of the flow pulses or plugs were quite short measured at 0.29 seconds (Figure 4.95 to Figure 4.97) and 0.36 seconds (Figure 4.98 to Figure 4.99).

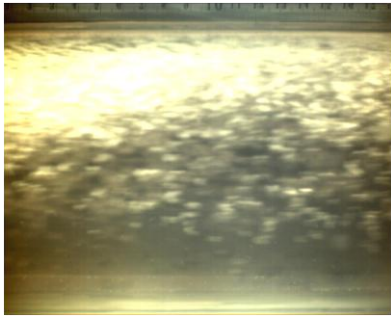
#### 4.1.4.6 Time Series Flow Rate, Pressure and Image Comparison at P3

Figure 4.100 shows the flow rate and pressure measurements for the corresponding 10 second period (325.05 to 335.05 seconds) that images were collected at P3 (downstream of Outlet C and F3) during Test 54.

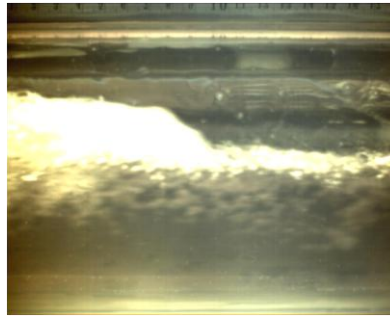


**Figure 4.100 Flow Rate and Pressure Measurement within the Horizontal Carrier Pipe during Test 54 (325.05 to 335.05 seconds)**

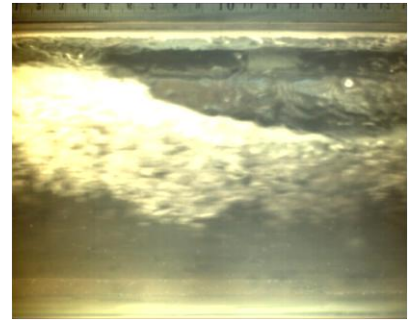
The following selected images correspond to the time series data shown in Figure 4.100.



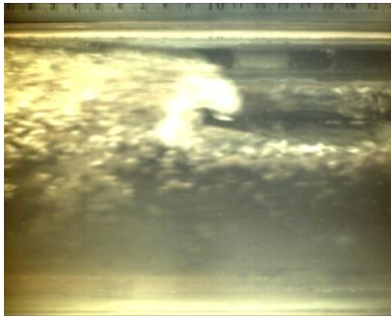
**Figure 4.101 Image at P3 at 325.20 seconds**



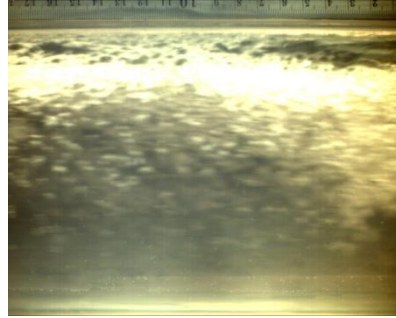
**Figure 4.102 Image at P3 at 325.38 seconds**



**Figure 4.103 Image at P3 at 333.17 seconds**



**Figure 4.104 Image at P3 at 334.04 seconds**



**Figure 4.105 Image at P3 at 335.05 seconds**

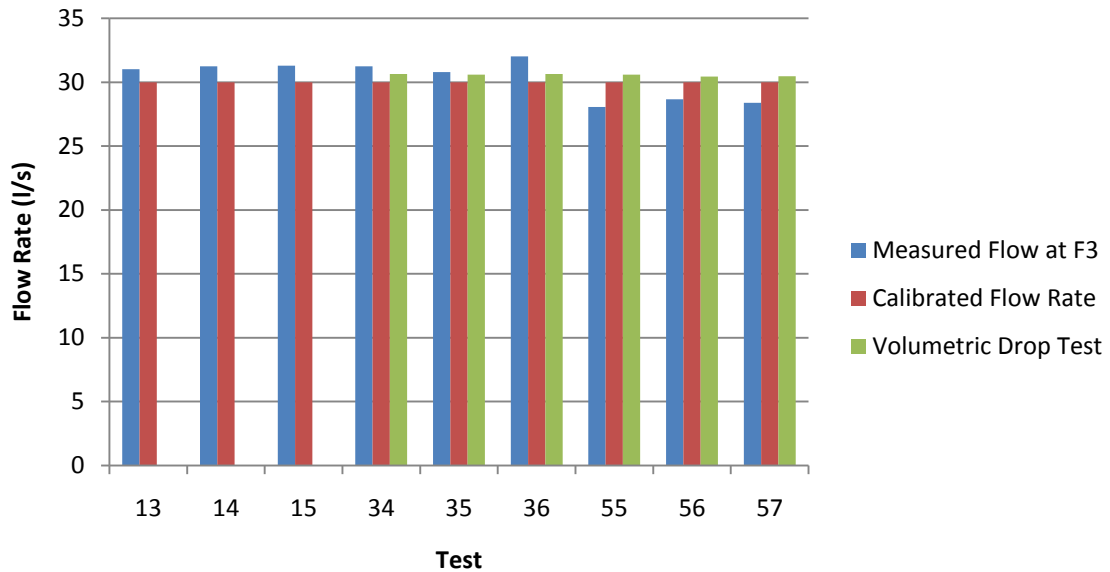
Flow at P3 during the steady flow tests completed at 24 l/s were dominated by aerated two-phase flow and a series of waves (Figure 4.102, Figure 4.103 and Figure 4.104) that both occupied and did not fully occupy the cross-sectional area of the pipe (Figure 4.101 and Figure 4.105). These waves were clearly measured in the corresponding time series data shown in Figure 4.100. There were no observed free-surface, plug flow or full bore flow conditions observed at P3.



## 4.1.5 Tests Completed at the Design Flow Rate

### 4.1.5.1 Mass Balance

Flow tests completed at the design flow rate showed an average difference between the mass balance measured using flourometry and the volumetric drop test of  $\pm 4.67\%$  and a maximum difference of  $+8.24\%$ . The measured mean flow rate varied between 28.06 l/s to 32.03 l/s and a comparison between the measured flow at F3, calibrated flow rate and the volumetric drop test is shown in Figure 4.106.

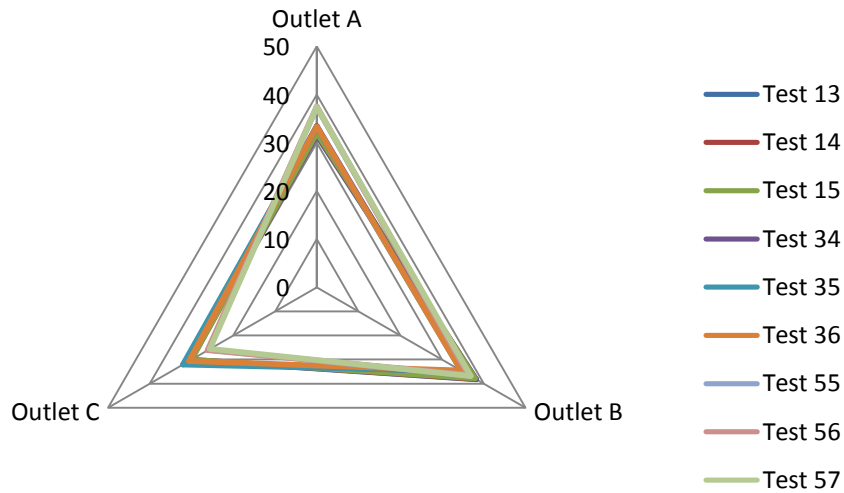


**Figure 4.106 Mass Balance Comparison for Tests Completed at the Design Flow Rate**

These results do not continue the trend of a decrease in the difference between the measured average flow rate and the volumetric drop tests. The results are slightly higher in comparison to the tests completed at 80% of the design flow rate and are more comparable to the tests completed at 40% and 60% of the design flow rate.

### 4.1.5.2 Flow Proportionality

Figure 4.107 shows a radar plot demonstrating the relative proportionality of flow through each outlet during the tests reported in Table 4.6.



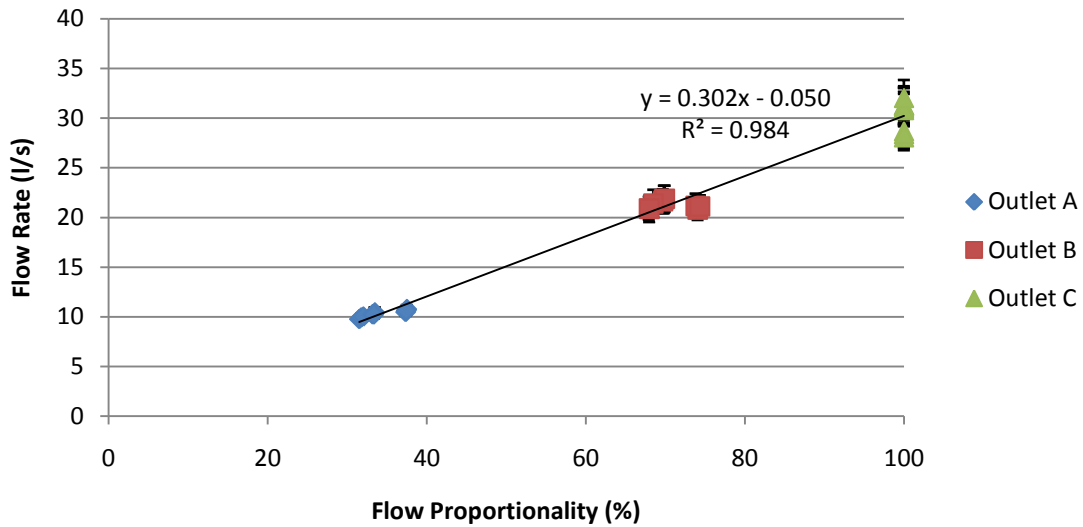
**Figure 4.107 Radar Plot Showing Flow Proportionality (%) at the Design Flow Rate**

These results show at the design flow rate, flow proportionality is not equal between the three outlets. Outlet B still dominates although less than the flow tests completed at 20%, 40%, 60% and 80% of the design flow rate. Outlet A and Outlet C have a relatively greater proportion in comparison to the flow tests completed less than the design flow rate. Maximum, minimum and average flow proportionality for the series of tests is shown in Table 4.20.

**Table 4.20 Maximum, Minimum and Average Flow Proportionality for Tests Completed at the Design Flow Rate**

Outlet	Maximum (%)	Minimum (%)	Average (%)
A	37.5	31.5	34.18
B	38.19	34.64	36.44
C	32.08	25.65	29.18

Figure 4.108 shows the measured component of flow through each outlet and relative standard deviation shown by the error bars for the series of flow tests.

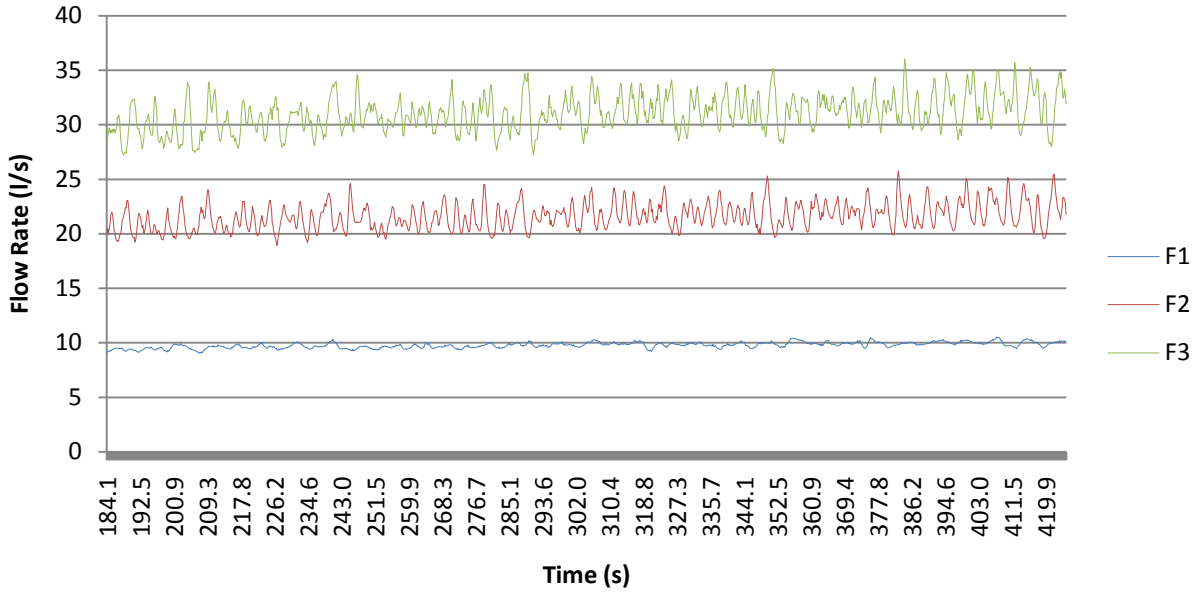


**Figure 4.108 Flow Proportionality at the Design Flow Rate with Standard Deviation shown by the Error Bars**

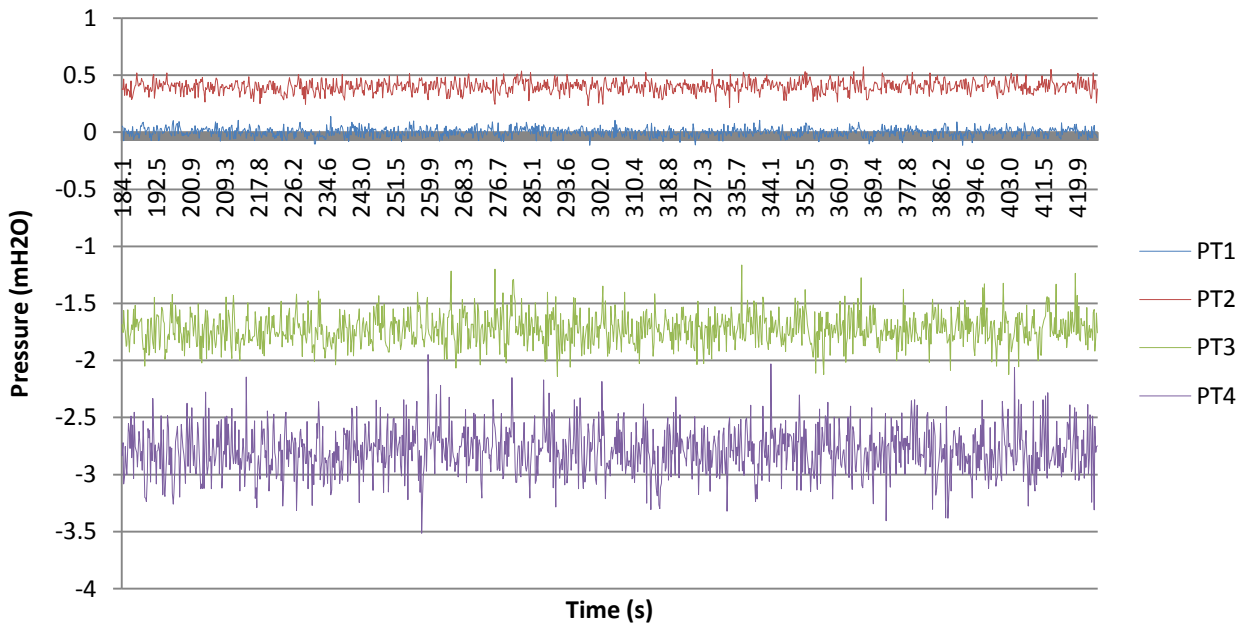
These results show that the standard deviation of the flow measured through each outlet is considerably less in comparison to the tests completed below the design rate. This would suggest comparably less variability in flow rate measured through each outlet.

#### 4.1.5.3 Time Series Flow Rate and Pressure Measurements

Figure 4.109 and Figure 4.82 show continuous flow measurement measured using flourometry through each outlet and system pressure within the horizontal carrier pipe for the same time period during Test 13.

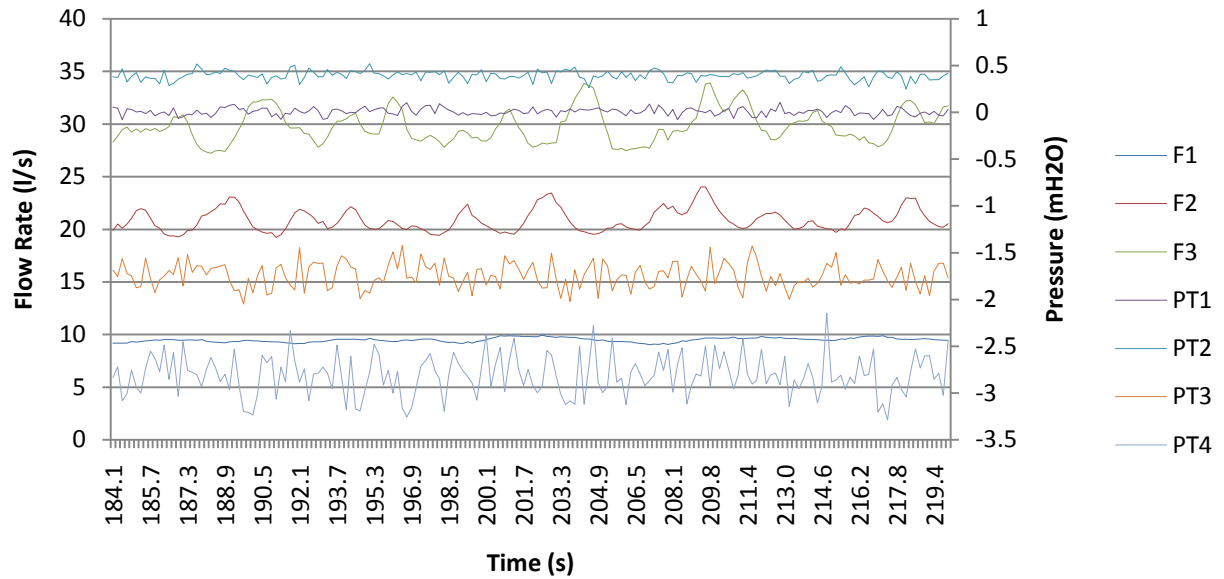


**Figure 4.109 Flow Rate Measurement within the Horizontal Carrier Pipe during Test 13**



**Figure 4.110 Pressure Measurement within the Horizontal Carrier Pipe during Test 13**

Figure 4.111 shows the measured flow rate and pressure for a selected time period during Test 13.

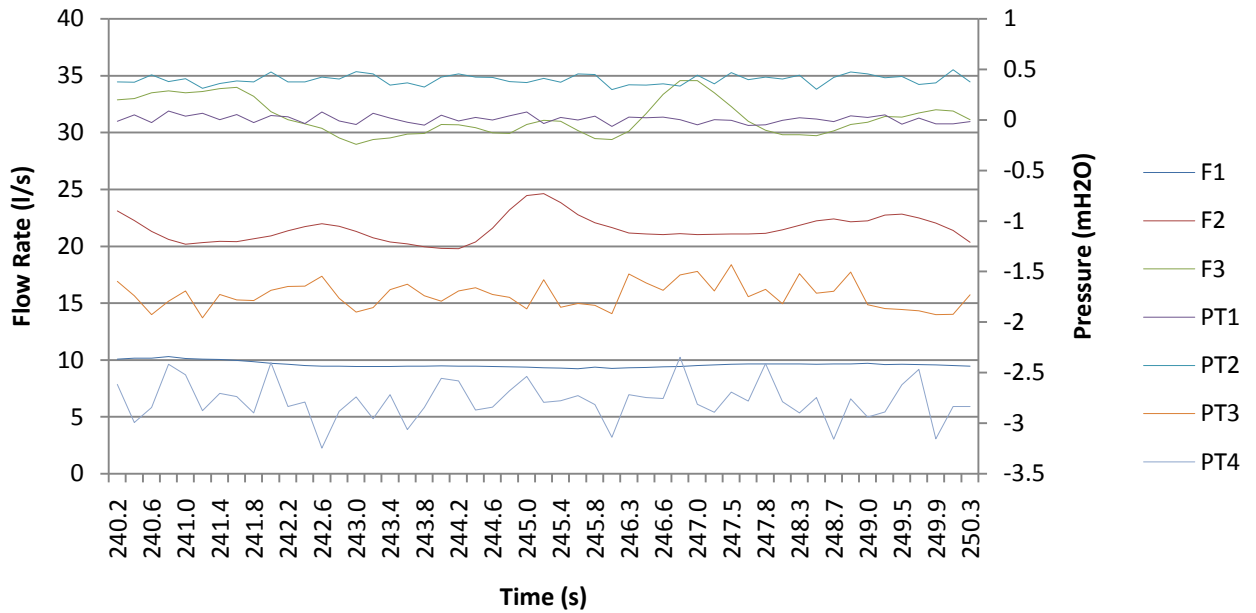


**Figure 4.111 Flow Rate and Pressure Comparison during Test 13**

Figure 4.109, Figure 4.110 and Figure 4.111 demonstrate that similar to the flow tests completed at 40%, 60% and 80% of the design flow rate, the flow profile through each outlet and the relative time series pressure data became increasingly variable moving downstream through the experimental test facility.

#### 4.1.5.4 Time Series Flow Rate, Pressure and Image Comparison at P1

Figure 4.84 shows the flow rate and pressure measurements for the corresponding 10 second period (240.20 seconds to 250.20 seconds) that images were collected at P1 (downstream of Outlet A and F1) during Test 13.

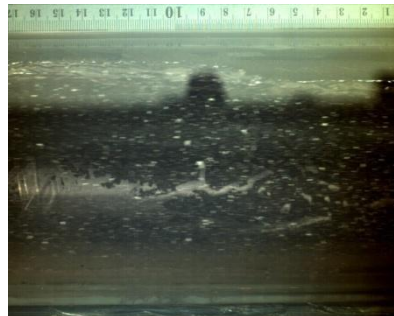


**Figure 4.112 Flow Rate and Pressure Measurement within the Horizontal Carrier Pipe during Test 13 (240.20 to 250.20 seconds)**

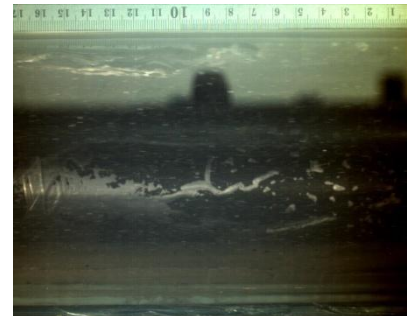
The following selected images correspond to the time series data shown in Figure 4.112.



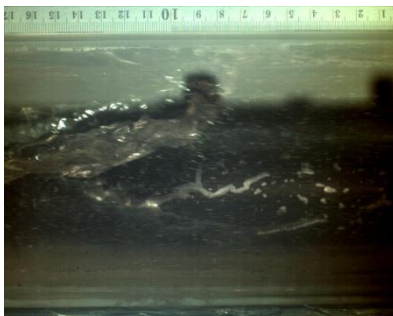
**Figure 4.113 Image at P1 at 248.23 seconds**



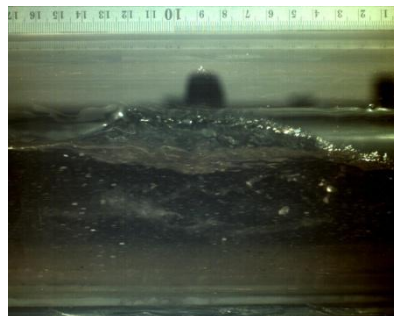
**Figure 4.114 Image at P1 at 248.47 seconds**



**Figure 4.115 Image at P1 at 249.14 seconds**



**Figure 4.116 Image at P1 at 249.41 seconds**



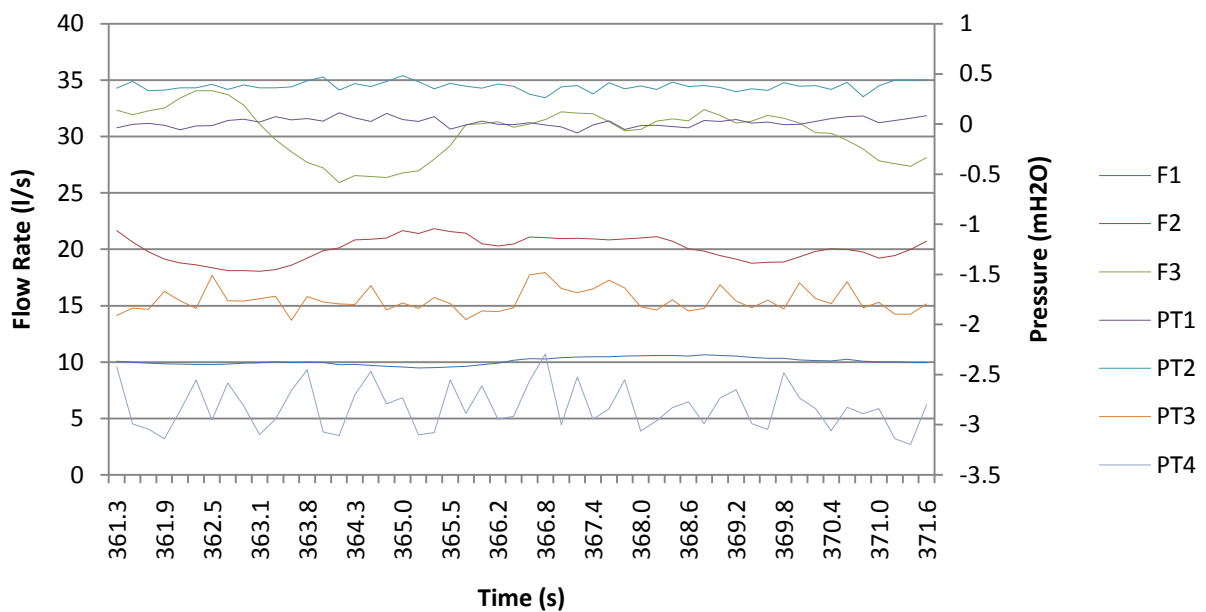
**Figure 4.117 Image at P1 at 249.54 seconds**

A series of flow pulses were observed throughout the 10 second measurement period during Test Reference 13. A series of free surface waves (Figure 4.113) were followed by free surface flow occupying the majority of the cross-sectional area of the pipe (Figure 4.114). Full bore flow conditions were observed interrupted by air pockets with little to no air

entrainment (Figure 4.115) before full bore flow ceased ( Figure 4.116) and the free surface waves resumed (Figure 4.117). This cycle was observed repeatedly throughout the measurement period.

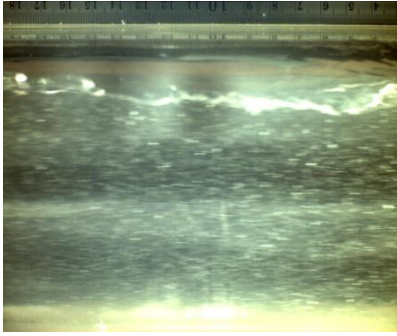
#### 4.1.5.5 Time Series Flow Rate, Pressure and Image Comparison at P2

Figure 4.118 shows the flow rate and pressure measurements for the corresponding 10 second period (361.48 to 371.48 seconds) that images were collected at P2 (downstream of Outlet B and F2) during Test 36.

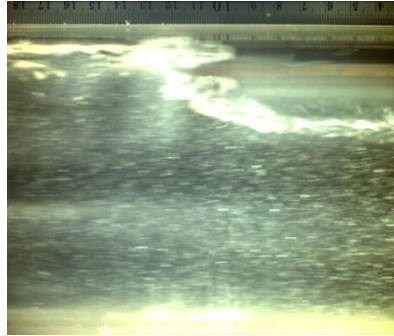


**Figure 4.118 Flow Rate and Pressure Measurements within the Horizontal Carrier Pipe during Test 36 (361.48 to 371.48 seconds)**

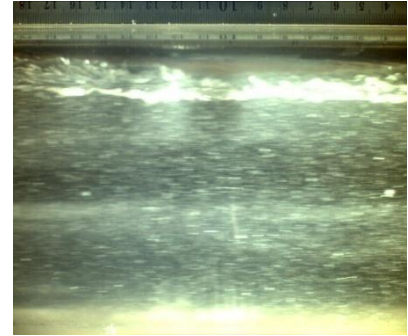
The following selected images correspond to the time series data shown in Figure 4.118.



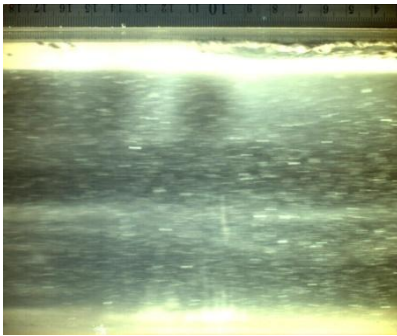
**Figure 4.119 Image at P2 at 363.06 seconds**



**Figure 4.120 Image at P2 at 363.18 seconds**



**Figure 4.121 Image at P2 at 363.32 seconds**



**Figure 4.122 Image at P2 at 363.84 seconds**



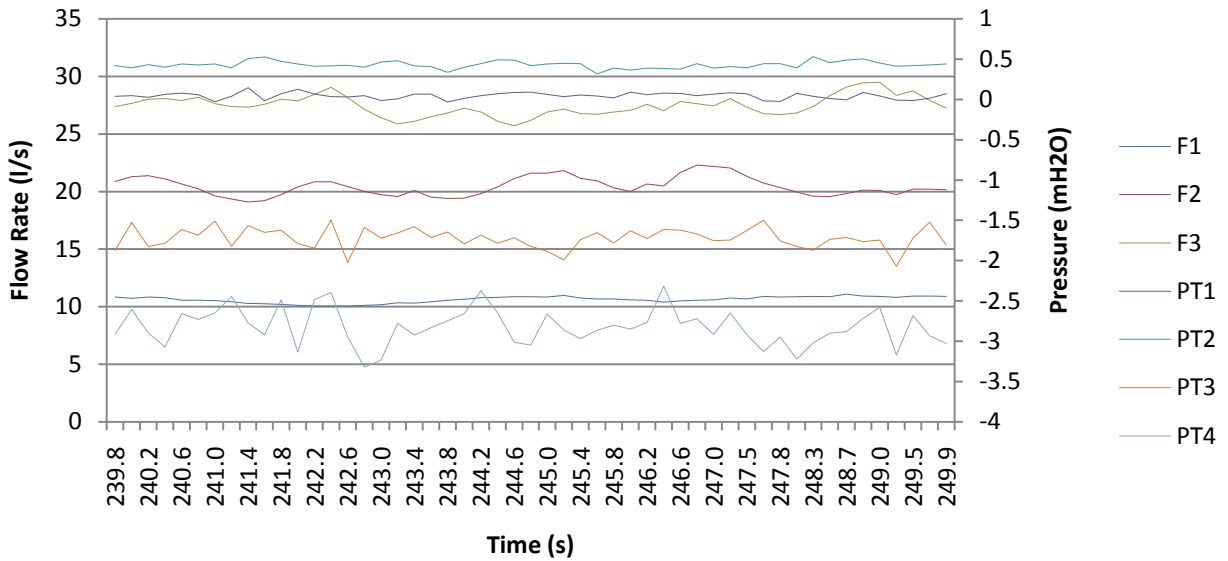
**Figure 4.123 Image at P2 at 364.09 seconds**

Similar to P1, a series of flow pulses were observed throughout the 10 second measurement period when the camera was positioned at P2 during Test Reference 36. Free surface flow was observed (Figure 4.119) followed by a series of turbulent waves (Figure 4.120). Free surface flow followed occupying the majority of the cross-sectional area of the pipe (Figure 4.121) preceding short periods (0.25 seconds) of full bore flow with little to no air entrainment (Figure 4.122). Full bore flow ceased (Figure 4.123) and the turbulent free surface waves resumed. This cycle was observed repeatedly throughout the measurement period.

#### 4.1.5.6 Time Series Flow Rate, Pressure and Image Comparison at P2

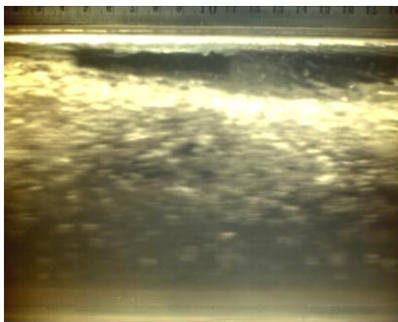
Figure 4.124 shows the flow rate and pressure measurements for the corresponding 10 second period (239.87 to 249.87 seconds) that images were collected at P3 (downstream of Outlet C and F3) during Test 57.



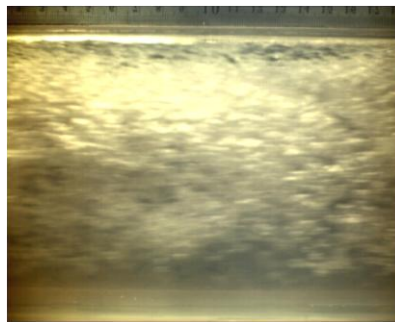


**Figure 4.124 Flow Rate and Pressure Measurement within the Horizontal Carrier Pipe during Test 57 (239.87 to 249.87 seconds)**

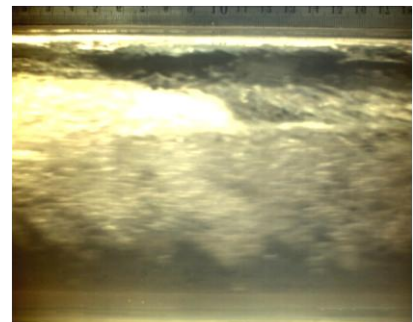
The following selected images correspond to the time series data shown in Figure 4.124.



**Figure 4.125 Image at P3 at 239.98 seconds**



**Figure 4.126 Image at P3 at 240.53 seconds**



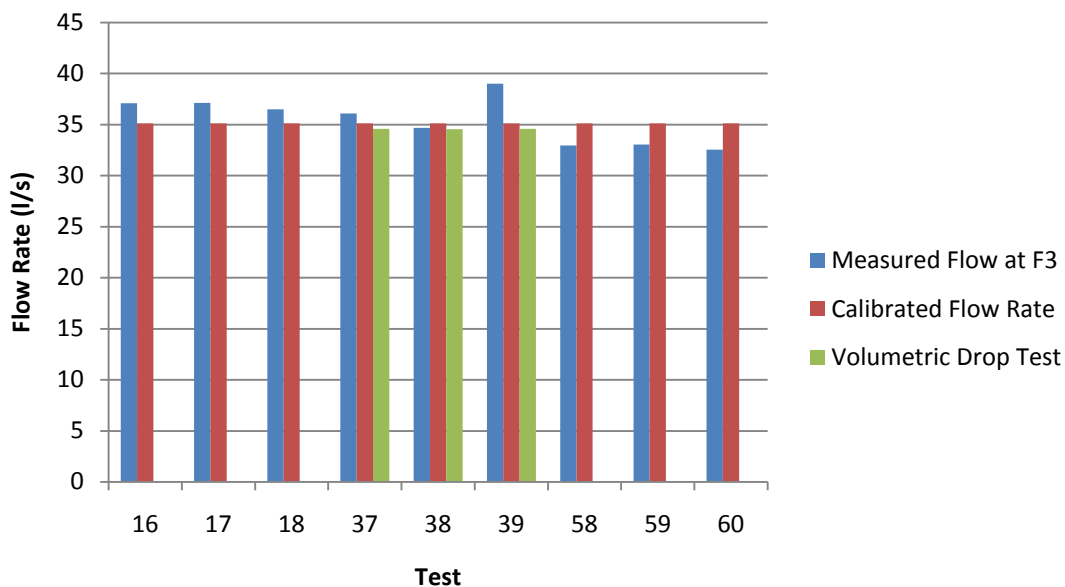
**Figure 4.127 Image at P3 at 241.39 seconds**

The images recorded at P3 during the steady flow tests completed at the design flow rate of 30 l/s showed heavily aerated two-phase flow that did not and did occupy the cross-sectional area of the pipe shown in Figure 4.125 and Figure 4.126 respectively. Figure 4.127 shows heavily aerated flow with a wave within the carrier pipe.

## 4.1.6 Tests Completed at the Ultimate Flow Rate

### 4.1.6.1 Mass Balance

Flow tests completed at the design flow rate showed an average difference between the mass balance measured using flourometry and the volumetric drop test of  $\pm 5.73\%$  and a maximum difference of  $+12.75\%$ . The measured mean flow rate varied between 32.54 l/s to 39.00 l/s and a comparison between the measured flow at F3 and the volumetric comparison is shown in Figure 4.128.

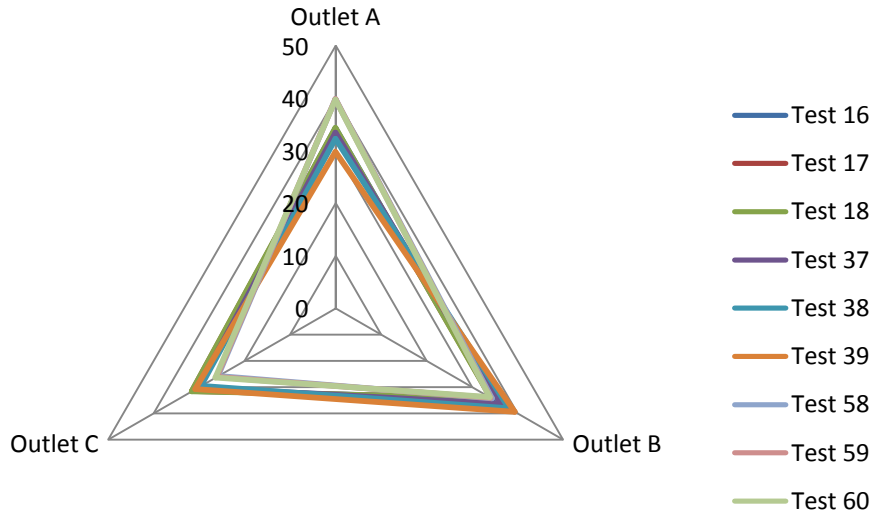


**Figure 4.128 Mass Balance Comparison for Tests Completed at the Ultimate Flow Rate**

These results show an increase in the difference between the measured average flow rate and the volumetric drop tests compared to the flow tests completed at the design flow rate. However, this comparison is limited as the volumetric comparison could only be completed for 3 of the 9 tests at the ultimate flow rate. One of these results (Test 39) has a greater relative difference compared to the other two.

### 4.1.6.2 Flow Proportionality

Figure 4.129 shows a radar plot demonstrating the relative proportionality of flow through each outlet during the tests reported in Table 4.7.



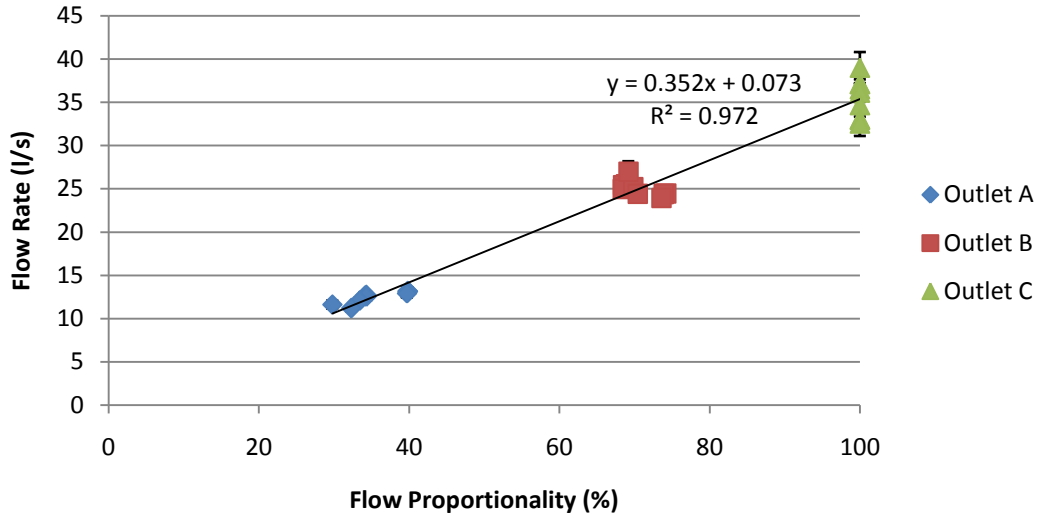
**Figure 4.129 Radar Plot Showing Flow Proportionality (%) at the Ultimate Flow Rate**

These results show at the ultimate flow rate, flow proportionality between Outlet A and Outlet B is within 0.56%. Average proportionality through Outlet C is consistently less in comparison with a slight increase of 0.27% compared to the design flow rate. Maximum, minimum and average flow proportionality for the series of tests is shown in Table 4.21.

**Table 4.21 Maximum, Minimum and Average Flow Proportionality for Tests Completed at the Ultimate Flow Rate**

Outlet	Maximum (%)	Minimum (%)	Average (%)
A	39.81	29.77	35.27
B	39.41	33.87	35.47
C	31.60	25.81	29.26

Figure 4.130 shows the measured component of flow through each outlet and relative standard deviation shown by the error bars for the series of flow tests.

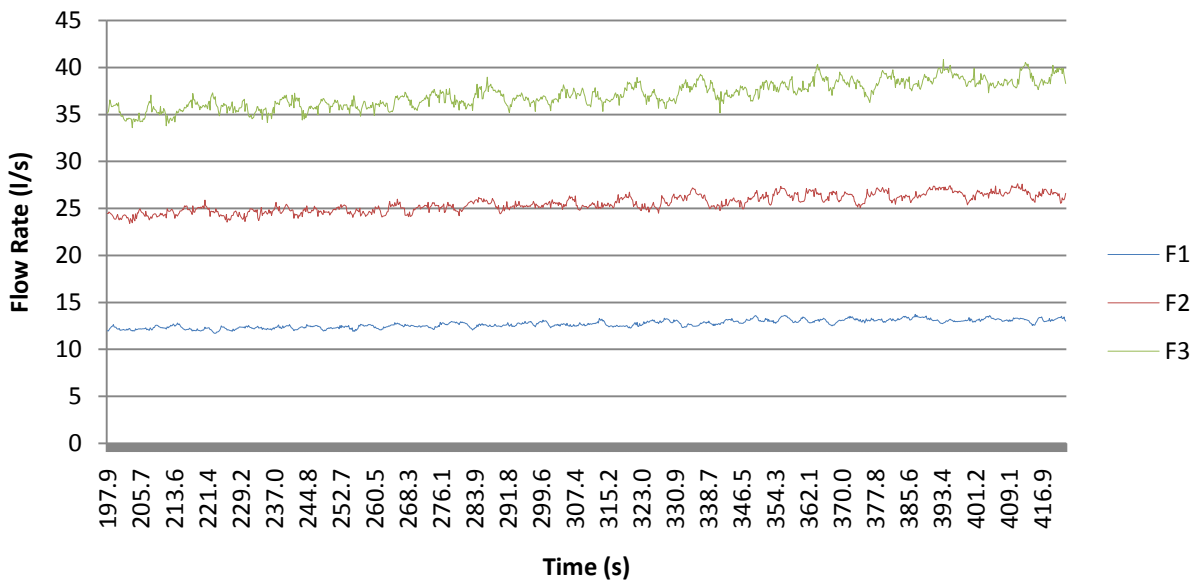


**Figure 4.130 Flow Proportionality at the Ultimate Flow Rate with Standard Deviation shown by the Error Bars**

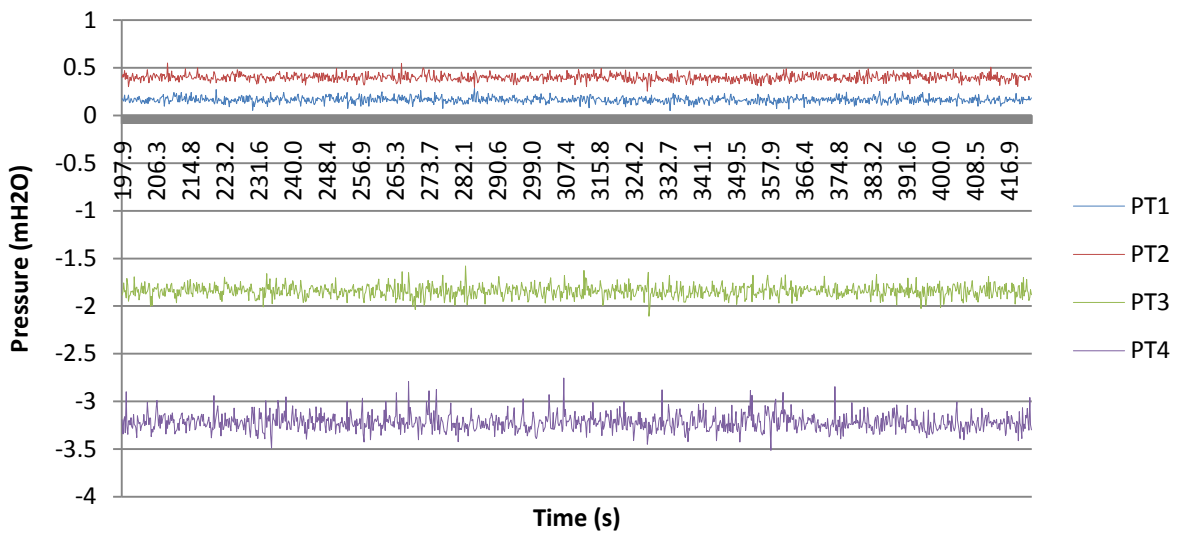
These results show that the standard deviation of the flow measured through each outlet is considerably less in comparison to the tests completed at and below the design flow rate. This suggests very little fluctuation in the flow rate measured through each outlet.

#### 4.1.6.3 Time Series Flow Rate and Pressure Measurements

Figure 4.131 and Figure 4.132 show continuous flow measurement measured using flourometry through each outlet and system pressure within the horizontal carrier pipe for the same time period during Test 16.



**Figure 4.131 Flow Rate Measurement within the Horizontal Carrier Pipe during Test 16**

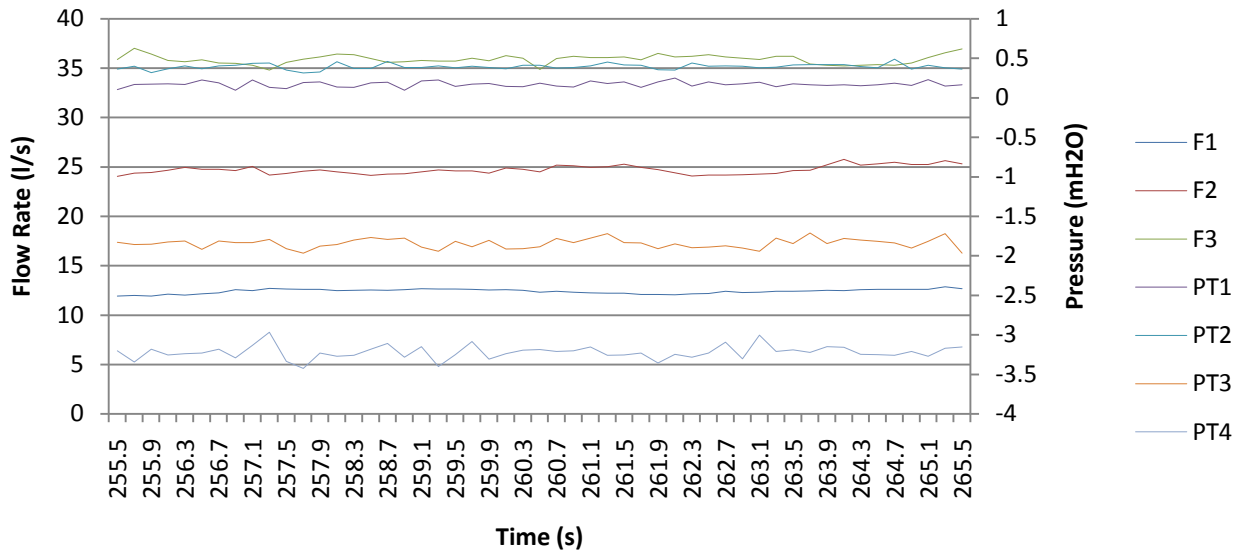


**Figure 4.132 Pressure Measurement within the Horizontal Carrier Pipe during Test 16**

Figure 4.131 and Figure 4.132 demonstrate that similar to previous flow tests, the flow profile through each outlet and the relative time series pressure data became increasingly variable moving downstream through the experimental test facility. However, variability of the flow rate measurement in particular during the tests completed in excess of the design flow rate is significantly less in comparison.

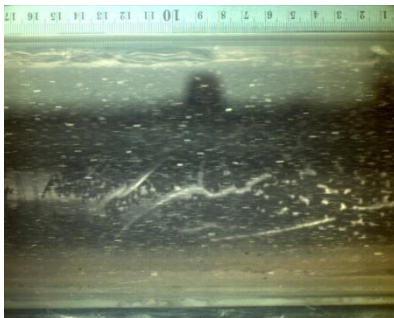
#### 4.1.6.4 Time Series Flow Rate, Pressure and Image Comparison at P1

Figure 4.133 shows the flow rate and pressure measurements for the corresponding 10 second period (255.49 seconds to 265.49 seconds) that images were collected at P1 (downstream of Outlet A and F1) during Test 16.

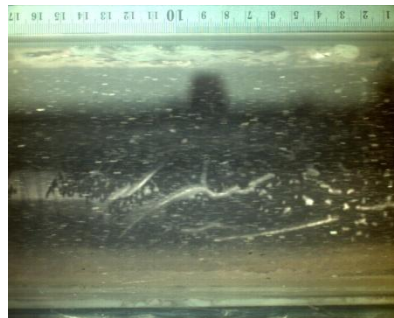


**Figure 4.133 Flow Rate and Pressure Measurement within the Horizontal Carrier Pipe during Test 16 (255.49 to 265.49 seconds)**

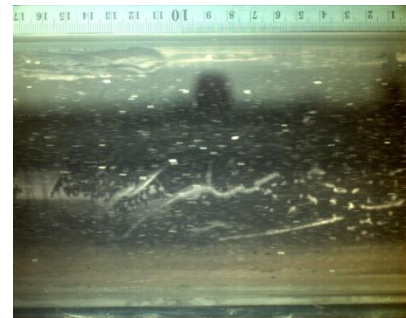
The following selected images correspond to the time series data shown in Figure 4.133.



**Figure 4.134 Image at P1 at 263.23 seconds**



**Figure 4.135 Image at P1 at 264.22 seconds**

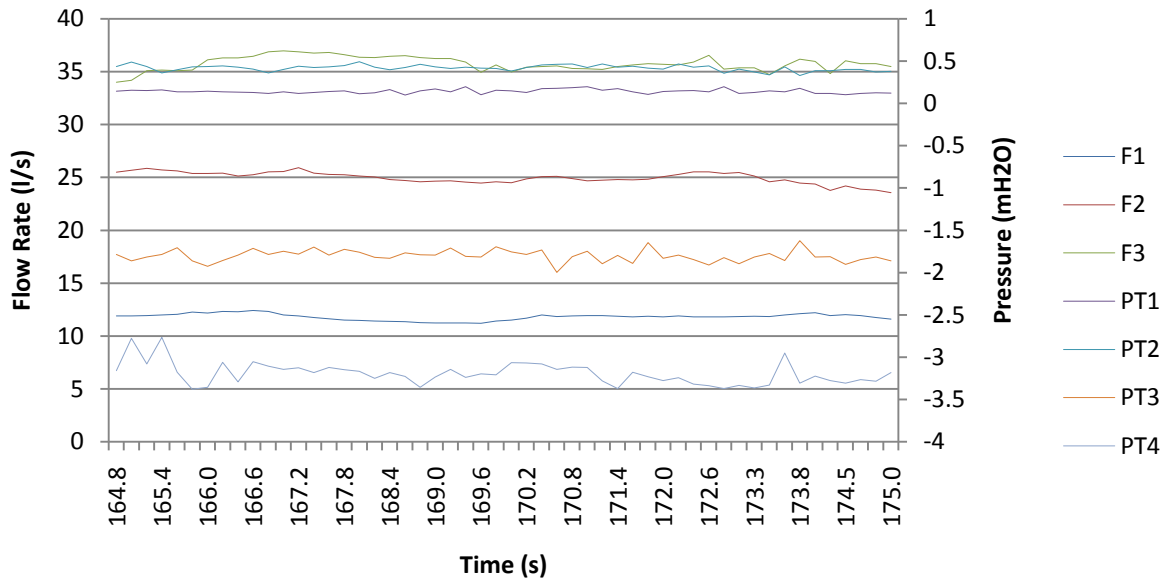


**Figure 4.136 Image at P1 at 264.67 seconds**

The images at P1 recorded at the ultimate flow rate showed full bore flow with no entrained air for the duration of the measured period. Small amounts of air at the crown of the pipe were observed repeatedly throughout the series of images. Examples are shown in Figure 4.134, Figure 4.135, and Figure 4.136.

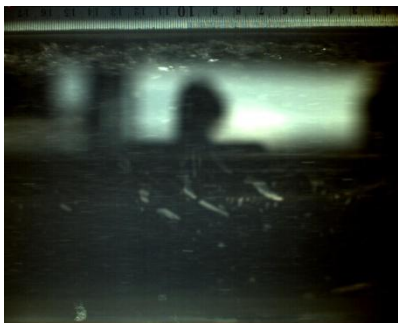
#### 4.1.6.5 Time Series Flow Rate, Pressure and Image Comparison at P2

Figure 4.137 shows the flow rate and pressure measurements for the corresponding 10 second period (164.87 to 174.87 seconds) that images were collected at P2 (downstream of Outlet B and F2) during Test 37.



**Figure 4.137 Flow Rate and Pressure Measurement within the Horizontal Carrier Pipe during Test 37 (164.87 to 174.87 seconds)**

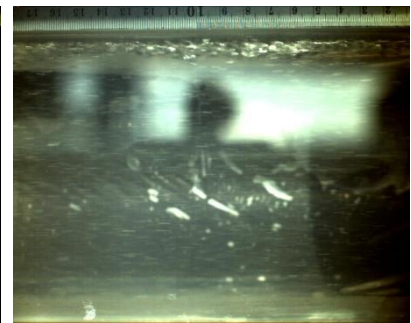
The following selected images correspond to the time series data shown in Figure 4.137.



**Figure 4.138 Image at P2 at 166.65 seconds**



**Figure 4.139 Image at P2 at 167.45 seconds**

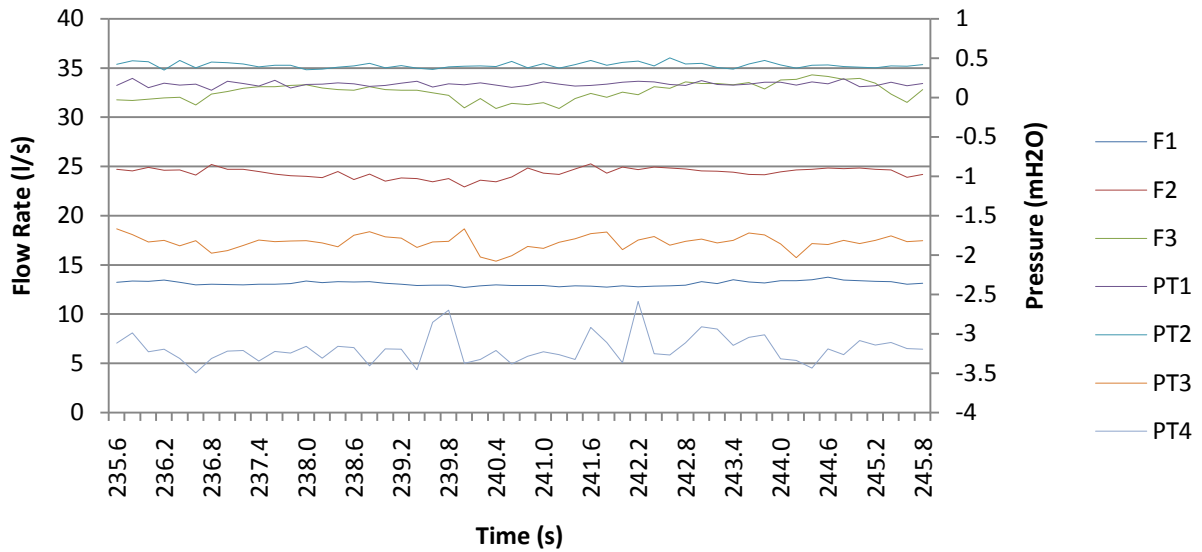


**Figure 4.140 Image at P2 at 170.93 seconds**

Similar to the results observed at P1, the images recorded during the flow tests completed at the ultimate flow rate at P2 showed full bore conditions with small amounts of entrained air sporadically throughout the measurement period. Examples are shown in Figure 4.138, Figure 4.139 and Figure 4.140.

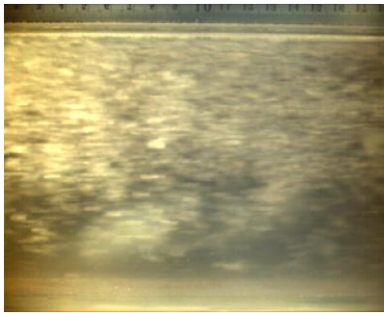
#### 4.1.6.6 Time Series Flow Rate, Pressure and Image Comparison at P3

Figure 4.141 shows the flow rate and pressure measurements for the corresponding 10 second period (235.69 to 245.69 seconds) that images were collected at P3 (downstream of Outlet C and F3) during Test 58.

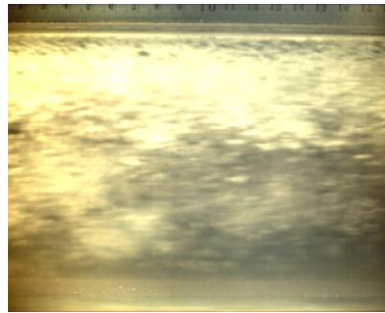


**Figure 4.141 Flow Rate and Pressure Measurement within the Horizontal Carrier Pipe during Test 58 (235.69 to 245.69 seconds)**

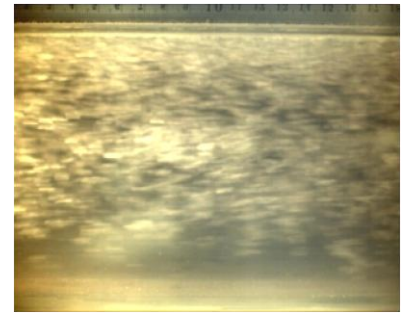
The following selected images correspond to the time series data shown in Figure 4.141.



**Figure 4.142 Image at P3 at 235.69 seconds**



**Figure 4.143 Image at P3 at 237.22 seconds**



**Figure 4.144 Image at P3 at 244.19 seconds**

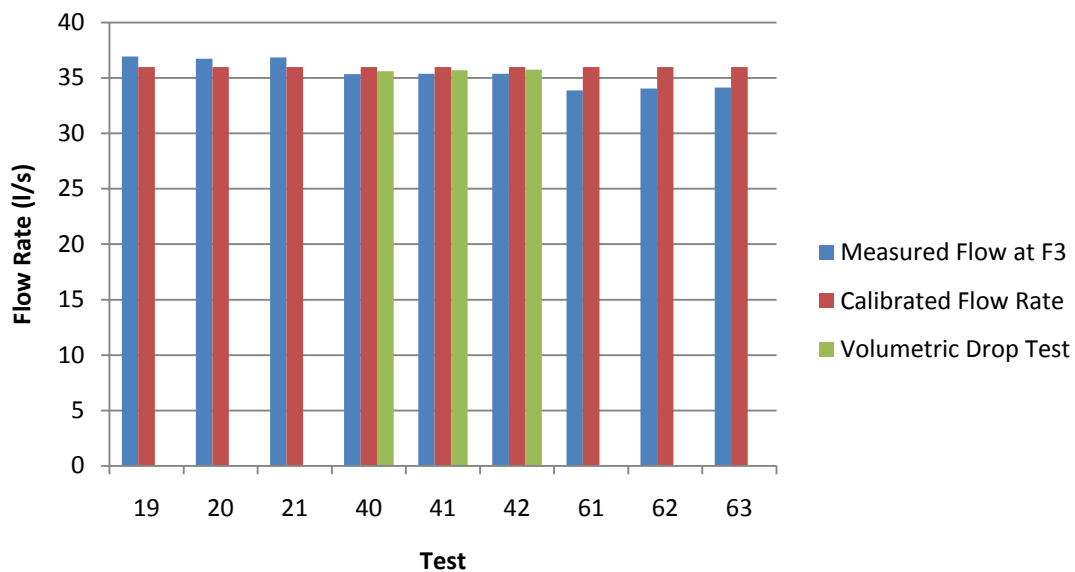
Images recorded at P3 for the tests completed at the ultimate flow rate showed heavily aerated two-phase flow occupying the cross-sectional area of the pipe for the duration of the measurement period. Examples are shown in Figure 4.142, Figure 4.143 and Figure 4.144.



## 4.1.7 Tests Completed at 120% of the Design Flow Rate

### 4.1.7.1 Mass Balance

Flow tests completed at 120% of the design flow rate showed an average difference between the mass balance measured using flourometry and the volumetric drop test of  $\pm 0.92\%$  and a maximum difference of  $-1.06\%$ . The measured mean flow rate varied between 33.87 l/s to 36.93 l/s and a comparison between the measured flow at F3, calibrated flow rate and the volumetric drop test is shown in Figure 4.145.

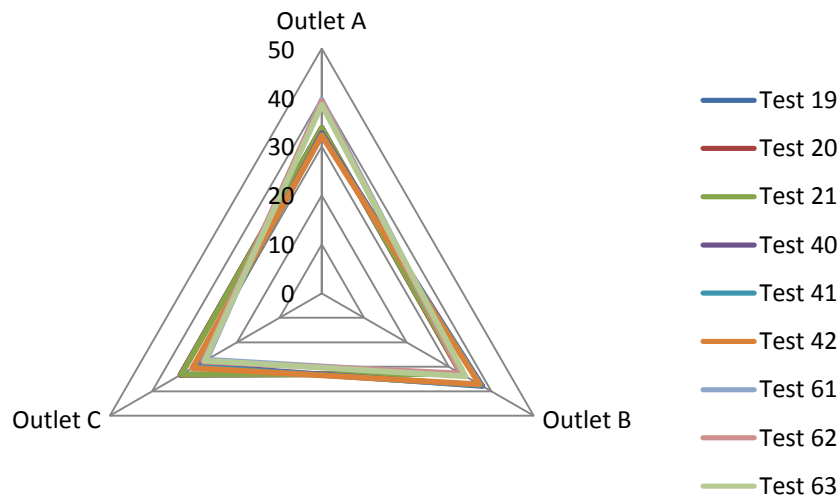


**Figure 4.145 Mass Balance Comparison for Tests Completed at 120% of the Design Flow Rate**

These results show the smallest comparable difference between the measured flow and volumetric comparison in relation to all of the other flow tests.. However, this comparison is limited as the volumetric comparison could only be completed for 3 of the 9 tests.

### 4.1.7.2 Flow Proportionality

Figure 4.146 shows a radar plot demonstrating the relative proportionality of flow through each outlet during the tests reported in Table 4.8.



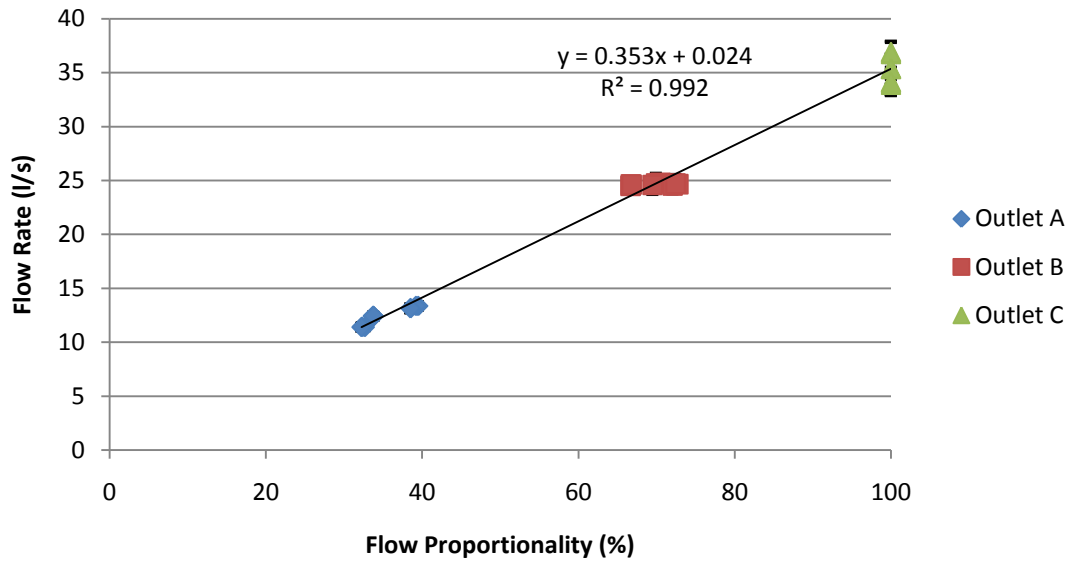
**Figure 4.146 Radar Plot Showing Flow Proportionality (%) at 120% of the Design Flow Rate**

These results show that at the flow tests completed at 120% of the design flow rate, Outlet A for the first time became the dominant outlet. The relative proportion through Outlet B was lowest in comparison to all previous flow tests reported. Conversely, the relative proportion through Outlet C was greatest at the flow tests undertaken at 120% of the design flow rate when compared to the analysis of flow tests at lesser flow rates. Maximum, minimum and average flow proportionality for the series of tests is shown in Table 4.22.

**Table 4.22 Maximum, Minimum and Average Flow Proportionality for Tests Completed at 120% of the Design Flow Rate**

Outlet	Maximum (%)	Minimum (%)	Average (%)
A	39.47	32.22	35.07
B	37.83	32.82	34.63
C	33.33	27.20	30.30

Figure 4.147 shows the measured component of flow through each outlet and relative standard deviation shown by the error bars for the series of flow tests.

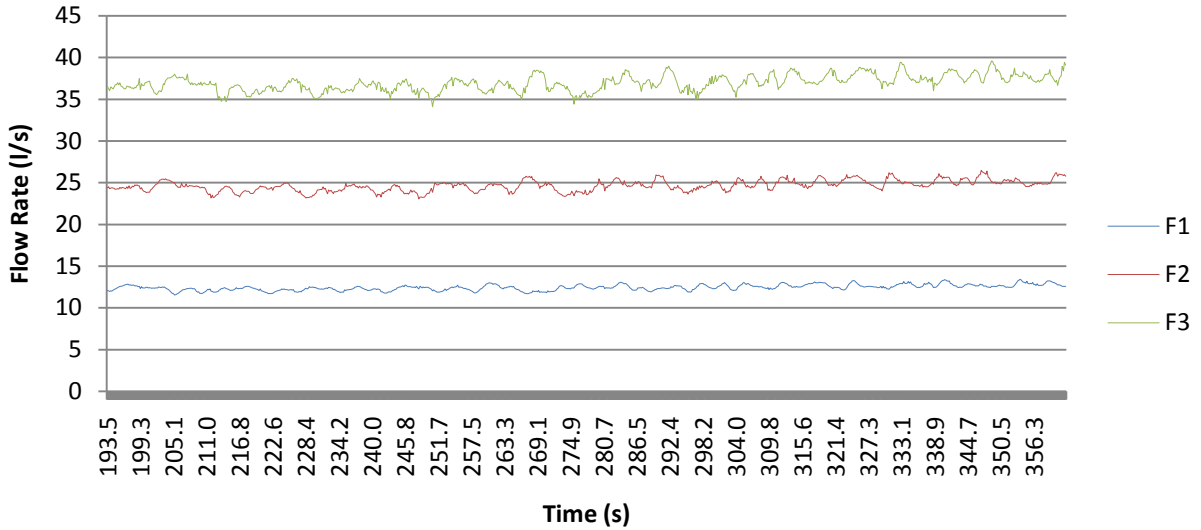


**Figure 4.147 Flow Proportionality at 120% of the Design Flow Rate with Standard Deviation shown by the Error Bars**

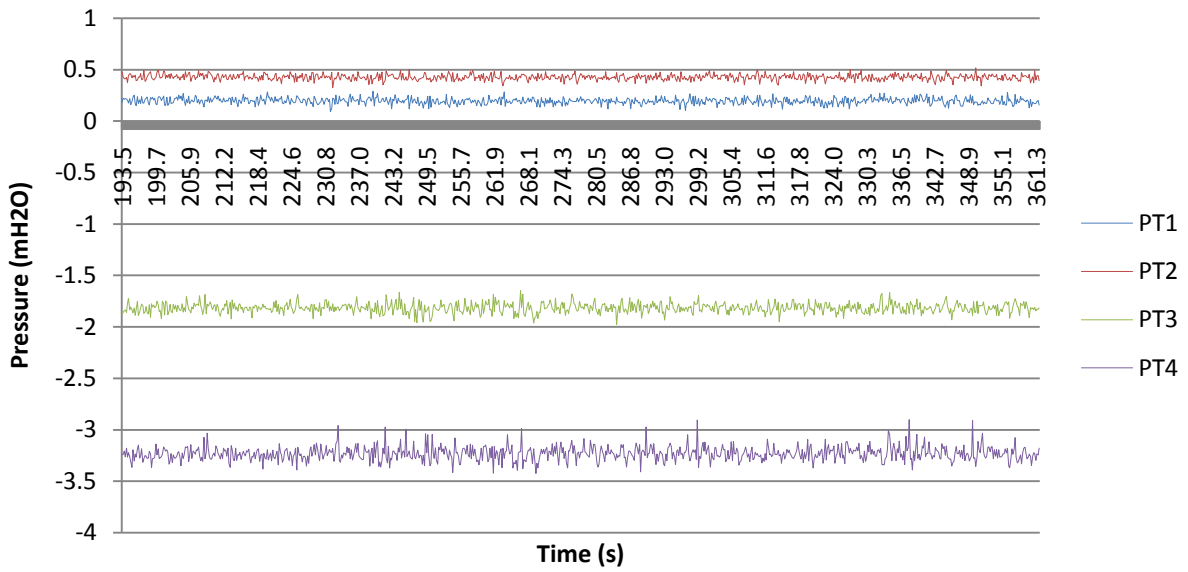
Similar to the results from the tests completed at the ultimate flow rate, these results show that the standard deviation of the flow measured through each outlet is minimal, indicative of minor fluctuations in the flow rate measured through each outlet. The variability in terms of measured flow through each outlet is also the lowest in comparison to previously report flow tests. This is supported by the regression of the linear relationship of the data points shown in Figure 4.147.

#### 4.1.7.3 Time Series Flow Rate and Pressure Measurements

Figure 4.148 and Figure 4.149 show continuous flow measurement measured using flourometry through each outlet and system pressure within the horizontal carrier pipe for the same time period during Test 19.

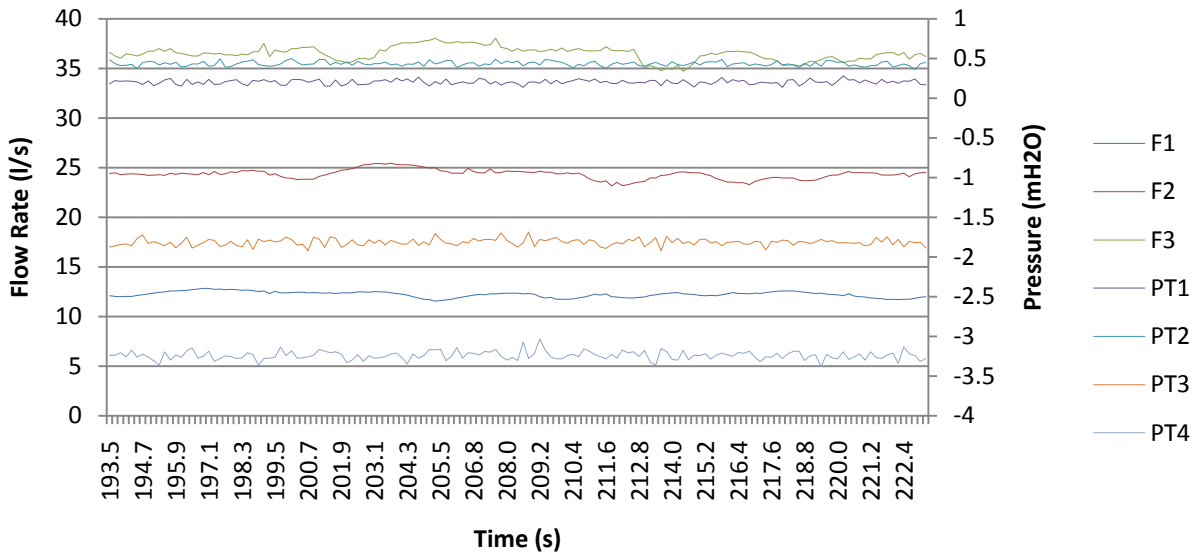


**Figure 4.148 Flow Rate Measurement within the Horizontal Carrier Pipe during Test 19**



**Figure 4.149 Pressure Measurement within the Horizontal Carrier Pipe during Test 19**

Figure 4.150 shows the measured flow rate and pressure for a selected time period during Test 19.

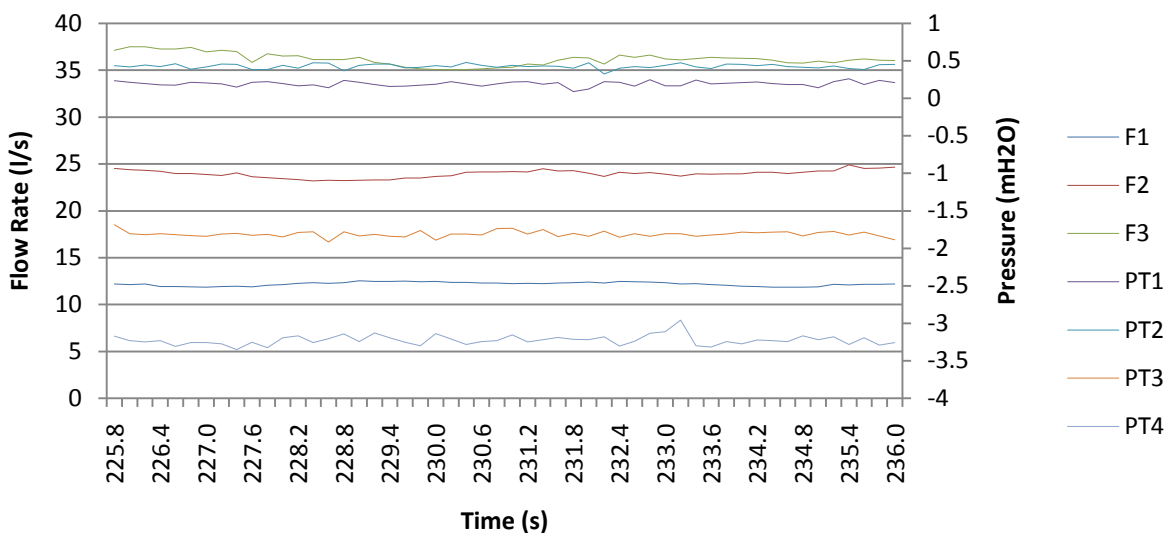


**Figure 4.150 Flow Rate and Pressure Comparison During Test 19**

Figure 4.149 and Figure 4.150 show very similar results to the flow tests completed at the ultimate flow rate. Variability of the flow rate and pressure measurements during these tests is less when compared to all other tests completed as part of this experimental research.

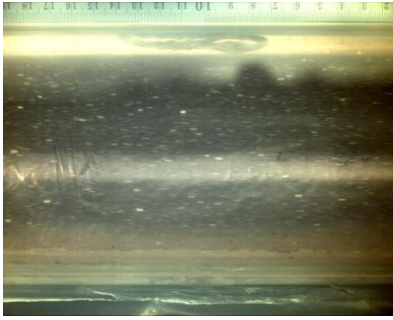
#### 4.1.7.4 Time Series Flow Rate, Pressure and Image Comparison at P1

Figure 4.151 shows the flow rate and pressure measurements for the corresponding 10 second period (225.89 seconds to 235.89 seconds) that images were collected at P1 (downstream of Outlet A and F1) during Test 19.

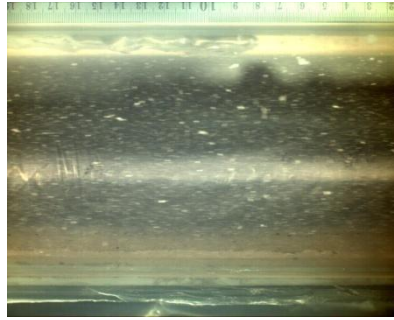


**Figure 4.151 Flow Rate and Pressure Measurement within the Horizontal Carrier Pipe during Test 19 (225.89 to 235.89 seconds)**

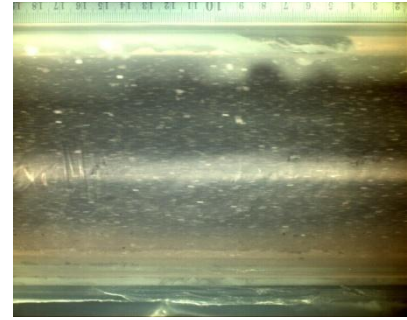
The following selected images correspond to the time series data shown in Figure 4.151.



**Figure 4.152 Image at P1 at 227.39 seconds**



**Figure 4.153 Image at P1 at 229.52 seconds**

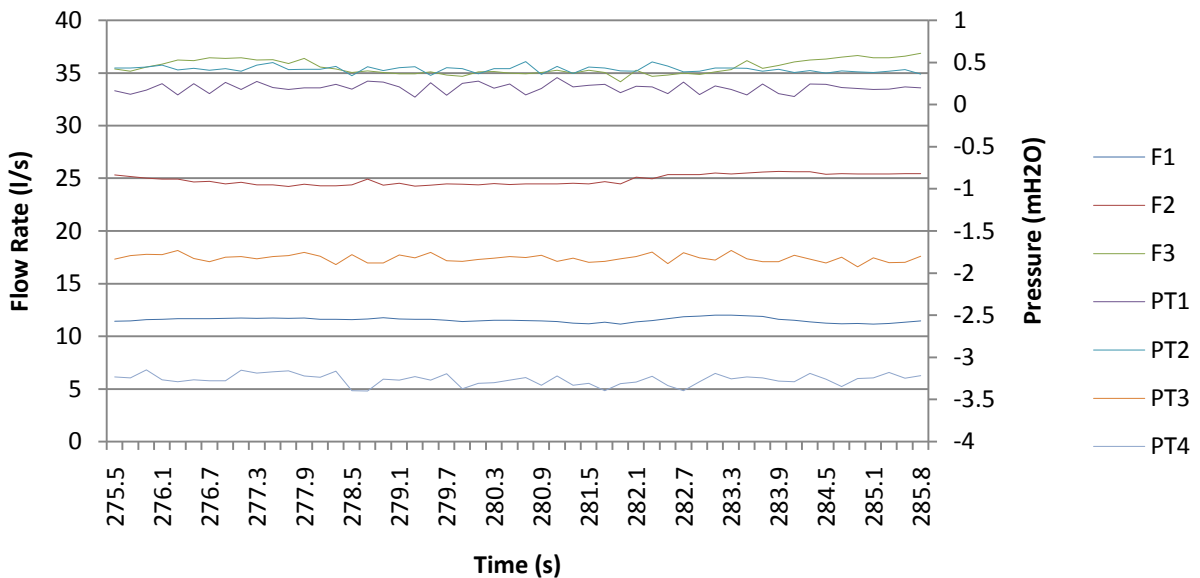


**Figure 4.154 Image at P1 at 235.12 seconds**

The images at P1 recorded at a flow rate of 36 l/s showed full bore flow with no entrained air for the duration of the measured period. Small amounts of air at the crown of the pipe were observed repeatedly throughout the series of images. Examples are shown in Figure 4.152, Figure 4.153 and Figure 4.154.

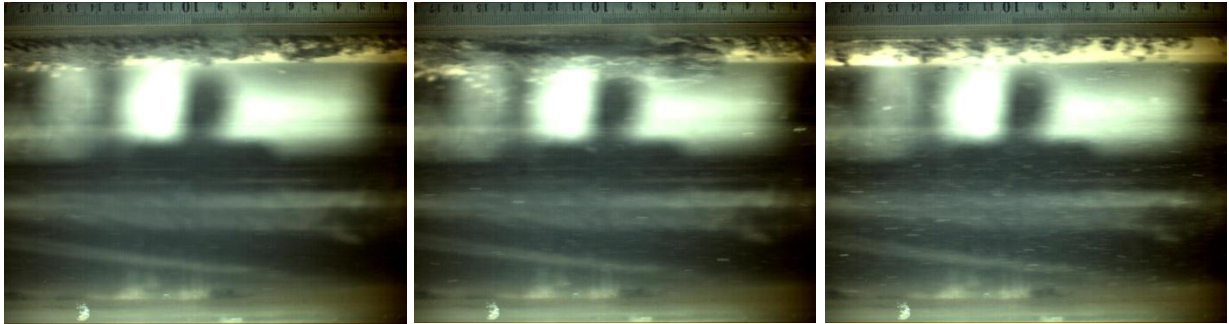
#### 4.1.7.5 Time Series Flow Rate, Pressure and Image Comparison at P2

Figure 4.155 shows the flow rate and pressure measurements for the corresponding 10 second period (275.69 to 285.69 seconds) that images were collected at P2 (downstream of Outlet B and F2) during Test 40.



**Figure 4.155 Flow Rate and Pressure Measurement within the Horizontal Carrier Pipe during Test 40 (275.69 to 285.69 seconds)**

The following selected images correspond to the time series data shown in Figure 4.155.



**Figure 4.156 Image at P2 at 278.50 seconds**

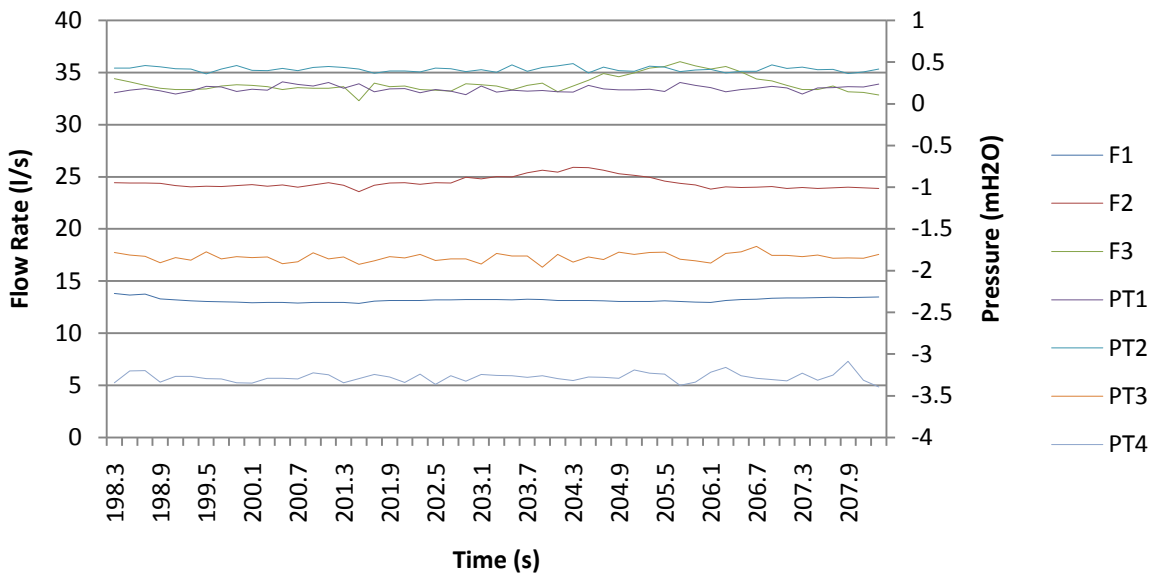
**Figure 4.157 Image at P2 at 281.82 seconds**

**Figure 4.158 Image at P2 at 284.62 seconds**

Similar to the results observed at P1, the images recorded during the flow tests completed at 36 l/s at P2 showed full bore conditions with small amounts of air at the crown of the pipe sporadically throughout the measurement period. Examples are shown in Figure 4.156, Figure 4.157 and Figure 4.158.

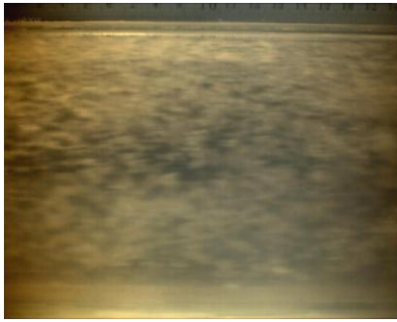
#### 4.1.7.6 Time Series Flow Rate, Pressure and Image Comparison at P3

Figure 4.159 shows the flow rate and pressure measurements for the corresponding 10 second period (198.31 to 208.31 seconds) that images were collected at P3 (downstream of Outlet C and F3) during Test 61.

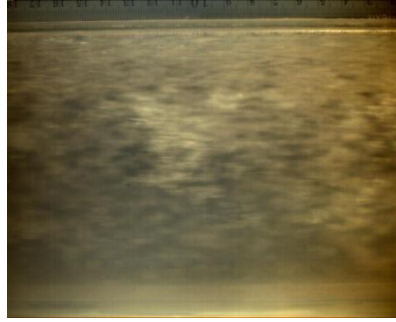


**Figure 4.159 Flow Rate and Pressure Measurement within the Horizontal Carrier Pipe during Test 61 (198.31 to 208.31 seconds)**

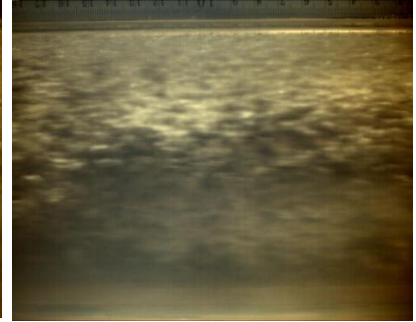
The following selected images correspond to the time series data shown in Figure 4.159.



**Figure 4.160 Image at P3 at  
198.31 seconds**



**Figure 4.161 Image at P3 at  
203.31 seconds**



**Figure 4.162 Image at P3 at  
207.37 seconds**

Images recorded at P3 for the tests completed at 120% of the design flow rate showed heavily aerated two-phase flow occupying the cross-sectional area of the pipe for the duration of the measurement period. Examples are shown in Figure 4.160, Figure 4.161 and Figure 4.162.



## 4.2 Key Findings and Discussion

Key findings from the experimental research programme are discussed in detail in the following section of this thesis and compared and contrasted to previous relevant experimental research and practice critically reviewed in Chapter 2. A summary of the key findings are:

1. The method of flourometry provides, for the first time, a robust, repeatable and accurate methodology for quantifying the relative proportion of flow through the components of a multi-outlet siphonic roof drainage system for both sub-prime and primed siphonic action, as detailed in Section 4.2.1;
2. Contrary to previously reported research, design standards and model based design software, flow proportionality through the multi-outlet test facility was not equal for the measured flow rates until the ultimate flow through the system was exceeded, as discussed in Section 4.2.2;
3. Measured system flow rates and pressure differed to the calculated values using the model based design software. Details are presented in Section 4.2.3;
4. The recognised and reported flow regimes within the horizontal carrier pipe of a siphonic roof drainage system varied temporally and spatially from the observations made during the steady flow tests completed as part of this experimental study, as set out in Section 4.2.4;
5. Air entrainment was observed throughout the series of steady flow tests that were completed at flow rates below, at and greater than the design flow conditions, as discussed in 4.2.5; and,
6. Observations following analysis of the measured flow velocity using high-speed image velocimetry and PIV analysis showed that the transverse velocity profile within the horizontal carrier pipe was variable and complex. These have been detailed in Section 4.2.6.

#### 4.2.1 Quantified Measurement of the Flow Proportionality within a Multi-Outlet Siphonic Roof Drainage Test Facility

The application of flourometry and the experimental system and methodology refined during this experimental investigation has, for the first time, provided a repeatable, robust and reliable approach to accurately measure the relative proportion and components of flow within a multi-outlet siphonic roof drainage system for a range of steady flows. Significantly, this is a non-intrusive methodology that does not affect the flow field. This is supported by the tabulated summary of results set out in Table 4.2 to Table 4.8 and the detailed analysis reported in Section 4.1.1 to 4.1.7 for each of the flow tests. A summary comparing the measured mass balance at F3 relative to the calibrated flow rate and volumetric drop test for each of the 63 flow tests are shown in Table 4.23 and Figure 4.163.

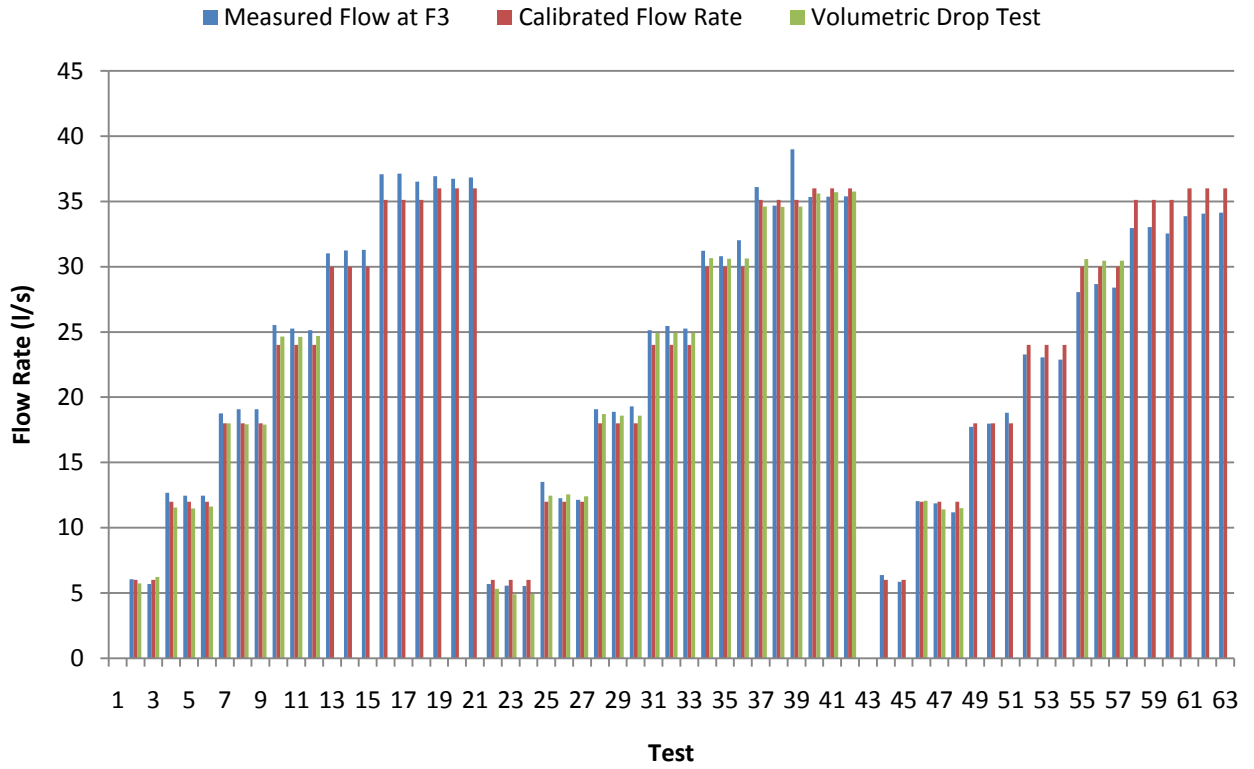
**Table 4.23 Summary of the Measured Flow at F3 Compared to the Calibrated Flow Rate and Volumetric Drop Test**

Test	Measured Flow at F3 (l/s)	Calibrated Flow Rate		Volumetric Drop Test	
		Flow Rate (l/s)	Difference (%)	Flow Rate (l/s)	Difference (%)
1	N/A	N/A	N/A	N/A	N/A
2	6.05	6	0.83	5.73	5.58
3	5.70	6	-5.00	6.22	-8.36
4	12.67	12	5.58	11.54	9.79
5	12.45	12	3.75	11.47	8.54
6	12.46	12	3.83	11.63	7.14
7	18.75	18	4.17	18.01	4.11
8	19.07	18	5.94	17.93	6.36
9	19.08	18	6.00	17.89	6.65
10	25.53	24	6.38	24.64	3.61
11	25.26	24	5.25	24.61	2.64
12	25.13	24	4.71	24.70	1.74
13	31.02	30	3.40	N/A	N/A
14	31.24	30	4.13	N/A	N/A
15	31.28	30	4.27	N/A	N/A
16	37.09	35.12	5.61	N/A	N/A
17	37.13	35.12	5.72	N/A	N/A
18	36.51	35.12	3.96	N/A	N/A
19	36.93	36	2.58	N/A	N/A
20	36.73	36	2.03	N/A	N/A
21	36.84	36	2.33	N/A	N/A
22	5.69	6	-5.17	5.33	6.75
23	5.56	6	-7.33	4.91	13.24
24	5.54	6	-7.67	4.92	12.60
25	13.52	12	12.67	12.47	8.42
26	12.26	12	2.17	12.55	-2.31
27	12.15	12	1.25	12.4	-2.02
28	19.08	18	6.00	18.7	2.03

---

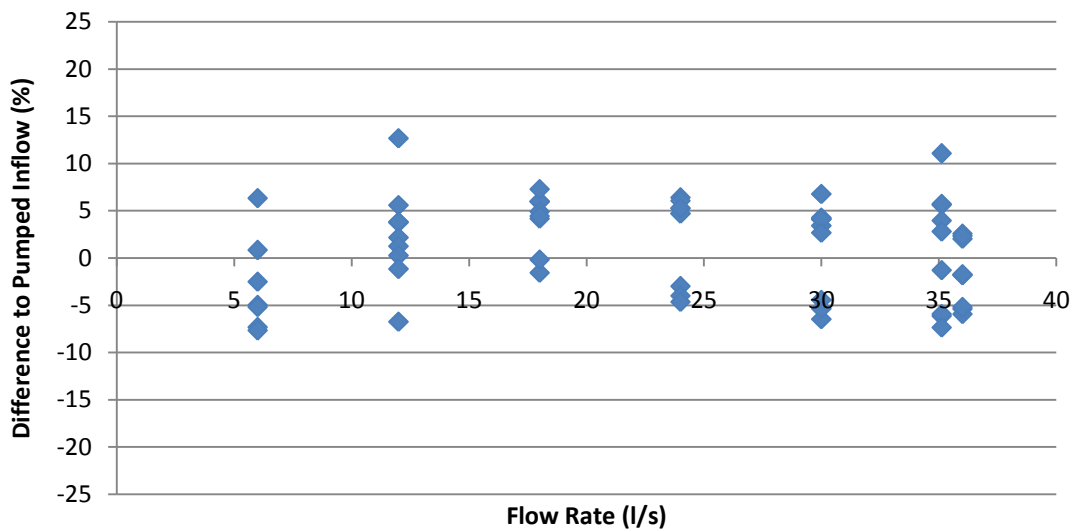
29	18.88	18	4.89	18.59	1.56
30	19.31	18	7.28	18.58	3.93
31	25.13	24	4.71	24.91	0.88
32	25.45	24	6.04	24.94	2.04
33	25.27	24	5.29	24.95	1.28
34	31.23	30	4.10	30.65	1.89
35	30.8	30	2.67	30.6	0.65
36	32.03	30	6.77	30.63	4.57
37	36.1	35.12	2.79	34.6	4.34
38	34.67	35.12	-1.28	34.57	0.29
39	39	35.12	11.05	34.59	12.75
40	35.34	36	-1.83	35.61	-0.76
41	35.37	36	-1.75	35.71	-0.95
42	35.38	36	-1.72	35.76	-1.06
43	N/A	N/A	N/A	N/A	N/A
44	6.38	6	6.33	N/A	N/A
45	5.85	6	-2.50	N/A	N/A
46	12.03	12	0.25	12.07	-0.33
47	11.86	12	-1.17	11.4	4.04
48	11.19	12	-6.75	11.51	-2.78
49	17.72	18	-1.56	N/A	N/A
50	17.97	18	-0.17	N/A	N/A
51	18.8	18	4.44	N/A	N/A
52	23.28	24	-3.00	N/A	N/A
53	23.04	24	-4.00	N/A	N/A
54	22.89	24	-4.63	N/A	N/A
55	28.06	30	-6.47	30.58	-8.24
56	28.67	30	-4.43	30.45	-5.85
57	28.39	30	-5.37	30.47	-6.83
58	32.96	35.12	-6.15	N/A	N/A
59	33.04	35.12	-5.92	N/A	N/A
60	32.54	35.12	-7.35	N/A	N/A
61	33.87	36	-5.92	N/A	N/A
62	34.06	36	-5.39	N/A	N/A
63	34.13	36	-5.19	N/A	N/A

---



**Figure 4.163 Measured Flow at F3 relative to the Calibrated Pumped Inflow and Volumetric Drop Test Comparison**

Figure 4.164 demonstrates the difference between the measured flow at F3 for each of the tests relative to the pumped inflow to the system.



**Figure 4.164 Scatter Plot Showing the Difference between the Measured Flow at F3 and the Calibrated Pumped Inflow**

During the full test program, a positive and negative difference in the mass balance was measured in comparison to the pumped inflow and volumetric drop test (where available) for all flow rates shown in Table 4.23, Figure 4.163 and Figure 4.164. The average difference considering both positive and negative values between the measured flow at F3 and the calibrated pumped inflow over the series of tests was 1.01% with a standard deviation of 5.05%. The average absolute difference and standard deviation was 4.54% and 2.37% respectively. Specifically, the mass balance measured during Tests 52 to 63 was less than the pumped inflow but, for all these tests, the measured difference was within 3 times the standard deviation of the absolute values, equivalent to 7.11%, with the exception of Test 60 which was 3.1 times the standard deviation. Hence, as these results are consistent in terms of their accuracy and repeatability with all other tests, they support the main conclusions of the research and confirm the accuracy of the methodology for flow rates below, at, and above the design criteria.

#### 4.2.1.1 Comparison to Previous Research and Practice

An off-line dye dilution technique was developed by Bramhall (2004) to investigate the flow rates through an experimental test facility with three outlets within a common gutter described in Section 2.4.4.2.5. An injection pump was used to inject dye of a known concentration into the upstream outlet. Dilution samples were retrieved from three sample points and an average concentration determined for each point. This average value was then used to determine the average flow of water through the individual outlets. This methodology was applied to one flow test at a constant inflow to the system of 36 l/s, selected as it was close to the calculated theoretical maximum capacity of the system (ultimate flow rate).

The results reported by Bramhall (2004) are analysed and compared to the results from tests 19, 20, 21, 40, 41 and 42. The results from these tests were selected as they were completed at a steady flow rate in excess of the ultimate system capacity of 35.12 l/s and the difference between the calibrated inflow rate and volumetric drop test was  $\pm 2.58\%$ . The comparative analysis includes sample size, mean measured value, proportionality through each outlet, standard deviation ( $\sigma$ ), sample variance ( $\sigma^2$ ), maximum measured value, number of standard deviations the maximum measured value was from the mean, the mean plus 3 standard deviations, minimum measured value, number of standard deviations the minimum measured value was from the mean and the mean minus 3 standard deviations. The results relative to Outlets A, B and C are shown in Table 4.24, Table 4.25 and Table 4.26 respectively.

**Table 4.24 Measurement Analysis Comparison to Bramhall (2004) for Outlet A**

Ref	Sample size	Outlet A									
		Mean (l/s)	Proportionality (%)	$\sigma$ (l/s)	$\sigma^2$ (l/s)	Max (l/s)	$\frac{\text{Max} - \text{Mean}}{\sigma}$	Mean +3 $\sigma$ (l/s)	Min (l/s)	$\frac{\text{Mean} - \text{Min}}{\sigma}$	Mean -3 $\sigma$ (l/s)
Bramhall	5	9.28	26.24	0.14	0.020	9.40	0.86	9.70	9.12	1.14	8.86
19	841	12.45	33.72	0.35	0.123	13.44	2.83	13.50	11.55	2.57	11.40
20	969	12.41	33.78	0.37	0.137	13.36	2.57	13.52	11.55	2.32	11.30
21	915	12.44	33.75	0.32	0.102	13.35	2.84	13.40	11.66	2.44	11.48
40	1046	11.41	32.65	0.35	0.123	12.54	3.23	12.46	10.49	2.63	10.36
41	1067	11.43	32.32	0.40	0.160	12.54	2.78	12.63	10.46	2.43	10.23
42	1081	11.40	32.22	0.37	0.137	12.40	2.70	12.51	10.34	2.86	10.29

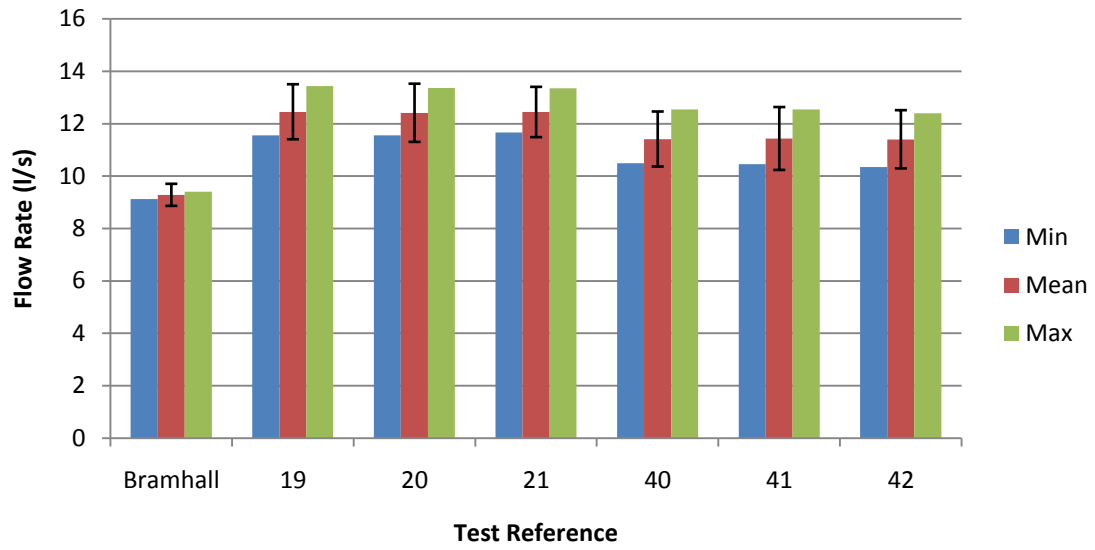
**Table 4.25 Measurement Analysis Comparison to Bramhall (2004) for Outlet B**

Ref	Sample size	Outlet B									
		Mean (l/s)	Proportionality (%)	$\sigma$ (l/s)	$\sigma^2$ (l/s)	Max (l/s)	$\frac{\text{Max} - \text{Mean}}{\sigma}$	Mean +3 $\sigma$ (l/s)	Min (l/s)	$\frac{\text{Mean} - \text{Min}}{\sigma}$	Mean -3 $\sigma$ (l/s)
Bramhall	5	23.24	39.47	0.05	0.003	23.31	1.40	23.39	23.18	1.20	23.09
19	841	24.63	32.97	0.65	0.423	26.45	2.80	26.58	23.04	2.45	22.68
20	969	24.49	32.89	0.78	0.608	26.15	2.13	26.83	22.82	2.14	22.15
21	915	24.62	33.06	0.64	0.410	26.30	2.63	26.54	23.14	2.31	22.70
40	1046	24.78	37.83	0.69	0.476	27.05	3.29	26.85	22.90	2.72	22.71
41	1067	24.73	37.60	0.96	0.922	27.76	3.16	27.61	22.60	2.22	21.85
42	1081	24.58	37.25	0.90	0.810	27.08	2.78	27.28	21.91	2.97	21.88

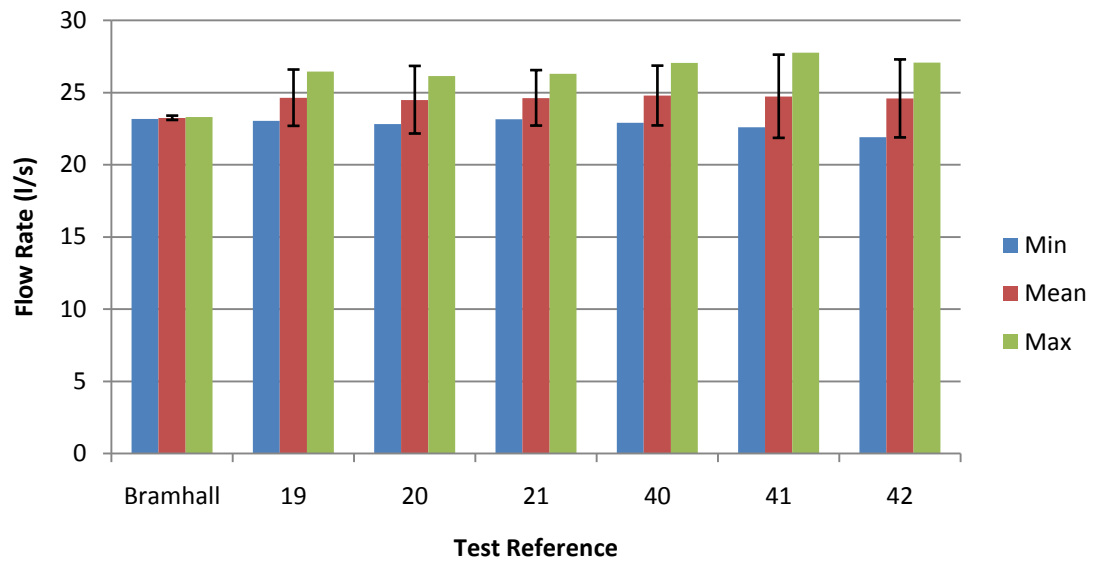
**Table 4.26 Measurement Analysis Comparison to Bramhall (2004) for Outlet C**

Ref	Sample size	Outlet C									
		Mean (l/s)	Proportionality (%)	$\sigma$ (l/s)	$\sigma^2$ (l/s)	Max (l/s)	$\frac{\text{Max} - \text{Mean}}{\sigma}$	Mean +3 $\sigma$ (l/s)	Min (l/s)	$\frac{\text{Mean} - \text{Min}}{\sigma}$	Mean -3 $\sigma$ (l/s)
Bramhall	5	35.37	34.29	0.29	0.084	35.99	2.14	36.24	35.27	2.48	34.50
19	841	36.93	33.32	0.95	0.903	39.59	2.80	39.78	34.10	2.98	34.08
20	969	36.73	33.33	1.21	1.464	39.37	2.18	40.36	33.61	2.58	33.10
21	915	36.84	33.19	0.93	0.865	39.40	2.75	39.63	34.44	2.58	34.05
40	1046	35.34	29.52	0.99	0.980	38.69	3.38	38.31	32.02	3.35	32.37
41	1067	35.37	30.08	1.42	2.016	39.62	2.99	39.63	31.90	2.44	31.11
42	1081	35.38	30.53	1.36	1.850	38.72	2.46	39.46	31.52	2.84	31.30

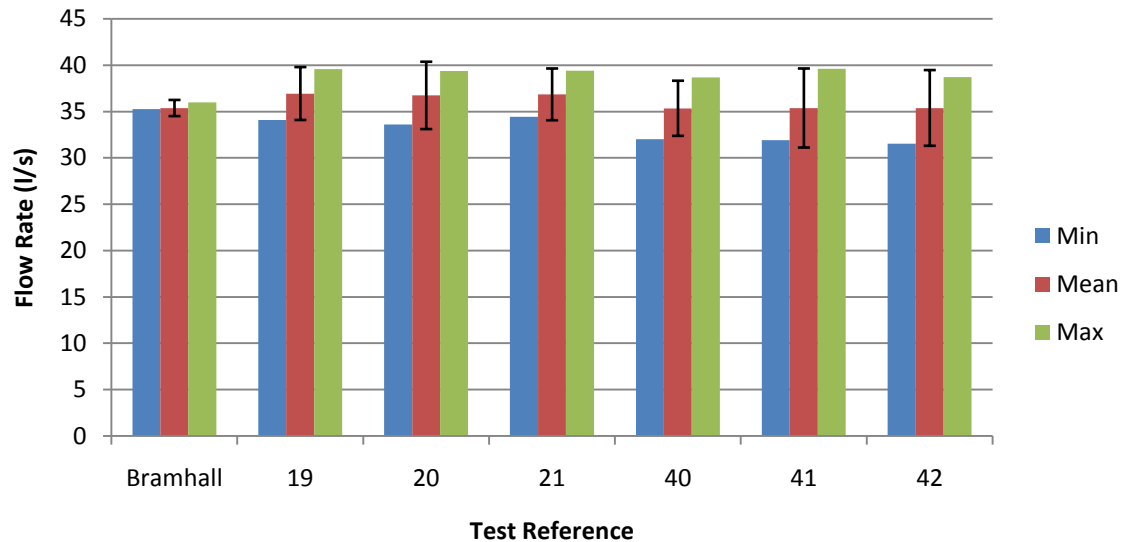
Comparative bar charts showing the measured minimum, mean and maximum flow rate through each outlet for each of the selected tests in comparison to the results reported by Bramhall (2004) are shown in Figure 4.165, Figure 4.166 and Figure 4.167. The error bars show the mean value  $\pm 3$  times the standard deviation.



**Figure 4.165 Minimum, Mean and Maximum Flow Rate Comparison for Outlet A**



**Figure 4.166 Minimum, Mean and Maximum Flow Rate Comparison for Outlet B**



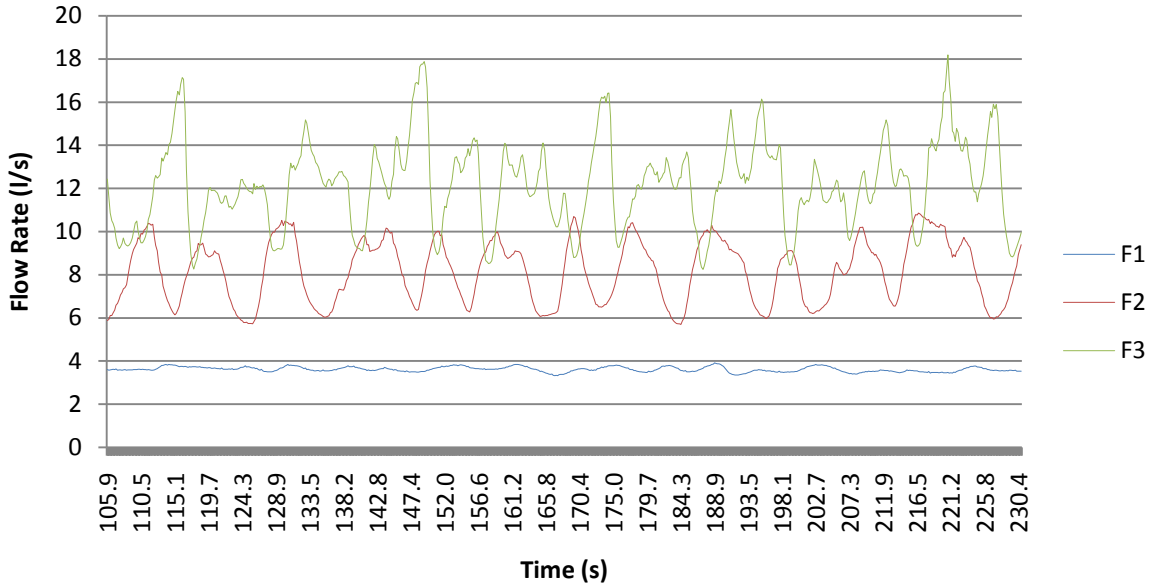
**Figure 4.167 Minimum, Mean and Maximum Flow Rate Comparison for Outlet C**

Whilst both techniques are successful, these results clearly show that the off-line sampling approach provides limited resolution in comparison to the in-line, continuous methodology developed within this experimental research. There is a significant difference in the sample size and variance which brings into question the validity of the maximum and minimum values recorded by Bramhall (2004). Specifically, the difference between the mean and the maximum and minimum measured values reported by Bramhall (2004) through Outlets A and B were all within 1.4 times the standard deviation. By comparison, the results from this research showed a range of 2.13 and 3.29 times the standard deviation. This confirms that a substantial data set is required to fully understand the range of flow rates through a multi-outlet siphonic system, even when the system is operating at the ultimate capacity. This presents a limitation of the sampling methodology.

This limitation would mean that application of the sampling methodology at system flow rates below the ultimate capacity would not be appropriate. The sampling methodology is not instantaneous and based on the limited resolution would not be able to detect the peak flows observed and measured repeatedly throughout this experimental research.

For example, Figure 4.168, shows a section of time-series flow data from Test 4 at a flow rate of 40% of the system design capacity or 12 l/s. The time series data is over a time period of 124.9 seconds with a sample size of 624 measurements.





**Figure 4.168 Time Series Flow Rate Measurements from Test 4**

Analysis of the time series data is shown in Table 4.27.

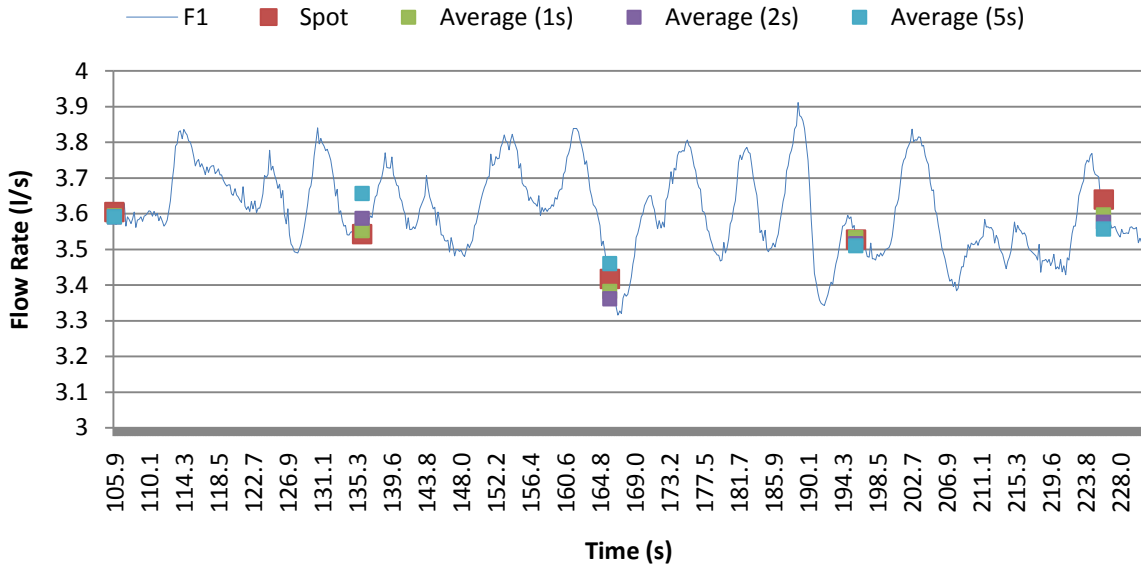
**Table 4.27 Test 4 Comparative Analysis**

Outlet	Mean (l/s)	Proportionality (%)	$\sigma$ (l/s)	$\sigma^2$ (l/s)	Max (l/s)	Mean + 3 $\sigma$ (l/s)	Min (l/s)	Mean - 3 $\sigma$ (l/s)
A	3.61	29.69	0.12	0.014	3.91	3.97	3.32	3.25
B	8.17	37.50	1.45	2.103	10.86	12.52	5.70	3.82
C	12.16	32.81	2.02	4.080	18.18	18.22	8.24	6.10

The measured mass balance (i.e. mean flow at C3) was 12.16 l/s, equivalent to 101.33% of the calibrated pump inflow of 12 l/s.

The data has been analysed to demonstrate the difference between the time series measurements recorded at 5 Hz during this experimental research and the sampling method reported by Bramhall (2004). The time series data has been compared to spot or instantaneous measurements and data averaged over a 1 second, 2 second and 5 second duration. These time periods were selected to represent the time required to obtain the necessary sample volume for measurement by the flourometer. The data points were calculated at a frequency of 30 seconds representing a realistic time between sample collection. The time taken to collect a sample and sampling frequency has been assumed as it was not reported by Bramhall (2004). This is a limitation of this method as time is required to extract the necessary sample volume from the system. Furthermore, the decanting process and diligence required to ensure that there was no contamination is a time-consuming procedure that will dictate the frequency at which samples can be taken.

The time series data measured by F1 through Outlet A during Test 4 is presented in Figure 4.169 with the corresponding data points determined using this approach.



**Figure 4.169 Time Series Data Measured by F1 during Test 4 and Comparison to a Sampling Method**

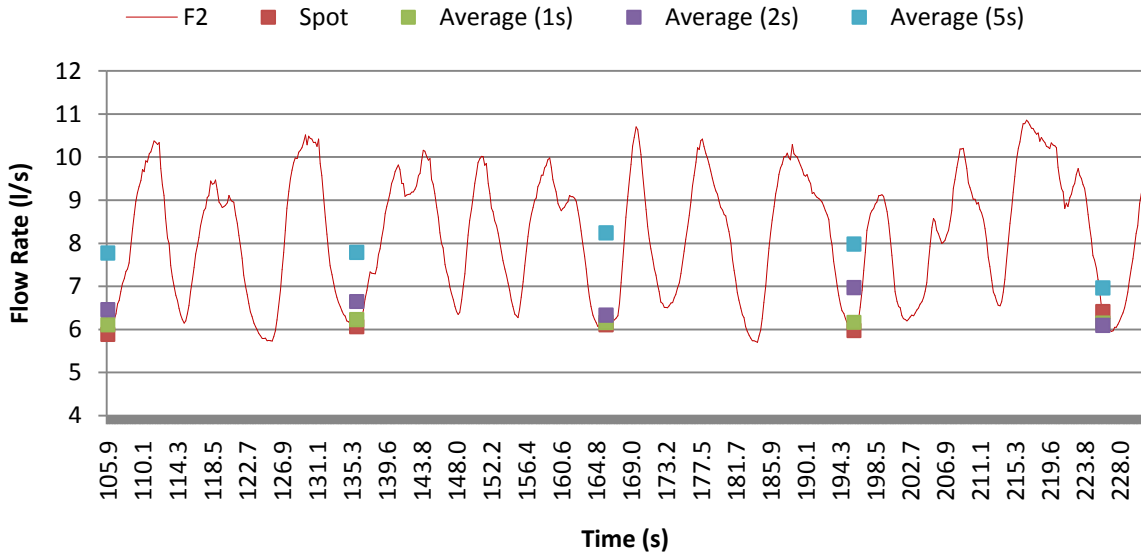
Analysis of the data presented in Figure 4.169 is shown in Table 4.28. Flow proportionality has been determined relative to the mass balance calculated according to the respective method included in Table 4.30.

**Table 4.28 Analysis of Time Series Data Measured by F1 during Test 4 and Comparison to a Sampling Method**

Method	Mean (l/s)	Proportionality (%)	$\sigma$ (l/s)	$\sigma^2$ (l/s)	Max (l/s)	Mean + 3 $\sigma$ (l/s)	Min (l/s)	Mean - 3 $\sigma$ (l/s)
F1	3.61	29.69	0.12	0.014	3.91	3.97	3.32	3.25
Spot	3.55	27.52	0.09	0.008	3.64	3.82	3.42	3.28
Average (1s)	3.53	28.08	0.09	0.008	3.60	3.80	3.38	3.26
Average (2s)	3.53	28.40	0.10	0.010	3.59	3.83	3.36	3.23
Average (5s)	3.56	32.28	0.08	0.006	3.66	3.80	3.46	3.32

Analysis of the flow rate data measured through Outlet A by F1 shows that the mean values are comparable. This is due to the relatively constant flow rate measured through Outlet A during this test. However, the sampling methodology is not able to achieve the resolution to detect the flow rate fluctuations measured using the inline method. This is demonstrated in the differences between the maximum and minimum values, standard deviation and sample variance.

The time series data measured by F2 through Outlet B during Test 4 is presented in Figure 4.170 with the corresponding data points.



**Figure 4.170 Time Series Data Measured by F2 during Test 4 and Comparison to a Sampling Method**

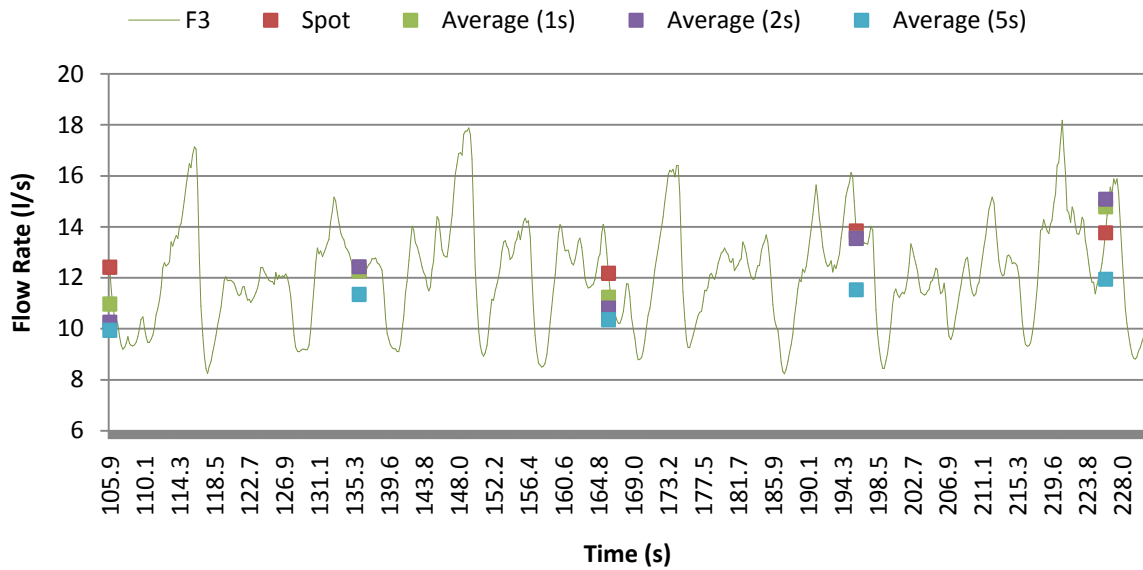
Analysis of the data presented in Figure 4.170 is shown in Table 4.29. Flow proportionality has been determined relative to the mass balance calculated according to the respective method included in Table 4.30.

**Table 4.29 Analysis of Time Series Data Measured by F2 during Test 4 and Comparison to a Sampling Method**

Method	Mean (l/s)	Proportionality (%)	$\sigma$ (l/s)	$\sigma^2$ (l/s)	Max (l/s)	Mean + 3 $\sigma$ (l/s)	Min (l/s)	Mean - 3 $\sigma$ (l/s)
F2	8.17	37.50	1.45	2.103	10.86	12.52	5.70	3.82
Spot	6.09	19.69	0.20	0.040	6.41	6.69	5.89	5.49
Average (1s)	6.17	21.00	0.04	0.002	6.23	6.29	6.11	6.05
Average (2s)	6.50	23.89	0.33	0.109	6.97	7.49	6.09	5.51
Average (5s)	7.75	37.99	0.48	0.230	8.24	9.19	6.96	6.31

Analysis of the flow rate data measured through Outlet B by F2 shows that the mean values are significantly different. The difference in comparison to the mean flow rate measured using the inline method ranged from -5.14% using the 5 second average to -25.46% using the spot measurements. A difference of -24.48% and -20.44% was measured using the 1 second average and 2 second average methods respectively. All sampling methods underestimated the flow rate measured through Outlet B which significantly affected the relative flow proportionality. The sampling method was also not able to detect the flow rate fluctuations shown clearly in Figure 4.170. This is confirmed by the data analysis including the maximum and minimum values, standard deviation and sample variance.

The time series data measured by F3 through Outlet C during Test 4 is presented in Figure 4.171 with the corresponding data points.



**Figure 4.171 Time Series Data Measured by F3 during Test 4 and Comparison to a Sampling Method**

Analysis of the data presented in Figure 4.171 is shown in Table 4.30. A comparison to the pumped inflow of 12 l/s is included in the analysis.

**Table 4.30 Analysis of Time Series Data Measured by F3 during Test 4 and Comparison to a Sampling Method**

Method	Mean (l/s)	Comparison to Pumped Inflow (%)	Proportionality (%)	$\sigma$ (l/s)	$\sigma^2$ (l/s)	Max (l/s)	Mean + 3 $\sigma$ (l/s)	Min (l/s)	Mean - 3 $\sigma$ (l/s)
F3	12.16	101.33	32.81	2.02	4.080	18.18	18.22	8.24	6.10
Spot	12.90	107.50	52.79	0.83	0.689	13.83	15.39	12.18	10.41
Average (1s)	12.57	104.75	50.92	1.61	2.592	14.79	17.40	10.97	7.74
Average (2s)	12.43	103.58	47.71	1.98	3.920	15.10	18.37	10.25	6.49
Average (5s)	11.03	91.92	29.73	0.84	0.706	11.96	13.55	9.95	8.51

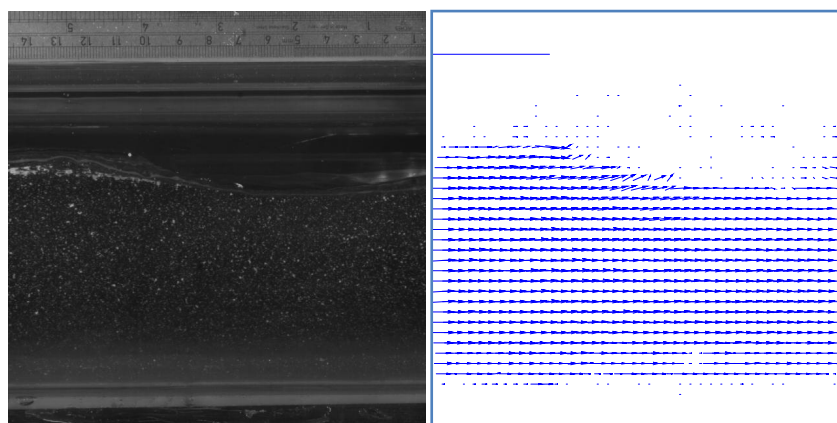
Analysis of the flow rate data measured through Outlet C by F3 shows that the mean values are variable with a difference ranging from -9.29% to 6.09%. Similar to the results measured by F1 and F2, the sampling methods were not able to detect the flow rate fluctuations shown in Figure 4.171. This is confirmed by the data analysis including the maximum and minimum values, standard deviation and sample variance.

A comparison between the time series data measured during this experimental research and sampling methods reported by Bramhall (2004) has shown that neither the accuracy or resolution of measurement can be achieved using the sampling approach. This is demonstrated by the variability and difference in the mean flow rate values significantly affecting the relative flow proportionality. Furthermore, the sampling method could not be

applied to time-varying flows, essential to be able to determine the time to prime and time to deprime of a siphonic system.

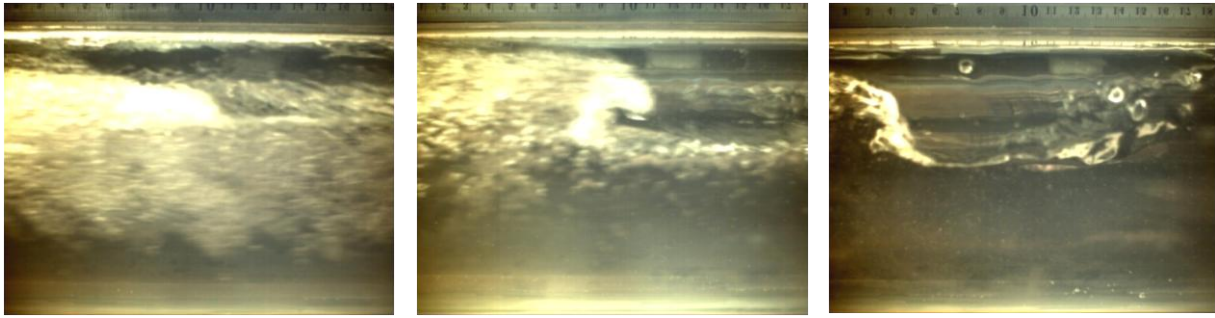
It is recognised from previous experimental research, for example Lucke et al. (2014), that quantifying flow rates through individual gutters and pipework in siphonic roof drainage is very difficult, particularly when the flow is aerated or does not fully occupy the cross-sectional area of the pipe. Accurate measurement of these flow conditions is complex. This is supported by May (1997) who identified that "the behaviour of two-phase flows with significant amounts of air can be complex, and at present it is not possible to predict accurately how a siphonic system will operate under part-full conditions."

Recent experimental research completed by Lucke et al (2014) reported a methodology of estimating the flow component through outlets within the full scale siphonic roof drainage test facility at the University of South Australia. The experimental method consisted of a propeller-type current meter installed within the tail pipe to measure velocity and a pressure transducer to measure water depth. Measurements from the instruments were then calibrated against known flow rates to generate a series of calibration curves. The output from these instruments during a series of tests was then used to estimate the flow rate through the individual outlets within the test facility. The current meter used during the experimental tests reported by Qu et al. (2011) was installed 1mm above the invert of the pipe to be able to measure the lowest flow depths. However, this type of instrument is only able to measure flow velocity within a limited area and it is unclear how representative this is of the cross-sectional velocity profile. This would be very difficult to determine due to the turbulent, oscillating flow conditions. Furthermore, the velocity profile is known to be variable, demonstrated by the series of images throughout this thesis and the PIV analysis undertaken during the feasibility tests. An example of an image taken during free surface flow conditions and the corresponding PIV analysis is shown in Figure 4.172.



**Figure 4.172 Image Showing Flow Conditions and Corresponding PIV Analysis**

Flow within the horizontal carrier pipe has been shown to be temporally and spatially variable as highlighted throughout this chapter. This is demonstrated by reference to three examples of complex flow conditions captured during this experimental research as shown in Figure 4.173.



**Figure 4.173 Examples of Complex Flow Conditions**

Hence, to estimate flow rate based on this method of measuring velocity and depth and applying a modified continuity equation should, in the opinion of the author, be used/applied with caution.

Disturbance testing was undertaken as part of the experimental research reported by Qu et al. (2011) to determine the effect of introducing the current meter into the flow field. A difference in water level within the test facility of up to 14% was reported although this was not regarded to significantly affect the flow rate. Furthermore, the results from the pressure transducers used by Qu et al. (2011), as a basis to estimate flow rate, were reported to be highly variable and alternative more suitable instruments were proposed for future experimental research (Lucke, et al. 2014).

It is concluded therefore, that the provision of such a measurement system represents a novel and original way in which to measure the flow components in a multi-outlet siphonic system for flow rates below the design criteria and for time varying changes. This is significant as reported by Wright et al. (2006a):

"Existing design methods cannot be used to analytically assess the ability of a system to prime. Furthermore, steady state design methods cannot predict performance when a system is exposed to rainfall events below the design criteria, when the flow may contain substantial quantities of entrained air, or events with time varying rainfall intensity. As such events are the norm, current design methods may not be suitable for determining the day-to-day performance characteristics of siphonic roof drainage systems. This is a major disadvantage, as it is during these events that the majority of operational problems tend to occur."

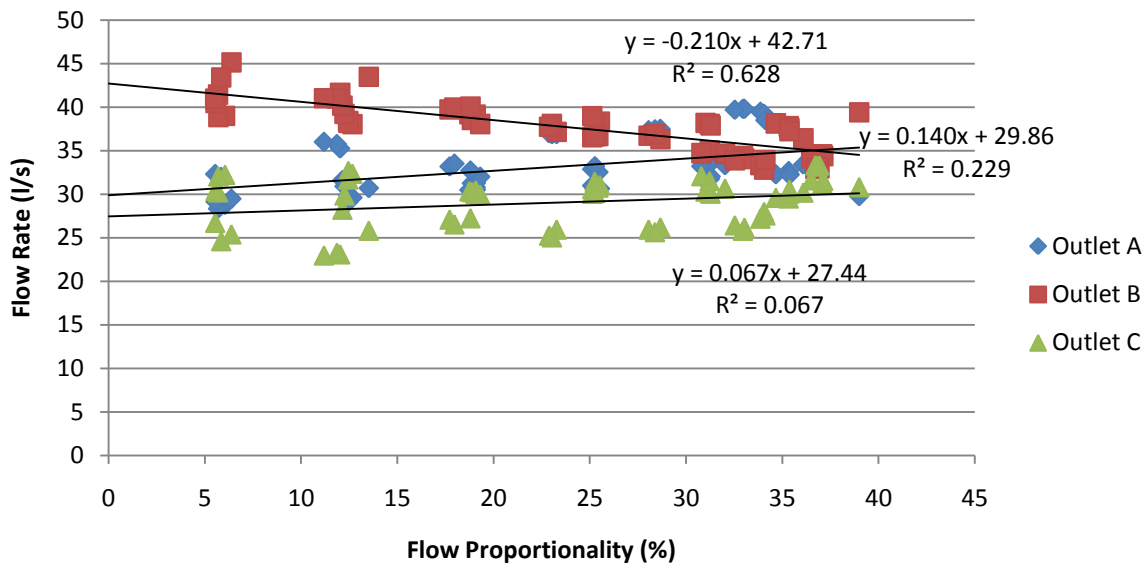
For the first time, this experimental research presents time-series flow rate measurements of key network components within a multi-outlet siphonic roof drainage system with the relative time-series system pressure and high resolution image data. Furthermore, the methodologies and measurement techniques developed throughout this experimental research are appropriate and applicable to flow rates at and below a systems operating capacity, to understand the

effect and impact of common operational problems (i.e. outlet blockages) in real time as well as critically, time-varying flows.

#### 4.2.2 Relative Flow Proportionality within a Multi-Outlet Siphonic Roof Drainage Test Facility

The results from this research using a sophisticated experimental test facility, has shown that the flow rate through the multi-outlet system was not equal and that the proportional flow through each outlet varied as a function of the magnitude of the total system flow rate. Previously reported research, design standards and design software used in the siphonic roof drainage industry and discussed in the literature review of this thesis, has been based on the assumption that there is equal flow proportionality through each outlet. This key finding is discussed relative to previous relevant research and practice in Section 4.2.2.1.

Figure 4.174 shows the measured relative flow component through each outlet as a percentage of the total system flow rate recorded in each steady flow test.



**Figure 4.174 Proportionality of Flow through each Outlet**

Analysis of the results showed that at the steady flow tests less than the ultimate flow rate of 35.12 l/s, flow through Outlet B was proportionally higher. The relative flow component was highest at the lowest flow rates measured and reduced as the flow rate increased. Conversely, flow proportionality through Outlets A and C were lowest at the lower steady flow tests and increased relative to the system flow rate. Average flow proportionality between Outlets A and B was within 0.65% during the steady flow tests completed at the ultimate flow rate. Flow through Outlet A exceeded the relative proportion compared to Outlet B during the steady flow tests completed in excess of the ultimate flow rate.

Although there is variability in the results, flow proportionality through the experimental test facility tended toward an equal state as the flow through the system increased. Flow proportionality was equal through each outlet for a number of tests (19, 20 and 21) completed



at 120% of the design flow rate. However, average flow proportionality through Outlet C throughout the series of tests was less than this highlighted in Figure 4.174.

This finding confirms that flow proportionality is not equal, but for the first time accurately quantifies and confirms this hypothesis.

#### 4.2.2.1 Comparison to Previous Research and Practice

These observations contrast research published by Arthur and Wright (2005), which stated that under free discharge conditions, "the flow splits evenly in any given gutter section irrespective of whether the gutter inflow is uniform or non-uniform". The steady flow tests completed as part of this experimental research has found this not to be the case as highlighted in Figure 4.174.

Arthur and Wright (2005) also identified that "the pipework in a siphonic system will run full-bore when operating at or near its design point and the flow division between outlets will be dependent on the relative losses associated with each branch". In contrast, this experimental programme of research has shown that full bore conditions were not observed throughout the siphonic test facility even at flow rates in excess of the calculated design and ultimate flows. At the design flow rate, for the experimental test facility at the University of Sheffield, full bore conditions were interspersed with free surface flow and the presence of air pockets at the crown of the pipe. Even at steady flow tests completed at 120% of the design flow rate, aerated two phase flow was observed within the horizontal carrier pipe downstream of Outlet C. A summary of the observed flow phases relative to each system flow rate have been included in Table 4.35 in Section 4.2.4.

Research completed in Australia by Lucke (2009) reported that "an ideal siphonic system will have a total calculated energy loss through the piping system precisely equal to the available head for each branch in the system". System balancing can only be achieved at the system flow rate where these energy losses are realised. At system flow rates less than this, energy losses will reduce and hence, system balancing will not be achieved. This research has demonstrated that the flow component through each outlet varied as a function of the magnitude of the total system flow rate. System balancing using the experimental test facility at the University of Sheffield was not achieved even at system flow rates in excess of the ultimate design capacity.

The development of a numerical model based on estimated flow rates from experimental research completed at the University of South Australia was reported by Lucke et al. (2014). The experimental test facility incorporated four outlets within a common gutter. The authors reported that the measured flow rate values for the downstream outlet (Outlet 4) were estimated by dividing the total flow rate supplied to the rig by the number of outlets, i.e. 25% each. However, the uncertainty in quantifying the flow proportionality using this approach was acknowledged as Lucke et al. (2014) recognised that "this estimation method assumes an equal distribution of the gutter flow between the outlets, which may not be the case for all

flow rates". To achieve an optimum fit between the measured and predicted flow at Outlet 4, a factor of 0.795 was applied. This corresponds to flow proportionality of 20% rather than 25% and hence brings into question the validity of the modelling approach adopted by Lucke et al (2014).

Although the results and observations from this experimental research are specific to the experimental test facility used, the outputs strongly indicate that a single factor is not sufficient to cover the full range of sub-prime and primed flow conditions. This will of course be specific to each system, but this research has demonstrated that flow proportionality is not equal or constant during steady flow tests. This contrasts with the research published by Lucke et al. (2014) which states that specific to the results reported as part of the experimental study "the underlying methodology used in this study to estimate flow rates through individual outlets is suitable".

Additional experimental research using the methodology developed within this study is therefore recommended to understand the effect of system design variables (e.g. outlet position, tailpipe size and configuration, number of outlets, etc) on flow proportionality through each outlet within a common gutter. This will help to enhance current design criteria and refine numerical models.

### 4.2.3 Comparison Between Measured System Flow Rates and Pressure to the Calculated Values using the Model Based Design Software

A comparison was made between the measured system flow rates and pressures with those computed using commercially available software. The sizing and configuration of the experimental test facility pipework was completed using commercially available software based on the Bernoulli Energy Equation and Colebrook White Equation. Design flow and operating pressure of the system was 30 l/s and -3.23 mH<sub>2</sub>O respectively with an ultimate flow of 35.12 l/s and ultimate operating pressure of -4.67 mH<sub>2</sub>O.

Measured system flow rates and pressure during the full test program completed using the experimental test facility at the University of Sheffield differed to the calculated values from the model based design software.

A comparison between the measured minimum system pressure, the mean pressure minus 3 standard deviations and the calculated system pressure of -3.23 mH<sub>2</sub>O for the tests completed at  $\pm 5\%$  of the design flow rate is shown in Table 4.31.

**Table 4.31 Comparison Between Measured and Calculated System Pressure at the Design Flow Rate**

Test	Measured Flow Rate (l/s)	Minimum Measured System Pressure (mH <sub>2</sub> O)	Difference to Calculated System Pressure (%)	Mean Pressure -3 $\sigma$ (mH <sub>2</sub> O)	Difference to Calculated System Pressure (%)
13	31.02	-3.51	8.67	-3.42	5.88
14	31.24	-3.38	4.64	-3.41	5.57
15	31.28	-3.45	6.81	-3.45	6.81
34	31.23	-3.52	8.98	-3.45	6.81
35	30.80	-3.46	7.12	-3.44	6.50
56	28.67	-3.46	7.12	-3.44	6.50

The results show there is a very close match between the minimum measured system pressure and the mean pressure minus 3 standard deviations. This demonstrates that the minimum measured value is valid. The average difference to the calculated system pressure of -3.23 mH<sub>2</sub>O is 7.22% and 6.35% respectively.

A comparison between the measured minimum system pressure, the mean pressure minus 3 standard deviations and the calculated system pressure of -4.67 mH<sub>2</sub>O for the tests completed at  $\pm 5\%$  of the ultimate flow rate is shown in Table 4.32.

**Table 4.32 Comparison Between Measured and Calculated System Pressure at the Ultimate Flow Rate**

Test	Measured Flow Rate (l/s)	Minimum Measured System Pressure (mH <sub>2</sub> O)	Difference to Calculated System Pressure (%)	Mean Pressure -3σ (mH <sub>2</sub> O)	Difference to Calculated System Pressure (%)
18	36.51	-3.58	23.34	-3.53	24.41
37	36.10	-3.61	22.70	-3.54	24.20
38	34.67	-3.57	23.55	-3.53	24.41
20	36.73	-3.42	26.77	-3.45	26.12
21	36.84	-3.46	25.91	-3.42	26.77
40	35.34	-3.45	26.12	-3.47	25.70
41	35.37	-3.44	26.34	-3.47	25.70
42	35.38	-3.48	25.48	-3.49	25.27
61	33.87	-3.49	25.27	-3.45	26.12
62	34.06	-3.43	26.55	-3.46	25.91
63	34.13	-3.47	25.70	-3.49	25.27

The results show there is a very close match between the minimum measured system pressure and the mean pressure minus 3 standard deviations. This demonstrates that the minimum measured value is valid. The average difference to the calculated system pressure of -4.67 mH<sub>2</sub>O is 25.25% and 25.44% respectively.

These results showed that there is a difference of between 4.64% and 8.98% between the measured and calculated system pressure at the design flow rate. There is a much more significant difference in the comparison of system pressures at the ultimate flow rate of between 22.70% and 26.77%.

Steady state hydraulic calculations of the experimental test facility were completed to account for differences between the measured data and those predicted using the commercially available software. Bernoulli's equation was used to calculate the head loss ( $\Delta H$ ) within each pipe in the system according to the following equation:

$$\left( h_1 + \frac{V_1^2}{2g} + z_1 \right) - \left( h_2 + \frac{V_2^2}{2g} + z_2 \right) = \Delta H_{12}$$

Where  $h_1$  is the upstream pressure head,  $V_1$  is the upstream velocity,  $z_1$  is the upstream vertical elevation,  $h_2$  is the downstream pressure head,  $V_2$  is the downstream velocity,  $z_2$  is the downstream vertical elevation and  $g$  is the acceleration due to gravity.

Two elements of  $\Delta H$  were calculated:

$$\Delta H = \Delta H_p + \Delta H_f$$

Where  $\Delta H_p$  is the head loss due to hydraulic resistance of the pipe walls and  $\Delta H_f$  is the head loss due to fittings.

The  $\Delta H_p$  component of the equation for each pipe length was determined according to the following equation:

$$\Delta H_p = iL$$

Where  $i$  is the head loss or energy gradient in metres per meter and  $L$  is the pipe length.

$i$  was calculated iteratively using the Colebrook White resistance equation:

$$\frac{1}{\sqrt{2gDi}} = -\frac{2.0A}{Q} \log_{10} \left[ \frac{k_s}{3.71D} + \frac{2.51\nu}{D\sqrt{2gDi}} \right]$$

Where  $D$  is the pipe diameter,  $A$  is the cross-sectional area of the pipe,  $k_s$  is the hydraulic roughness of the pipe material taken as 0.00025 mm and  $\nu$  is the kinematic viscosity of the fluid equivalent to 1.004E-06. Both coefficients were obtained from the commercially available software used for the design of this system such that a like for like comparison could be made.

$\Delta H_f$  was calculated according to the following equation:

$$\Delta H_f = \frac{KQ^2}{2gA^2}$$

Where  $K$  is the head-loss coefficient for the fitting specifically 0.35 and 0.65 for a 45° and 90° bend respectively obtained from the commercially available software used for the design of this system such that a like for like comparison could be made.

The operational pressure for each pipe length was calculated according to the following equation:

$$P_k = (O_h - N_h) - \sum P_L - \frac{V^2}{2g}$$

Where  $P_k$  is operational pressure,  $O_h$  is outlet head elevation,  $N_h$  is pipe section head elevation,  $P_L$  is the head loss between the outlet and the pipe section and  $V$  is the velocity of the flow within the pipe section.

The pressure reserve was calculated according to the following equation:

$$\text{Pressure Reserve} = R_T - L$$

$$\text{Reserve Capacity (\%)} = 1 - \frac{L}{R_T} \times 100$$

Where  $R_T$  is the height of the outlet minus height of the discharge point and  $L$  is the sum of all losses between the outlet and the discharge point including the discharge loss.

Results from the calculations of the experimental test facility at the design flow rate are summarised in Table 4.33 and detailed in Appendix 2.

**Table 4.33 Comparison between Commercially Available Software and Steady State Theory at the Design Inflow**

Outlet	Design inflow (l/s)	Commercially Available Software Pressure Reserve		Steady State Theory Calculations Pressure Reserve	
		m	%	m	(%)
A	10.00	2.69	27	2.44	25
B	10.00	2.60	26	2.42	25
C	10.00	2.70	27	2.54	27

Steady state hydraulic calculations of the system at the design inflow of 30 l/s estimated at a minimum design operating pressure of -3.07 mH<sub>2</sub>O compared to -3.23 mH<sub>2</sub>O estimated using the commercially available software.

Results from the calculations of the experimental test facility at the design flow rate are summarised in Table 4.34 and detailed in Appendix 2.

**Table 4.34 Comparison between Commercially Available Software and Steady State Theory at the Ultimate Inflow**

Outlet	Ultimate inflow (l/s)	Commercially Available Software Pressure Reserve		Steady State Theory Calculations Pressure Reserve	
		m	%	m	(%)
A	11.74	0.00	0	-0.09	-1
B	11.25	-0.03	0	-0.02	0
C	12.14	0.02	0	0.05	1

Steady state hydraulic calculations of the system at the design inflow of 35.12 l/s estimated at a minimum design operating pressure of -4.55 mH<sub>2</sub>O compared to -4.67 mH<sub>2</sub>O estimated using the commercially available software.

This analysis shows that the commercially available software and calculations performed using steady state hydraulic theory are in agreement. The differences in terms of the pressure reserve and minimum operating pressures at the design and ultimate inflow calculated are minimal. This is due to the commercially available software being based on the Bernoulli equation and Colebrook White resistance equation. The minor differences can be attributed to

the pipe roughness ( $k_s$ ) value which is estimated and affects the energy gradient ( $i$ ) and therefore the head loss due to the pipe walls ( $\Delta H_p$ ) and ultimately the total head loss ( $\Delta H$ ). Differences can also occur due to the head loss coefficient ( $K$ ) which is based on manufacturers published data, available text books and research documents. The head loss coefficient will have a direct effect on the head loss estimated at fittings  $\Delta H_f$ , affecting the total head loss ( $\Delta H$ ).

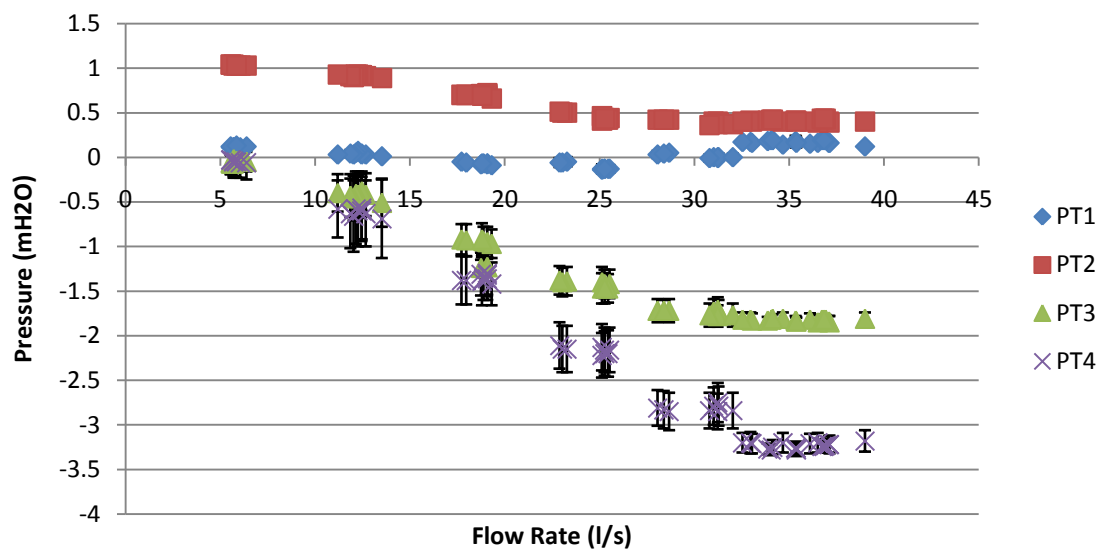
The differences between the measured system pressures and flow rates and those estimated using the commercially available software and steady state hydraulic calculations can be attributed to five reasons:

1. Steady state hydraulic theory is based on the pipes within system being full of water and free of air. During this experimental research, a range of flow conditions were observed during the tests completed at the design flow rate that varied both spatially and temporally summarised in Table 4.35 and discussed in Section 4.2.4. Furthermore, during the tests completed at the ultimate capacity of the system, a homogenous mixture of air and water was observed downstream of Outlet C. The different flow regimes and aerated flow will be a source of error between the measured results and the software predictions;
2. The flow observed within the horizontal carrier pipe contained unquantified amounts of air at the crown of the carrier pipe and as a homogenous mixture that varied temporally and spatially. This will result in a difference to the estimated pipe losses and the friction losses where these flow conditions are present. This error source was also identified by Arthur et. al. (2005);
3. The steady state hydraulic calculations used within the software are based on certain assumptions, specifically the pipe roughness ( $k_s$ ) and the head loss coefficient ( $K$ ). Arthur et al (2005) identified that erroneous  $k_s$  and  $K$  values are a source of error. This experimental research has shown that the interaction of flows between intermediate tail pipes and the horizontal carrier pipe are very complex. Thus, any assumption of head loss within the system at this point is very difficult to estimate and open to error. May and Escarameia (1996) identified that loss coefficient at tee junctions for example, are difficult to predict as head losses can vary considerably depending on the ratios of the flow areas and flow rates and on the junction angle. Furthermore, the variable flow regimes observed during this experimental research meant that the estimation of head losses in these circumstances in particular is very complex and a source of error;
4. Head loss due to fittings within the software are assumed to be local to the fitting. In reality, this head loss may be realised further down the system which would result in a difference between the experimental measurements and software predictions;
5. In practice, any slight displacement or imperfection in the pipe joints will affect the head loss at that fitting and be a source of error. The HDPE pipes within the experimental test facility were jointed using a combination of electro-fusion and electro-welding. May and Escarameia (1996) identified that within electro-fusion the amount of current applied to form the joint needs to be carefully controlled. Too little current and the joint may not seal properly, too much, and the pipes may melt and

deform. Intrusion of melted plastic or deformation of the joint will affect the head loss and the assumed head loss coefficient may no longer be applicable. The electro-welding technique results in a joint with an internal bead. The presence of this bead may have a significant effect on the hydraulic resistance of the pipe (May and Escarameia, 1996).

#### 4.2.3.1 Measured Pressure and Flow Comparison

Figure 4.175 shows a comparison between average system pressure measured by each pressure transducer and standard deviation shown by the error bars for the steady flow tests completed as part of this experimental research.



**Figure 4.175 Plot Comparing System Pressure and Flow Rate**

Average pressure within the horizontal carrier pipe downstream of Outlet A (P1) was measured between  $-0.14 \text{ mH}_2\text{O}$  and  $0.19 \text{ mH}_2\text{O}$ . The greatest negative and positive pressures measured at P1 were recorded during the tests completed at system flow rates of 80% and 120% of the design flow rate respectively. The standard deviation of the pressure measurements varied relatively little with a minimum of  $0.02 \text{ mH}_2\text{O}$  and maximum of  $0.06 \text{ mH}_2\text{O}$ .

Average system pressure downstream of Outlet B was measured at  $1.04 \text{ mH}_2\text{O}$  during the tests completed at 20% of the design flow rate decreasing to  $0.39 \text{ mH}_2\text{O}$  measured during the tests completed in excess of the design flow rate of 30 l/s. Similar to P1, standard deviation across the range of flow tests completed varied relatively little with a minimum of  $0.02 \text{ mH}_2\text{O}$  and a maximum of  $0.07 \text{ mH}_2\text{O}$ .

System pressure at P3 steadily decreased from an average pressure of  $-0.04 \text{ mH}_2\text{O}$  during the tests completed at a system flow rate of 20% of the design flow rate to between  $-1.82 \text{ mH}_2\text{O}$

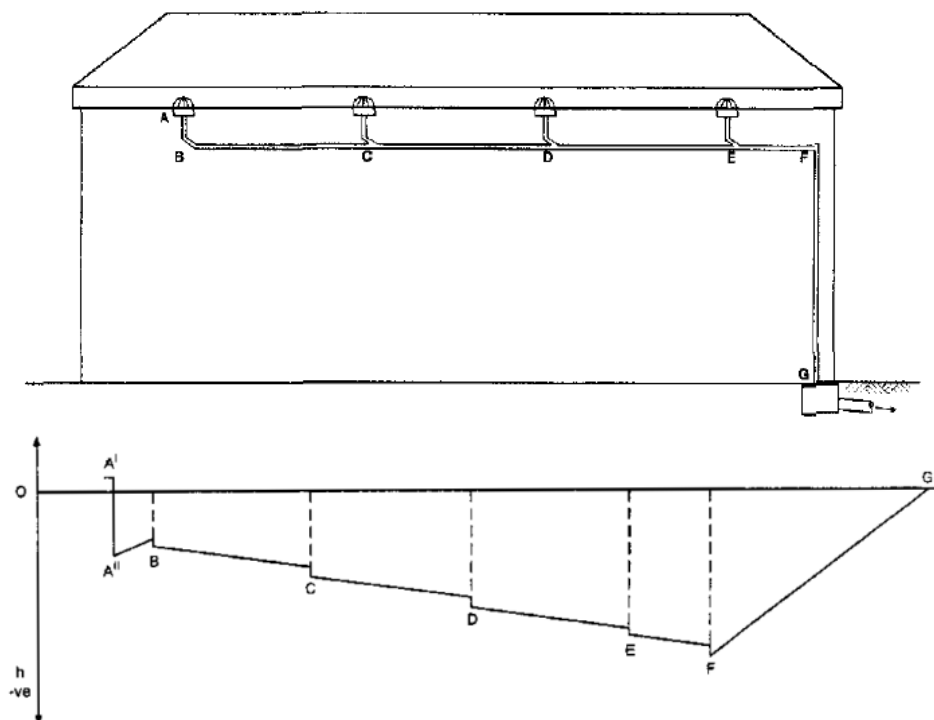


and  $-1.85 \text{ mH}_2\text{O}$  for the tests completed in excess of the design flow rate. Standard deviation was greatest during the flow tests completed at 40% of the design flow rate with a maximum of  $-0.27 \text{ mH}_2\text{O}$  and least during the flow tests completed at 120% of the design flow rate measured at  $0.04 \text{ mH}_2\text{O}$ .

The greatest negative pressure was measured at P4 located at the junction between the horizontal carrier pipe and the vertical downpipe. Average system pressure was measured at  $-0.05 \text{ mH}_2\text{O}$  during the flow tests completed at 20% of the design flow rate and  $-3.28 \text{ mH}_2\text{O}$  during the flow tests completed at 120% of the design flow rate. The greatest standard deviation was recorded during the flow tests completed at 40% of the design flow rate at  $0.44 \text{ mH}_2\text{O}$ . This was the maximum standard deviation measured by any of the pressure transducers throughout the experimental test program. The lowest standard deviation was measured at  $0.06 \text{ mH}_2\text{O}$  during the tests completed at 120% of the design flow rate.

#### 4.2.3.2 Comparison to Previous Research and Practice

These results and analysis are not in agreement with siphonic system theory reported by May (1997). The author provided an example of a siphonic system with four outlets within a common gutter and the associated pressure characteristics. This is shown in Figure 4.176.



**Figure 4.176 Siphonic System Theory Pressure Characteristics (May, 1997)**

The pressure characteristics from this reported example were summarised by May (1997):

1. Positive pressure at the upstream outlet ( $A^1$ ) equal to the depth of water within the gutter;

2. As the flow accelerates into the upstream tailpipe ( $A^{11}$ ), the pressure decreases below atmospheric due to the increase in kinetic energy. Energy is lost within the tailpipe, but this is less than the pressure energy gained due to the change in level. Therefore the pressure at B is less negative than at  $A^{11}$ ;
3. Energy is lost between points B and F due to frictional resistance and losses at bends and junctions;
4. The greatest negative pressure is at the junction between the horizontal carrier pipe section and the top of the vertical pipe (F); and
5. As the flow descends the vertical discharge pipe, the change in potential energy more than offsets the frictional losses and the pressure increases until the flow discharges (G) at atmospheric pressure.

May (1997) reported that these characteristics were typical of a siphonic system with negative pressures and high velocities operating under full-bore conditions. However, he recognised that increases in flow rate at junctions and changes in pipe diameter can produce large local variations in comparison to this profile.

This research has highlighted some significant differences in the pressure profiles for individual outlets. Although pressure became increasingly negative at P3 and P4 during the flow tests completed as part of this experimental research, the average pressure at P2 remained positive irrespective of the system flow rate. This is a new finding that requires further exploration and is in contrast to previous research reported by May. Clearly there are differences in the experimental technique where during this experimental research, pressure around the circumference of the pipe was recorded compared to single point measurements. A series of pressure transducers fitted around the circumference of the horizontal carrier pipe would help further understand pressure variation throughout the cross-sectional area. The location of the pressure measurement point along the horizontal carrier pipe could also make a significant difference to any measured results. Different measurement points along the length of the horizontal carrier pipe would help to understand local pressure variation as a function of flow. From a design perspective this would help to understand the location of greatest negative pressure relative to each outlet, associated standard deviation and whether this changes as a function of the system flow rate.

Previous experimental research completed by Wright et al. (2002) provided a comparison of system pressures within a two outlet experimental test facility to those calculated by a design program used by industry. For the steady flow tests completed where the experimental system was operating in a fully primed state, the system pressures predicted by the design software were up to ~40% lower than those measured experimentally (Wright, 2002). However, to achieve a balanced state within the experimental test facility used by Wright et al. (2002), the inflow into gutter 2 was reported to be significantly higher than into gutter 1 (Wright et al. 2006a). Although the experimental system was significantly different in scale, design and configuration to that used within this experimental research, a similar trend was observed. For the tests completed during this experimental research where the flow through the test facility was in a fully primed state, the commercially available design software used, the

critical operating pressure was between 22.70% and 26.77% lower. Grant et al. (2002) accounted for these differences:

"These discrepancies were considered to be due to inaccuracies in the predicted head losses across fittings and the simplifying assumptions employed within the program."

These findings bring into question the accuracy of the model based design software to estimate system pressure within a multi-outlet siphonic drainage systems at flow rates in excess of the design conditions. In practical terms this could lead to the incorrect specification of pipe sizes and system configuration. Hence, systems may not achieve their optimal performance and be over or under designed.

#### 4.2.4 Observed Flow Regimes within the Multi-Outlet Siphonic Roof Drainage Test Facility

The flow regimes within the horizontal carrier pipe of a siphonic roof drainage system were shown to vary temporally and spatially from the observations made during the steady flow tests during both sub-primed and primed flow conditions completed as part of this experimental study. These observations are summarised in Table 4.35.

**Table 4.35 Observed Flow Regimes**

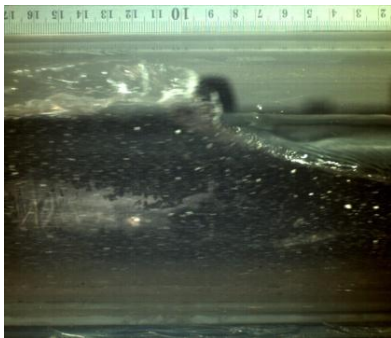
Flow Rate	Camera Position		
	P1	P2	P3
20% of Design	Free surface flow	Free surface flow	Free surface flow
	Free surface flow with entrained air	Plug flow	Free surface flow with entrained air Plug flow Full bore flow
40% of Design	Free surface flow	Free surface flow	Free surface flow
	Plug flow	Plug flow	Aerated two-phase flow
	Full bore flow	Full bore flow	
60% of Design	Free surface flow	Free surface flow	Free surface flow
	Full bore flow	Plug flow	Aerated two-phase flow
		Full bore flow with air pockets	
80% of Design	Free surface flow	Plug flow	Aerated two-phase flow
	Plug flow	Full bore flow with air pockets and entrained air	
	Full bore flow with air pockets		
Design	Free surface flow	Free surface flow	Aerated two-phase flow
	Full bore flow with air pockets	Full bore flow with air pockets	
Ultimate	Full bore flow with air pockets	Full bore flow with air pockets	Aerated two-phase flow
120% of Design	Full bore flow with air pockets	Full bore flow with air pockets	Aerated two-phase flow

This experimental research did not focus on the priming process as the observations and measurements were made when the inflow to the system was steady and established. One of the major findings of this research is that there are several flow regimes that were observed prior to priming. Therefore the time to prime and time to deprime (the time and flow rate through each outlet at the time of priming, siphonic operation and depriming) cannot be estimated in steady flow tests. Hence, the priming mechanism for multi-outlet systems remains unclear and cannot be resolved fully.

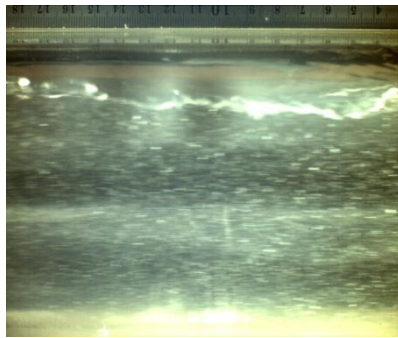
A significant observation made during each of the tests was the interaction of flow within the horizontal carrier pipe and tailpipe junctions. Any existing flow regime within the horizontal carrier pipe was interrupted by the introduction of additional flow and air at the junction

between each of the horizontal carrier pipe and tail pipe junctions. This resulted in very complex and turbulent hydraulic regimes immediately downstream of this point.

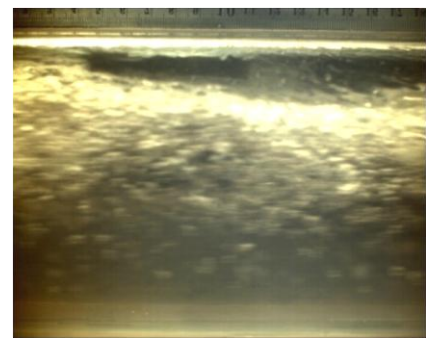
At the calculated design flow rate, flow within the experimental test facility was not fully primed for the duration of the measurement period. Periods of full bore flow were observed throughout these tests, however these conditions were interspersed by periods of free-surface flow. Air within the horizontal carrier pipe was observed downstream of Outlets A (P1), B (P2) and Outlet C (P3). Examples are shown in Figure 4.177, Figure 4.178 and Figure 4.179 respectively.



**Figure 4.177 Image at P1 during Test Reference 13**

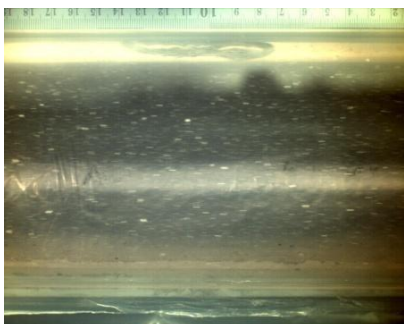


**Figure 4.178 Image at P2 during Test Reference 36**

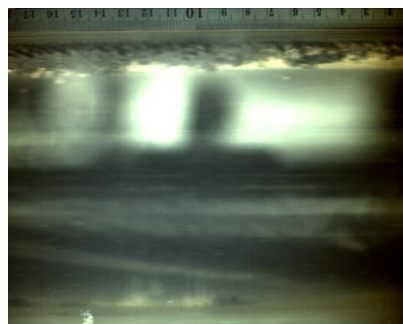


**Figure 4.179 Image at P3 during Test Reference 57**

In contrast, flow conditions at the ultimate flow rate and at 120% of the design flow rate were significantly different. Full bore flow conditions with small pockets of air were observed downstream of Outlet A (P1) and B (P2). Aerated, two phase flow occupying the cross-sectional area of the pipe was observed downstream of Outlet C (P3). Examples of the flow within the horizontal carrier pipe during tests performed at 120% of the design flow rate are shown in Figure 4.180, Figure 4.181 and Figure 4.182.



**Figure 4.180 Image at P1 during Test Reference 19**



**Figure 4.181 Image at P2 during Test Reference 40**

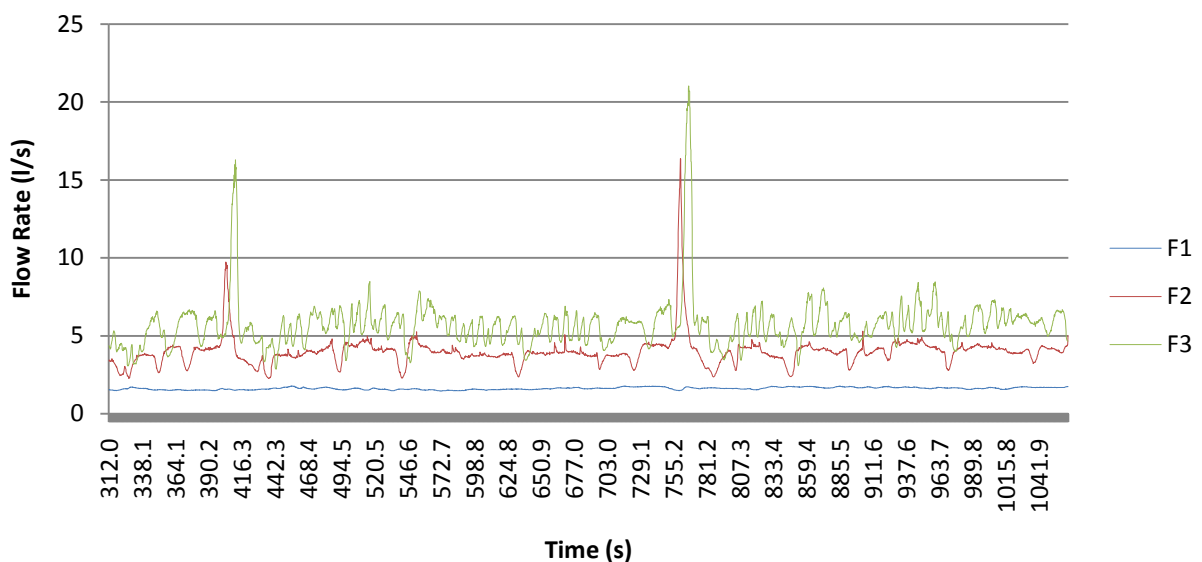


**Figure 4.182 Image at P3 during Test Reference 61**

These results showed that small quantities of air were entrained through Outlets A and B which moved downstream at the local velocity of the flow. A greater degree of air entrainment was observed downstream of Outlet C (P3). This was as a result of the increased flow through Outlet C mixing any air already within the carrier pipe as well as the introduction of air through Outlet C. The result was a homogenous mixture of air and water highlighted in Figure 4.182.

#### 4.2.4.1 Comparison to Previous Research and Practice

These observations support the research reported by Öngören and Materna (2006) and Arthur and Swaffield (2001a) which focussed on a single outlet application with images taken from within a short section of the horizontal carrier pipe. Three distinct flow regimes were observed (free surface flow, unsteady two-phase flow and full bore flow) but they recognised that this did not take into account any temporal or spatial variations within the carrier pipe. Importantly, they concluded that as the flow within the system increased, some components began to flow full while others remained partially filled depending on the volume of air within the system. Such findings support the observations made throughout the range of steady flow tests completed as part of this program of experimental research. A good example is highlighted by reference to the results from Test Reference 22. The measured flow rate through each outlet during this test is shown in Figure 4.183.



**Figure 4.183 Flow Measured through each Outlet during Test Reference 22**

The average flow rate during this test was measured at 5.69 l/s, or 18.97% of the calculated design flow for the experimental system. The time series data shows that during the steady flow test different flow regimes were recorded both spatially and temporally, summarised in Table 4.35 and supported by the series of images throughout Section 4.1.1. Clearly the flow regime within the carrier pipe changes significantly and needs to be taken into account to better understand the performance of siphonic systems.

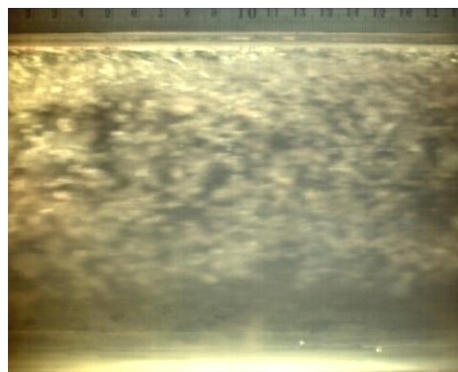
Experimental research completed by Wright et al. (2002) using a two outlet experimental test facility observed that the priming process for the multi-outlet siphonic system was similar to that which occurs with a single outlet system highlighted in Figure 2.8 and described in Section 2.4.1. Wright et al. (2002) reported that:

"The only significant difference is that the increased complexity of the multi-outlet system results in more complex flow conditions,

particularly with respect to the formation and movement of trapped air within the system."

Wright et al. (2002) reported evidence of the formation and downstream movement of "bubbly flow" where air within the downstream tailpipe became entrained by the flow within the horizontal carrier pipe. The observations reported by Wright et al. (2002) were made when the experimental test facility was operating in a fully primed state. However, to achieve a balanced state within the experimental test facility used by Wright et al. (2002), the inflow into gutter 2 was reported to be significantly higher than into gutter 1 (Wright et al. 2006a). Although the test facilities are considerably different, these results are consistent with the observations made during this experimental research at comparable flow regimes highlighted in Figure 4.182. However, for the first time, time series flow rate, pressure and high resolution image data has been collected to enable the relative discharge through each key component within the system to be determined.

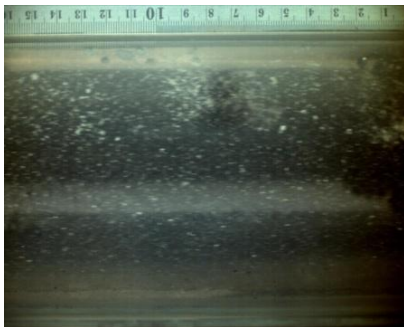
At steady inflows to the system between 15% and 40% of the design criteria, Wright et al (2002) observed that siphonic action could only be sustained for short periods. Flow through the system was dominated by cyclical periods of positive and negative pressures. This is consistent with the observations made during the steady flow tests completed at 20% and 40% of the system design during this experimental research. Cyclical pressure was observed particularly at PT2, PT3 and PT4. The pressure at PT1 was less variable throughout the measurement period. For the first time, the corresponding time series flow rate has been measured combined with a series of high resolution images. These measurements show the cyclical nature of the flow regime particularly at F2 and F3. Although similar flow regimes were observed at F1, the effect is much less pronounced. During the tests completed at 40% of the system design, periods of full bore flow were observed at P1 and P2 but not at P3. The flow regimes within the carrier pipe were observed to be cyclical, however, the quantity of air already within the siphonic system as well as additional air introduced through Outlet C meant that full bore flow conditions at P3 were not achieved. Short periods of heavily aerated flow were observed where the turbulence within the carrier pipe entrained the air within the system into a homogenous mixture highlighted in Figure 4.184



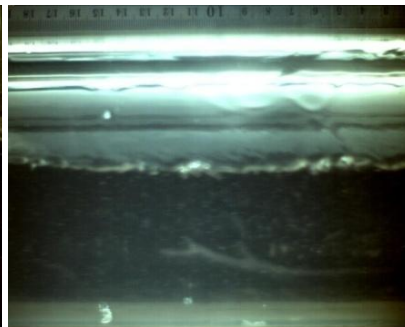
**Figure 4.184 Aerated Flow Observed at P3 during a Test Completed at 40% of the Design Capacity (Test Reference 46)**

This is in contrast to the observations made by Grant et al. (2002) which can be explained by the difference in the two experimental systems in terms of the number of outlets.

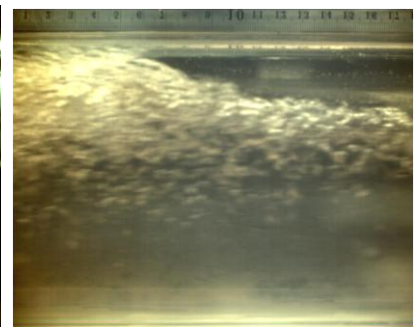
At flow tests completed between 40% and 60% of the design criteria, Grant et al. (2002) observed that the inflow created oscillating negative pressure greater than that measured when the system was fully primed. Continuous siphonic action was reported with large amounts of air entrained resulting in lower flow rates and higher pressures than those measured when the system was fully primed. A similar oscillating pressure profile was measured at the comparable flow tests during this experimental research. Pressure at P1, P3 and P4 were all negative, however, pressure at P2 remained positive throughout the measurement period. This difference is due to the experimental configurations, positioning of the pressure transducers and method of pressure measurement. In contrast to Wright et al. (2002), continuous siphonic action was not observed at the comparable flow tests during this experimental research. Instead, a number of flow regimes were measured and reported (Table 4.35) including free surface flow, full-bore flow and aerated two-phase flow. Examples are shown in Figure 4.185, Figure 4.186 and Figure 4.187.



**Figure 4.185 Full-bore Flow at P1 at 60% of the Design Flow Rate**



**Figure 4.186 Free Surface Flow at P2 at 60% of the Design Flow Rate**



**Figure 4.187 Aerated Two-Phase Flow at P3 at 60% of the Design Flow Rate**

For the first time, this experimental research has quantified the measurement of flow through each outlet with corresponding time series pressure and image data. The measured flow rate reported in Section 4.1.3 demonstrates the variability in flow rate, particularly downstream of Outlets B and C for the tests completed with a steady inflow at 60% of the design flow rate (18 l/s).

Similar to the observations made between 40% and 60% of the design criteria inflow, Wright et al. (2002) reported similar results for the tests completed at system inflows above 60% of the design criteria. A number of flow regimes were observed throughout the tests completed at steady inflow rates above 60% (i.e. 80%) during this experimental research including free surface flow, plug flow, full bore flow and aerated two-phase flow. An oscillating pressure regime was measured at levels lower than steady flow tests completed at 40% and 60% of the design capacity although greater than those measured at the design and ultimate capacity.

Arthur and Swaffield (2001a) commented that "if a system is suitably sized, the momentum of the water removes the air present in the pipes more quickly than it can enter through the



outlets. This causes the pipes to fill and flow full with a bubbly two phase mixture". This experimental research clearly identified the existence of such air flows and hence supports these observations confirmed by the results of this experimental study summarised in Table 4.35. Furthermore, the maximum system flow tests completed at 120% of the design flow rate was not sufficient to create a water depth in the gutter that completely eliminated any air entering the system prior to gutter overtopping.

Results from static, independent, water depth measurements made within the gutter during the feasibility tests ranged from 61.3mm to 79.4mm for the flow tests with a steady inflow of 36 l/s equivalent to 120% of the design. This depth of water within the gutter meant that air could be entrained into the pipework through the outlet. As the negative pressure was greatest downstream of Outlet C, air was more readily entrained through this outlet. A narrower gutter would increase the relative depth of water within the gutter for the same inflow rates and hence reduce the quantity of air that could be entrained within the siphonic system. This is confirmed by Bramhall (2004):

"The gutter sole width was shown to have an influence upon the water depth required around an outlet for a given flow rate. Flow depths were observed to increase as the gutter sole width was reduced."

The results from this experimental research are specific to the three outlet experimental test facility shown in Figure 3.2 and tail pipe configurations highlighted in Figure 3.10 to Figure 3.15. Previous experimental research using a multi-outlet test facility (Bramhall, 2004) identified that the position of an outlet within a gutter has no detrimental effect upon the performance of the siphonic system, providing all the design parameters are met. Bramhall (2004) stated that:

"The performance of the siphonic system is independent of the position of the outlets within the system. What is important is the position of the outlet and the relationship between the resultant depth of flow in the gutter."

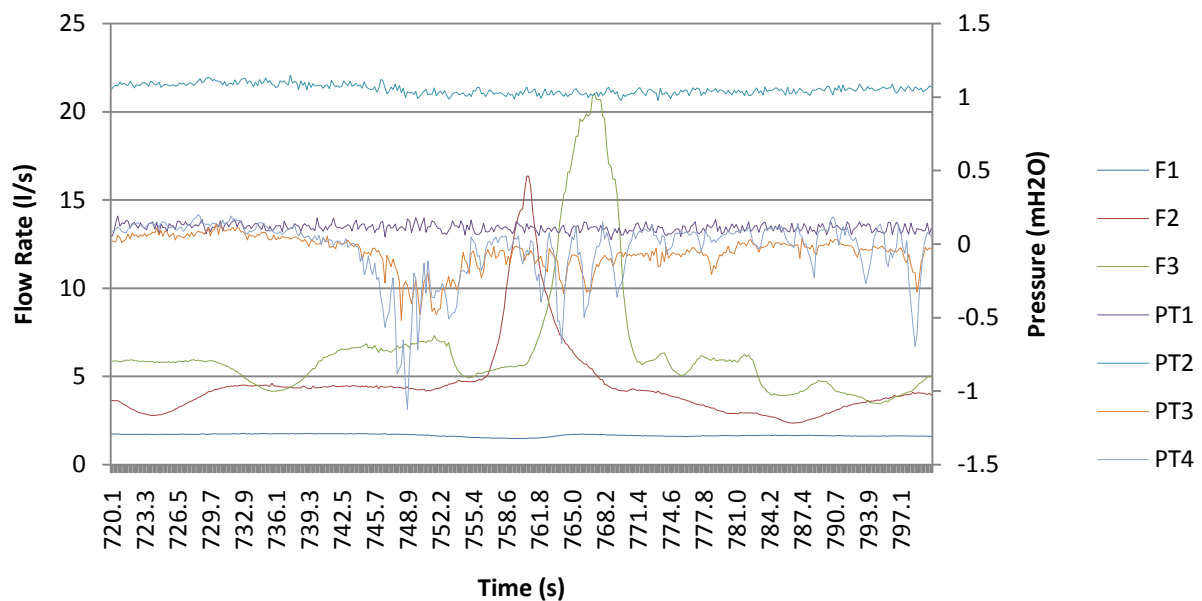
The tail pipe configurations and horizontal carrier pipe dimensions were determined using commercially available design software. All of the required design checks were passed for the system in terms of minimum velocities, critical operating pressure and balance range between the outlets at the design and ultimate operating capacity.

The results and observations from this experimental research are all relative as one system configuration was used throughout the feasibility tests and full test program. Changing key network components would have an effect on the flow and associated air entrainment within the system affecting the relative proportionality and priming mechanism, however, this cannot be quantified.

#### 4.2.5 Observed Air Entrainment During Steady Flow Tests within the Multi-Outlet Siphonic Roof Drainage Test Facility

This experimental research study successfully demonstrated the relationship between localised system pressure, the relative flow through each component outlet of the system and a visual representation of air entrainment along the length of the horizontal carrier pipe using sophisticated high speed image apparatus and methodology. This relationship was investigated for a series of steady tests for flow conditions below, at and above the design threshold.

Previous researchers, Lucke (2009) identified that the relationship between system pressure and air entrainment within siphonic roof drainage was not well understood. Arthur and Swaffield (1999) recognised that any sudden changes in the proportion of air in the inflow resulted in a sudden change in the local pressure that was subsequently transmitted throughout the system at the propagation velocity. This phenomenon was also observed and reported by Lucke et al. (2014). The experimental research reported in this thesis has confirmed, for the first time, that such pressure changes may be observed and a typical result is demonstrated in the time series data shown in Figure 4.188 which highlights a sudden pressure drop recorded by PT3 and PT4 and the subsequent response in the system flow rate recorded by F2 and F3.



**Figure 4.188 Time Series Data during Test Reference 22**

The relationship between system pressure and flow rate as a pressure wave propagates through the horizontal carrier pipe may be clearly seen in Figure 4.160. These results suggest that full bore conditions have occurred at PT3 and PT4 indicated by the negative pressure spike shown after 748 seconds. This negative pressure resulted in the changes to the flow through Outlets B and C measured by the flourometers F2 and F3. This change in pressure

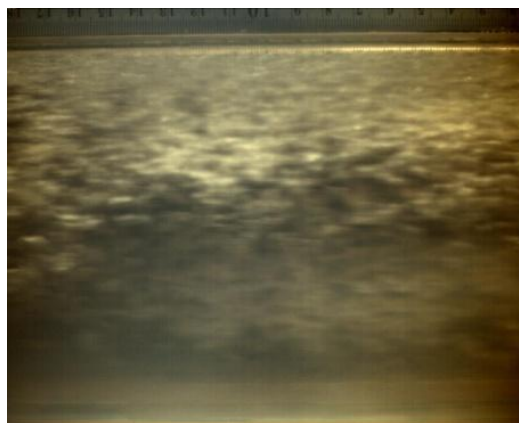
may be observed to have little to no effect on the flowmeter measurement of the flow through the most upstream outlet (Outlet A).

The time series data and corresponding images presented throughout this chapter for the range of steady flow tests, have provided the data to establish a much greater understanding of the interaction between the flow rate through each outlet and the pressure fluctuations that cause such changes. This is shown in the tabulated summary of results set out in Table 4.2 to Table 4.15 and the detailed analysis reported in Section 4.1.1 to 4.1.7. This new data has provided a much greater understanding of the interaction between these variables which needs to be taken into account at the time of system design.

In summary therefore, this experimental research has, for the first time, demonstrated the relationship between localised system pressure, the relative flow through each component outlet of the system and a visual representation of air entrainment along the length of the horizontal carrier pipe. Arthur et al. (2005) recognised that to estimate the air content in turbulent two-phase flows was complex, but clearly, the results of this experimental research have demonstrated that, with further analysis, the image data collected would enable the level of air entrainment to be quantified. This is recommended in the future work chapter of this thesis.

#### 4.2.5.1 Comparison to Previous Research and Practice

As part of the study, a comparison was made with the results reported in this thesis by those completed by other researchers. Experimental research by May and Escarameia (1996) reported that air concentration was no greater than 1% at maximum capacity. Measurements were taken using a void-fraction meter and these results were significantly less than those reported by Arthur et al (2005) and Arthur and Swaffield (2001) who claimed that values of air entrainment may be as high as 10%. In this study, the problems associated with air entrainment did not form part of the objectives and hence was not quantified as part of this experimental research. However, the image data collected at P3 for tests completed greater than the design flow rate showed evidence of entrained air. An example is shown in Figure 4.189.



**Figure 4.189 Air Entrainment within the Horizontal Carrier Pipe at P3**

Although, it can only be estimated, air entrainment in this example would appear to be greater than 10% and hence the results from this study contrast with the results reported by May and Escarameia (1996), Arthur et al (2005) and Arthur and Swaffield (2001a).

May and Escarameia (1996) claimed that the small amounts of air were generated by the turbulent inflow of water and from air coming out of solution due to pressure reductions along the system. The series of steady tests completed as part of this experimental research has demonstrated that flow rate, pressure and the quantity of air within the horizontal carrier pipe varied temporally and spatially, even when the system was operating above the design capacity. What is clear is that the quantity of air entrainment is extremely difficult to both accurately measure and model as such entrainment varied as a function of the flow conditions and configuration of the pipework. May and Escarameia (1996) and May (1997) recognised that the behaviour of two-phase flows is complex, very difficult to predict and identify the following important factors:

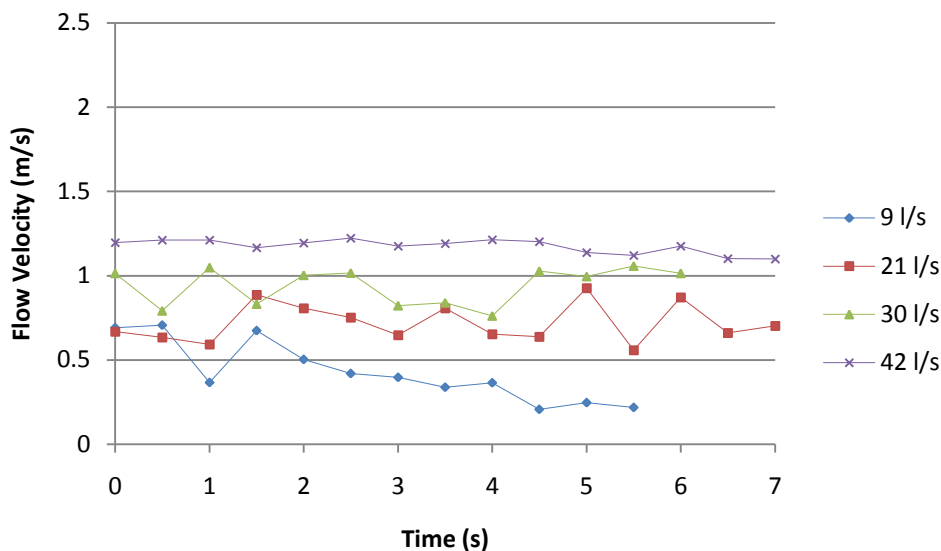
- expansion of the air bubbles as the flow travels from regions of high pressure to low pressure in siphonic systems;
- effect of the air on the frictional resistance of the pipes and fittings;
- flow velocities and turbulence levels needed to prevent the air bubbles from coalescing to form distinct air and water phases.

Arthur and Swaffield (2001a) identified that even a small amount of air within the inflow can substantially influence the local transient propagation velocity discussed in Section 2.4.2.7. Multi-phase and two-phase flows specifically air and water beyond siphonic roof drainage is an area that has been much researched and reported in several studies. Arthur and Swaffield (2001a) reported that two-phase friction models are available but these do require accurate estimation of the level of air content. As reported by May and Escarameia (1996) and May (1997) this is incredibly complex and very difficult to predict. This experimental research has demonstrated that a number of significant flow regimes were observed, each with different time-variable air entrainment processes. This experimental research is the most comprehensive study to date, however, it has not been possible to be able to accurately quantify the error of the measurement of multi-phase flows using the method of fluorometry. Hence, it is recommended that further research, both modelling and experimental, is undertaken to investigate this issue.

#### 4.2.6 Measured Flow Velocity During Steady Flow Tests within the Multi-Outlet Siphonic Roof Drainage Test Facility

A sophisticated system of measurement was developed and refined to record the transverse velocity of the flow within the horizontal carrier pipe. The methodology and apparatus used during this study are described in Section 3.6 of this thesis. This is a unique approach of measuring velocity in siphonic systems and provides a novel method of measurement without interrupting the flow field.

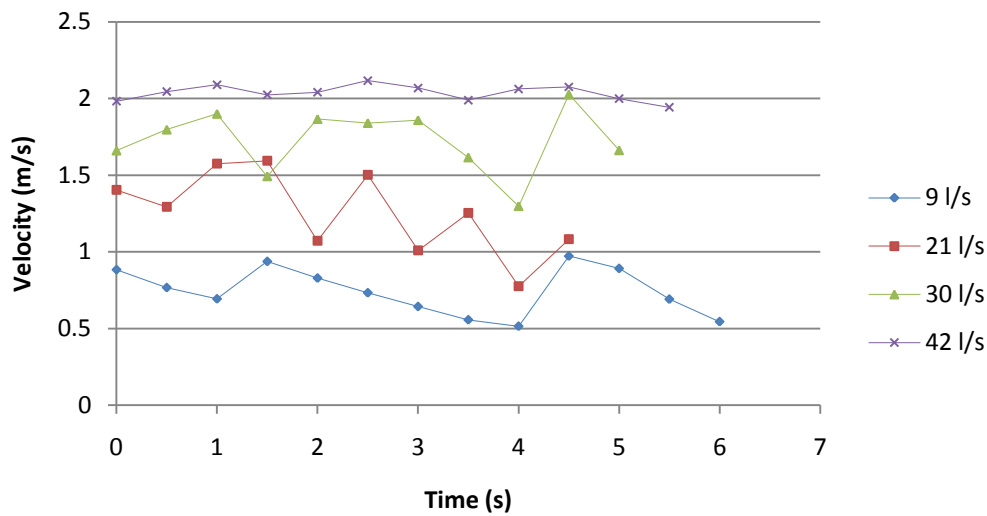
Particle Image Velocimetry (PIV) analysis described in Section 3.6.1 was completed for the series of feasibility tests undertaken at steady flow rates of 30% (9 l/s), 70% (21 l/s), 100% (30 l/s) and 140% (42 l/s) of the calculated design system capacity at positions P1 and P2. Figure 4.190 provides an example of flow velocity results within the horizontal carrier pipe based on the PIV analysis of the images collected using the high speed camera positioned at P1 downstream of Outlet A.



**Figure 4.190 Flow Velocity Results for Feasibility Tests Downstream of Outlet A (P1)**

A clear difference can be seen in terms of the flow velocity profile for each of the tests reported. The measured velocity at system flow rates at and below the design threshold of 30 l/s demonstrated a much more variable time-series profile in comparison to the results measured at a system flow rate of 140% of the system design. This would suggest that there are considerable fluctuations in the velocity profile of the flow within the carrier pipe during sub-primed conditions and at the system design. It is not until the system flow rate exceeded the design threshold that the velocity field tended to a uniform state. However, even at flow conditions significantly in excess of the system design, variability in the flow velocity was measured. This is a new finding that requires further exploration.

Figure 4.191 shows the flow velocity results based on the PIV analysis of the images collected with the camera positioned downstream of Outlet B (P2).



**Figure 4.191 Flow Velocity Results for Feasibility Tests Downstream of Outlet B (P2)**

Similar to the results reported in Figure 4.190, the results presented in Figure 4.191 show that fully primed flow conditions were evident during the test completed at 140% of the design capacity (42 l/s). However, even during these steady flow tests, the measured flow velocity was not uniform and a series of pulses were observed despite the full bore flow conditions.

The flow velocity measured during the test completed at 30% of the design capacity (9 l/s) demonstrated a profile indicative of pulsed or plug flow. This was not observed at P1 (Figure 4.190) during the same steady flow conditions. These results support the findings reported in Section 4.2.4 and summarised in Table 4.35 where different flow regimes were evident along the length of the horizontal carrier pipe during the same steady flow tests.

This methodology provides a non-intrusive method of being able to measure velocity of the flow within the horizontal carrier pipe of a siphonic system. These results support the key findings from this experimental research that within a multi-outlet siphonic system, different flow regimes occur along the length of the horizontal carrier pipe during steady flow tests.

Further analysis of the image data using PIV with the corresponding time series flow rate and pressure measurements would further the understanding of the relative proportion of air within the system based on the continuity equation. This is discussed in further detail in Section 4.3.7.

Clearly, this research has shown that there are differences in the measured velocity during steady flow tests completed below, at and above the design threshold. Previous experimental research using alternative methods of measuring and estimating flow rate and velocity, for example Lucke et al. (2014) discussed in Sections 4.2.1.1 and 4.2.2.1, may not be able to

accurately determine these conditions at the required resolution and further work is required to address this shortfall in knowledge.

### **4.3 Practical Implications of the Research on Design Practice**

Section 2.4.2 of the Literature Review of this thesis provided a critical appraisal of current design practice from the perspective of accepted design standards and relevant experimental research. This was presented in the context of seven key areas essential to the design of siphonic roof drainage systems (Arthur and Swaffield 2001a; Arthur and Wright 2007; BSI 2000; BSI 2007):

1. Hydraulic design
2. Design criteria
3. System balancing
4. Minimum flow velocities
5. Speed of priming
6. Minimum allowable pressures
7. Air within siphonic systems

Key findings from this experimental study are discussed in the following section of this chapter in relation to these key design areas with recommendations for further research.

#### **4.3.1 Hydraulic Design**

Siphonic system design is based on steady-state hydraulic relationships as each system is designed to accommodate a specified storm or system flow rate. This experimental research demonstrated that at the design system flow rate of 30 l/s, a fully primed system was not achieved and a range of flow regimes along the length of the carrier pipe were observed (summarised in Table 4.35). Significantly, Arthur et al. (2005) identified that these design methods may not be suitable for system flow rates below the design criteria or with time varying rainfall intensity. This research has demonstrated that for steady flow tests below the system design, a range of flow conditions were observed and measured along the length of the horizontal carrier pipe and flow proportionality through the gutter outlets was not equal and varied as a function of the overall system flow rate. In this study percentage changes of 5.40% (Outlet A), 6.70% (Outlet B) and 2.53% were recorded over the range of flow rates.

A comparison was made between the measured system flow rates and pressures with those computed using commercially available software based on the Bernoulli Energy Equation and Colebrook White Equation. It was observed that the measured system flow rates and pressure differed to the calculated values from the model based design software at significant levels at flow rates in excess of the design criteria. In practical terms this could lead to the incorrect specification of pipe sizes and system configuration. Hence, siphonic systems designed using software based on steady-state hydraulic relationships may not achieve their optimal performance and be over or under designed.



### 4.3.2 Design Criteria

Arthur and Wright (2007) identified that increasing the design capacity of a system by 10% corresponded to a subsequent increase of 20% to 40% in the design rainfall return period. This may mean that the system may not operate in a fully primed state.

Experimental research completed by Lucke (2009) recommended using a safety factor of 1.2 for systems designed using Bernoulli's energy equation and to account for losses derived by the effects of air entrainment, to multiply the calculated losses by 1.2. This research has demonstrated that air entrainment was present even at system flow rates completed at 120% of the system design flow rate and varied temporally and spatially along the length of the horizontal carrier pipe during steady flow tests. Hence, it is clear that air entrainment is a significant factor to influence system performance and enhance siphonic system design criteria within multi-outlet siphonic roof drainage systems. A blanket factor to take account of these changes, as proposed by Lucke (2009), does not reflect the observations in this thesis. Further experimental research is required to confirm whether a standard safety factor is applicable for both sub-prime and primed siphonic action. This investigation would require a detailed experimental study over a range of flow conditions for different system configurations.

### 4.3.3 System Balancing

Previous experimental research and design practice, for example May (1997), Slater et al. (1999), Sommerhein (1999), ASPE (2006), Ross (2006) and Lucke et al. (2007) recognised the importance of system balancing within siphonic system design. However, the design of any siphonic system will have a number of restrictions which consequently affect balancing (ASPE 2006):

- Pipes sizes are only available in nominal diameters;
- The type and placement of fittings are limited;
- The number of iterations to the energy loss calculations are excessive and unreasonable to achieve perfect balance;
- Flow variation caused by random and transient air entrainment.

Arthur and Wright (2007) suggested a value of  $\pm 2.5\%$  is an acceptable level of variation within the design of a siphonic system, however, the ASPE (2006) recommended a maximum imbalance of 0.5m or 10% of the available head. This experimental research has measured quantitatively for the first time through robust, repeatable methodologies, that flow proportionality within a multi-outlet siphonic roof drainage system is not equal. Furthermore, proportionality varied as a function of the overall system flow rate and the imbalance within the experimental test facility during low flow rates was as much as 11.46%. The relative difference in flow proportionality reduced as the system flow rate increased to system flow rates in excess of the design. This experimental research therefore suggests that if system balancing is achieved for the system design, this is not consistent for flow rates less than the design conditions. Further experimental research is therefore required to investigate system

balancing for a range of outlet and pipework configurations. The experimental techniques and methodology developed and enhanced during this experimental research are transferable and appropriate to this proposed research.

#### **4.3.4 Minimum Flow Velocities**

May and Escarameia (1996) identified that where the flow velocity was low within the horizontal carrier pipe, air will not be prevented from rising to form air pockets along the pipe soffit. There were numerous examples during this experimental research where air pockets were observed at the pipe soffit along the length of the horizontal carrier pipe. Results and observations from the range of steady flow tests demonstrated that flow rate within the horizontal carrier pipe varied spatially and temporally. Flow conditions also varied during the experimental programme of tests and free surface flow, plug flow, flow with air pockets at the soffit and entrained air were all observed. Any suggested minimum velocities used to inform design would need to take into consideration that flow rates below the system design are not idealised and are time varying.

Further experimental research is required to investigate whether the equation proposed by Volkart (1982) and the Froude number suggested by Arthur and Wright (2007) are appropriate for both sub-primed and primed siphonic action, as described in Section 2.4.2.4. Again the experimental techniques and methodologies developed during this experimental research would be appropriate for such a study.

#### **4.3.5 Speed of Priming**

Previously reported research (May 1997; Sommerhein 1999; Arthur and Swaffield 2001a; Arthur and Wright 2007; Bramhall and Wearing 2008) recognised that factors controlling the speed of priming and rate of air entrainment are complex and no analytical method is available to determine how long or even if a system will prime. Observations and measurements made during this experimental programme have demonstrated and quantified the complexity of flows within the horizontal carrier pipe of a siphonic test facility during both sub-prime and primed siphonic action.

Current design practice assumes that tail pipes and carrier pipes are empty prior to priming. In practice this is not the case and the drainage system is likely to be partially filled and therefore part-primed at the onset of a rainfall event. Furthermore, the current British Standard, BS 8490:2007 'Guide to Siphonic Roof Drainage Systems', assumes that tail pipes should prime instantly and fill the system within 60 seconds. However, since siphonic systems within the UK are designed for two minute storm events, May and Escarameia (1996) identify that it is not feasible to estimate the speed to priming due to the unavailability of an appropriate quantitative method of prediction. Therefore in practice, siphonic systems are typically designed with tail pipes that are oversized to meet this specification.

The methodologies and experimental techniques developed during this experimental research study could be applied and used to examine the speed of priming. This would involve a series of time varying flow tests within a multi-outlet siphonic roof drainage test facility. This experimental research would provide much needed data and be used to inform and update current British Standards and be incorporated within existing design software and models. Tail pipe configurations could then be sized more accurately improving the efficiency and design of future siphonic roof drainage systems as well as providing safety and security against failure.

#### **4.3.6 Minimum Allowable Pressures**

Existing British and EU standards recommend a minimum pressure of  $-7.8\text{m H}_2\text{O}$  (BSI 2000; BSI 2007). Current methods used to estimate pressures do not consider localised turbulence (Arthur and Wright 2007) and system pressures can vary based on (Arthur and Swaffield 2001a):

- Interaction with the underground system;
- Partial or total blockage of an outlet;
- Changes in pipework configuration from the original design during installation;
- Volumes of air entering the system.

This experimental research has provided a significant quantified set of continuous pressure data and corresponding system flow rate data. The pressure along the length of the horizontal carrier pipe was measured at four locations so localised turbulence other than in the immediate vicinity of the pressure transducer cannot be accounted for. However, variations in system pressure due to the interaction with the underground system and volumes of air observed throughout the horizontal carrier pipe were measured. The results demonstrated that pressure fluctuations are greatest at low flow rates which decreased at system flow rates at and above the system design of 30 l/s. The same measurement techniques could also be applied to investigate the effect of partial and total blockages within an outlet and changes in pipework configuration. This understanding could be applied and used to inform system and outlet design.

Cavitation was not part of the scope of this experimental research study. Comprehensive experimental research has been completed at the University of South Australia, described in Section 2.3.5.3.1. May and Escarameia (1996) identified four factors that can cause an increase in the cavitation index:

- An increase in flow velocity;
- An increase in temperature;
- A reduction in the mean static pressure;
- A reduction in the value of atmospheric pressure.

The methods of continuous flow rate and pressure measurement developed and enhanced during this experimental study could be applied to further experimental research to investigate and quantify the effect of these factors.

#### 4.3.7 Air within Siphonic Systems

Existing siphonic roof drainage design is completed on the assumption that no air is present when the system is fully primed and operating at full bore. However, air can be easily entrained into the system via three identified mechanisms (Arthur and Swaffield 2001a; Arthur and Swaffield 2001b):

1. Air already within the system prior to any inflow;
2. Air held within the inflowing rainwater;
3. Air entrained into the system through the siphonic outlet.

The steady flow energy equation used in the design of siphonic systems is dependent on the density of the inflow. Any air within the system will cause a change in local pressure which may be transmitted through the whole system causing a reduction in system capacity (Arthur and Swaffield 2001a). Quantification of the volume of air within siphonic systems has been estimated by previous research, for example, May and Escarameia (1996) and Arthur and Swaffield (1999), and is regarded as very difficult to accurately measure. Observations and corresponding time-series data from this experimental research has demonstrated the temporal and spatial variability of air entrainment throughout the horizontal carrier pipe for the range of steady flow tests.

To improve current design practice, more detailed knowledge is required specific to the volume of air within siphonic roof drainage systems and the associated effect of system flow rate and pipework configuration.

During the 63 steady flow tests completed during this experimental research, continuous time-series data was collected along the length of the horizontal carrier pipe specifically pressure, flow rate measured using flourometry and images of the flow using high speed image velocimetry.

Therefore for each steady flow test, discharge ( $Q$ ) has been measured. Calculation of the corresponding flow velocity using PIV based on the associated images collected using high speed image velocimetry would provide  $V$ . Based on the continuity equation:

$$\frac{Q}{V} = A_f$$

Where  $Q$  is the discharge,  $V$  is the flow velocity and  $A_f$  is the cross-sectional area of flow within the pipe.

Hence:

$$A_a = A_p - A_f$$

Where  $A_a$  is the cross-sectional area of air entrainment and  $A_p$  is the cross-sectional area of the pipe.

This method of estimating the amount of air entrainment continuously is based on the robust and repeatable methods of measurement, developed and enhanced through this experimental research study.

Further work is therefore recommended to undertake PIV analysis of the series of images from the steady flow tests to examine and test this proposed method. The corresponding time-series pressure data would complement this analysis further to develop a much needed data set and provide a detailed understanding of the interaction between flow rate, flow velocity, system pressure and volume of air entrainment within a multi-outlet siphonic roof drainage system.

#### **4.4 Results and Discussion Close**

Chapter 4 of this thesis presented a summary of the results, followed by detailed analysis of the series of 63 steady flow tests. These results were then critically reviewed in the context of previous, relevant experiential research and presented as key findings and discussion. Section 4.3 of this chapter set out the practical implications of this experimental research in the context of current design practice from the perspective of accepted design standards and relevant experimental research. The following section of this thesis presents the conclusions followed by recommendations for further work. A succinct, summary of these conclusions is presented in Chapter 6 of this thesis.

## 5 Conclusions and Recommendations for Further Research

The work presented in this thesis describes a comprehensive experimental programme of research to increase the understanding of the hydraulic performance of multi-outlet siphonic roof drainage systems with three outlets in order to deliver a step change and better understanding of the performance of such systems and how they may be better designed.

The following objectives were investigated:

- Enhance the existing full-scale siphonic roof drainage experimental test facility at the University of Sheffield using commercially available design software based on steady-state hydraulic theory.
- Design, develop and refine experimental techniques specifically:
  - The measurement of system pressure;
  - A non-intrusive method of flow rate measurement through each outlet using flourometry;
  - Image data capture of the flow using high speed image velocimetry;
  - A non-intrusive method of flow velocity measurement using particle image velocimetry.
- Complete a series of performance evaluations under steady flow conditions below, at, and above the system design capacity to enable the simultaneous and high-resolution measurement of system pressure, flow rate and collation of image data within the horizontal carrier pipe.
- Quantify the proportionality of flow through each outlet during steady flow tests below, at, and above the system design capacity.
- Classify the flow regimes within the horizontal carrier pipe during steady flow tests below, at, and above the system design capacity.
- Examine the performance of the experimental system within the context of key network components and the interaction between multiple outlets.
- Apply the products of the research and compare with commercially available design software, steady state hydraulic theory, previously reported experimental research, methodologies and appropriate tools to predict siphonic system performance.
- Make recommendations to enhance the research into design practice.

Conclusions are presented in the following section of this thesis corresponding to the key findings of this experimental research. Recommendations for further research are included in Section 5.7 corresponding to the practical implications of this study on current design practice and system performance.

## **5.1 Flow Measurement within a Multi-Outlet Siphonic Roof Drainage System**

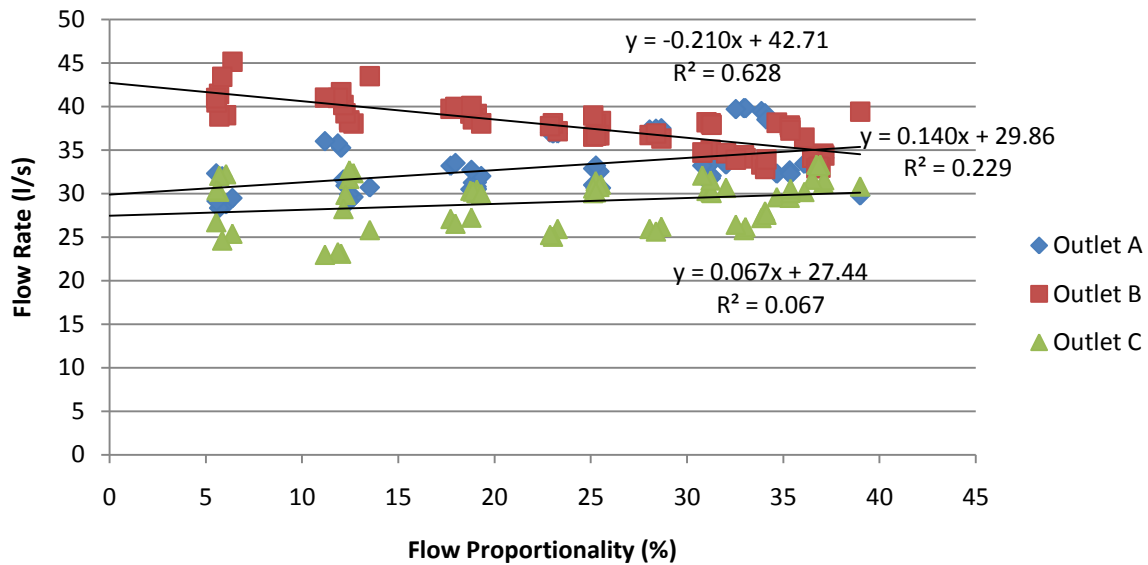
The application of flowometry within the experimental system and methodology refined during this research has for the first time, provided a repeatable, robust and reliable approach to simultaneously measure the relative proportion and components of flow within a multi-outlet siphonic roof drainage system. A range of steady flow tests were used in the study including sub-primed and primed siphonic conditions. The average difference between the flow measured by the flowmeter positioned downstream of Outlet C (termed F3) and the calibrated pumped inflow over the series of steady flow tests was 1.01%. This confirms the accuracy of the methodology for flow rates below, at, and above the design criteria.

Significantly, this non-intrusive methodology enabled the continuous measurement of flow through each outlet without affecting the hydraulic performance or generating additional, uncalculated losses. It is concluded therefore, that the provision of such a measurement system represents a novel and original way in which to measure the flow components in a multi-outlet siphonic roof drainage system.



## 5.2 Flow Proportionality

The research has shown that the flow rate through the multi-outlet test facility was not equal and flow proportionality through each outlet varied as a function of the magnitude of the total system flow rate shown in Figure 5.1.



**Figure 5.1 Flow Proportionality as a Function of the System Flow Rate**

This highlights that current design criteria are fundamentally flawed as the assumption is made that this is the case. In this study percentage changes of 5.40% (Outlet A), 6.70% (Outlet B) and 2.53% were recorded, as summarised in Table 5.1.

**Table 5.1 Average Flow Proportionality Relative to System Flow Rate**

Flow Rate Relative to System Design (%)	Average Flow Proportionality (%)		
	Outlet A	Outlet B	Outlet C
20	29.87	41.33	28.80
40	32.09	40.13	27.77
60	31.75	39.14	29.11
80	33.51	37.57	28.92
Design	34.18	36.44	29.18
Ultimate	35.27	35.47	29.26
120	35.07	34.63	30.30

### 5.3 Measured and Calculated System Flow Rate and Pressure

Measured system flow rates and pressure using the experimental test facility at the University of Sheffield differed to the calculated values from the model based design software.

A comparison between the measured minimum system pressure, the mean pressure minus 3 standard deviations and the calculated system pressure of -3.23 mH<sub>2</sub>O for the tests completed at  $\pm 5\%$  of the design flow rate is shown in Table 5.2.

**Table 5.2 Comparison Between Measured and Calculated System Pressure at the Design Flow Rate**

Test	Measured Flow Rate (l/s)	Minimum Measured System Pressure (mH <sub>2</sub> O)	Difference to Calculated System Pressure (%)	Mean Pressure -3 $\sigma$ (mH <sub>2</sub> O)	Difference to Calculated System Pressure (%)
13	31.02	-3.51	8.67	-3.42	5.88
14	31.24	-3.38	4.64	-3.41	5.57
15	31.28	-3.45	6.81	-3.45	6.81
34	31.23	-3.52	8.98	-3.45	6.81
35	30.80	-3.46	7.12	-3.44	6.50
56	28.67	-3.46	7.12	-3.44	6.50

A comparison between the measured minimum system pressure, the mean pressure minus 3 standard deviations and the calculated system pressure of -4.67 mH<sub>2</sub>O for the tests completed at  $\pm 5\%$  of the ultimate flow rate is shown in Table 5.3.

**Table 5.3 Comparison Between Measured and Calculated System Pressure at the Ultimate Flow Rate**

Test	Measured Flow Rate (l/s)	Minimum Measured System Pressure (mH <sub>2</sub> O)	Difference to Calculated System Pressure (%)	Mean Pressure -3 $\sigma$ (mH <sub>2</sub> O)	Difference to Calculated System Pressure (%)
18	36.51	-3.58	23.34	-3.53	24.41
37	36.10	-3.61	22.70	-3.54	24.20
38	34.67	-3.57	23.55	-3.53	24.41
20	36.73	-3.42	26.77	-3.45	26.12
21	36.84	-3.46	25.91	-3.42	26.77
40	35.34	-3.45	26.12	-3.47	25.70
41	35.37	-3.44	26.34	-3.47	25.70
42	35.38	-3.48	25.48	-3.49	25.27
61	33.87	-3.49	25.27	-3.45	26.12
62	34.06	-3.43	26.55	-3.46	25.91
63	34.13	-3.47	25.70	-3.49	25.27

These results show there is a difference of between 4.64% and 8.98% between the measured and calculated system pressure for the steady flow tests completed at  $\pm 5\%$  of the design flow rate. There is a much more significant difference of between 22.70% and 26.77% in the

comparison between the calculated system pressure and the measured results recorded during the steady flow tests completed at  $\pm 5\%$  of the ultimate flow rate.

The differences between the measured system pressures and flow rates and those estimated using the commercially available software and steady state hydraulic calculations can be attributed to five reasons:

1. Steady state hydraulic theory is based on the pipes within system being full of water and free of air;
2. The flow observed within the horizontal carrier pipe contained unquantified amounts of air at the crown of the carrier pipe and as a homogenous mixture that varied temporally and spatially;
3. The steady state hydraulic calculations used within the software are based on certain assumptions, specifically the pipe roughness ( $k_s$ ) and the head loss coefficient ( $K$ );
4. Head loss due to fittings within the software are assumed to be local to the fitting;
5. In practice, any slight displacement or imperfection in the pipe joints will affect the head loss at that fitting and be a source of error.

These findings bring into question the accuracy of the model based design software to estimate system pressure within multi-outlet siphonic drainage systems at flow rates in excess of the design conditions. In practical terms, this could lead to the incorrect specification of pipe sizes and system configuration. Hence, siphonic systems designed using software based on steady state hydraulic relationships may not achieve their optimal performance and be over or under designed.

## 5.4 Flow Regimes

This experimental research has for the first time quantified the measurement of flow through each outlet with corresponding time series pressure and image data. The change in pressure and flow regimes within the horizontal carrier pipe of a siphonic system has been shown to be an extremely complex phenomena. A summary of the observed regimes are shown in Table 5.4.

**Table 5.4 Observed Flow Regimes**

Flow Rate	Camera Position		
	P1	P2	P3
20% of Design	Free surface flow	Free surface flow	Free surface flow
	Free surface flow with entrained air	Plug flow	Free surface flow with entrained air Plug flow Full bore flow
40% of Design	Free surface flow	Free surface flow	Free surface flow
	Plug flow	Plug flow	Aerated two-phase flow
	Full bore flow	Full bore flow	
60% of Design	Free surface flow	Free surface flow	Free surface flow
	Full bore flow	Plug flow	Aerated two-phase flow
		Full bore flow with air pockets	
80% of Design	Free surface flow	Plug flow	Aerated two-phase flow
	Plug flow	Full bore flow with air pockets and entrained air	
	Full bore flow with air pockets		
Design	Free surface flow	Free surface flow	Aerated two-phase flow
	Full bore flow with air pockets	Full bore flow with air pockets	
Ultimate	Full bore flow with air pockets	Full bore flow with air pockets	Aerated two-phase flow
120% of Design	Full bore flow with air pockets	Full bore flow with air pockets	Aerated two-phase flow

The recognised and reported flow regimes within the horizontal carrier pipe of a siphonic roof drainage system varied temporally and spatially from the observations made during this experimental research during both sub-primed and primed flow conditions. These observations support the research reported by Öngören and Materna (2006) and Arthur and Swaffield (2001a). Current design criteria do not take these observed regimes and changes into account.

## 5.5 Air Entrainment

The experimental research demonstrated that flow rate, pressure and the quantity of air within the horizontal carrier pipe varied temporally and spatially, even when the system was operating above the design capacity. What is clear is that the quantity of air entrainment is extremely difficult to both accurately measure and model as such entrainment varied as a function of the magnitude of flow. Hence it is recommended that further research, both modelling and experimental, is completed to address this issue.

The experimental research has, for the first time, demonstrated the relationship between localised system pressure, the relative flow through each component outlet of the system and a visual representation of air entrainment along the length of the horizontal carrier pipe. Arthur et al. (2005) recognised that to estimate the air content in turbulent two-phase flows was complex, but clearly, the results of this experimental research have demonstrated that, with further analysis, the image data collected would enable the level of air entrainment to be quantified.

Lucke (2009) identified that the relationship between system pressure and air entrainment within siphonic roof drainage was not well understood. Arthur and Swaffield (1999) recognised that any sudden changes in the proportion of air in the inflow resulted in a sudden change in the local pressure that was subsequently transmitted throughout the system at the propagation velocity. The experimental research reported in this thesis has confirmed, for the first time, that such pressure changes may be observed.

## 5.6 Flow Velocity

A sophisticated system of measurement was developed and refined to record the transverse velocity of the flow within the horizontal carrier pipe. This is a unique approach of measuring velocity in siphonic systems and provides a novel and non-intrusive method of measurement without interrupting the flow field. Observations following analysis of the measured flow velocity using high-speed image velocimetry and PIV analysis showed that the transverse velocity profile within the horizontal carrier pipe was variable and complex. Hence, the use of flow velocity measurement at individual locations within a siphonic drainage system may not be appropriate to estimate flow rate.

Considerable fluctuations in the velocity profile of the flow within the horizontal carrier pipe were measured during sub-primed conditions and at the system design. It was not until the system flow rate exceeded the design threshold that the velocity field tended to a uniform state. However, even at full bore flow conditions significantly in excess of the system design, variability in the flow velocity was recorded. This is a new finding that requires further exploration. Previous experimental research using alternative methods of measuring and estimating flow rate and velocity may not be able to accurately determine these conditions at the required resolution and further work is recommended to address this shortfall in knowledge.

Results from this study support key findings that within a multi-outlet siphonic system, different flow regimes occur along the length of the horizontal carrier pipe during steady flow tests. The results have highlighted new understanding of the way in which the 3 outlet siphonic system performed and that the flow rate through each outlet is not constant which is in contrast to the philosophy used in existing design software. Hence, the basic siphonic drainage system design principles which utilise conventional pipe flow theories should be reviewed. This thesis has highlighted that further research is required to investigate these issues further.

## **5.7 Recommendations for Further Research**

The outputs from this programme of research have highlighted the need for further research to better understand the performance of multi-outlet siphonic roof drainage systems and to inform and update current design practice.

### **5.7.1 Hydraulic Design**

Further experimental research is required to confirm whether a standard safety factor is applicable for both sub-prime and primed siphonic action.

### **5.7.2 Design Criteria**

Quantification of air entrainment is important to enhance siphonic system design criteria within multi-outlet siphonic roof drainage systems. The development of analytical measurement techniques is required to be able to accurately quantify air entrainment relative to system flow rate. These techniques could then be applied to increasing numbers of outlets within a gutter to investigate the relationship between system flow rate, number of outlets and level of air entrainment.

### **5.7.3 System Balancing**

Further experimental research is required to investigate system balancing for a range of outlet and pipework configurations. The experimental techniques and methodology developed and enhanced during this experimental research are transferable and appropriate to this proposed research.

### **5.7.4 Minimum Flow Velocities**

Further experimental research is required to investigate whether the equation proposed by Volkart (1982) and the Froude number suggested by Arthur and Wright (2007) are appropriate for both sub-primed and primed siphonic action. Again the experimental techniques and methodologies developed during this experimental research would be appropriate for such a study.

### **5.7.5 Speed of Priming**

The methodologies and experimental techniques developed during this experimental research study could be applied and used to examine the speed of priming. This would involve a series of time varying flow tests within a multi-outlet siphonic roof drainage test facility. This experimental research would provide much needed data and be used to inform and update current British Standards and be incorporated within existing design software and models. Tail pipe configurations could then be sized more accurately improving the efficiency and

design of future siphonic roof drainage systems as well as providing safety and security against failure.

#### **5.7.6 Minimum Allowable Pressures**

The methods of continuous flow rate and pressure measurement developed and enhanced during this experimental study could be applied to further experimental research to investigate and quantify the effect of the four factors identified by May and Escarameia (1996) that can cause an increase in the cavitation index:

- a. An increase in flow velocity;
- b. An increase in temperature;
- c. A reduction in the mean static pressure;
- d. A reduction in the value of atmospheric pressure.

The methods of continuous flow rate and pressure measurement developed and enhanced during this experimental study could be applied to further experimental research to investigate and quantify the effect of these factors.

#### **5.7.7 Air within Siphonic Systems**

Further work is therefore recommended to complete the PIV analysis of the series of steady flow tests to examine and test this proposed method. The corresponding time-series pressure data would complement this analysis further to provide a much needed data set and provide a detailed understanding of the interaction between flow rate, flow velocity, system pressure and volume of air entrainment within a multi-outlet siphonic roof drainage system.

All of these topics may be addressed with the technology and methodologies that have been developed within this thesis and hence procedures are now in place to tackle such further work.

Furthermore, the data that has been collected within the experimental programme of research may be made available to assist any programme of further work.



## 6 Summary Conclusions

This experimental research presents novelty in several aspects:

- The application of flourometry within the experimental system and methodology refined during this research has for the first time, provided a repeatable, robust and reliable approach to simultaneously measure the relative proportion and components of flow within a multi-outlet siphonic roof drainage system over a range of steady flow tests below, at, and above the design criteria. Significantly, this non-intrusive methodology enabled the continuous measurement of flow through each outlet without affecting the hydraulic performance or generating additional, uncalculated losses. It is concluded therefore, that the provision of such a measurement system represents a novel and original way in which to measure the flow components in a multi-outlet siphonic roof drainage system;
- Flow rate through the multi-outlet test facility was not equal and flow proportionality through each outlet varied as a function of the magnitude of the total system flow rate. This highlights that current design criteria are fundamentally flawed as the assumption is made that this is the case;
- Commercially available model based software based on steady state hydraulic theory was used to calculate the design and ultimate flow capacity through the system. It was observed that the measured system flow rates and pressure using the experimental test facility differed to the calculated values from the model based design software. The differences can be attributed to five reasons:
  1. Steady state hydraulic theory is based on the pipes within system being full of water and free of air;
  2. Flow observed within the horizontal carrier pipe contained unquantified amounts of air at the crown of the carrier pipe and as a homogenous mixture that varied temporally and spatially;
  3. Steady state hydraulic calculations used within the software are based on certain assumptions, specifically the pipe roughness ( $k_s$ ) and the head loss coefficient ( $K$ );
  4. Head loss due to fittings within the software are assumed to be local to the fitting;
  5. In practice, any slight displacement or imperfection in the pipe joints will affect the head loss at that fitting and be a source of error.

These findings bring into question the accuracy of the model based design software to estimate system pressure within a multi-outlet siphonic drainage system at flow rates in excess of the design conditions. In practical terms this could lead to the incorrect specification of pipe sizes and system configuration. Hence, siphonic systems designed using software based on steady-state hydraulic relationships may not achieve their optimal performance and be over or under designed;

- The change in pressure and flow regime within the horizontal carrier pipe of a siphonic system has been shown to be an extremely complex process with many observed phenomena. The recognised and reported flow regimes within the horizontal carrier pipe of a siphonic roof drainage system varied temporally and spatially from

the observations made during the steady flow tests during both sub-primed and primed flow conditions. Current design criteria do not take these observed regimes and changes into account;

- Flow rate, pressure and the quantity of air within the horizontal carrier pipe varied temporally and spatially, even when the system was operating above the design capacity. What is clear is that the quantity of air entrainment is extremely difficult to accurately measure and model as such entrainment varied as a function of the magnitude of flow;
- For the first time, the relationship between localised system pressure, the relative flow through each component outlet of the system and a visual representation of air entrainment along the length of the horizontal carrier pipe, has been clearly demonstrated;
- A sophisticated system of measurement was developed and refined to record the transverse velocity of the flow within the horizontal carrier pipe. This is a unique approach of measuring velocity in siphonic systems and provides a novel, non-intrusive method of measurement without interrupting the flow field. Observations following analysis of the measured flow velocity using high-speed image velocimetry and PIV analysis showed that the transverse velocity profile within the horizontal carrier pipe was variable and complex. Hence, the use of flow velocity measurement at individual locations within a siphonic drainage system may not be appropriate to estimate flow rate;
- Considerable fluctuations in the velocity profile of the flow within the horizontal carrier pipe were measured during sub-primed conditions and at the system design. Even at full bore flow conditions significantly in excess of the system design, variability in the flow velocity was recorded. This is a new finding that requires further exploration. Previous experimental research using alternative methods of measuring and estimating flow rate and velocity may not be able to accurately determine these conditions at the required resolution and further work is recommended to address this shortfall in knowledge.

In summary, the results from this study support several key findings: within a multi-outlet siphonic system the flow rate through each individual outlet is not the same; that significantly different flow regimes occurred along the length of the horizontal carrier pipe during steady flow tests; that air entrainment is a major influence on system performance and that differences were observed between the experimental pressure and flow rate results with those computed using software based on steady-state hydraulic relationships. Hence, the current approaches applied in conventional siphonic roof drainage design should be reviewed. Design engineers should also be made aware of these findings.

## References

- Arthur, S. and J. A. Swaffield (1999a). "Numerical Modelling of the Priming of a Siphonic Rainwater Drainage System." Building Serv Eng Res Technol **20**(2): 83-91.
- Arthur, S. and J. A. Swaffield (2001a). "Siphonic Roof Drainage: Current Understanding." Urban Water **3**(1): 43-52.
- Arthur, S. and J. A. Swaffield (2001b). "Siphonic Roof Drainage System Analysis Utilising Unsteady Flow Theory." Building and Environment **36**: 939-948.
- Arthur, S. and G. B. Wright (2005). "Recent and Future Advances in Roof Drainage Design and Performance." Building Serv Eng Res Technol **26**(4): 337-348.
- Arthur, S., G. B. Wright and J. A. Swaffield (2005). "Operational Performance of Siphonic Roof Drainage Systems." Building and Environment **40**: 788-796.
- Arthur, S. and G. B. Wright (2007). "Siphonic Roof Drainage Systems - Priming Focused Design." Building and Environment **42**: 2421-2431.
- ASPE (2006). Siphonic Roof Drainage Design Standard (Draft Version 3). Chicago, USA, American Society of Plumbing Engineers.
- Bowler, R. and S. Arthur (1999). Siphonic Roof Rainwater Drainage - Design Considerations. Proceedings of water supply and drainage: CIB W62, Edinburgh, UK.
- Bramhall, M. (2004). The Performance of Syphonic Rainwater Outlets within Gutters. Civil & Structural Engineering, The University of Sheffield. **PhD**.
- Bramhall, M. and M. J. Wearing (2008). Siphonic Roof Drainage Systems - Priming of Tailpipes. 11th International Conference on Urban Drainage, Edinburgh.
- BSI (1974). "British Standards Institution. CP 308:1974. Drainage of roofs and paved areas."
- BSI (1983). "British Standards Institution. BS 6367:1983. Code of practice for the drainage of roofs and paved areas."
- BSI (2000). British Standards Institute. BS EN 12056-3:2000. Gravity Drainage Systems Inside Buildings. Part 3: Roof Drainage, Layout and Calculation.
- BSI (2007). "British Standards Institute. BS 8490:2007. Guide to Siphonic Roof Drainage Systems."
- Chadwick, A. and J. Morfett (1993). Hydraulics in Civil and Environmental Engineering, E & FN Spon.
- Fullflow Group Ltd (2016) "Syphonic Explained" <http://www.fullflow.com/pages/syphonic-explained/> [accessed 23 Jan 2016]
- Lucke, T. (2009). The role of air entrainment in the performance of siphonic roof drainage systems. School of Natural and Built Environments, University of South Australia. **PhD**.
- Lucke, T. and S. Beecham (2009). "Cavitation, aeration and negative pressures in siphonic roof drainage systems." Building Serv Eng Res Technol **30**(2): 103-119.
- Lucke, T. and S. Beecham (2010). "Capacity Loss in Siphonic Roof Drainage Systems due to Aeration". Building Research and Information **38**(2), 206-217.
- Lucke, T., S. Beecham and G. Zillante (2007). "Rainwater Harvesting Options for Commercial Buildings using Siphonic Roof Drainage Systems - Lessons for Building Surveyors." AIBS: 44-54.

- Lucke, T., S. Beecham and Y. Y. Qu (2011) Determining Flowrates through Individual Outlets in Siphonic Roof Drainage Systems. 12th International Conference on Urban Drainage, Porto Alegre, Brazil.
- Lucke, T., S. Beecham and Y. Y. Qu (2014) Estimating Flow Rates Through Individual Outlets of Siphonic Roof Drainage Systems. Building Research and Information. Routledge, doi: 10.1080/09613218.2014.987030.
- May, R. W. P. and M. Escarameia (1996). Performance of Siphonic Drainage Systems for Roof Gutters, HR Wallingford.
- May, R. W. P. (1997). "The Design of Conventional and Siphonic Roof Drainage Systems." J. CIWEM **11**: 56-60.
- Öngören, A. and R. Materna (2006). Multi-phase flow characteristics of a siphonic roof drainage system under part load conditions. 32nd International Symposium on CIB W062 Water Supply and Drainage for Buildings, Taipei.
- Qu, Y. Y., T. Lucke and S. Beecham (2011). Measuring Flows in Partially-Filled Pipes in Siphonic Roof Drainage Systems. MAPAN - Journal of Metrology Society of India. **26**(4): 315-327.
- Ross, W. (2006). Understanding siphonic drainage - the why's and how's. PM engineer magazine website.
- Slater, J. A., G. Cockerham and P. D. Williams (1999). Loss factors in siphonic roof drainage. Proceedings of Water Supply and Drainage for Buildings, CIB W62 1999, Edinburgh.
- Sommerhein, P. (1999). Design parameters for roof drainage systems. Proceedings of water supply and drainage: CIB W62, Edinburgh, UK.
- Thorne Rainwater Systems (2016) "Syphonic Cast Iron System"  
[http://thornerws.com/trws\\_syphonic\\_cast\\_iron.html](http://thornerws.com/trws_syphonic_cast_iron.html) [accessed Jan 23 2016]
- Unwin, D. (2008). Real Time Monitoring/Control of Sewers and Sewer Systems including Flooding, The University of Sheffield. **PhD**.
- Volkart, P. U. (1982) Self-aerated flow in steep, partially filled pipes. Proceedings of American Society of Civil Engineers, Vol 108, HY9: 1029-1046, September.
- Wearing, M. J. (2004). Give a sucker an even chance. AJ Focus.
- Wilson, J. F. Jr. (1968). Fluorometric Procedures for Dye Tracing. Techniques for Water Resources Investigations of the U.S. Geological Survey, Book 3, Applications of Hydraulics, Chapter A12:VIII, U.S. Government Printing Office. Washington D.C.
- Wright, G. B., J. A. Swaffield and S. Arthur (2002). "The Performance Characteristics of Multi-Outlet Siphonic Roof Drainage Systems." Building Serv Eng Res Technol **23**(3): 127-141.
- Wright, G. B., S. Arthur and J. A. Swaffield (2006a). "Numerical Simulation of the Dynamic Operation of Multi-Outlet Siphonic Roof Drainage Systems." Building and Environment **41**: 1279-1290.
- Wright, G. B., L. B. Jack and J. A. Swaffield (2006b). "Investigation and Numerical Modelling of Roof Drainage Systems Under Extreme Events." Building and Environment **41**: 126-135.
- Wylie, E. B. and V. L. Streeter (1978) Fluid Transients. New York. McGraw-Hill, Inc.

## Appendix 1 - Commercial System Software Design

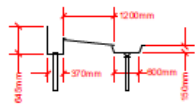
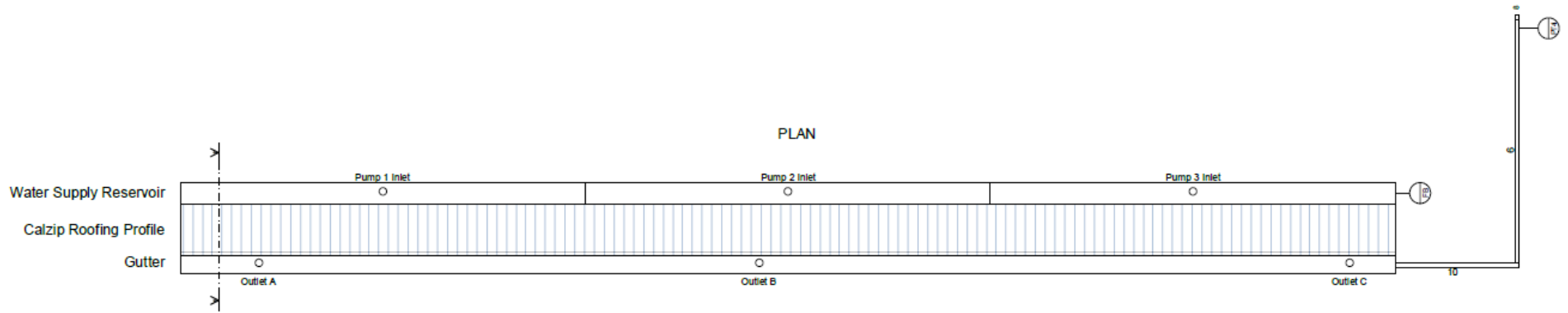
### Pipe Run List

Node Top	Node Bottom	Dir	Diameter (mm)	Length (m)	Flow (l/s)	Velocity (m/s)	Loss (m/m)	OpP (m)	Material
26	25	+Z	63	0.300	10.00	3.92	0.81	-1.29	HDPE9910
25	24	-Y+Z	63	0.190	10.00	3.92	0.35	-1.51	HDPE9910
24	12	+X- Y+Z	63	0.180	10.00	3.92	0.54	-1.92	HDPE9910
23	22	+Z	75	0.250	10.00	2.67	0.28	-0.39	HDPE9910
22	21	-Y+Z	75	0.270	10.00	2.67	0.27	-0.47	HDPE9910
21	15	+X- Y+Z	110	0.130	10.00	1.24	0.05	-0.15	HDPE9910
20	19	+Z	110	0.250	10.00	1.24	0.08	0.09	HDPE9910
19	18	-Y+Z	110	0.350	10.00	1.24	0.06	0.28	HDPE9910
18	17	+X	110	3.430	10.00	1.24	0.07	0.21	HDPE9910
17	16	+X	110	6.000	10.00	1.24	0.12	0.09	HDPE9910
16	15	+X	110	6.000	10.00	1.24	0.13	-0.04	HDPE9910
15	14	+X	110	5.120	20.00	2.48	0.40	-0.78	HDPE9910
14	13	+X	110	6.000	20.00	2.48	0.49	-1.28	HDPE9910
13	12	+X	125	6.000	20.00	1.92	0.27	-1.42	HDPE9910
12	11	+X	125	0.580	30.00	2.88	0.20	-1.85	HDPE9910
11	10	+X+Z	125	0.490	30.00	2.88	0.19	-1.70	HDPE9910
10	9	+X	125	3.870	30.00	2.88	0.62	-2.32	HDPE9910
9	8	+Y	125	7.000	30.00	2.88	0.91	-3.23	HDPE9910
8	7	+Z	125	4.500	30.00	2.88	0.68	0.59	HDPE9910
7	6	+Y	125	1.245	30.00	2.88	0.39	0.20	HDPE9910
6	5	+X	125	5.580	30.00	2.88	0.78	-0.58	HDPE9910
5	4	+Z	125	0.265	30.00	2.88	0.17	-0.48	HDPE9910
4	3	+Y+Z	125	1.490	30.00	2.88	0.28	0.29	HDPE9910
3	2	+Z	125	2.310	30.00	2.88	0.36	2.24	HDPE9910
2	1	+Y+Z	125	1.310	30.00	2.88	0.27	2.90	HDPE9910
1	0	+Y	125	3.360	30.00	2.88	0.73	2.18	HDPE9910

### System Design Summary

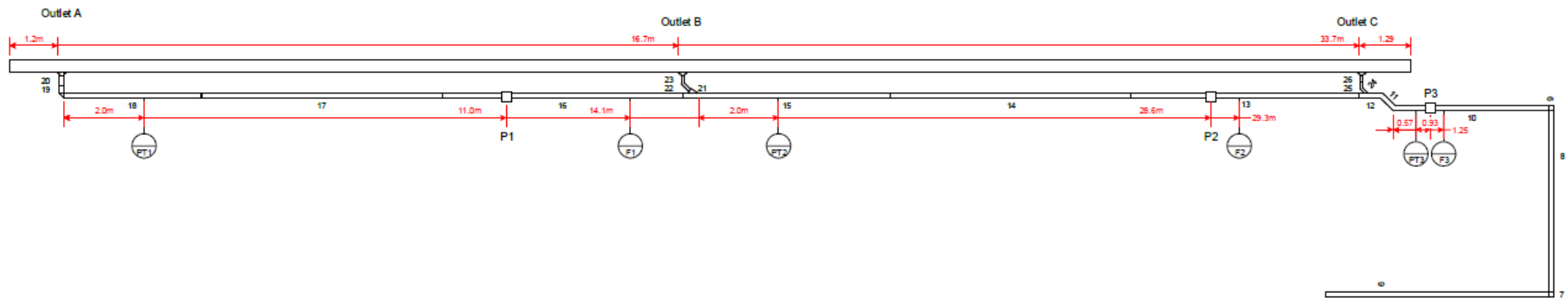
Node	Original Inflow (l/s)	Reserve		Ultimate Inflow (l/s)	Reserve	
		m	%		m	%
26	10.00	2.690	27	11.74	0.000	0
23	10.00	2.600	26	11.25	-0.025	0
20	10.00	2.700	27	12.14	0.024	0

Design flow (l/s): 30.00  
 Ultimate flow (l/s): 35.12  
 Design OpP (m): -3.23  
 Ultimate OpP (m): -4.67

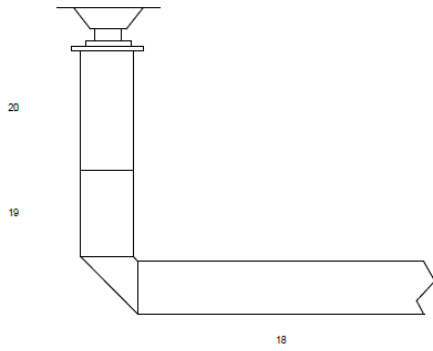


SECTION A-A

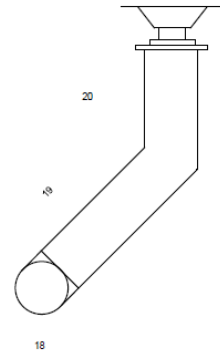
### SIDE ELEVATION



**Outlet A**

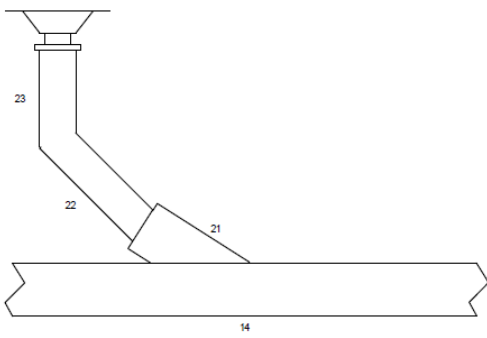


SIDE ELEVATION

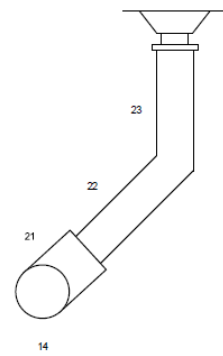


END ELEVATION

**Outlet B**

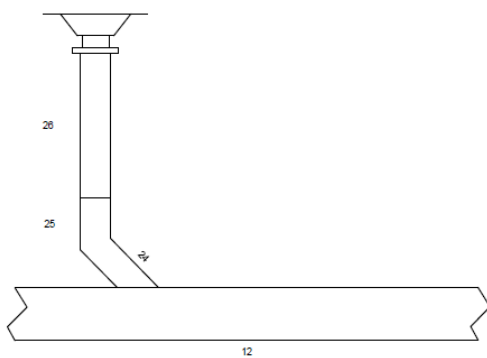


SIDE ELEVATION

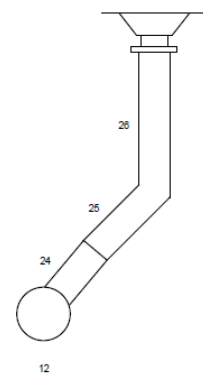


END ELEVATION

**Outlet C**



SIDE ELEVATION



END ELEVATION

## Appendix 2 - Steady State Hydraulic Equations of the Experimental Test Facility

### Design Flow Rate (30 l/s)

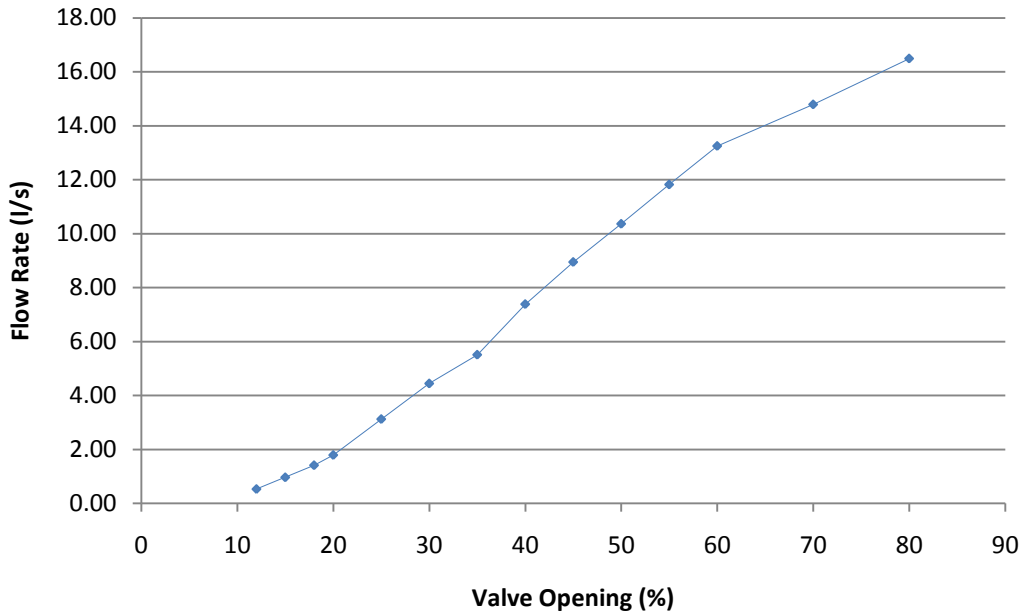
Node Top	Node Bottom	Dir	D (mm)	L (m)	Q (l/s)	V (m/s)	$z_1$ (m)	$z_2$ (m)	$h_1$ (m)	$h_2$ (m)	$i$ (m/m)	$\Delta H_p$ (m)	K	$\Delta H_f$ (m)	$\Delta H$ (m)	$P_k$ (m)
26	25	+Z	63	0.300	10.00	3.92	9.75	9.45	-4.77	-5.29	0.41	0.12	0.88	0.78	0.81	-1.29
25	24	-Y+Z	63	0.190	10.00	3.92	9.45	9.32	-5.29	-5.51	0.41	0.08	0.35	0.27	0.35	-1.51
24	12	+X-Y+Z	63	0.180	10.00	3.92	9.32	9.19	-5.51	-5.96	0.41	0.07	0.65	0.51	0.58	-1.92
23	22	+Z	75	0.250	10.00	2.67	9.72	9.47	-4.63	-4.65	0.15	0.04	0.65	0.24	0.27	-0.39
22	21	-Y+Z	75	0.270	10.00	2.67	9.47	9.28	-4.65	-4.74	0.15	0.04	0.65	0.24	0.28	-0.47
21	15	+X-Y+Z	110	0.130	10.00	1.24	9.28	9.19	-4.74	-4.70	0.02	0.00	0.65	0.05	0.05	-0.15
20	19	+Z	110	0.250	10.00	1.24	9.69	9.44	-4.87	-4.70	0.02	0.01	1.00	0.08	0.08	0.09
19	18	-Y+Z	110	0.350	10.00	1.24	9.44	9.19	-4.70	-4.51	0.02	0.01	0.65	0.05	0.06	0.28
18	17	+X	110	3.430	10.00	1.24	9.19	9.19	-4.51	-4.58	0.02	0.07	0.00	0.00	0.07	0.21
17	16	+X	110	6.000	10.00	1.24	9.19	9.19	-4.58	-4.70	0.02	0.12	0.00	0.00	0.12	0.09
16	15	+X	110	6.000	10.00	1.24	9.19	9.19	-4.70	-4.82	0.02	0.12	0.00	0.00	0.12	-0.03
15	14	+X	110	5.120	20.00	2.48	9.19	9.19	-4.82	-5.22	0.08	0.40	0.00	0.00	0.40	-0.67
14	13	+X	110	6.000	20.00	2.48	9.19	9.19	-5.22	-5.71	0.08	0.47	0.05	0.02	0.49	-1.15
13	12	+X	125	6.000	20.00	1.92	9.19	9.19	-5.71	-5.96	0.04	0.24	0.00	0.00	0.24	-1.27
12	11	+X	125	0.580	30.00	2.88	9.19	9.19	-5.96	-6.16	0.09	0.05	0.35	0.15	0.20	-1.70
11	10	+X+Z	125	0.490	30.00	2.88	9.19	8.84	-6.16	-6.00	0.09	0.04	0.35	0.15	0.19	-1.90
10	9	+X	125	3.870	30.00	2.88	8.84	8.84	-6.00	-6.62	0.09	0.35	0.65	0.28	0.62	-2.17
9	8	+Y	125	7.000	30.00	2.88	8.84	8.84	-6.62	-7.53	0.09	0.63	0.65	0.28	0.90	-3.07
8	7	+Z	125	4.500	30.00	2.88	8.84	4.34	-7.53	-3.70	0.09	0.40	0.65	0.28	0.68	0.75
7	6	+Y	125	1.245	30.00	2.88	4.34	4.34	-3.70	-4.09	0.09	0.11	0.65	0.28	0.39	0.36
6	5	+X	125	5.580	30.00	2.88	4.34	4.34	-4.09	-4.87	0.09	0.50	0.35	0.28	0.78	-0.41
5	4	+Z	125	0.265	30.00	2.88	4.36	4.09	-4.87	-4.77	0.09	0.02	0.35	0.15	0.17	-0.34
4	3	+Y+Z	125	1.490	30.00	2.88	4.09	3.24	-4.77	-1.90	0.09	0.13	0.35	0.15	0.28	0.23
3	2	+Z	125	2.310	30.00	2.88	3.24	0.93	-1.90	0.06	0.09	0.21	0.35	0.15	0.36	2.18
2	1	+Y+Z	125	1.310	30.00	2.88	0.93	0.00	0.06	0.72	0.09	0.12	0.35	0.15	0.27	2.84
1	0	+Y	125	3.360	30.00	2.88	0.00	0.00	0.72	0.00	0.09	0.30	1.00	0.42	0.72	2.12



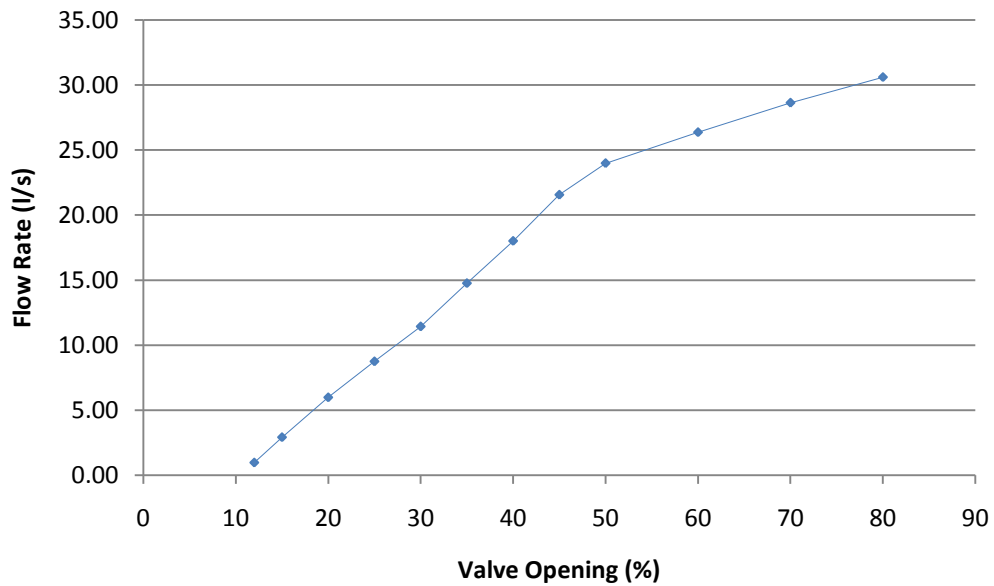
**Ultimate Flow Rate (35.12 l/s)**

Node Top	Node Bottom	Dir	D (mm)	L (m)	Q (l/s)	V (m/s)	z <sub>1</sub> (m)	z <sub>2</sub> (m)	h <sub>1</sub> (m)	h <sub>2</sub> (m)	i (m/m)	ΔH <sub>p</sub> (m)	K	ΔH <sub>F</sub> (m)	ΔH (m)	P <sub>k</sub> (m)
26	25	+Z	63	0.300	11.74	4.60	9.75	9.45	0.16	-0.65	0.56	0.17	0.88	0.95	1.12	-1.90
25	24	-Y+Z	63	0.190	11.74	4.60	9.45	9.32	-0.65	-1.08	0.56	0.11	0.35	0.38	0.48	-2.25
24	12	+X-Y+Z	63	0.180	11.74	4.60	9.32	9.19	-1.08	-1.75	0.56	0.10	0.65	0.70	0.80	-2.68
23	22	+Z	75	0.250	11.25	3.00	9.72	9.47	0.20	0.10	0.19	0.05	0.65	0.30	0.35	-0.55
22	21	-Y+Z	75	0.270	11.25	3.00	9.47	9.28	0.10	-0.06	0.19	0.05	0.65	0.30	0.35	-0.72
21	15	+X-Y+Z	110	0.130	11.25	1.39	9.28	9.19	-0.06	-0.04	0.03	0.00	0.65	0.06	0.07	-0.33
20	19	+Z	110	0.250	12.14	1.51	9.69	9.44	-0.05	0.08	0.03	0.01	1.00	0.12	0.12	0.01
19	18	-Y+Z	110	0.350	12.14	1.51	9.44	9.19	0.08	0.24	0.03	0.01	0.65	0.08	0.09	0.18
18	17	+X	110	3.430	12.14	1.51	9.19	9.19	0.24	0.14	0.03	0.10	0.00	0.00	0.10	0.08
17	16	+X	110	6.000	12.14	1.51	9.19	9.19	0.14	-0.04	0.03	0.18	0.00	0.00	0.18	-0.10
16	15	+X	110	6.000	12.14	1.51	9.19	9.19	-0.04	-0.21	0.03	0.18	0.00	0.00	0.18	-0.28
15	14	+X	110	5.120	23.39	2.90	9.19	9.19	-0.21	-0.76	0.11	0.55	0.00	0.00	0.55	-1.14
14	13	+X	110	6.000	23.39	2.90	9.19	9.19	-0.76	-1.42	0.11	0.64	0.05	0.02	0.66	-1.80
13	12	+X	125	6.000	23.39	2.25	9.19	9.19	-1.42	-1.75	0.06	0.33	0.00	0.00	0.33	-1.96
12	11	+X	125	0.580	35.12	3.37	9.19	9.19	-1.75	-2.03	0.12	0.07	0.35	0.20	0.27	-2.55
11	10	+X+Z	125	0.490	35.12	3.37	9.19	8.84	-2.03	-1.94	0.12	0.06	0.35	0.20	0.26	-2.82
10	9	+X	125	3.870	35.12	3.37	8.84	8.84	-1.94	-2.79	0.12	0.48	0.65	0.38	0.85	-3.32
9	8	+Y	125	7.000	35.12	3.37	8.84	8.84	-2.79	-4.03	0.12	0.86	0.65	0.38	1.24	-4.55
8	7	+Z	125	4.500	35.12	3.37	8.84	4.34	-4.03	-0.46	0.12	0.55	0.65	0.38	0.93	-0.98
7	6	+Y	125	1.245	35.12	3.37	4.34	4.34	-0.46	-0.99	0.12	0.15	0.65	0.38	0.53	-1.51
6	5	+X	125	5.580	35.12	3.37	4.34	4.34	-0.99	-1.87	0.12	0.69	0.35	0.20	0.89	-2.40
5	4	+Z	125	0.265	35.12	3.37	4.36	4.09	-1.87	-1.86	0.12	0.03	0.35	0.20	0.24	-2.39
4	3	+Y+Z	125	1.490	35.12	3.37	4.09	3.24	-1.86	-1.40	0.12	0.18	0.35	0.20	0.39	-1.93
3	2	+Z	125	2.310	35.12	3.37	3.24	0.93	-1.40	0.43	0.12	0.28	0.35	0.20	0.49	-0.10
2	1	+Y+Z	125	1.310	35.12	3.37	0.93	0.00	0.43	0.99	0.12	0.16	0.35	0.20	0.36	0.46
1	0	+Y	125	3.360	35.12	3.37	0.00	0.00	0.99	0.00	0.12	0.41	1.00	0.58	0.99	-0.53

## Appendix 3 - Pump Calibration Results



### Pump 1 Calibration Results



### Pump 3 Calibration Results

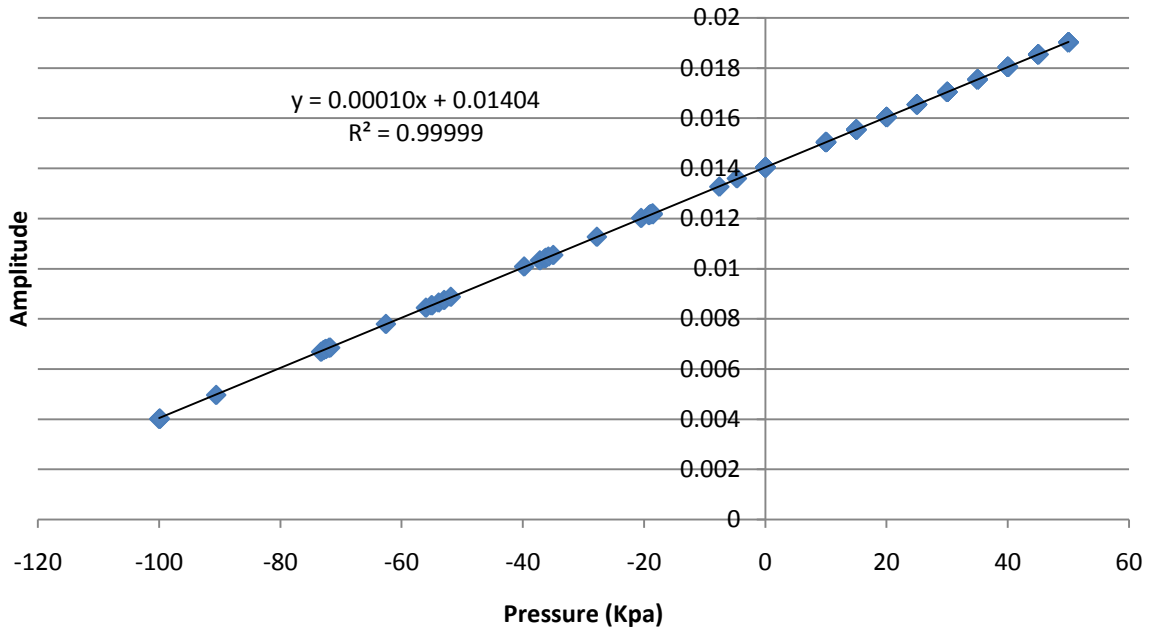
### Pump 1 Calibration Results

Valve Opening (%)	Start (ft)	Finish (ft)	Time 1 (s)	Time 2 (s)	Time 3 (s)	Average time (s)	Average time per ft (s)	Calibration	Average flow rate (l/s)
12	1	1.5	796.21	798.32	810.93	801.82	1603.64	849.505	0.53
15	1	1.5	440.41	440.15	440.13	440.23	880.46	849.505	0.96
18	1	2	605.33	595.29	603.48	601.37	601.37	849.505	1.41
20	1	2	474.01	471.59	477.27	474.29	474.29	849.505	1.79
25	1	3	544.81	538.99	548.37	544.06	272.03	849.505	3.12
30	1	3	383.95	380.89	382.20	382.35	191.17	849.505	4.44
35	1	4	465.02	462.06	460.81	462.63	154.21	849.505	5.51
40	1	4	342.00	346.98	346.37	345.12	115.04	849.505	7.38
45	1	4	283.47	284.07	287.15	284.90	94.97	849.505	8.95
50	1	4	245.35	244.89	247.66	245.97	81.99	849.505	10.36
55	1	4	214.35	215.09	217.47	215.64	71.88	849.505	11.82
60	1	4	192.73	192.13	192.33	192.40	64.13	849.505	13.25
70	1	4	172.53	172.33	172.21	172.36	57.45	849.505	14.79
80	1	4	154.76	154.47	154.47	154.57	51.52	849.505	16.49

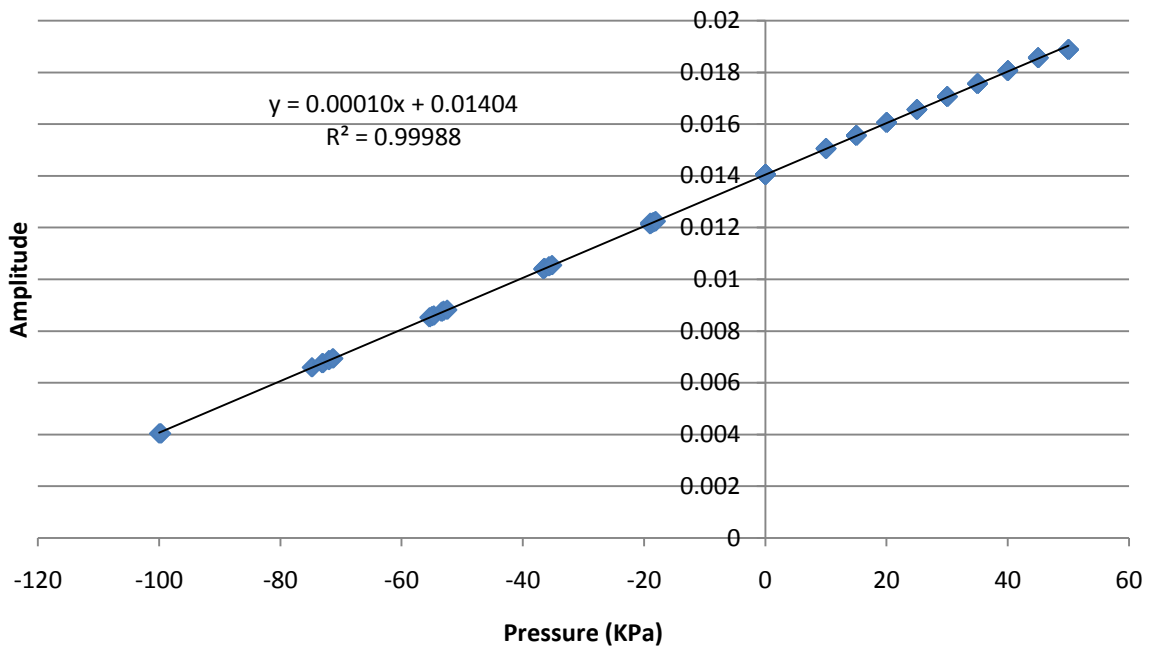
### Pump 3 Calibration Results

Valve Opening (%)	Start (ft)	Finish (ft)	Time 1 (s)	Time 2 (s)	Time 3 (s)	Average time (s)	Average time per ft (s)	Calibration	Average flow rate (l/s)
12	1	1.5	453.23	427.04	432.47	437.58	875.16	849.505	0.97
15	1	2	288.80	292.49	292.34	291.21	291.21	849.505	2.92
20	1	3	281.87	283.90	286.64	284.14	142.07	849.505	5.98
25	1	3	191.83	195.50	195.50	194.28	97.14	849.505	8.75
30	1	3	148.53	149.05	148.40	148.66	74.33	849.505	11.43
35	1	4	173.30	172.40	172.57	172.76	57.59	849.505	14.75
40	1	4	141.34	141.12	142.31	141.59	47.20	849.505	18.00
45	1	4	117.34	117.83	119.62	118.26	39.42	849.505	21.55
50	1	4	105.36	106.56	106.98	106.30	35.43	849.505	23.97
60	1	4	96.93	96.54	96.65	96.71	32.24	849.505	26.35
70	1	4	88.59	89.42	89.13	89.05	29.68	849.505	28.62
80	1	4	83.61	83.30	83.07	83.33	27.78	849.505	30.58

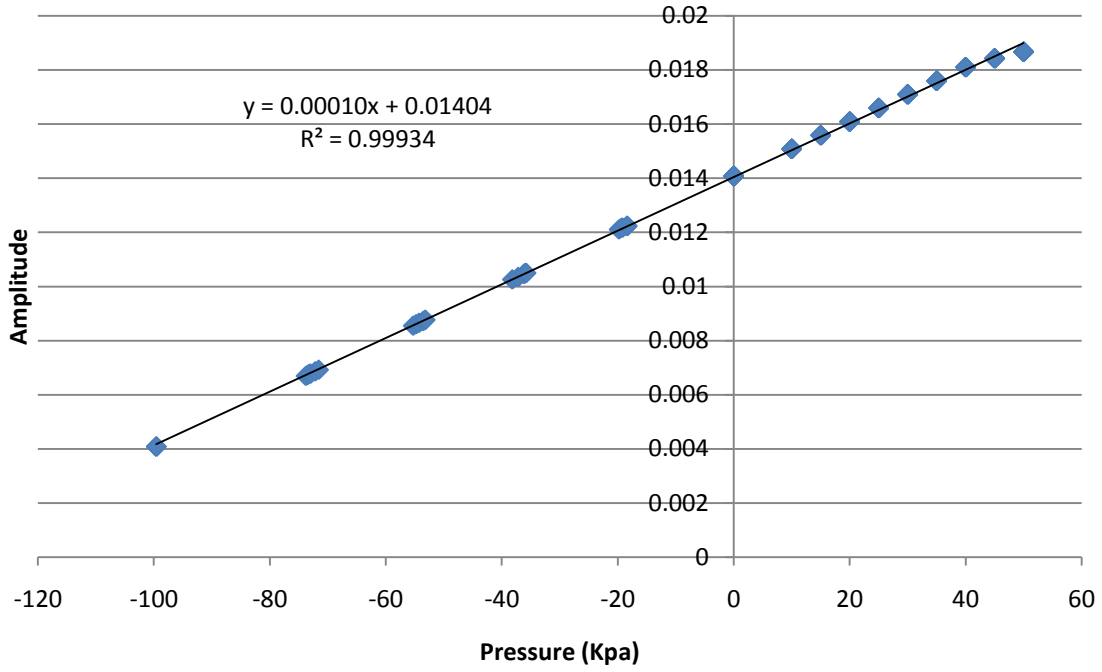
## Appendix 4 - Pressure Transducer Calibration Results



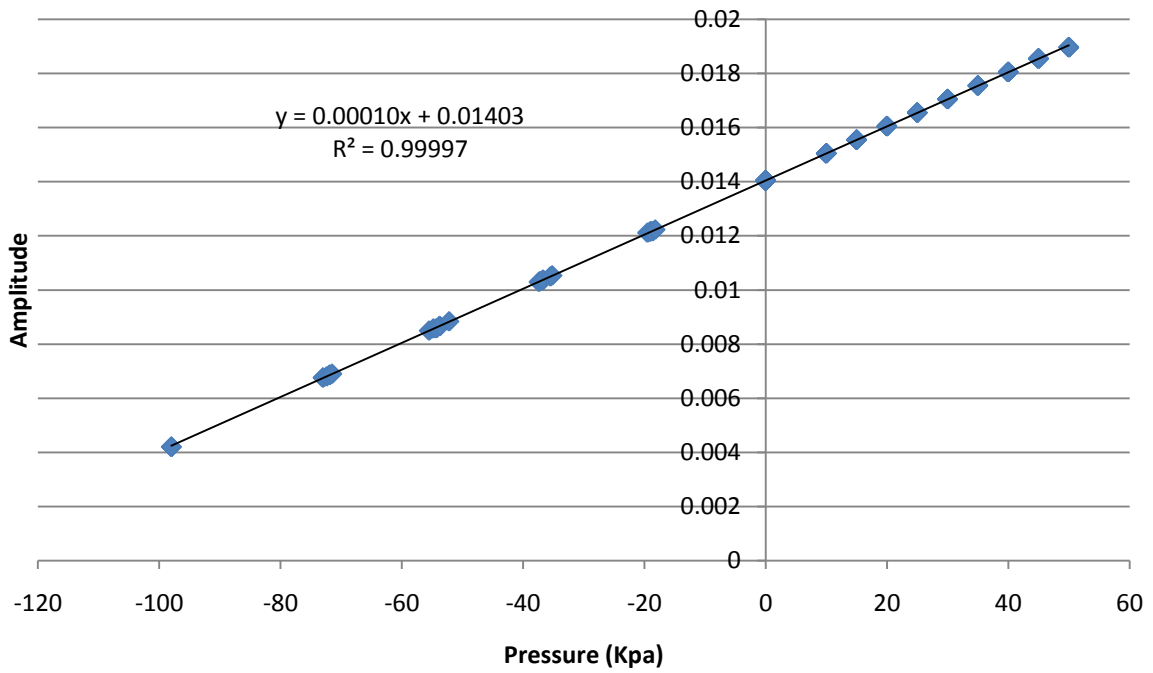
**PT1 Calibration**



**PT2 Calibration**

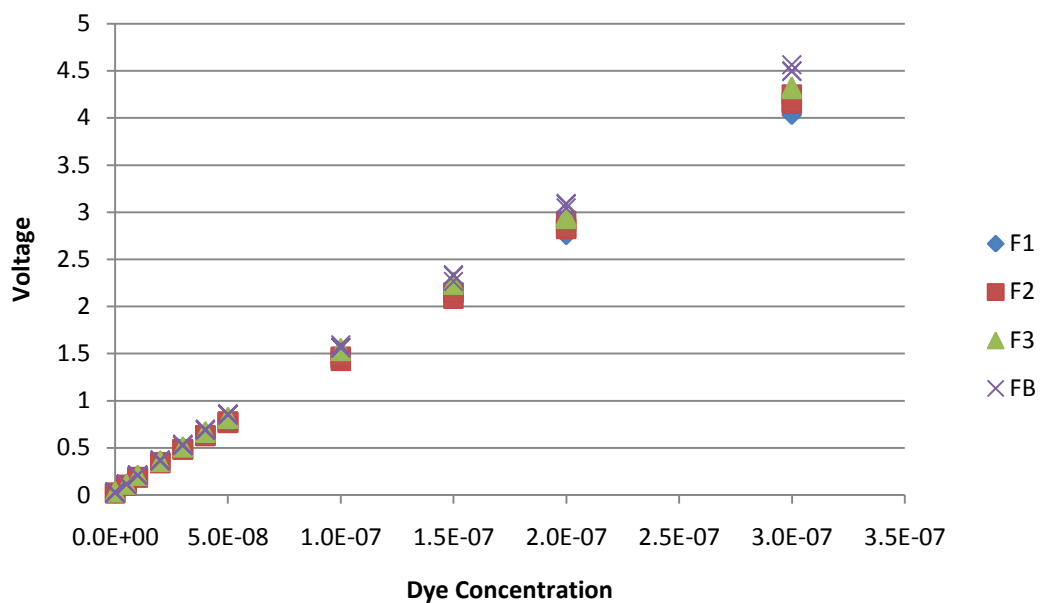


**PT3 Calibration**



**PT4 Calibration**

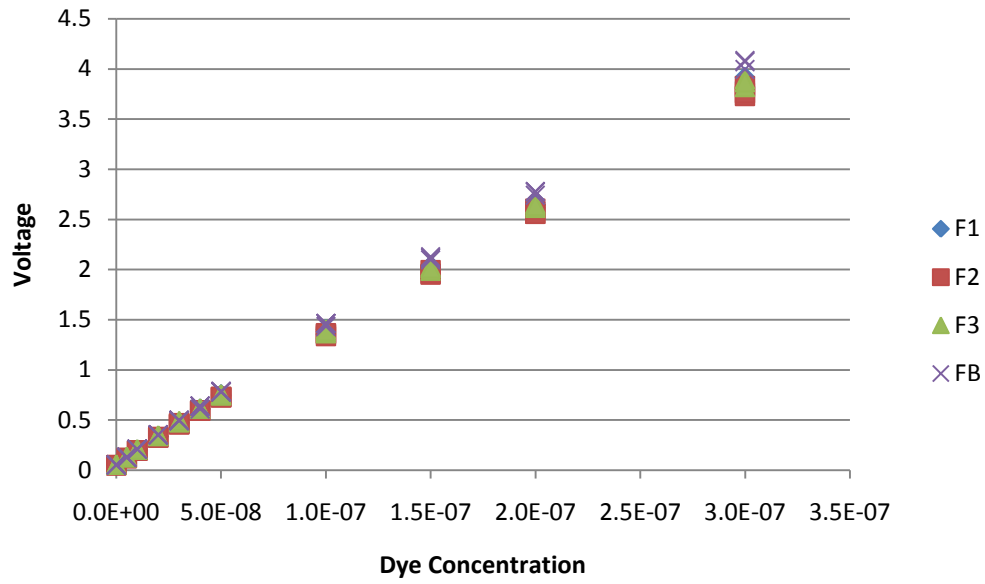
## Appendix 5 - Flourometer Calibration Results



### Flourometer Calibration 14.08.13

#### Flourometer Calibration 14.08.13 Summary

Flourometer	Equation	Regression
F1	$y = 13,534,576x + 0.080717$	0.999
F2	$y = 13,853,140x + 0.056031$	0.999
F3	$y = 14,286,935x + 0.077776$	0.999
FB	$y = 14,920,708x + 0.068745$	0.999

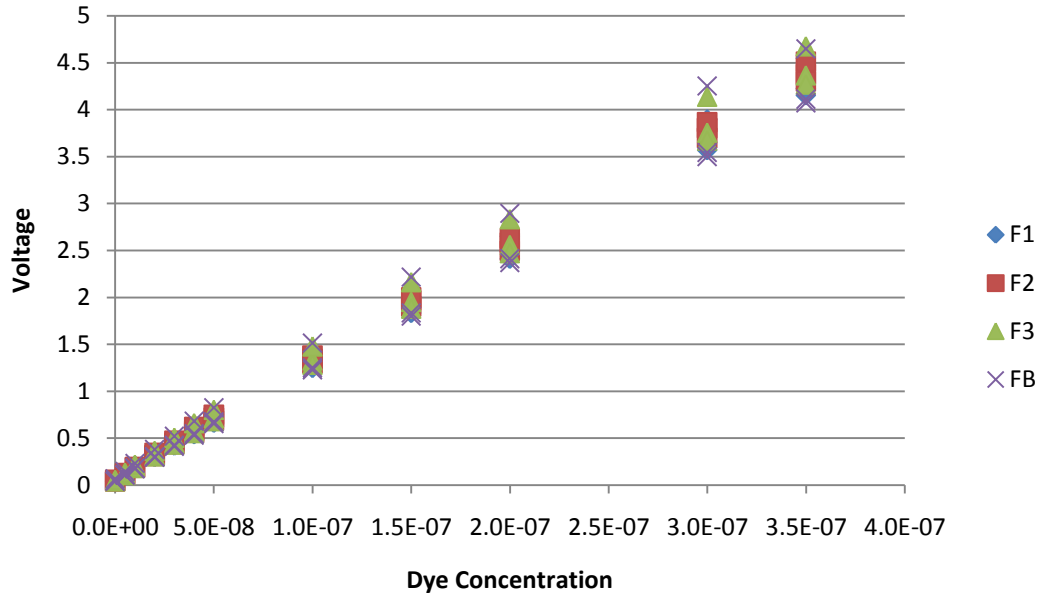


### Flourometer Calibration 10.09.13

#### Flourometer Calibration 10.09.13 Summary

Flourometer	Equation	Regression
F1	$y = 12,668,968x + 0.090856$	0.999
F2	$y = 12,415,482x + 0.081173$	0.999
F3	$y = 12,668,968x + 0.090856$	0.999
FB	$y = 13,327,667x + 0.087426$	0.999

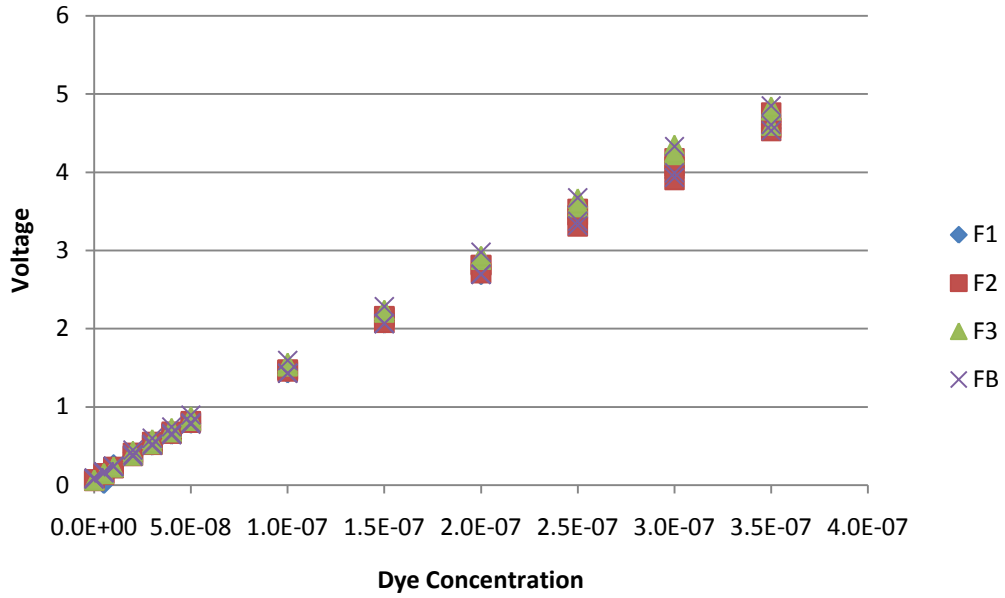




### Flourometer Calibration 08.10.13

#### Flourometer Calibration 08.10.13 Summary

Flourometer	Equation	Regression
F1	$y = 12,124,494x + 0.076550$	0.997
F2	$y = 12,395,476x + 0.077988$	0.999
F3	$y = 12,547,154x + 0.084776$	0.995
FB	$y = 12,159,109x + 0.090159$	0.986



### Flourometer Calibration 09.12.13

#### Flourometer Calibration 09.12.13 Summary

Flourometer	Equation	Regression
F1	$y = 12,922,116x + 0.112571$	0.999
F2	$y = 13,073,081x + 0.124625$	0.998
F3	$y = 13,623,388x + 0.133913$	0.998
FB	$y = 13,131,950x + 0.138237$	0.996

## **Appendix 6 - Published Papers**

# **An Investigation into the Measurement of Flow Proportionality through Multi-Outlet Siphonic Roof Drainage Systems**

**K. J. Williams (1,2), A. J. Saul (2)**

1. kwilliams@em-solutions.co.uk

2. a.j.saul@sheffield.ac.uk

1. Environmental Monitoring Solutions Ltd, 7 President Buildings, Savile Street East, Sheffield, S4 7UQ, UK

2. Department of Civil and Structural Engineering, University of Sheffield, Sir Frederick Mappin Building, Mappin Street, Sheffield, S1 3JD, UK

## **Abstract**

Recent trends in the development of our urban landscape have seen the introduction of larger buildings with vast roof areas. It is anticipated that the onset of climate change will see increased intensities and volumes of rainfall which will place significant pressures on the roof drainage systems for these buildings potentially leading to failure and major flooding. There is an urgent need to adapt and the principal solution is the use of siphonic roof drainage systems. However, it has been identified that there is a universal lack of understanding of the hydraulic performance of siphonic systems. Current design methodologies assume that the proportions of flow through each outlet within a common gutter are the same, previous research has reported that this is not the case.

An experimental study has been undertaken using the full-scale test facility at the University of Sheffield to improve the understanding of the hydraulic performance of multi-outlet siphonic roof drainage systems. This paper presents the results from the feasibility tests and an assessment of the suitability of the experimental measurement methods. The reported tests include a series of novel experiments using high speed image velocimetry and a unique approach that uses a fluorescein tracer to measure the flow component through each outlet. Proposed future tests are also reported including a systematic study of changes to the configuration of the outlets within the common gutter.

## **Keywords**

Siphonic Roof Drainage, Priming, Flow Measurement

## **1 Introduction**

We are living in a changing world and recent trends in the development of our urban landscape have seen the introduction of larger buildings with vast roof areas. It is anticipated that the onset of climate change will see increased intensities and volumes of rainfall which will place significant pressures on the roof drainage systems for these buildings potentially leading to failure and major flooding. There is an urgent need to adapt and the principal solution is the use of siphonic roof drainage systems. However, it has been identified that

there is a universal lack of the understanding of the hydraulic performance of siphonic systems, particularly when flow conditions are time varying.

Conventionally, roof drainage systems have been designed to safely convey the rainfall that runs off roof surfaces to the below ground drainage system. It is usual for the rainfall to be collected in a gutter and then conveyed to a downpipe, or series of downpipes, that are used to transfer the water from roof level to ground level. These gravity driven systems have worked well for many years and, in the UK, their design is based on methodologies outlined in BS EN 12056-3: 2000 Part 3: 'Gravity Roof Drainage, Layout and Calculation' (BSI 2000). However, in recent years the footprint of many buildings has increased significantly leading to large buildings with vast roof areas. Similarly architectural practice has changed with the use of new materials and exterior surface finishes which provide elegance and intricate aesthetic appearance that incorporates concealed roof drainage systems. The use of conventional roof drainage for such buildings requires large gutters and a large number of downpipes and associated pipework.

As a consequence the worldwide construction industry has seen the introduction of siphonic roof drainage systems. These have the advantage that their capacity is significantly greater than that of conventional systems and hence can drain much larger volumes of rainfall in a shorter period of time. They also require less pipework as a single carrier is used to drain several outlets within the gutter. Siphonic systems also have the advantage that they can be more easily upgraded or retro-fitted onto existing buildings to accommodate future increases in the frequency and severity of extreme rainfall events with the onset of climate change.

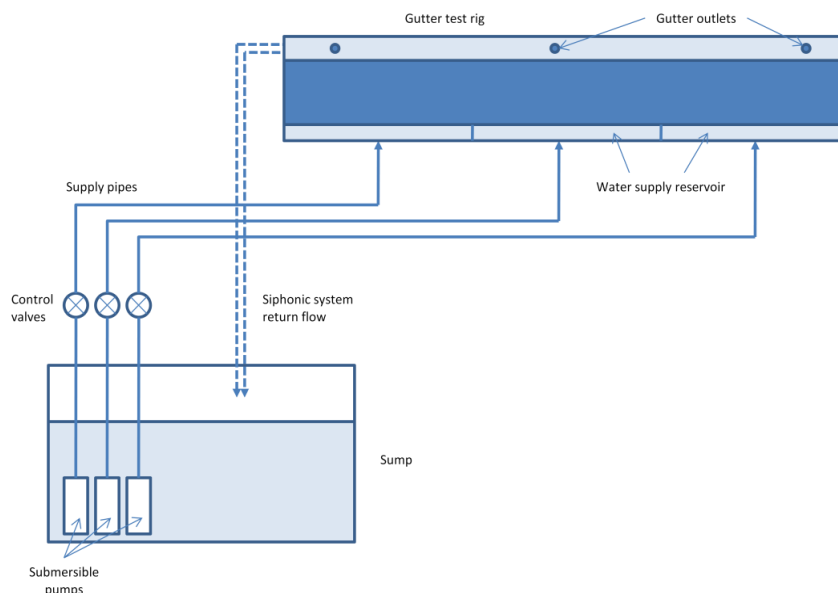
Previous research has reported the benefits of siphonic systems (Arthur and Swaffield 2001; Wright et al. 2002). However, to achieve these benefits, the system must prime. The priming mechanism is extremely complex and existing design standards (BSI 2000; BSI 2007), recognise that there is no available analytical method that satisfactorily describes the process. Of equal significance and concern is that it is not certain that any given system will prime (Arthur and Wright 2007). Guidance is given in Section 8.8 of BS 8490:2007, 'Guide to Siphonic Roof Drainage Systems', but this has been demonstrated to be based on a number of fallacies (Arthur and Wright 2007).

Whilst some current design methodologies assume that the proportions of flow through each outlet within a common gutter are the same, previous research has reported that this is not the case. Furthermore, under time-varying flow conditions it has been shown that pressure fluctuations may cause the system to deprime with the catastrophic consequence that there is a rapid rate of the rise of flow depth within the gutter resulting in system failure.

An experimental study has been undertaken using the full-scale test facility at the University of Sheffield to improve the understanding of the hydraulic performance of multi-outlet siphonic roof drainage systems. This paper presents the results from the feasibility tests and an assessment of the suitability of the experimental measurement methods. The reported tests include a series of novel experiments using high speed image velocimetry and a unique approach that uses a fluorescein tracer to measure the flow component through each outlet. Proposed future tests are also reported including a systematic study of changes to the configuration of the outlets within the common gutter.

## 2 Experimental Study

The full scale siphonic roof drainage experimental test facility is positioned on the mezzanine roof of the structures laboratory of the Sir Frederick Mappin Building of the University of Sheffield. Figure 1 provides a schematic of the experimental test facility.



**Figure 1 Schematic of the Experimental Test Facility (not to scale)**

The test facility has a gutter length of 35 m and a working head of 9.5 m. The supply of water to the rig is transferred from a 272 m<sup>3</sup> sump via three independent pumps highlighted in Figure 1. Each supply pipe incorporates a computer controlled butterfly valve controlled using real time control technology and recorded using LabView software. The water is supplied from the pipes into three supply reservoirs from where it spills over a knife-edged weir, onto the roof section and into the gutter.

The gutter dimensions are 600 mm wide by 150 mm deep with a 1.2 m wide roof section constructed from profiled roofing sheet at a pitch of 6°. Both the roof and gutter are fitted according to standard construction industry practice (Bramhall 2006).

The tailpipes and carrier pipes are manufactured from annealed cast acrylic with a wall thickness of 5 mm. The sizing and configuration of the pipework was completed using commercially available software based on the Bernoulli Energy Equation and the Colebrook White Equation. The system was designed as a primary system with three commercially available siphonic outlets fitted within the gutter sole. Design flow and operating pressure of the system was 30.0 l/s and -3.23 mH<sub>2</sub>O respectively with an ultimate flow of 35.1 l/s and ultimate operating pressure of -4.67 mH<sub>2</sub>O (Table 1).

**Table 1 Summary of Outlet Inflows and Reserves**

Outlet	Design inflow (l/s)	Reserve		Ultimate inflow (l/s)	Reserve	
		m	%		m	(%)
A	10.0	2.69	27	11.7	0.000	0
B	10.0	2.60	26	11.3	-0.025	0
C	10.0	2.70	27	12.1	0.024	0

## 2.1 Methodology

A series of feasibility tests were undertaken to assess, review and optimise the methods of flow measurement. The tests were completed to refine the measurement and data collection techniques and to determine the relative proportions of flow passing through each outlet. A number of tests were undertaken covering a range of flow rates that included both sub-prime and primed siphonic action. It was important to examine and understand the hydraulic performance over this flow range as siphonic systems predominantly perform at sub-prime conditions (Öngören and Materna 2006). Each section of the gutter was supplied with the same flow rate from 2 l/s to 14 l/s in 1 l/s increments. This is equivalent to a total flow rate through the system from 6 l/s to 42 l/s.

For each feasibility test, the following measurements were recorded:

1. Water depth within the common gutter
2. System pressure within the horizontal carrier pipe
3. Flow rate within the horizontal carrier pipe measured using flourometry
4. Flow velocity within the horizontal carrier pipe measured using high speed image velocimetry

### 2.1.1 Water Depth Measurements

Water depth measurements were made using a digital depth micrometer fitted to a frame that could be moved along the length of the gutter (Figure 2).



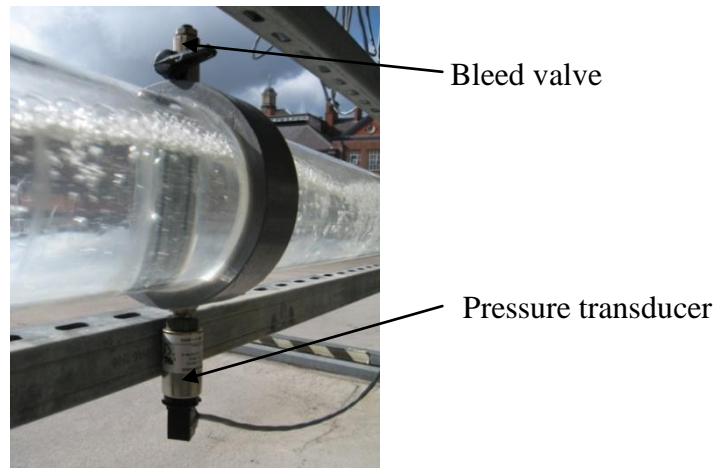
**Figure 2 Digital Depth Micrometer and Frame**

Water depth measurements were made 150 mm either side of each outlet in accordance with Section B.2.6 of BS 8490:2007 Guide to Siphonic Roof Drainage Systems (BSI 2007). Two further depth measurements were made at 50 mm around the perimeter of the outlet to monitor the effect of draw down. Five water depth measurements were also made between each outlet including the midpoint, 0.5 metres and 1 metre either side of the midpoint. Two further water depth measurements were also made 0.5 metres and 1 metre from each gutter end.

### 2.1.2 System Pressure

Five pressure transducers were installed within the system to monitor pressure with a range of -1 Bar to 0.6 Bar (equivalent to -10 m to 6 m pressure head) with an accuracy of 0.15%, equivalent to 24 mm. Three transducers were positioned 2 metres downstream of where each tail pipe entered the horizontal carrier pipe. This distance from the junction was selected to reduce the risk of high pressure fluctuations closer to the fittings. A further transducer was located at the end of the horizontal carrier pipe and at the system outlet.

To record an average pressure around the circumference of the pipe, a unique collar was designed and manufactured. The collar featured two rubber o-rings either side of a 6 mm by 6 mm bevel. Four 4 mm holes were drilled into the carrier pipe at the crown, invert and horizontal sides of the pipe wall and the collar slid over the pipe so the holes were positioned in the bevel. Sealant was then applied between the edge of the collar and the carrier pipe to create an airtight seal. Each pressure transducer was positioned at the invert of the collar and a simple bleed valve attached to the crown to enable the removal of any air blocks (Figure 3). This configuration enabled the average pressure to be taken around the circumference of the carrier pipe.



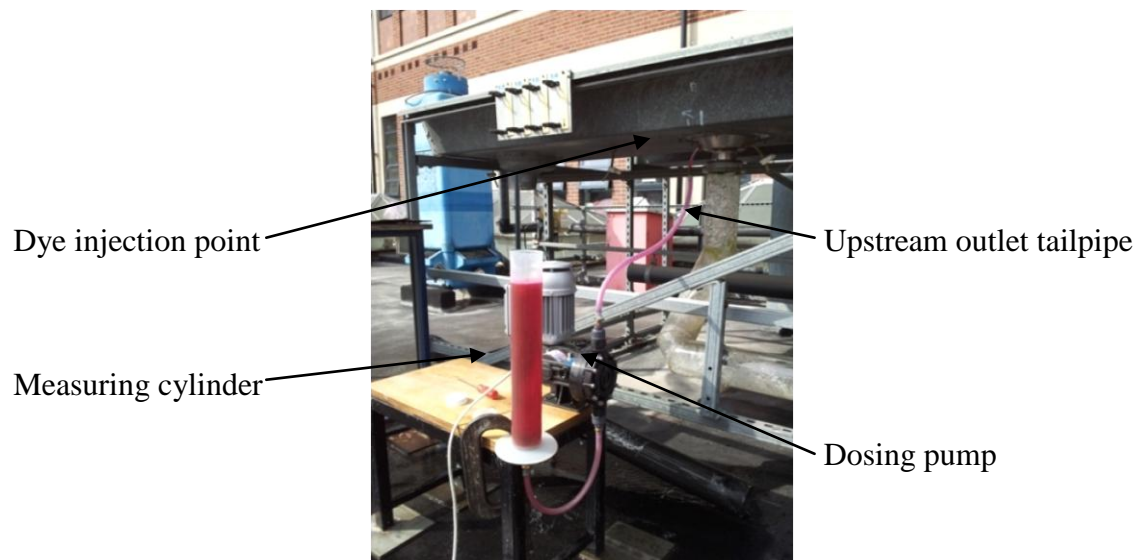
**Figure 3 Pressure Transducer Collar In-Situ**

### *2.1.3 Fluorometry*

To measure the flow rate within the horizontal carrier pipe a unique approach using a fluorescein tracer was used to measure the flow component through each outlet. Three submersible fluorimeters were fitted within the horizontal carrier pipe downstream of each tail pipe such that the sensor was exposed to the main body of the flow, but with a minimum of disruption. A further fluorimeter was fitted within the supply reservoir to record the background solute levels.

The fluorimeters are able to detect a change in solute concentration of Rhodamine WT with a sensitivity of 4 ppb. A temperature probe with an accuracy of  $\pm 0.3^{\circ}\text{C}$  was also fitted within the supply reservoir to allow for temperature correction. For the feasibility tests, Rhodamine WT dye was injected into the outlet bowl of the upstream outlet using a dosing pump. The configuration of the apparatus is shown in Figure 4.





**Figure 4 Feasibility Tests Dye Injection Apparatus Configuration**

For each feasibility test, 1 litre of Rhodamine WT dye at a concentration of  $5 \times 10^{-4}$  ( $C_{in}$ ) was pumped from the measuring cylinder into the bowl of the upstream outlet. The turbulence within the outlet bowl and tail pipe was sufficient to ensure the dye was fully mixed before reaching the first measurement point. The dye injection rate ( $q_{in}$ ) was measured volumetrically recording the time taken to dose every 100 ml of dye.

The raw values recorded by each fluourometer were first resolved to a common temperature according to the following calculation (Wilson, 1968):

$$F_r = F_s e^{[n(T_s - T_r)]}$$

Where  $F_r$  is the calculated fluorescent reading at the reference temperature,  $F_s$  is the observed fluorescence reading of the sample at the time of reading the sample temperature,  $e$  is the base of natural log,  $n$  is the temperature coefficient of the dye used (0.026 for Rhodamine WT),  $T_s$  is the sample temperature at the time of reading  $F_s$  and  $T_r$  is the reference temperature.

For the feasibility tests the observed fluorescence readings were resolved to a common temperature of 20°C. The appropriate calibration was then applied to the resolved readings to calculate the concentration of dye ( $C$ ) at each measurement point.

The position of each of the fluoumeters within the test facility was selected to assess the flow rate through each outlet based on the measured dilution of the dye:

$$q_{in} C_{in} = Q_{F1} C_{F1}$$

Where  $q_{in}$  is the dye injection rate,  $C_{in}$  the concentration of dye injected,  $Q_{F1}$  the flow rate at fluoumeter point 1 and  $C_{F1}$  is the concentration of dye at  $F1$ . This equation can be rearranged to:

$$Q_{F1} = \frac{q_{in} C_{in}}{C_{F1}}$$

The background solute level was measured to accurately determine the flow rate at the location of each flourometer:

$$Q_{Fn} = \frac{q_{in} C_{in}}{C_{Fn} - C_{FB}}$$

Where  $C_{FB}$  the concentration of the background solute level,  $C_{Fn}$  and  $Q_{Fn}$  is the concentration of dye and flow rate at each flourometer location respectively.

#### 2.1.4 High Speed Image Velocimetry

High speed image velocimetry feasibility tests were necessary to assess the quality of image produced within the test environment and the flow velocity results following Particle Image Velocimetry (PIV) analysis.

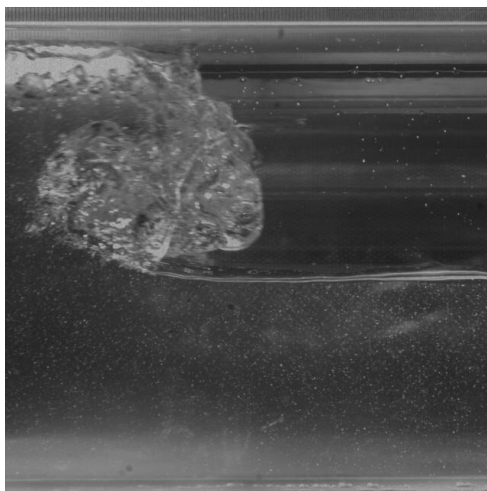
The feasibility tests were completed using a Photron Fastcam XLR high speed camera to record images of the flow within the horizontal carrier pipe. To reduce distortion of the images as a result of the curvature of the pipe, a glass fronted water box was designed, manufactured and installed at three points along the length of the carrier pipe downstream of each tailpipe. The configuration of the apparatus is shown in Figure 5.



**Figure 5 Configuration of the High Speed Image Velocimetry Apparatus**

For each test, the flow was seeded using inert, white, plastic particles with a diameter of 150  $\mu\text{m}$  and density of 1000  $\text{kg}/\text{m}^3$ . Blackout material was fitted to the pipe behind the water box to provide sufficient contrast for the particle seeding to be observed. Additional lighting was required to be able to view the images being recorded at the required frequency.

Prior to testing, the water box was filled with water and a graduated steel rule placed along the crown of the pipe. The rule was required to be able to scale the images for analysis. The camera was positioned in front of the water box and the image field adjusted to include the pipe and steel rule. An example image is shown in Figure 6.



**Figure 6 Image of Seeded Flow within the Horizontal Carrier Pipe**

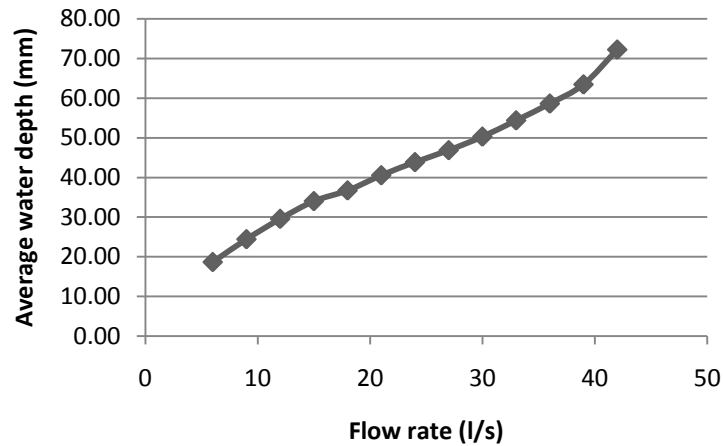
For the feasibility tests the camera was set to record images at a frequency of 2000 Hz. 10 consecutive images every 1000 were selected for analysis representing a flow measurement point every 0.5 seconds. The images were then analysed using PIV software to determine the local flow velocity within the horizontal carrier pipe at each measurement point:

1. For each set of images the field of view was adjusted for the size of the image
2. Cross-referencing of each image relative to the next one was completed producing nine vector analysis results
3. Range validation was applied to the vector analysis results to eliminate spurious readings detected outside of the flow field
4. Statistical analysis of the validated, vector analysis results was completed. One result was generated of the average flow velocity from the nine, validated, vector analysis results.
5. The average of the flow velocity results from was calculated. Any results less than 0.01 m/s were excluded from the average so that stationary objects within the image did not skew the resulting mean.
6. The average flow velocity for that half second interval was plotted.

## **2.2 Results**

### *2.2.1 Water Depth Results*

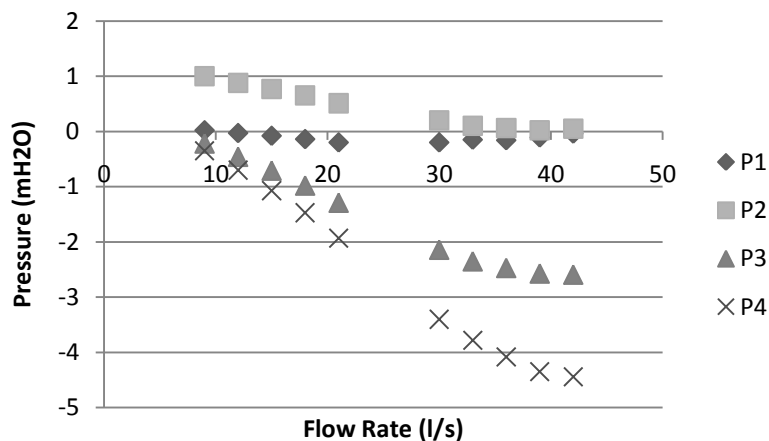
The water depth along the length of the gutter was recorded three times for each steady flow test in accordance with the methodology outlined in Section 2.1.1. Figure 7 shows the average water depth along the length of the gutter at the different test flow rates.



**Figure 7 Average Water Depth within the Gutter**

2.2.2 System Pressure Results

Figure 8 shows a plot of the mean pressure values at each measurement point for the series of feasibility tests.



**Figure 8 Plot of Feasibility Test Pressure Measurements**

The results show that at the upstream monitoring position (P1), there was minimal change in pressure irrespective of the flow rate through the system. A maximum pressure of -0.2 mH<sub>2</sub>O was recorded during the tests completed at 21 l/s and 30 l/s. The system pressure after the second tailpipe (P2) steadily decreased from a positive pressure of 1 mH<sub>2</sub>O to less than 0.1 mH<sub>2</sub>O at test flow rates greater than 36 l/s. The pressure transducer located downstream of the third tailpipe (P3) showed a steady pressure decrease throughout the tests from -0.22 mH<sub>2</sub>O at 9 l/s to -2.59 mH<sub>2</sub>O at 42 l/s. The transducer located at the top of the downpipe (P4) showed the most significant change in system pressure. The results decreased from -0.35 mH<sub>2</sub>O at 9 l/s to -4.44 mH<sub>2</sub>O at 42 l/s.

Table 2 provides a comparison of the calculated and measured system pressures at the design and ultimate flow rates outlined in Section 2.

**Table 2 Calculated and Measured System Pressure Comparison**

Flow Rate (l/s)	Calculated System Pressure (mH <sub>2</sub> O)	Measured System Pressure (mH <sub>2</sub> O)
30 (Design)	-3.23	-3.40
35.12 (Ultimate)	-4.67	-4.00 (extrapolated)

The results in Table 2 show that although the calculated and measured system pressures at the design flow rate of 30 l/s were similar, there is a difference in the ultimate flow results. Even at a flow rate of 42 l/s, the measured system pressure of -4.44 mH<sub>2</sub>O was less than the calculated pressure at ultimate flow.

### 2.2.3 Fluorometry Results

Figure 9 provides an example of the results measured using fluorometry. The graph shows the individual components of flow measured by each fluorometer at the design flow rate of 30 l/s.

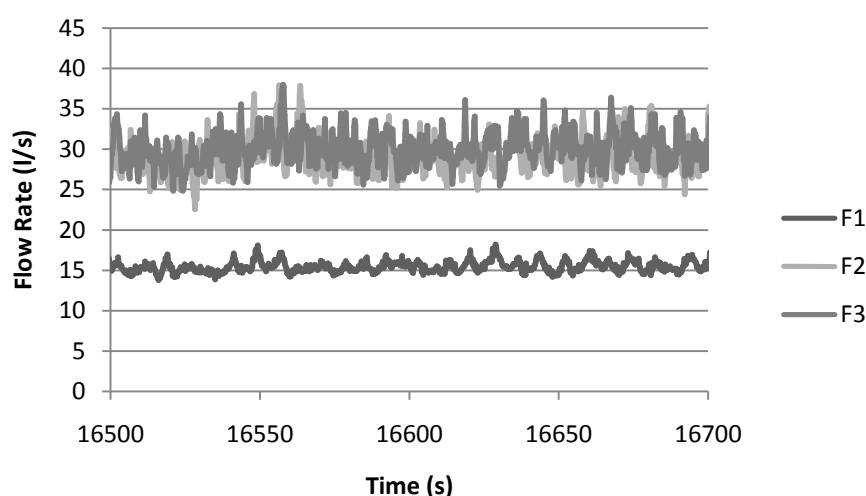
**Figure 9 Flow Proportionality Measured at the Design Flow Rate of 30 l/s**

Table 3 shows the average flow rate and flow proportionality measured by each fluorometer for the series of feasibility tests.

**Table 3 Flow Proportionality Measured using Fluorometry**

Test l/s	F1		F2		F3
	l/s	%	l/s	%	l/s
9	4.82	52.1	8.85	95.7	9.25
15	7.42	48.8	15.4	101	15.2
18	8.99	49.7	19.2	106	18.1
21	9.95	47.2	20.1	95.3	21.1
30	15.6	51.8	29.6	98.3	30.1
33	18.9	59.6	32.4	102	31.7
36	20.0	57.3	33.5	96.0	34.9
39	20.5	52.6	33.3	85.4	39.0
42	21.0	50.0	35.0	83.3	42.0

The results in Table 3 show that equal proportions of flow were not measured through each outlet. For the design flow rate of 30 l/s, 51.8% of the flow was measured through the upstream outlet (A) and a further 46.5% through Outlet B. This is a consistent observation for

each of the tests. The total flow through the system measured downstream of Outlet C (F3) was within 4% of the volumetrically calibrated flow input.

2.2.3 High Speed Image Velocimetry Results

Figure 10 shows the flow velocity results based on the PIV analysis of the images collected using the high speed camera positioned downstream of Outlet A.

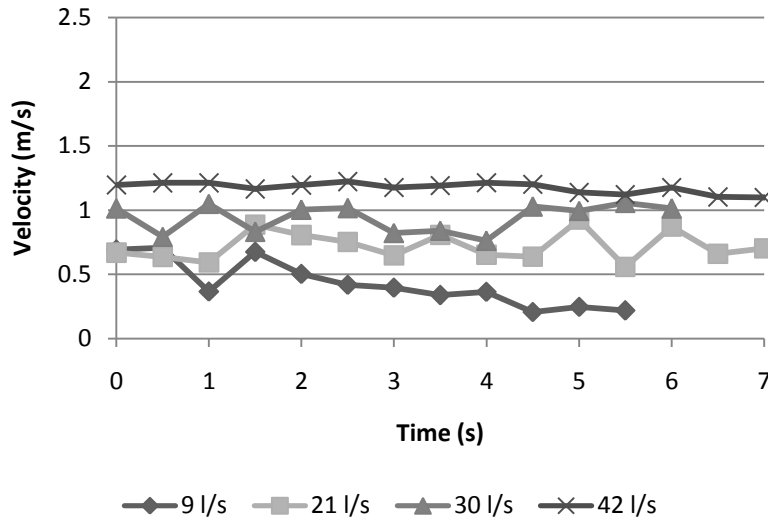


Figure 10 Flow Velocity Results Measured using Fluorometry (Outlet A)

The results are limited in terms of the duration of each test at less than 7 seconds. However, clear difference can be seen in terms of the flow velocity profile for each of the tests reported. Fully primed flow conditions were observed during the 42 l/s test which is reflected in the velocity results. Sub-prime conditions were observed in each of the other tests which demonstrate a greater degree of flow variation.

Figure 11 shows the flow velocity results based on the PIV analysis of the images collected using the high speed camera positioned downstream of Outlet B.

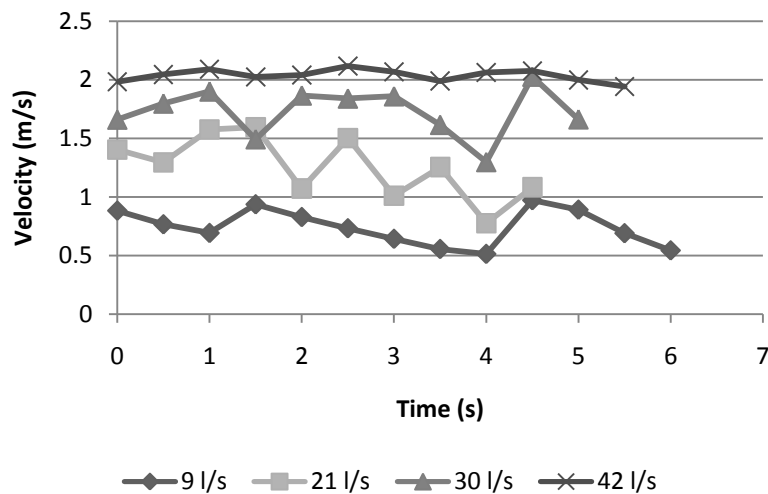


Figure 11 Flow Velocity Results Measured using Fluorometry (Outlet B)

Similar to the results observed in Figure 10, fully primed flow conditions were evident during the test completed at 42 l/s. For each of the other tests reported, the flow velocity varied in comparison. The flow velocity measured during the 9 l/s test demonstrated a profile indicative of pulsed or plug flow. This was not observed downstream of Outlet A (Figure 10). This would suggest that within a multi-outlet siphonic system, different flow phases occur along the length of the horizontal carrier pipe.

### 2.3 Proposed Future Tests

During the feasibility tests, the methods of measurements were conducted independently to refine each scientific technique. The next phase of steady state tests will involve running each method of flow and pressure measurement simultaneously. This will provide a direct, temporal and spatial comparison between each of the methods of measurement. Furthermore, this will enable an evaluation of the interaction of flow and system pressures on proportionality and priming within a multi-outlet siphonic system for both sub-prime and primed conditions. Following this phase of testing and analysis, a systematic study of changes to the configuration of the outlets within the common gutter will be undertaken.

### Acknowledgments

The authors would like to thank the help and support of Dr Martyn Bramhall of Fullflow Group Ltd, Dr Terry Lucke of the University of the Sunshine Coast and Professor Simon Tait of the University of Bradford.

### 3 References

- Arthur, S. and J. A. Swaffield (2001). "Siphonic Roof Drainage: Current Understanding." *Urban Water* 3(1): 43-52.
- Arthur, S. and G. B. Wright (2007). "Siphonic Roof Drainage Systems - Priming Focused Design." *Building and Environment* 42: 2421-2431
- Bramhall, M. (2006). *The Performance of Syphonic Rainwater Outlets within Gutters*. Civil & Structural Engineering, The University of Sheffield. PhD
- BSI (2000). British Standards Institute. BS EN 12056-3:2000. Gravity Drainage Systems Inside Buildings. Part 3: Roof Drainage, Layout and Calculation.
- BSI (2007). "British Standards Institute. BS 8490:2007. Guide to Siphonic Roof Drainage Systems."
- Öngören, A. and R. Materna (2006). Multi-phase flow characteristics of a siphonic roof drainage system under part load conditions. 32nd International Symposium on CIB W062 Water Supply and Drainage for Buildings, Taipei.
- Wilson, J. F. (1968). *Fluorometric Procedures for Dye Tracing*. Techniques of Water-Resources Investigations of the U.S. Geological Survey, Book 3 (Applications of Hydraulics), Chapter A12, 31 p.
- Wright, G. B., J. A. Swaffield and S. Arthur (2002). "The Performance Characteristics of Multi-Outlet Siphonic Roof Drainage Systems." *Building Serv Eng Res Technol* 23(3): 127-141

## 4 Presentation of Authors

Kieran Williams is the Development Manager at Environmental Monitoring Solutions Ltd. He has a BSc (Hons) in Environmental Science and Geography, an MSc in Water and Environmental Engineering and an MPhil on In-Sewer Sedimentation. He has worked as a Senior Research Scientist for Thames Water, is a Chartered Scientist, member of CIWEM and is currently undertaking a part-time PhD on the Hydraulic Performance of Siphonic Roof Drainage Systems at the University of Sheffield.



Professor Adrian Saul is the Yorkshire Water Professor of Water Engineering, Director of the Pennine Water Group at the University of Sheffield and a Fellow of the Institution of Civil Engineers. He has over 30 years post-doctoral experience working in the areas of urban storm drainage and potable water distribution systems and has published over 200 papers, with awards including a Millennium Product Award and an ICE Telford prize.





## **Appendix 7 - Details of Equipment Used**

## 2200 Series / 2600 Series – General Purpose Industrial Pressure Transducers

- ▶ Gauge, Absolute, Vacuum and Compound Pressure Models Available
- ▶ Submersible, General Purpose and Wash Down Enclosures
- ▶ High Stability Achieved by CVD Sensing Element
- ▶ Millivolt, Voltage and Current Output Models

The 2200 series features stability and accuracy in a variety of enclosure options. The 2600 series extends the packaging options via an all welded stainless steel back end for demanding submersible and industrial applications. The 2200 and the 2600 feature proven CVD sensing technology, an ASIC (amplified units), and modular packaging to provide a sensor line that can easily accommodate specials while not sacrificing high performance.

### Specifications

<b>Input</b>	
<b>Pressure Range</b>	Vacuum to 6000 psi (400 bar)
<b>Proof Pressure</b>	2 x Full Scale (FS) (1.5 x Fs for 400 bar, ≥ 5000 psi)
<b>Burst Pressure</b>	>35 x FS ≤ 100 psi (6 bar); >20 x FS ≥ 1000 psi (60 bar); >5 x FS ≤ 6000 psi (400 bar)
<b>Fatigue Life</b>	Designed for more than 100 million FS cycles
<b>Performance</b>	
<b>Long Term Drift</b>	0.2% FS/year (non-cumulative)
<b>Accuracy</b>	0.25 % FS typical (optional 0.15% FS)
<b>Thermal Error</b>	1.5% FS typical (optional 1% FS)
<b>Compensated Temperatures</b>	-5°F to +180°F (-20°C to +80°C)
<b>Operating Temperatures</b>	-40°F to +260°F (-40°C to +125°C) for elec. codes A, B, C, 1 -5°F to +180°F (-20°C to +80°C) for elec. codes 2, D, G, 3 -5°F to +125°F (-20°C to +50°C) for elec. codes F, M, P Amplified units >100°C maximum 24 VDC supply
<b>Zero Tolerance</b>	1% of span
<b>Span Tolerance</b>	1% of span
<b>Response Time</b>	0.5 ms
<b>Mechanical Configuration</b>	
<b>Pressure Port</b>	See ordering chart
<b>Wetted Parts</b>	17-4 PH Stainless Steel
<b>Electrical Connection</b>	See ordering chart
<b>Enclosure</b>	316 ss, 17-4 PH ss IP65 NEMA 4 for elec. codes A, B, C, D, G, 1, 2, 3 IP67 for elec. code "F" IP68 for elec. codes M, (max depth 200 meters H <sub>2</sub> O) IP30 for elec. code "3" with flying leads
<b>Vibration</b>	70g, peak to peak sinusoidal, 5 to 2000 Hz (Random Vibration: 20 to 2000 Hz @ ≈20g Peak per MIL-STD.-810E Method 514.4)
<b>Acceleration</b>	100g steady acceleration in any direction 0.032% FS/g for 15 psi (1 bar) range decreasing logarithmically to 0.0007% FS/g for 6000 psi (400 bar) range.
<b>Shock</b>	20g, 11 ms, per MIL-STD.-810E Method 516.4 Procedure I
<b>Approvals</b>	CE, UR (22IC, 26IC, 22CS, 26CS)
<b>Weight</b>	Approx. 100 grams (additional cable; 75 g/m)

Series 2200



Series 2600



## Individual Specifications

<b>Millivolt Output units</b>	
Output	100 mV (10 mv/v)
Supply Voltage (Vs)	10 VDC (15 VDC max.) Regulated
Bridge resistance	2600-6000 ohms
<b>Voltage Output units</b>	
Output	see ordering chart
Supply Voltage (Vs)	1.5 VDC above span to 35 VDC @ 6 mA
Supply Voltage Sensitivity	0.01% FS/Volt
Min. Load Resistance	(FS output / 2) Kohms
Current Consumption	approx 6 mA at 7.5V output
<b>Current Output units</b>	
Output	4-20 mA (2 wire)
Supply Voltage (Vs)	24 VDC, (7-35 VDC)
Supply Voltage Sensitivity	0.01% FS/Volt
Max. Loop Resistance	(Vs-7) x 50 ohms

## Electromagnetic Capability

Meets the requirement for CE marking of EN50081-2 for emissions and EN50082-2 for susceptibility.

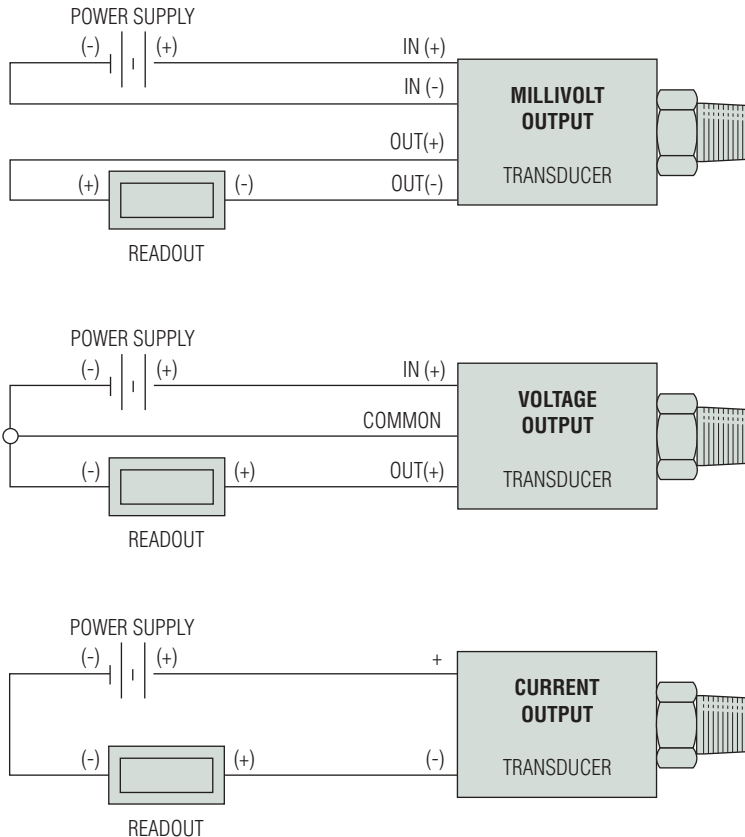
### Test Data:

- EN61000-4-2 Electrostatic Discharge. 8kV air discharge, 4kV contact discharge. Unit survived.
- ENV50140 Radiated RF Susceptibility. 10V/m, 80MHz-1GHz, 1kHz mod. Maximum recorded output error was  $<\pm 1\%$
- ENV50204 Radiated RF Susceptibility to Mobile Telephones. 10V/m, 900MHz. Maximum recorded output error was  $<\pm 1\%$ .
- EN61000-4-4 Fast Burst Transient. 2kV, 5/50ns, 5kHz for 1 minute. Unit survived.
- ENV50141 Conducted RF Susceptibility. 10Vms, 1kHz mod, 150kHz - 80MHz. Maximum recorded output error was  $<\pm 1\%$

Connection Code		mV units				Voltage units				Current units (4-20mA)		
		IN+	OUT+	OUT-	IN-	IN+	COM	OUT+	EARTH	(+)	(-)	EARTH
A, B, G	"DIN" PIN	1	2	3	E	1	2	3	4	1	2	4
C	"10-6 Bayonet" PIN	A	B	C	D	A	C	B	E	A	B	E
D	"cable"	R	Y	BL	G	R	BK	W	DRAIN	R	BK	DRAIN
F	"IP 67 cable"	R	Y	BL	G	R	BK	W	DRAIN	R	BK	DRAIN
M	"Immersible"	R	Y	BL	W	R	W	Y	DRAIN	R	BL	DRAIN
1	"8-4 Bayonet" PIN	A	B	C	D	A	C	B	D	A	B	D
2	"cable"	R	W	G	BK	R	BK	W	DRAIN	R	BK	DRAIN
3	"conduit & cable"	R	W	G	BK	R	BK	W	DRAIN	R	BK	DRAIN


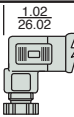
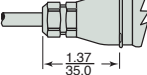
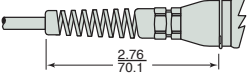
### Cable Legend:

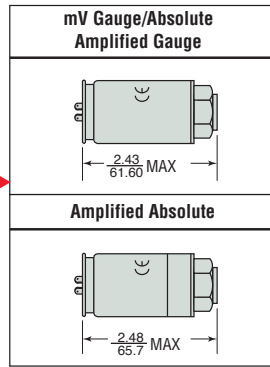
R = Red  
 BL = Blue  
 BK = Black  
 W = White  
 Y = Yellow



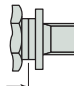
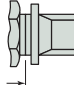
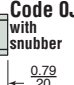
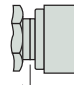
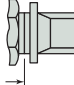
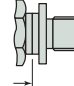
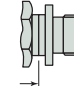

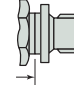
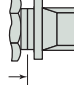
## Dimensions

### 2200 Series

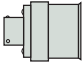
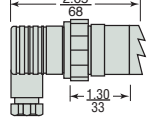
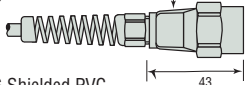
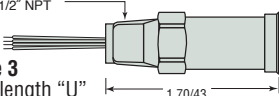
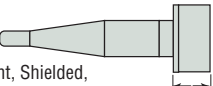
<b>Mini 4 Pin - No Connector</b>
<b>Code B</b> 
<b>Mini 4 Pin - With Connector</b>
<b>Code A</b>  1.02 26.02
<b>IP67 Cable (Waterproof)</b>
<b>Code F</b>  1.37 35.0
24 AWG Shielded PVC
<b>IP65 or NEMA4 Cable</b>
<b>Code D or 2</b>  2.76 70.1
24 AWG Shielded PVC

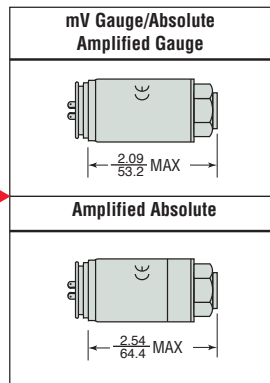


Maximum diameter 1.07" (27.3 mm)

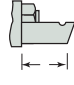
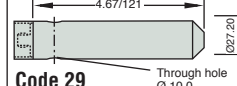
<b>1/8-27 NPT</b>
<b>Code 08</b>  0.59 15
<b>1/4 - 18 NPT</b>
<b>Code 02 with snubber</b>  0.79 20
<b>Code OJ with snubber</b> 
<b>1/4-18 NPT Internal</b>
<b>Code 0E</b>  0.95 24
<b>1/2-14 NPT</b>
<b>Code 0H</b>  1.02 26.0
<b>7/16-20 UNF-2A</b>
<b>Code 04</b>  0.75 19
<b>9/16-18 UNF-2A</b>
<b>Code 1P</b>  0.67 17
<b>G 1/8 Internal</b>
<b>Code 09</b> 
<b>G 1/4 External</b>
<b>Code 01</b>  0.67 17
<b>R 1/4</b>
<b>Code 0A</b>  0.79 20

### 2600 Series

<b>10-6 or 8-4 Mil-C Connector</b>
<b>10-6 Code C</b>  0.87 22
<b>8-4 Code 1</b>
<b>Large DIN 43650 Plug</b>
<b>Code G</b>  2.65 68 1.30 33
<b>Conduit Connector with Cable</b>
<b>Code 3</b> 1/2" NPT  43 1.70
24 AWG Shielded PVC
<b>Conduit Connector with Flying Leads</b>
<b>Code 3</b> 1/2" NPT with length "U"  1.70/43
<b>Moulded, Immersible Cable</b>
<b>Code M</b> 24 AWG, Vent, Shielded, Polyurethane  0.90 23



Maximum diameter 1.07" (27.3 mm)

<b>Nose Cone - Black Acetal</b>
<b>Code 19</b>  0.75 19
<b>Nose Cone Sink Weight</b>
<b>Code 29</b>  4.67/121 0.87/20 Through hole Ø 10.0

inch  
mm

## How to Order

Use the **bold** characters from the chart below to construct a product code

<p><b>Series</b></p> <p><b>2200</b>      <b>2600</b></p> <p><b>Output</b></p> <p><b>A</b> - 100 mV    <b>C</b> - 1-6V      <b>J</b> - 0.5-5.5V    <b>G</b> - 0.2-10.2V  <b>B</b> - 4-20mA    <b>D</b> - 1-11V     <b>R</b> - 0-5V        <b>F</b> - 0.1-5.1V                       <b>H</b> - 1-5V      <b>S</b> - 0-10V</p> <p><b>Pressure Datum</b></p> <p><b>A*</b> - Absolute    <b>G</b> - Gauge  *Max absolute range is 25 bar. (≤ 300 psi)</p> <p><b>Pressure Range<sup>3</sup> - psi</b></p> <table border="0"> <tr> <td><b>F07</b> - 0-7.5</td> <td><b>G60</b> - 0-600</td> <td><b>Vac</b> = -15 psi</td> </tr> <tr> <td><b>F15</b> - 0-15</td> <td><b>H10</b> - 0-1,000</td> <td><b>1F5</b> - Vac-0</td> </tr> <tr> <td><b>F30</b> - 0-30</td> <td><b>H15</b> - 0-1,500</td> <td><b>3F0</b> - Vac-15</td> </tr> <tr> <td><b>F60</b> - 0-60</td> <td><b>H20</b> - 0-2,000</td> <td><b>6F0</b> - Vac-45</td> </tr> <tr> <td><b>G10</b> - 0-100</td> <td><b>H30</b> - 0-3,000</td> <td><b>1G0</b> - Vac-85</td> </tr> <tr> <td><b>G15</b> - 0-150</td> <td><b>H40</b> - 0-4,000</td> <td><b>1G5</b> - Vac-135</td> </tr> <tr> <td><b>G20</b> - 0-200</td> <td><b>H50</b> - 0-5,000</td> <td><b>2G0</b> - Vac-185</td> </tr> <tr> <td><b>G30</b> - 0-300</td> <td><b>H60</b> - 0-6,000</td> <td><b>3G0</b> - Vac-285</td> </tr> <tr> <td><b>G50</b> - 0-500</td> <td></td> <td></td> </tr> </table> <p><b>Pressure Range - bar</b></p> <table border="0"> <tr> <td><b>A10</b> - 0-1</td> <td><b>B25</b> - 0-25</td> <td><b>Vac</b> = -1 bar</td> </tr> <tr> <td><b>A16</b> - 0-1.6</td> <td><b>B40</b> - 0-40</td> <td><b>1A0</b> - Vac-0</td> </tr> <tr> <td><b>A25</b> - 0-2.5</td> <td><b>B60</b> - 0-60</td> <td><b>1A6</b> - Vac-0.6</td> </tr> <tr> <td><b>A40</b> - 0-4</td> <td><b>C10</b> - 0-100</td> <td><b>2A5</b> - Vac-1.5</td> </tr> <tr> <td><b>A60</b> - 0-6</td> <td><b>C16</b> - 0-160</td> <td><b>4A0</b> - Vac-3</td> </tr> <tr> <td><b>B10</b> - 0-10</td> <td><b>C25</b> - 0-250</td> <td><b>6A0</b> - Vac-5</td> </tr> <tr> <td><b>B16</b> - 0-16</td> <td><b>C40</b> - 0-400</td> <td><b>1B0</b> - Vac-9</td> </tr> <tr> <td></td> <td></td> <td><b>1B6</b> - Vac-15</td> </tr> <tr> <td></td> <td></td> <td><b>2B5</b> - Vac-24</td> </tr> <tr> <td></td> <td></td> <td><b>4B0</b> - Vac-39</td> </tr> </table> <p><b>Pressure Port</b></p> <table border="0"> <tr> <td><b>08</b> - 1/8-27 NPT External</td> <td><b>09</b> - G1/8 Internal</td> </tr> <tr> <td><b>02</b> - 1/4-18 NPT External</td> <td><b>01</b> - G1/4 External</td> </tr> <tr> <td><b>0J</b> - 1/4 NPT External w/snubber</td> <td><b>0A</b> - R1/4 External</td> </tr> <tr> <td><b>0E</b> - 1/4 NPT Internal</td> <td>Submersible (2600 only)</td> </tr> <tr> <td><b>0H</b> - 1/2-14 NPT External</td> <td><b>19</b> - Plastic Nose Cone</td> </tr> <tr> <td><b>04</b> - 7/16-20 External (SAE #4, J514)</td> <td><b>29</b> - Sink Weight Nose Cone</td> </tr> <tr> <td><b>1P</b> - 9/16-18 External (SAE #6, J1926-2)</td> <td></td> </tr> <tr> <td><b>1J</b> - 7/16-20 External (SAE #4, J1926-2)</td> <td></td> </tr> </table>	<b>F07</b> - 0-7.5	<b>G60</b> - 0-600	<b>Vac</b> = -15 psi	<b>F15</b> - 0-15	<b>H10</b> - 0-1,000	<b>1F5</b> - Vac-0	<b>F30</b> - 0-30	<b>H15</b> - 0-1,500	<b>3F0</b> - Vac-15	<b>F60</b> - 0-60	<b>H20</b> - 0-2,000	<b>6F0</b> - Vac-45	<b>G10</b> - 0-100	<b>H30</b> - 0-3,000	<b>1G0</b> - Vac-85	<b>G15</b> - 0-150	<b>H40</b> - 0-4,000	<b>1G5</b> - Vac-135	<b>G20</b> - 0-200	<b>H50</b> - 0-5,000	<b>2G0</b> - Vac-185	<b>G30</b> - 0-300	<b>H60</b> - 0-6,000	<b>3G0</b> - Vac-285	<b>G50</b> - 0-500			<b>A10</b> - 0-1	<b>B25</b> - 0-25	<b>Vac</b> = -1 bar	<b>A16</b> - 0-1.6	<b>B40</b> - 0-40	<b>1A0</b> - Vac-0	<b>A25</b> - 0-2.5	<b>B60</b> - 0-60	<b>1A6</b> - Vac-0.6	<b>A40</b> - 0-4	<b>C10</b> - 0-100	<b>2A5</b> - Vac-1.5	<b>A60</b> - 0-6	<b>C16</b> - 0-160	<b>4A0</b> - Vac-3	<b>B10</b> - 0-10	<b>C25</b> - 0-250	<b>6A0</b> - Vac-5	<b>B16</b> - 0-16	<b>C40</b> - 0-400	<b>1B0</b> - Vac-9			<b>1B6</b> - Vac-15			<b>2B5</b> - Vac-24			<b>4B0</b> - Vac-39	<b>08</b> - 1/8-27 NPT External	<b>09</b> - G1/8 Internal	<b>02</b> - 1/4-18 NPT External	<b>01</b> - G1/4 External	<b>0J</b> - 1/4 NPT External w/snubber	<b>0A</b> - R1/4 External	<b>0E</b> - 1/4 NPT Internal	Submersible (2600 only)	<b>0H</b> - 1/2-14 NPT External	<b>19</b> - Plastic Nose Cone	<b>04</b> - 7/16-20 External (SAE #4, J514)	<b>29</b> - Sink Weight Nose Cone	<b>1P</b> - 9/16-18 External (SAE #6, J1926-2)		<b>1J</b> - 7/16-20 External (SAE #4, J1926-2)		<p><b>2200</b>    <b>B</b>    <b>G</b>    <b>A60</b>    <b>01</b>    <b>A</b>    <b>3</b>    <b>U</b>    <b>A</b></p> <p>Performance Code</p> <p>Accuracy/Thermal  <b>A</b> - .25%/1.5%  <b>B</b> - .15%/1.0%</p> <p>Cable Length<sup>1</sup>  <b>U</b> - No Cable Fitted<sup>1 2</sup>  <b>D</b> - 1 Metre (3 feet)  <b>E</b> - 3 Metres (9 feet)  <b>F</b> - 5 Metres (16 feet)  <b>G</b> - 10 Metres (32 feet)</p> <p>Apparatus Protection  <b>2</b> - mV Only Transient Protection CE Mark, UR  <b>3</b> - Amplified Only RFI Protected CE Mark, UR</p> <p>Electrical Connection (See Notes)</p> <p>2200 Series  <b>A</b> - 4 PIN DIN (Micro) Mating Connector Supplied  <b>B</b> - 4 PIN DIN (Micro) Mating Connector Not Supplied  <b>2</b> - Cable Nema 4 USA  <b>D</b> - Cable European Color Code  <b>F</b> - Cable Gland Metal IP67</p> <p>2600 Series  <b>C</b> - Fixed Plug Size 10-6 Mating Plug Not Supplied  <b>G</b> - Fixed Plug To DIN 43650 Mating Plug Supplied  <b>M</b> - Moulded Cable Immersible  <b>1</b> - Fixed Plug Size 8-4 Mating Plug Not Supplied  <b>3</b> - Conduit Connector 1/2NPT Ext. 1M Cable<sup>2</sup></p> <p>Notes:</p> <ol style="list-style-type: none"> <li>When electrical connection is cable please select a cable length from Table 1 below. When electrical connection is DIN or plug style "U" must be specified.</li> <li>Where electrical connection -<b>3</b> and cable length -<b>U</b> occur in part number, the unit will be supplied with flying leads (4-1/2" IP30).</li> <li>Additional Pressure Ranges are available. Please consult factory.</li> </ol>
<b>F07</b> - 0-7.5	<b>G60</b> - 0-600	<b>Vac</b> = -15 psi																																																																								
<b>F15</b> - 0-15	<b>H10</b> - 0-1,000	<b>1F5</b> - Vac-0																																																																								
<b>F30</b> - 0-30	<b>H15</b> - 0-1,500	<b>3F0</b> - Vac-15																																																																								
<b>F60</b> - 0-60	<b>H20</b> - 0-2,000	<b>6F0</b> - Vac-45																																																																								
<b>G10</b> - 0-100	<b>H30</b> - 0-3,000	<b>1G0</b> - Vac-85																																																																								
<b>G15</b> - 0-150	<b>H40</b> - 0-4,000	<b>1G5</b> - Vac-135																																																																								
<b>G20</b> - 0-200	<b>H50</b> - 0-5,000	<b>2G0</b> - Vac-185																																																																								
<b>G30</b> - 0-300	<b>H60</b> - 0-6,000	<b>3G0</b> - Vac-285																																																																								
<b>G50</b> - 0-500																																																																										
<b>A10</b> - 0-1	<b>B25</b> - 0-25	<b>Vac</b> = -1 bar																																																																								
<b>A16</b> - 0-1.6	<b>B40</b> - 0-40	<b>1A0</b> - Vac-0																																																																								
<b>A25</b> - 0-2.5	<b>B60</b> - 0-60	<b>1A6</b> - Vac-0.6																																																																								
<b>A40</b> - 0-4	<b>C10</b> - 0-100	<b>2A5</b> - Vac-1.5																																																																								
<b>A60</b> - 0-6	<b>C16</b> - 0-160	<b>4A0</b> - Vac-3																																																																								
<b>B10</b> - 0-10	<b>C25</b> - 0-250	<b>6A0</b> - Vac-5																																																																								
<b>B16</b> - 0-16	<b>C40</b> - 0-400	<b>1B0</b> - Vac-9																																																																								
		<b>1B6</b> - Vac-15																																																																								
		<b>2B5</b> - Vac-24																																																																								
		<b>4B0</b> - Vac-39																																																																								
<b>08</b> - 1/8-27 NPT External	<b>09</b> - G1/8 Internal																																																																									
<b>02</b> - 1/4-18 NPT External	<b>01</b> - G1/4 External																																																																									
<b>0J</b> - 1/4 NPT External w/snubber	<b>0A</b> - R1/4 External																																																																									
<b>0E</b> - 1/4 NPT Internal	Submersible (2600 only)																																																																									
<b>0H</b> - 1/2-14 NPT External	<b>19</b> - Plastic Nose Cone																																																																									
<b>04</b> - 7/16-20 External (SAE #4, J514)	<b>29</b> - Sink Weight Nose Cone																																																																									
<b>1P</b> - 9/16-18 External (SAE #6, J1926-2)																																																																										
<b>1J</b> - 7/16-20 External (SAE #4, J1926-2)																																																																										

**PRESSURE TRANSDUCERS**



**Table 1 - Cable Length**  
(2600 Series) (2200 Series select "U" through "G")

Code	Length (M)	Code	Length (M)
<b>U</b>	No Cable Fitted	<b>M</b>	40
<b>D</b>	1	<b>N</b>	50
<b>E</b>	3	<b>P</b>	75
<b>F</b>	5	<b>Q</b>	100
<b>G</b>	10	<b>R</b>	125
<b>H</b>	15	<b>S</b>	150
<b>J</b>	20	<b>4</b>	170
<b>K</b>	25	<b>5</b>	200
<b>L</b>	30	<b>6</b>	225

Note: Maximum cable length on a 2200 is 10 meters.

# GigaView™

## Are You Sure You're Seeing the Whole Picture?

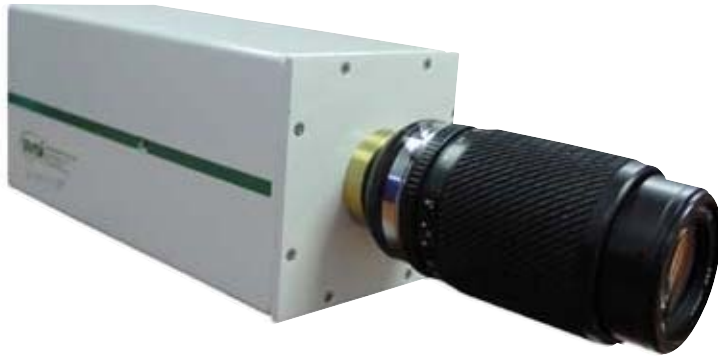
Record High Definition 1280x720 video at 750-fps to memory for 30-seconds when troubleshooting machinery, VGA 640x480 video at 250-fps to disk for 8-hours for monitoring and surveillance, or both at the same time. GigaView – a Gigabit Ethernet equipped high-speed digital video camera system is specifically designed for the difficulties of the production environment. GigaView is the only complete video solution that delivers the images you need to solve the problem...every time.



### Features

- 1280 x 720 HD resolution @ 750-fps to memory
- 640 x 480 VGA resolution @ 250-fps to hard disk
- 10 bit grayscale – More information per image
- Gigabit Ethernet Interface (GigE) – Robust TCP/IP connection for plant environment
- Up to 16 GB of memory – Extends traditional record times
- Image-Cued Triggering – Offers solution when an external trigger is unavailable
- Digital output for alarm or strobe





# GigaView™

## Specifications

### Continuous Streaming

Resolution: 640 x 480 @ 250-fps

Record Time: Up to 8-hours

### High Definition to Camera Memory

Resolution: 1280 x 720 @ 750-fps

Record Time: Up to 30-seconds

### Camera

Shutter: 1/50 – 1/500,000

Sensor: 10-bit mono or 24-bit color

Trigger Source: Standard TTL or

Image-Cued

Multiple-event recording capability

Lens Mount: C-mount\*

Interface: TCP/IP 100/1000-BaseT

Size: 4.25"x4.25"x11"

Weight: 3.4 lbs

Software: Video Record/Playback

*\* C-mount to F-mount adapter available.*

Process inspection, high-speed motion capture, and machine troubleshooting just got easier with SVSi's GigaView high-speed camera. Designed for true networked (TCP/IP) operation, GigaView can record an entire 8-hour shift of high-resolution high-speed video to diagnose equipment failures, power disruptions, or external interference. With the easiest-to-use software on the market (just turn it on and GigaView begins recording video), you can concentrate on maximizing efficiency.

GigaView reduces even the highest speed processes to slow-motion video that can be analyzed frame-by-frame. Through the combination of the highest resolution, longest record times, and fastest frame-rates, GigaView is the clear performance leader in high-speed video solutions for the production and packaging environments.

Mode	Resolution	Frame Rate (fps)	Recording Time	
			16-GB Memory	2.4-TB Hard Disk
Streaming	160 x 120	4,000	N/A	8-hours
	320 x 240	1,000	N/A	8-hours
	640 x 480	250	N/A	8-hours
	1280 x 1024	60	N/A	8-hours
Burst	320 x 240	2,200	25-sec	N/A
	640 x 480	1,135	25-sec	N/A
	1280 x 720	750	56-sec	N/A
	1280 x 1024	530	112-sec	N/A

### Image-Cued Trigger

A troubleshooting aid unique to GigaView is the ability to trigger the recording process from an event in the camera's field-of-view. If you know what happens but not when, GigaView can look for the event itself and record digital video before and after the fact with a minimum of excess frames so that you can go straight to the cause of the problem.

Southern Vision Systems, Inc.  
 8215 Madison Blvd, Suite 150  
 Madison, AL 35758  
 Phone: (256) 461-7143  
 Fax: (256) 461-7145  
 www.southernvisionsystems.com  
 email: info@southernvisionsystems.com



# CYCLOPS-7

SUBMERSIBLE SENSORS



## Cyclops-7 Submersible Sensors

The CYCLOPS-7 line of submersible sensors is a high performance, compact sensor at a significantly lower price than traditional submersible sensors. The CYCLOPS-7 combination of price, performance and size makes the sensor very attractive for oceanographic, freshwater and dye tracing applications.

## Designed for Integration

Cyclops-7 was designed specifically for integration into any platform that supplies power and datalogging.



## Cyclops-7 Highlights

- Extremely small size
  - 5.7" x 0.9" (SSt or Ti)
  - 5.7" x 1.25" (Delrin)
- Affordable price / excellent value
- Built-in light scatter rejection
- Low power consumption
- Integrates into a C6 Multi-Sensor Platform or any third-party platform
- Interfaces with DataBank Datalogger
- Cyclops-7 Submersible Logger Available
- Cyclops Explorer enables various lab applications

## Available Sensors

- Blue Green Algae
  - Phycoerythrin (marine)
  - Phycocyanin (freshwater)
- CDOM/FDOM
- Chlorophyll *in vivo*
  - Blue excitation
  - Red excitation
- Fluorescent Dye Tracing
  - Fluorescein
  - PTSA
  - Rhodamine
- Hydrocarbons
  - Crude Oil
  - Refined Fuels
- Turbidity
- Wastewater Monitoring
  - Optical Brighteners
  - Tryptophan

Custom Optics Available : 260-900 nm



## Fluorometer Performance

Linearity: 0.99R<sup>2</sup>

APPLICATION	MINIMUM DETECTION LIMIT	DYNAMIC RANGE
CDOM/FDOM	0.15 ppb**	0-1250 ppb**
	0.5 ppb***	0-5000 ppb***
Chlorophyll <i>in vivo</i>		
Blue excitation	0.025 µg/L	0-500 µg/L
Red excitation	0.5 µg/L	>500 µg/L
Fluorescein Dye	0.01 ppb	0-500 ppb
Oil - Crude	0.2 ppb***	0-2700 ppb***
Oil - Fine	10 ppb*	>10,000 ppb*
	10 ppm****	>100 ppm****
Optical Brighteners	0.6 ppb***	0-15,000 ppb***
Phycocyanin	2 ppb <sup>PC</sup>	0-40,000 ppb <sup>PC</sup>
Phycocerythrin	0.15 ppb <sup>PE</sup>	0-750 ppb <sup>PE</sup>
PTSA Dye	0.1 ppb***	0-650 ppb***
Rhodamine Dye	0.01 ppb	0-1000 ppb
Tryptophan	3 ppb	>20,000 ppb
Turbidity	0.05 NTU	0-3000 NTU

\* 1,5 Naphthalene Disulfonic Disodium Salt

\*\* Quinine Sulfate

\*\*\* PTSA (1,3, 6, 8 - Pyrenetetrasulfonic Acid Tetrasodium Salt)

\*\*\*\* BTEX (Benzene, Toluene, Ethylbenzene, Xylenes)

<sup>PC</sup> Phycocyanin pigment from Prozym diluted in Deionized water

<sup>PE</sup> Phycocerythrin pigment from Prozym diluted in Deionized water

## Physical Dimensions

Length x Diameter:

5.7" x 0.9"; 14.48 x 2.23 cm (SSt or Ti)

5.7" x 1.25"; 14.48 x 3.18 cm (Delrin)

Weight: 5.0 oz; 142 grams

## Environmental Characteristics

Temperature Range:

Ambient: 0 to 50 deg C

Water Temp: -2 to 50 deg C

Depth Range: 600 meters

Signal Output: 0 - 5 VDC

Supply Voltage Range: 3 - 15 VDC

Power Requirements: <300mW typical

## Ordering Information

### AVAILABLE INSTRUMENTS

Blue Green Algae - Phycocerythrin (freshwater) or Phycocyanin (marine)

CDOM/FDOM

Chlorophyll *in vivo*

- Blue excitation

- Red excitation

Crude Oil

Fluorescent Dye Tracing - Fluorescein, PTSA or Rhodamine

Refined Fuels

Turbidity

Wastewater Monitoring - Optical Brighteners or Tryptophan

Contact us for Custom Optics

**Titanium and Plastic Housings also available. Titanium and Plastic withstand corrosion better than stainless steel and are recommended for stationary deployments in highly corrosive environments.**

## Contact Us

Toll-Free : 1.877.316.8049

Email : sales@turnerdesigns.com

Address:

Phone : 408.749.0994

Web : www.turnerdesigns.com

845 West Maude Avenue

Fax : 408.749.0998

Sunnyvale, CA 94085

### CYCLOPS-7 ACCESSORIES

Solid Secondary Standards

Flowthrough Cap

Shade Cap (Recommended for most deployments)

0.6 Meter Pigtail Cable with Locking Sleeve

5 Meter Pigtail Cable with Locking Sleeve

10 Meter Pigtail Cable with Locking Sleeve

25 Meter Pigtail Cable with Locking Sleeve

50 Meter Pigtail Cable with Locking Sleeve

Cyclops Explorer

*DataBank Datalogger available.*

*For details visit [www.turnerdesigns.com](http://www.turnerdesigns.com).*



Spring return mechanical diaphragms metering pumps

*Pompe dosatrici a membrana meccanica con ritorno a molla*

**MB**

**155** l/h

**MC**

**420** l/h



**BLACKLINE**  
series



D\_MB/MC\_GB.IT\_07'11

## Mechanical diaphragms metering pumps

The **OBL MB/MC** series are mechanical diaphragm pumps with spring return mechanism, eccentric shaft and thrust ring. They combine the working characteristics of a plunger pump with the sealing advantages of a diaphragm pump.

Thanks to the quality and simple-design of the diaphragm, these pumps are easy-handling.

*Le pompe dosatrici OBL a membrana meccanica della serie MB/MC con meccanismo a ritorno a molla con albero eccentrico e disco di spinta, associano le caratteristiche funzionali delle pompe a pistone e i vantaggi delle pompe a membrana.*

*Grazie alla qualità e alla semplicità della membrana queste pompe sono di facile gestione.*

**MB**



Flow rate/Portata Max: • 155 L/h  
Stroke/Corsa: • 1 mm. 2 mm. 4 mm.

### General features

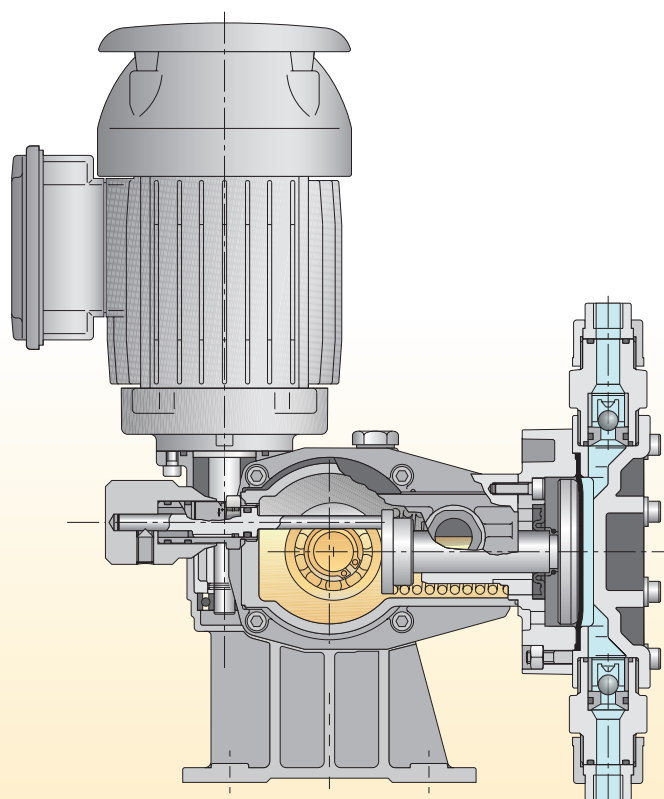
- Diaphragm, economic, robust, compact metering pump.
- The mechanical diaphragm works, both giving the swept volume, acting basically as plunger, and as separator between crank gear and the handled fluid.
- Easy and minimum maintenance required, thanks to the reduced number of components.
- The OBL's unique mechanical diaphragm design ensures linearity between flow rate and percentage of stroke. The flow rate is virtually unaffected by the working pressure variations.
- Leak-free pump, due to OBL's stress-proof diaphragm.
- High working safety:
  - No external moving parts.
  - Leak-free operations.

### Caratteristiche generali

- Pompa a membrana economica, robusta e compatta.
- La membrana meccanica svolge il duplice ruolo di trasmissione della cilindrata, agendo in pratica come un pistone, e di separatore tra manovellismo e fluido da pompare.
- Manutenzione semplice e ridotta al minimo, grazie al basso numero di componenti.
- La particolare struttura fisica della membrana meccanica OBL assicura una proporzionalità lineare fra portata e percentuale di regolazione. La portata risulta quasi insensibile alle variazioni di pressione d'esercizio.
- Perfetta tenuta idraulica grazie all'elasticità della membrana.
- Sicurezza operativa grazie all'assenza di perdite del liquido dosato e di organi esterni in movimento.

### Sectional view

Sezione



## Pompe dosatrice a membrana meccanica

**MC****Control systems**

Sistemi di regolazione

- Manual: With 0-10 scale micrometer knob.
- Electric: Via OBL designed Z type electrical actuator.
- Pneumatic: By means of a 3÷15 PSI, type W pneumatic actuator.

- *Manuale: Manopola con numeri in sequenza da 0 a 10.*
- *Elettrico: Mediante servocomando OBL tipo Z.*
- *Pneumatico: Mediante servocomando pneumatico 3÷15 PSI tipo W.*

**Standard manual adjustment**

Regolazione manuale

- Adjustment via 0-10 scale micrometer knob.
- *Regolazione con manopola con numeri in sequenza da 0 a 10.*

**Electric actuator**

Servocomando elettrico

**MB/MC** series can be equipped with Z type electrical actuator, with following characteristics:

- IP 66 STD
- Manual emergency override
- Anticondensation heater (on demand)
- Non standard voltages and frequencies
- External automatic/manual selector

**Z**

Flow rate is adjusted according to following input signals:

- 4-20 mA, 0-20 A, 20-4 mA e 0-10 V
- Pulses (0÷2 Hz - 0÷30 Hz)
- RS 485 protocol
- Profibus DP - VØ

Le **MB/MC** possono essere fornite con servocomando elettrico tipo Z avente le seguenti caratteristiche:

- IP 66 standard
- Regolazione manuale d'emergenza
- Resistenza anticondensa (su richiesta)
- Frequenze e tensioni non STD
- Selettore esterno automatico/manuale

La regolazione della portata avviene in funzione dei seguenti segnali regolanti:

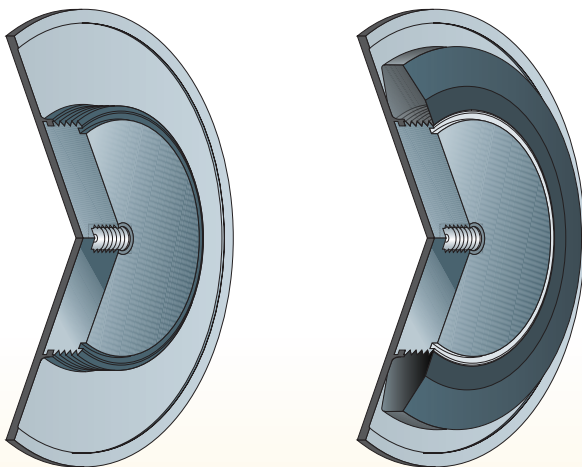
- 4-20 mA, 0-20 mA, 20-4 mA e 0-10 V
- Impulsi (0÷2 Hz - 0÷30 Hz)
- Protocollo di comunicazione RS 485
- Profibus DP - VØ

**PROFI**  
**BUS**

Flow rate/Portata Max: • **420 L/h**  
Stroke/Corsa: • **6 mm.**

**Diaphragm sectional view**

Sezione della membrana



METALLIC  
SUPPORT  
SUPPORTO  
METALLICO

RUBBER  
GOMMA

PTFE  
TEFLON  
RUBBER  
GOMMA  
PTFE  
TEFLON  
NYLON NET  
RETE

Technical data

TYPE TIPO	STROKES/ COLPI/AL 1"	FLOW RATE PORTATA MAX l/h	MAX PRESS. BAR PRESS. MAX BAR			CONNECTIONS/ ATTACCHI					
			3PH 0,20	IPH 0,24	KW 0,37	THREADED/FILETTATI g.f. BSPF			FLANGED/FLANGIATI DN 15 - ANSI 150		
						P	PP	A	P	PP	A
<b>50 Hz</b>											
MB 1	36	1	12	12	12	1/4"	-	1/4"	1/2"	-	1/2"
MB 1,6	50	1,5	12	12	12	1/4"	-	1/4"	1/2"	-	1/2"
MB 2,4	70	2,4	12	12	12	1/4"	-	1/4"	1/2"	-	1/2"
MB 3,5	95	3,5	12	12	12	1/4"	-	1/4"	1/2"	-	1/2"
MB 4	115	4	12	12	12	1/4"	-	1/4"	1/2"	-	1/2"
MB 5,5	155	5,5	12	12	12	1/4"	-	1/4"	1/2"	-	1/2"
MB 7	25	7	12	10	12	3/8"	3/8"	3/8"	1/2"	1/2"	1/2"
MB 11	36	11	12	10	12	3/8"	3/8"	3/8"	1/2"	1/2"	1/2"
MB 16	50	16	12	10	12	3/8"	3/8"	3/8"	1/2"	1/2"	1/2"
MB 23	70	23	12	10	12	3/8"	3/8"	3/8"	1/2"	1/2"	1/2"
MB 31	95	31	8	6	8	3/8"	3/8"	3/8"	1/2"	1/2"	1/2"
MB 37	115	37	8	6	8	3/8"	3/8"	3/8"	1/2"	1/2"	1/2"
MB 50	155	50	8	6	8	3/8"	3/8"	3/8"	1/2"	1/2"	1/2"
MB 35	36	35	6	4	6	3/8"	3/8"	3/8"	1/2"	1/2"	1/2"
MB 49	50	49	6	4	6	3/8"	3/8"	3/8"	1/2"	1/2"	1/2"
MB 75	70	75	6	4	6	3/8"	3/8"	3/8"	1/2"	1/2"	1/2"
MB 101	95	101	6	4	6	3/8"	3/8"	3/8"	1/2"	1/2"	1/2"
MB 120	115	120	6	3	5	-	3/8"	1/2"	1/2"	1/2"	1/2"
MB 155	155	155	6	3	5	-	3/8"	1/2"	1/2"	1/2"	1/2"
<b>60 Hz</b>											
MB 0,8	30	9	12	12	12	1/4"	-	1/4"	1/4"	-	1/4"
MB 1,2	30	9	12	12	12	1/4"	-	1/4"	1/4"	-	1/4"
MB 2,9	30	9	12	12	12	1/4"	-	1/4"	1/4"	-	1/4"
MB 4,2	30	9	12	12	12	1/4"	-	1/4"	1/4"	-	1/4"
MB 4,8	30	9	12	12	12	1/4"	-	1/4"	1/4"	-	1/4"
MB 9	30	9	12	10	12	3/8"	3/8"	3/8"	1/2"	1/2"	1/2"
MB 14	43	14	12	10	12	3/8"	3/8"	3/8"	1/2"	1/2"	1/2"
MB 28	84	28	12	10	12	3/8"	3/8"	3/8"	1/2"	1/2"	1/2"
MB 36	114	36	8	6	8	3/8"	3/8"	3/8"	1/2"	1/2"	1/2"
MB 45	138	45	8	6	8	3/8"	3/8"	3/8"	1/2"	1/2"	1/2"
MB 42	43	42	6	4	6	3/8"	3/8"	3/8"	1/2"	1/2"	1/2"
MB 58	60	58	6	4	6	3/8"	3/8"	3/8"	1/2"	1/2"	1/2"
MB 90	84	90	6	4	6	3/8"	3/8"	3/8"	1/2"	1/2"	1/2"
MB 121	115	121	6	3	5	-	3/8"	1/2"	1/2"	1/2"	1/2"
MB 145	138	145	6	3	5	-	3/8"	1/2"	1/2"	1/2"	1/2"

Model number

Esempio composizione sigla

KEY TO SYMBOL	LEGENDA
PUMP MODEL / POMPA TIPO	
FLOW RATE l/h   PORTATA l/h	
PP	PP CONSTRUCTION   ESECUZIONE POLIPROPILENE
P	PVC HEAD, CERAMIC SEATS AND BALLS   VALVOLA E SEDE IN PVC
A	AISI-316L CONSTRUCTION   ESECUZIONE AISI-316L
PP11	PP CONSTRUCTION+AISI-316L VALVE AND SEAT   ESEC. PP+VALVOLA E SEDE IN AISI-316L
PP32	PP CONSTRUCTION + HASTELLOY C VALVE - INCOLOY 825 SEAT ESECUZIONE PP+VALVOLA HASTELLOY C - SEDE INCOLOY 825
Z	OBL 4÷20 mA ELECTRIC ACTUATOR   SERVOCOMANDO ELETTRICO OBL 4÷20 mA
W	3÷15 PSI PNEUMATIC ACTUATOR   SERVOCOMANDO PNEUMATICO 3÷15 PSI
F	UNI-DIN FLANGED CONNECTIONS   ATTACCHI FLANGIATI UNI-DIN
FA	ANSI FLANGED CONNECTIONS   ATTACCHI FLANGIATI ANSI

Two-headed MB pump, first head PP wetted parts, second head AISI 316L.

Pompa MB a doppia testata con una testata in PP e la seconda in AISI 316L.



Caratteristiche tecniche



• MB series diaphragm metering pump with PP pump head.

• Pompa dosatrice a membrana serie MB con testata in PP.

Flow rates/Portate: • 1÷155 L/h

Motors/Motori: • Threephase special 0,20/0,30 kW  
Trifase con flangia speciale - 0,20/0,30 kW  
4 Poles/poli - IP55 - I.C.L.F - S1 - IEC 34-1

Δ - 230 V - 50 Hz
λ - 400 V - 50 Hz
Δ - 220÷290 V - 60 Hz
λ - 380÷500 V - 60 Hz

• Singlephase special 0,24/0,37 kW  
Monofase con flangia speciale - 0,24/0,37 kW  
4 Poles/poli - IP55 - I.C.L.F - S1 - IEC 34-1

220÷240 V - 50 Hz
110÷115 V - 50 Hz
220÷230 V - 60 Hz
110÷115 V - 60 Hz

Pump/Pompa: • Single and multiple unit / Singola e multipla

< MB pumps can be supplied with multiheaded arrangement; heads can have different max flow rates and different wetted materials.

Le pompe MB possono essere fornite con testata multipla con possibilità di fornire diverse portate ed anche diversi materiali a contatto con il liquido dosato.

Adjustm./Regolaz.: • 0-10 scale micrometer knob.  
Manopola con numeri in sequenza da 0 a 10

Materials/Materiale: • Aluminium casing  
Corpo meccanismo: alluminio  
• Glass reinforced PP pump head, PVC \* or AISI 316 L  
Testata popmpante:  
PP (Polipropilene), PVC \* o AISI 316L

Weigth/Peso: • 10÷20 Kgs/Kg

\* 0,8÷5,5 only / Solo 0,8÷5,5.

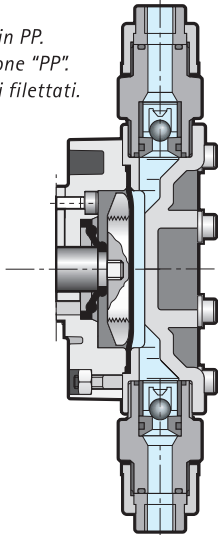
# Pump heads

Testate pompanti

## PP

PP heads. "PP" execution. Threaded connections.

Testate in PP. Esecuzione "PP". Attacchi filettati.



- Single valve ball (Double check valve for PVC version).
- Suction and discharge connections both threaded and flanged (on demand).
- Max. temperature of dosed chemical: 45 °C.

- L'esecuzione prevede valvole a sfera singole (VALVole doppie per versione PVC).
- Gli attacchi di aspirazione e mandata sono forniti sia filettati che flangiati.
- Temperatura massima del liquido dosato: 45 °C.

### Materials of construction

Materiali di costruzione

PARTS / PARTICOLARI	PP	PP II	PP32	A	P
LIQUID END / CORPO TESTATA	PP	PP	PP	AISI 316L	PVC
VALVE GUIDE / GUIDA VALVOLA	PP	PP	PP	PP	PP
VALVE SEAT / SEDE VALVOLA	PVC	AISI 316L	INCOLOY 825	AISI 316L	CERAMIC
VALVE / VALVOLA	PYREX	AISI 316L	HASTELLOY C-276	AISI 316L	CERAMIC
VALVE SEAL / TENUTA VALVOLA	FPM (VITON)	FPM (VITON)	FPM (VITON)	FPM (VITON)	FPM (VITON)
VALVE HOUSING / CONT. VALVOLA	PP	PP	PP	AISI 316L	PVC
DIAPHRAGM / MEMBRANA	PTFE (TEFLON)	PTFE (TEFLON)	PTFE (TEFLON)	PTFE (TEFLON)	PTFE

### Overall dimensions

Misure d'ingombro

#### Construction characteristics

Caratteristiche costruttive

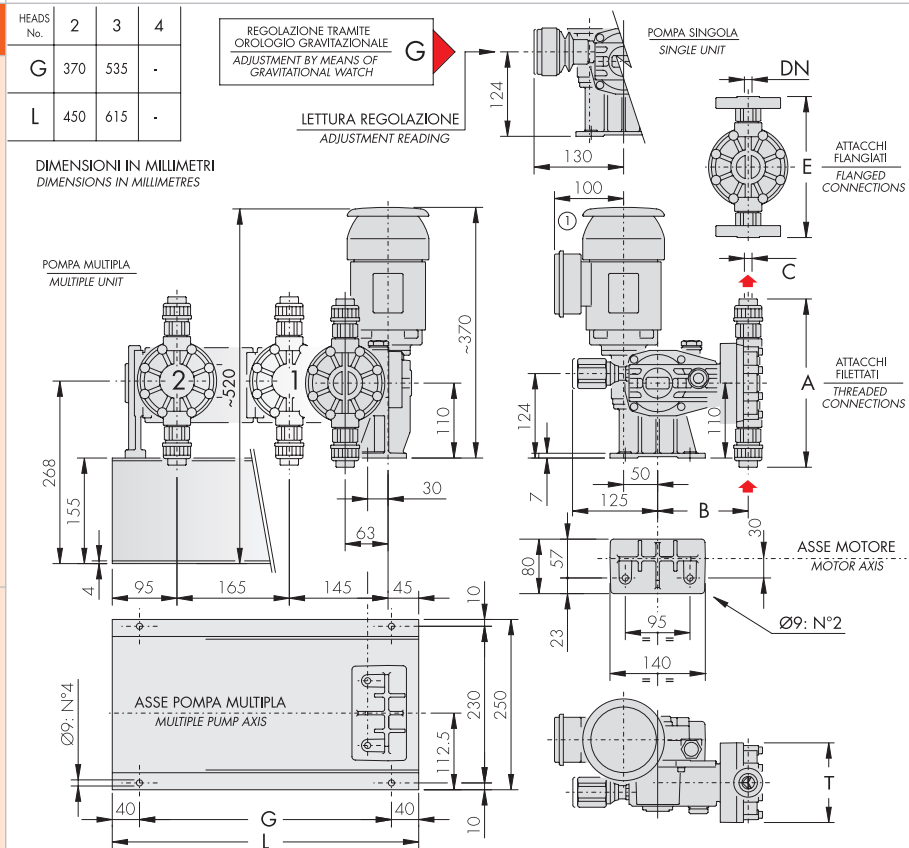
- Glass reinforced PP pump head support ensures chemical compatibility with any dosed liquid.
- Leak-free diaphragm pump head.
- Smooth and linear adjustment, either stationary or running, by means of micrometer knob.
- ± 2% accuracy rating from 10 to 100% of the nominal flow rate.

• Supporto della testata pompante realizzato in PP per consentire una ottima protezione dal liquido dosato.

• Testata a membrana a tenuta stagna del liquido pompato.

• Regolazione continua della portata sia a pompa ferma che in moto, tramite manopola graduata.

• Precisione ± 2% tra il 10 ed il 100% della portata di targa.



TYPE / TIPO		A AISI 316 L					PP POLYPROP.					P PVC					DN	
50Hz	60Hz	A	B	C	E	TØ	A	B	C	E	TØ	ADV	B	C	EDV	TØ	UNI	ANSI
		g.f. BSPF					g.f. BSPF					g.f. BSPF						
MB 1=5.5	MB 0.8=4.8	-	-	-	-	-	-	-	-	-	-	256	144	1/4"	198	118	15	1/2"
MB7		166	132,5	3/8"	180	114	237	133	3/8"	201	117	-	-	-	-	-	15	1/2"
MB11	MB9	166	132,5	3/8"	180	114	237	133	3/8"	201	117	-	-	-	-	-	15	1/2"
MB16	MB14	166	132,5	3/8"	180	114	237	133	3/8"	201	117	-	-	-	-	-	15	1/2"
MB23		166	132,5	3/8"	180	114	237	133	3/8"	201	117	-	-	-	-	-	15	1/2"
MB31	MB28	166	132,5	3/8"	180	114	237	133	3/8"	201	117	-	-	-	-	-	15	1/2"
MB37	MB36	166	132,5	3/8"	180	114	237	133	3/8"	201	117	-	-	-	-	-	15	1/2"
MB50	MB45	166	132,5	3/8"	180	114	237	133	3/8"	201	117	-	-	-	-	-	15	1/2"
MB35		181	132	3/8"	195	129	251	133	3/8"	215	133	-	-	-	-	-	15	1/2"
MB49	MB42	181	132	3/8"	195	129	251	133	3/8"	215	133	-	-	-	-	-	15	1/2"
MB75	MB58	181	132	3/8"	195	129	251	133	3/8"	215	133	-	-	-	-	-	15	1/2"
MB101	MB90	181	132	3/8"	195	129	251	133	3/8"	215	133	-	-	-	-	-	15	1/2"
MB120	MB121	200	133,5	1/2"	200	129	251	133	3/8"	215	133	-	-	-	-	-	15	1/2"
MB155	MB145	200	133,5	1/2"	200	129	251	133	3/8"	215	133	-	-	-	-	-	15	1/2"

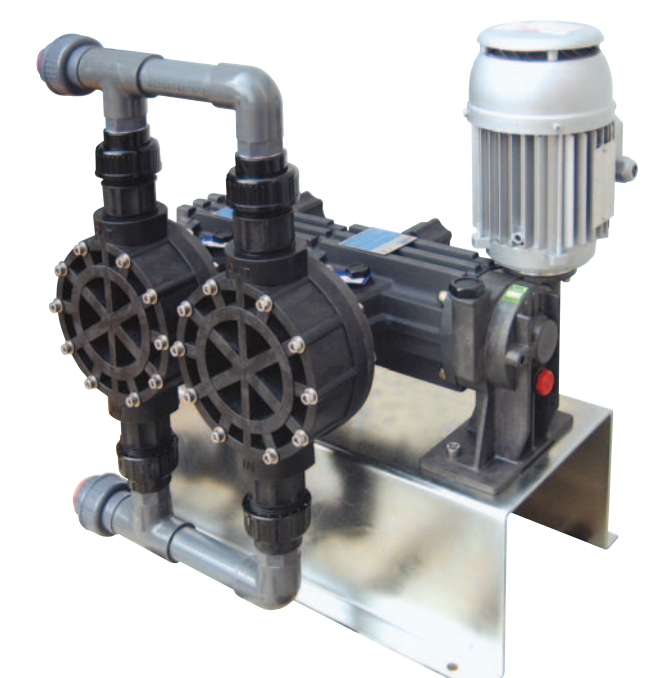
Technical data

TYPE TIPO	STROKES/1" CORSI/1"	FLOW RATE l/h PORTATA MAX l/h	MAX PRESS. BAR PRESS. MAX. BAR		CONNECTIONS ATTACCHI			
			3PH	1PH	THREADED FILETTATI g.f.		FLANGED FLANGIATI	
					PP	A	PP	A
<b>50 Hz</b>								
MC101	36	100	7	6	3/4" BSPF	DN20 - 3/4"ANSI		
MC131	50	132	7	6	3/4" BSPF	DN20 - 3/4"ANSI		
MC201	70	197	7	6	3/4" BSPF	DN20 - 3/4"ANSI		
MC261	95	260	7	6	3/4" BSPF	DN20 - 3/4"ANSI		
MC321	115	320	5	4	1" BSPF	DN25 - 3/4"ANSI		
MC421	155	420	5	4	1" BSPF	DN25 - 3/4"ANSI		
<b>60 Hz</b>								
MC120	43	120	7	6	3/4" BSPF	DN20 - 3/4"ANSI		
MC158	60	158	7	6	3/4" BSPF	DN22 - 3/4"ANSI		
MC236	84	236	7	6	3/4" BSPF	DN20 - 3/4"ANSI		
MC312	114	312	5	4	1" BSPF	DN25 - 3/4"ANSI		
MC384	138	384	5	4	1" BSPF	DN25 - 3/4"ANSI		

Model number

Esempio composizione sigla

KEY TO SYMBOL		LEGGENDA
PUMP MODEL   POMPA TIPO		
FLOW RATE l/h   PORTATA l/h		
PP	PP CONSTRUCTION   ESECUZIONE POLIPROPILENE	
A	AISI-316L CONSTRUCTION   ESECUZIONE AISI-316L	
PP11	PP CONSTRUCTION+AISI-316L VALVE AND SEAT   ESEC. PP-VALVOLA E SEDE IN AISI-316L	
PP32	PP CONSTRUCTION + HASTELLOY C VALVE - INCOLOY 825 SEAT ESECUZIONE PP+VALVOLA HASTELLOY C - SEDE INCOLOY 825	
Z	OBL 4÷20 mA ELECTRIC ACTUATOR   SERVOCOMANDO ELETTRICO OBL 4÷20 mA	
W	3÷15 PSI PNEUMATIC ACTUATOR   SERVOCOMANDO PNEUMATICO 3÷15 PSI	
F	UNI-DIN FLANGED CONNECTIONS   ATTACCHI FLANGIATI UNI-DIN	
FA	ANSI FLANGED CONNECTIONS   ATTACCHI FLANGIATI ANSI	



Two-headed MC PP pump head with PVC manifold (1" BSP f threaded connections). Max flow rate 840 l/h, max pressure 5 bar g.

Pompa MC a doppia testata in PP con collettore in PVC con attacchi filettati 1" gas femmina. Portata massima 840 l/h, pressione massima 5 bar g.

Caratteristiche tecniche



- MC series diaphragm metering pump with PP pump head.
- Pompa dosatrice a membrana serie MC con testata in PP.

Flow rates/Portate: • 100÷420 L/h (Stroke/Corsa membrana 6mm.)

Motors/Motori: • Threephase special 0,30 kW  
Trifase con flangia speciale - 0,30 kW  
4 Poles/poli - IP55 - I.C.L.F - S1 - IEC 34-1

Δ - 230 V - 50 Hz
λ - 400 V - 50 Hz
Δ - 220÷290 V - 60 Hz
λ - 380÷500 V - 60 Hz

• Singlephase special 0,24/0,37 kW  
Monofase con flangia speciale - 0,24/0,37 kW  
4 Poles/poli - IP55 - I.C.L.F - S1 - IEC 34-1

220÷240 V - 50 Hz
110÷115 V - 50 Hz
220÷230 V - 60 Hz
110÷115 V - 60 Hz

Pump/Pompa: • Single and multiple unit / Singola e multipla

< MC pumps can be supplied with multiheaded arrangements; heads can have different max flow rates and different wetted materials. MC pumps can be supplied with suction and discharge manifold reaching max flow rates of 1200 litres per hour at max pressure of 4 bar g.

Le pompe MC possono essere fornite con testata multipla con possibilità di fornire diverse portate ed anche diversi materiali a contatto con il liquido dosato. Le pompe MC possono essere fornite con un collettore in PVC (aspirazione e mandata) in modo da raggiungere portate massime fino a 1200 litri ora con pressioni massime fino a 4 bar g.

Adjustm./Regolaz.: • 0-10 scale micrometer knob.  
Manopola con numeri in sequenza da 0 a 10

Materials/Materiale: • Aluminium casing  
Corpo meccanismo: alluminio  
• Glass reinforced PP pump head or AISI 316 L  
Testata popmpante:  
PP (Polipropilene), o AISI 316L

Weigth/Peso: • 10÷25 Kgs/Kg

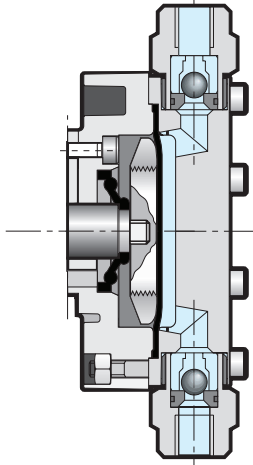
## Pump heads

Testate pompanti

### AISI 316L

AISI 316L heads. "A" execution.  
Threaded connections.

Testate in AISI 316L. Esecuzione "A".  
Attacchi filettati.



- Single valve ball.
- Suction and discharge connections both threaded and flanged (on demand).
- Max. temperature of dosed chemical: 45 °C.

- L'esecuzione prevede valvole a sfera singole.
- Gli attacchi di aspirazione e mandata sono forniti sia filettati che flangiati.
- Temperatura massima del liquido dosato: 45 °C.

### Materials of construction

PARTS / PARTICOLARI	Materiali di costruzione			
	PP	PPII	PP32	A
LIQUID END   CORPO TESTATA	PP	PP	PP	AISI 316L
VALVE GUIDE   GUIDA VALVOLA	PP	PP	PP	PP
VALVE SEAT   SEDE VALVOLA	PVC	AISI 316L	INCOLOY 825	AISI 316L
VALVE   VALVOLA	PYREX	AISI 316L	HASTELLOY C-276	AISI 316L
VALVE SEAL   TENUTA VALVOLA	FPM (VITON)	FPM (VITON)	FPM (VITON)	FPM (VITON)
VALVE HOUSING   CONT. VALVOLA	PP	PP	PP	AISI 316L
DIAPHRAGM   MEMBRANA	PTFE (TEFLON)	PTFE (TEFLON)	PTFE (TEFLON)	PTFE (TEFLON)

### Overall dimensions

Misure d'ingombro

### Construction characteristics

Caratteristiche costruttive

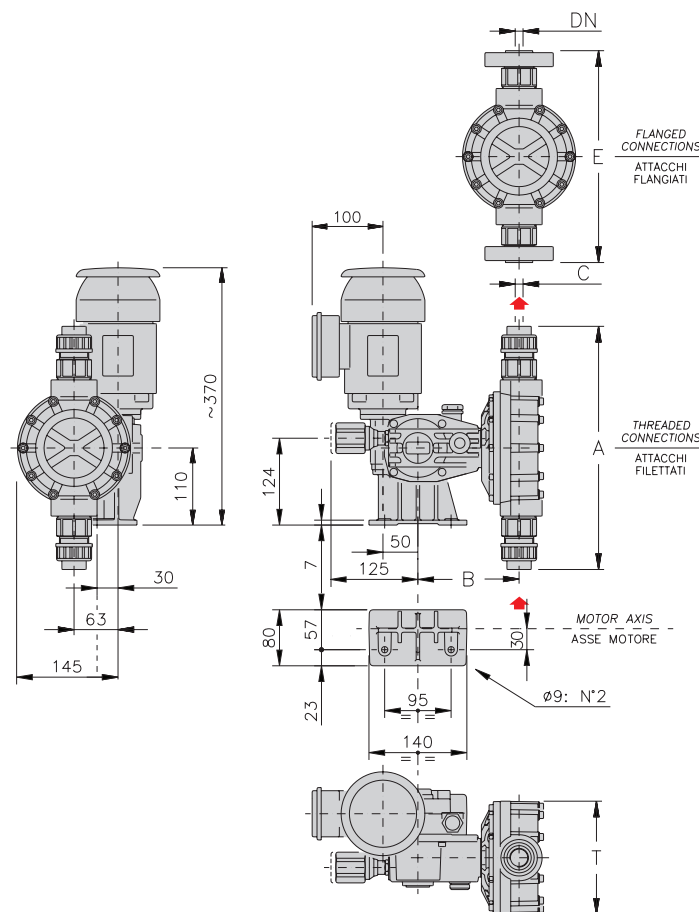
- PTFE coated aluminium pump head support ensures chemical compatibility with any dosed liquid.
- Leak-free diaphragm pump head.
- Smooth and linear adjustment, either stationary or running, by means of micrometer knob.
- ± 2% accuracy rating from 10 to 100% of the nominal flow rate.

• Supporto della testata pompante realizzato in alluminio rivestito in teflon per consentire una ottima protezione dal liquido dosato.

• Testata a membrana a tenuta stagna del liquido pompato.

• Regolazione continua della portata sia a pompa ferma che in moto, tramite manopola graduata.

• Precisione ± 2% tra il 10 ed il 100% della portata di targa.



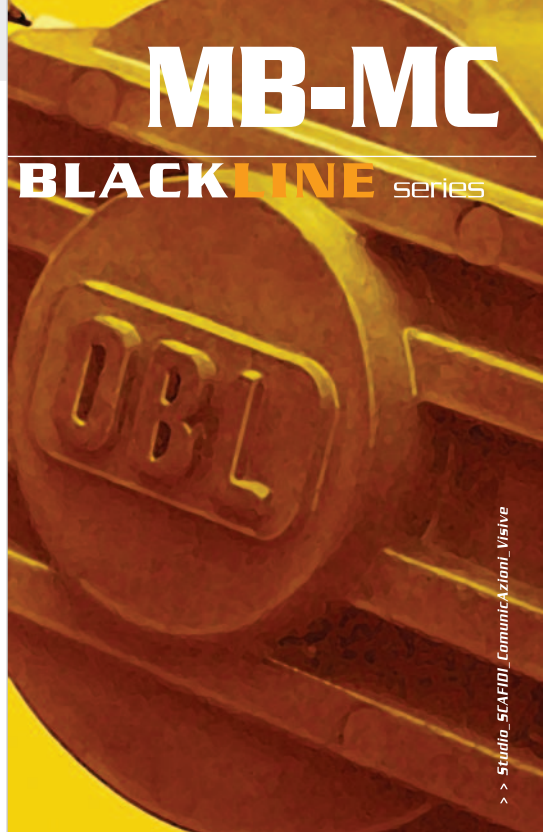
TYPE / TIPO		AISI 316 L					PP					DN	
50Hz	60Hz	A	B	C g.f.	E	T Ø	A	B	C g.f.	E	T Ø	UNI	ANSI
MC101	MC120	235	142	3/4" g.f. BSPF	235	159	347	145	3/4" g.f. BSPF	303	162	20	3/4"
MC131	MC158	235	142	3/4" g.f. BSPF	235	159	347	145	3/4" g.f. BSPF	303	162	20	3/4"
MC201	MC236	235	142	3/4" g.f. BSPF	235	159	347	145	3/4" g.f. BSPF	303	162	20	3/4"
MC261		235	142	3/4" g.f. BSPF	235	159	347	145	3/4" g.f. BSPF	303	162	20	3/4"
MC321	MC312	276	140	1" g.f. BSPF	261	159	355	145	1" g.f. BSPF	303	162	25	1"
MC421	MC384	276	140	1" g.f. BSPF	261	159	355	145	1" g.f. BSPF	303	162	25	1"





# MB-MC

BLACKLINE series



> > Studio SCAFIDI Comunicazione Visiva



Quality System ISO 9001 Certified

**OBL s.r.l.**

20090 Segrate - MILANO

Via Kennedy, 12

Tel. +39-02.269191

Fax +39-02.2133893

[www.oblitalia.com](http://www.oblitalia.com)

[obl.info@idexcorp.com](mailto:obl.info@idexcorp.com)

Technical data are subject to modifications without prior notice. - I dati tecnici possono essere modificati senza preavviso.

# PLASCOAT TALISMAN 30

## Performance Polymer Alloy Coating



### GENERAL DESCRIPTION

Plascoat Talisman 30 has been developed to provide a long lasting, hard, tough coating for mild steel. It is based on an alloy of polyolefins. Therefore it is halogen free and the combustion fumes are low in smoke and have a low toxicity index.

The coating is the hardest in our range. As such it has excellent scuff and abrasion resistance. The coating has excellent adhesion to metal without the need of a separate primer. The coating has FDA food contact approval.

Note: Not all Talisman 30 colours are specifically UV stabilised. Please contact Plascoat for further details. Alternatively, please consider the use of PPA 571.

### TYPICAL USES

Food shelving.  
Metal furniture coating.

### GUIDE TO TYPICAL COATING CONDITIONS

#### Recommended Pretreatment:

For mild steel, ensure metal is clean by thorough degreasing and removal of mill scale. To get the full benefits of the material, the metal can also be blast cleaned to Swedish standard SA 2½-3 or phosphated.

#### Batch Operation:

Metal preheat temperature 250°C - 380°C, depending on metal thickness. Dip for 3 - 10 seconds. A postheat cycle at 170°C may be required to develop fully the surface finish on thin wires.

Water quenching is not necessary except for handling purposes. If present, water quenching should take place at least 30 seconds after all parts have flowed out to a smooth coating and at least 90 seconds after dipping in the powder.

### TYPICAL PROPERTIES OF THE POWDER

Coverage (100% efficiency)	3.3 m <sup>2</sup> /Kg at 300 microns
Particle Size	95% less than 250 microns
Bulk Density (at rest)	0.40 g/cm <sup>3</sup>
Fluidising Characteristics	Excellent
Packaging	20 kg paper sacks

### TYPICAL PROPERTIES OF THE MATERIAL

Specific Gravity		0.99 g/cm <sup>3</sup>
Tensile Strength	ISO 527 (100mm/min)	16 MPa
Elongation at Break	ISO 527 (100mm/min)	160%
Hardness	Shore A	98
	Shore D	58
Pencil Hardness		H/B
Vicat Softening Point	ISO 306	103°C
Melting Point		155°C
Environmental Stress Cracking	ASTM D1693	>1000 hrs
Dielectric Strength	ASTM D149	49.6 KV/mm at 400 microns

### STORAGE

Stored in a clean dry area at 10-25°C and out of sunlight, the material should not deteriorate. However, in the interest of good housekeeping, old stocks should be used first.

### HEALTH AND SAFETY

Plascoat Talisman 30 is supplied as a finely divided powder. Whilst there are no known health hazards associated with Talisman 30, normal handling precautions for dealing with fine organic powders should be taken - i.e. excessive dust generation and inhaling of the powder should be avoided. Facilities may be required for removing excess dust from the working area during the coating of more difficult items.

As with all polymeric powders, the material can ignite if brought into contact with a high temperature source or ignition - particularly in the fluidised condition.

Reference should be made to the respective Plascoat Health and Safety Data Sheet, available on request.

# PLASCOAT Talisman 30

## Performance Polymer Alloy Coating



### TYPICAL PROPERTIES OF THE COATING

The following data applies to a 350 micron coating applied under standard conditions onto 3mm thick steel or aluminium. The pretreatment consisted of degreasing and gritblasting unless otherwise stated.

Recommended Coating Thickness		200-600 microns
Appearance		Smooth/Glossy
Gloss	ISO 2813	60
Impact Strength	Gardner (drop weight) ISO 6272	
	Direct 23°C (water quenched)	1.9 Joules
	Indirect 0°C	6.5 Joules
Abrasion	Taber ASTM D4060/84	
	H18, 500g load, 1000 cycles	69 mg weight loss
	CS17, 500g load, 1000 cycles	20 mg weight loss
Salt Spray	ISO 7253 and NF 41-002	
	Steel - Scribed	Loss of adhesion less than 15 mm from scribe after 500 hrs
	Steel - Unscribed	No loss of adhesion
Chemical Resistance*	- Dilute Acids 70°C	Good
	- Dilute Alkali 70°C	Good
	- Salts (except peroxides) 70°C	Good
	- Solvents 23°C	Poor
Adhesion	PSL, TM/19	A-1
Resistance to Staining	Carrot Juice	Good
	Tomato Juice	Good
	Blackcurrant Juice	Good
	Eosin Dye	Good
	Beetroot Juice	Good
Safe Working Temperature (in air)		100°C max

\* The results given are for full immersion in the chemicals for a prolonged period of time. The coating is resistant to splashes and short term contact of most chemicals. *Further technical advice may be obtained from Plascoat concerning the effects of particular chemicals or mixtures.*

### QUALITY

Plascoat is committed to the manufacture and supply of a wide range of thermoplastic coating powders. This service is backed by the unrivalled experience of over 50 years of powder coating application. With a policy of continuous improvement to its range of products, Plascoat reserves the right to alter or amend any item. Stringent quality control procedures are carried out at every relevant stage of manufacture and Plascoat operates a quality management system approved by BSI in accordance with ISO 9001:2008.

*Plascoat can also offer, through its factories in Europe, specialist plastic coating equipment, an extensive custom coating service and a size reduction service for plastics and other materials.*

*Plascoat is a subsidiary member of the IPT Group of companies. Plascoat is an EU registered trade name.*

#### Plascoat Systems Limited

Trading Estate, Farnham  
Surrey,  
GU9 9NY  
United Kingdom  
Tel: +44(0)1252 733777  
Fax: +44(0)1252 721250  
Web site: [www.plascoat.com](http://www.plascoat.com)  
email: [sales@plascoat.com](mailto:sales@plascoat.com)

#### Plascoat Europe BV

Meeuwenoordlaan 19  
Postbus 9  
3214VT Zuidland  
The Netherlands  
Tel:+31 (0) 181 458 888  
Fax:+31 (0) 181 458 877  
[salespce@plascoat.nl](mailto:salespce@plascoat.nl)

### DISCLAIMER

The information given here is, to the best of our knowledge, true and accurate.

Product and item design, pre-treatment, coating conditions, quality assurance and conditions of product end use are among the factors that affect performance of the coated products and are outside Plascoat's control.

Conditions under which our materials may be used are beyond our control. The suitability for application and performance of finished goods coated with Plascoat material is the sole responsibility of the customer and end user.

Plascoat expressly denies specific or implied warranties including warranties for fitness for a particular use or purpose.

#### Plascoat Corp

Crown Center  
Suite 600  
5005 Rockside Rd  
Cleveland  
OH44131 U.S.A.  
Tel: 800 489 7236  
Fax: 216 520 1273  
[plascoat@nls.net](mailto:plascoat@nls.net)

#### Plascoat Corp (Sales & Dist)

Punda Mercantile Inc  
4115 Sherbrooke Str West,  
6th Floor, Montreal,  
Quebec H3Z 1K9  
Call: 800 489 7236  
Tel: +1 514 931 7278  
Fax: +1 514 931 7200  
[sales@punda.com](mailto:sales@punda.com)